NAA-SR-6320
VOLUME IV OF VI
TRW REPORT No. ER-6041
AEC CATEGORY C-92B, M-3679 (43rd EDITION)
MERCURY RANKINE PROGRAM (SNAP 2) TOPICAL REPORT No. 28

MERCURY RANKINE PROGRAM (SNAP 2)

DEVELOPMENT OF LIQUID-MERCURY-LUBRICATED BEARINGS

VOLUME IV

THREE-SECTOR BEARING EXPERIMENTAL RESULTS

(TITLE UNCLASSIFIED)

AEC RESEARCH AND DEVELOPMENT REPORT

PREPARED UNDER SUBCONTRACT N843 FS-101221
FOR

ATOMICS INTERNATIONAL
A Division of North American Aviation Inc.

TRW EQUIPMENT LABORATORIES
A DIVISION OF TRW INC. • CLEVELAND, OHIO 44117

DISCLAIMER

LEGAL NOTICE

Printed in USA Charge $4.40. Available from the

U. S. Atomic Energy Commission
Division of Technical Information Extension,
P. O. Box 62
Oak Ridge, Tennessee.

Please direct to the same address inquiries covering the procurement of other classified AEC reports.

CONFIDENTIAL UNCLASSIFIED

NAA-SR-6320
VOLUME IV OF VI
TRW REPORT No. ER-6041
AEC CATEGORY C-92B, M-3679 (43rd EDITION)
MERCURY RANKINE PROGRAM (SNAP 2) TOPICAL REPORT No. 28

MERCURY RANKINE PROGRAM (SNAP 2)

DEVELOPMENT OF LIQUID-MERCURY-LUBRICATED BEARINGS

VOLUME IV

THREE-SECTOR BEARING EXPERIMENTAL RESULTS

(TITLE UNCLASSIFIED)

CLASSIFICATION CANCELLED UNCLASSIFIED
OR CHANGED TO
BY AUTHORITY OF DOC
BY J E Brown DATE 3 Nov 71
Exempt from CCRP Re-review Requirements
(per 7/22/82 Duff/Caudle memorandum) 3/4/01 HR

By

OTTO DECKER

DEFENSE INFORMATION

"THIS MATERIAL CONTAINS INFORMATION AFFECTING THE NATIONAL DEFENSE OF THE UNITED STATES WITHIN THE MEANING OF THE ESPIONAGE LAWS, TITLE 18 U.S.C., SECTIONS 793 AND 794. THE TRANSMISSION OR REVELATION OF WHICH IN ANY MANNER TO AN UNAUTHORIZED PERSON IS PROHIBITED BY LAW."

GROUP III

DOWNGRADED AT 12 YEAR INTERVALS,
NOT AUTOMATICALLY DECLASSIFIED

PREPARED UNDER SUBCONTRACT N843 FS-101221

FOR

ATOMICS INTERNATIONAL
A Division of North American Aviation Inc.

DISTRIBUTION OF THIS DOCUMENT IS UNLIMITED

TRW EQUIPMENT LABORATORIES
A DIVISION OF TRW INC. • CLEVELAND, OHIO 44117

UNCLASSIFIED

CONTRACT: AT(11-1)-GEN-8
ISSUED:

CONFIDENTIAL

DISTRIBUTION LIST

SYSTEMS FOR NUCLEAR AUXILIARY POWER (SNAP)
REACTOR SNAP PROGRAM
M-3679 (43rd Ed.)

No. of Copies	
1	AEC Patent Office
6	Aerojet-General Corporation (NASA)
1	Aerojet-General Corporation, Sacramento
1	Aerojet-General Nucleonics
1	Aerojet-General Nucleonics (NASA)
2	Aeronautical Systems Division
1	Aerospace Corporation
1	Air Force Foreign Technology Division
1	Air Force Headquarters
1	Air Force Surgeon General
1	Air Force Technical Applications Center
3	Air Force Weapons Laboratory
1	Air University Library
1	AiResearch Manufacturing Company, Phoenix
1	Allison Division - GMC
1	Argonne National Laboratory
1	Army Ballistic Research Laboratories
1	Army Director of Transportation
1	Aro, Inc.
2	Atomic Energy Commission, Washington
66	Atomics International
1	Battelle Memorial Institute
2	Battelle-Northwest
1	Bendix Corporation (NASA)
1	Brookhaven National Laboratory
2	Bureau of Naval Weapons
2	Bureau of Ships
1	California Patent Group
2	Canoga Park Area Office
1	Central Intelligence Agency
1	Chicago Patent Group
1	Director of Defense Research and Engineering (OAP)
1	Douglas Aircraft Company, Inc. Newport Beach
1	Du Pont Company, Aiken
1	Du Pont Company, Wilmington
1	Electro-Optical Systems, Inc.
1	General Atomic Division
1	General Dynamics/Convair (AF)
1	General Dynamics/Fort Worth
1	General Electric Company, Cincinnati
2	General Electric Company (FPD)
1	General Electric Company (MSVD)
2	General Electric Company, San Jose
1	Hughes Research Laboratories
1	Institute for Defense Analyses
2	Jet Propulsion Laboratory
1	Johns Hopkins University (APL)
1	Lockheed-Georgia Company
1	Los Alamos Scientific Laboratory
1	Minnesota Mining and Manufacturing Company
1	Monsanto Research Corporation
1	Mound Laboratory
1	NASA Ames Research Center
2	NASA Goddard Space Flight Center
7	NASA Lewis Research Center
1	NASA Manned Spacecraft Center
3	NASA Marshall Space Flight Center
3	NASA Scientific and Technical Information Facility
2	National Aeronautics and Space Administration, Washington
4	National Reactor Testing Station (PPCO)
1	Naval Air Development Center
1	Naval Radiological Defense Laboratory
2	Naval Research Laboratory
1	Navy Marine Engineering Laboratory
1	New York Operations Office
1	Nuclear Weapons Training Center Pacific
1	Oak Ridge Operations Office
2	Office of Naval Research
1	Office of the Chief of Engineers
3	Office of the Chief of Naval Operations
2	Office of the Chief of Naval Operations (OP-03EG)
1	Pratt and Whitney Aircraft Division (NASA)
1	Radio Corporation of America
1	Rand Corporation
1	Sandia Corporation
8	Union Carbine Corporation (ORNL)
1	United Nuclear Corporation (NDA)
1	University of California, Livermore
1	Westinghouse Electric Corporation, Lima
1	Westinghouse Electric Corporation, Lima (AF)
1	Westinghouse Electric Corporation (NASA)
1	Westinghouse Electric Corporation (WAL)
2	White Sands Missile Range
10	Division of Technical Information Extension
9	TRW Inc.

FOREWORD

This Development of Liquid-Mercury-Lubricated Bearings Topical Report defines the analytical and experimental results obtained with fluid film bearings lubricated by liquid mercury. This report includes the design approach, analytical techniques, procedures, test results, and experimental activity performed by TRW Inc. as a facet of the Mercury Rankine Power Conversion Program during the period of January 1961 through June 1963.

This report consists of the following six volumes:

Volume I	Analytical Design Approach and Status of Bearing Systems (With Appendixes)
Volume II	Plain Bearing Experimental Results
Volume III	Tilting-Pad Bearing Experimental Results
Volume IV	Three-Sector Bearing Experimental Results
Volume V	Three-Pad Bearing Experimental Results
Volume VI	Spiral-Groove Thrust Bearing Experimental Results

For convenience of the reader, citations of reference works are the same in each volume; e. g., Reference 6 cited in Volume I and Reference 6 cited in Volume II are the same publication.

Volume I contains the Nomenclature and the References on the study. All other Appendixes are also included in Volume I.

ABSTRACT

This volume presents the results of part of the activity associated with the development of the hybrid three-sector bearings with and without orifice compensation.

On the basis of previous development work and the system requirements, the three-sector bearing is selected, sized, analyzed, and tested. The initial tests utilize inherent compensation and several supply configurations. Diametral clearance, axial length, and alignment are the principle variables experimentally evaluated. The overall performance characteristics reviewed are satisfactory except for poor stability characteristics. The reduced data is utilized to modify the supply pad configuration and orifice diameter resulting in partial orifice compensation. Improved stability characteristics are achieved at the expense of load capacity and flow for a given supply pressure. To improve stability performance further, complete orifice compensation is utilized. Combined with a diametral clearance of 0.0015-inch, complete orifice compensation assures freedom from half-frequency whirl over the entire speed and load range.

Experimental performance for each type of three-sector bearing tested is compared with predicted performance based on semi-empirical turbulent flow correction factors. Semi-empirical equations and non-dimensional design curves are generated to predict load capacity, flow, and power loss while operating at Reynolds numbers from $0 < Re < 10,000$. The influence of high Reynolds numbers in the clearance space on load capacity is secondary to the hybrid contribution. Power loss is increased and flow is decreased due to superlaminar flow regime in the clearance space.

The three-sector bearing meets the major CRU requirements with the following exceptions: (1) Without orifice compensation the threshold of half-frequency whirl is below the design speed, and (2) with orifice compensation the load capacity is compromised. (3) The experimental program completed to date has shown that the surface damage due to cavitation-erosion is not a problem.

TABLE OF CONTENTS

TABLE OF CONTENTS (Continued)

TABLE OF CONTENTS (Continued)

LIST OF ILLUSTRATIONS

LIST OF ILLUSTRATIONS (Continued)

LIST OF ILLUSTRATIONS (Continued)

LIST OF ILLUSTRATIONS (Continued)

LIST OF ILLUSTRATIONS (Continued)

LIST OF ILLUSTRATIONS (Continued)

LIST OF ILLUSTRATIONS (Continued)

LIST OF ILLUSTRATIONS (Continued)

LIST OF ILLUSTRATIONS (Continued)

LIST OF ILLUSTRATIONS (Continued)

LIST OF ILLUSTRATIONS (Continued)

LIST OF TABLES

I. INTRODUCTION AND SUMMARY

A large number of developmental tests were conducted on a variety of three-sector bearings in support of the SNAP 2 program. The three-sector bearing is essentially a plain journal bearing with three equally sized and spaced axial drain grooves or slots. The three-sector bearing was selected primarily because it offered a more stable operating envelope under the influence of zero-g operation than did the plain cylindrical bearing developed for application earlier and discussed in Volume II. Combined with the high supply pressures required to force fluid through the clearance space this type of bearing becomes a hybrid bearing, having both hydrostatic capacity at zero and any other speed, as well as hydrodynamic capacity by virtue of the shearing action generated as a function of speed.

The development tests concentrated on a single diameter of 0.625 inch and evaluated the influence of length (0.312 - 0.450 inch), clearance (0.0008 - 0.0022 inch), orifice size (0.020 - 0.018 inch), number of orifices (1 or 3 per pad), supply pad geometry, and degree of alignment (up to 0.0025 inch/inch), on performance.

Major test variables were speed, load (both unidirectional and rotating), lube flow-pressure and temperature, and time. The measured output variables included deflection characteristics, attitude angle, damping, radial and fluid film stiffness, power loss, and phase angle.

The three-sector bearings were subjected to four distinctive test series during this report period:

1) Limited parametric tests to evaluate the influence of clearance, axial length, degree of alignment, and loads on the performance and endurance characteristics of the uncompensated bearing (i.e., no orifice compensation)

2) Parametric tests on individually fed three-sector bearings in which each supply pad is fed and controlled separately

3) Parametric tests on a partially orifice-compensated bearing

4) Parametric and endurance tests on fully-orifice-compensated bearing

The experimental performance was correlated with predicted performance which was based on empirical correction factors for superlaminar (turbulent) flow. Measured power loss, attitude angle (for the uncompensated orifice), and threshold of stability agreed reasonably well with predicted performance. Semi-analytical prediction techniques and non-dimensional design curves were generated for load capacity and flow-pressure requirements which, when combined with existing techniques, can form the basis for future analytical estimates of hybrid three-sector bearing performance.

The development tests verified many of the predicted performance characteristics of bearings operating in the nonlaminar regime. In comparing laminar performance with measured performance, the mercury-lubricated, three-sector bearing had higher power loss, lower flow for a given supply pressure, and poorer stability characteristics. However, in terms of load capacity, the influence of high Reynolds number operation was overshadowed by the increase in load capacity resulting from the hybrid action in the bearing. This was especially true for the smaller clearance bearing operating at eccentricity ratios below 0.5. At eccentricity ratios approaching 1.0 and for larger clearance, load capacity performance approached that predicted by laminar hydrodynamic theory. Orifice compensation reduced the hydrostatic load capacity contribution as a result of the pressure drop through the supply orifice. The prediction that load capacity with an axial groove was less than the load capacity into a pad (i.e., between axial slots) was verified.

Stable operation (freedom from half- or fractional-frequency whirl) within the speed envelope and load range was achieved by reducing the diametral clearance of the uncompensated bearing to 0.001 inch. At 0.0012 inch, the threshold was below 40,000 rpm. By providing orifice compensation, the same three-sector bearing was stable at all operating modes for clearances up to 0.0015 inch. Increasing the clearance to 0.002 inch lowered the threshold to 20,000 rpm, but it could be raised to above 44,000 rpm by applying a supply pressure of 250 to 300 psi. Although half-frequency whirl was present, the three-sector bearing demonstrated its ability to operate satisfactorily for 1000 hours.

Orifice compensation also enhanced flow reliability to each sector for large displacements of the shaft. Without compensation it was possible to choke or throttle off all the flow out of the loaded pad and, hence, to depend on flow swept across the axial slot to assure adequate lubrication.

Flow requirements for available supply pressures were adequate although orifice compensation reduced the flow for a given supply pressure.

The analytical and experimental bearing development program demonstrated the capability of the three-sector bearing to meet the specific requirements of stable operation at any possible operating mode with orifice compensation but at a considerable compromise in load capacity. However, on the basis of the experimental component tests, the load capacity was still in excess of that required by CRU specifications. No evidence of cavitation-erosion damage was detected during any of the three-sector bearing tests even though large amplitudes of motion were encountered for long periods of time (in hundreds of hours). Critical speeds were controllable by supply pressure, flow, and clearance manipulations. Operation between first and second mode critical was assured with satisfactory bearing clearances. Crudding (deposition of corrosion products) was not encountered in the small orifices although on occasion scum-like deposits were observed on the journal surface. The performance characteristics of the uncompensated three-sector bearing in early CRU's (CRU III) was very poor. The ability of the improved (stability) orifice-compensated bearing in the current CRU's remains unknown at the conclusion of this report period.

II. THREE-SECTOR BEARING

As indicated in Table 1 a large number of tests have been conducted on a variety of three-sector bearings in support of the SNAP 2 development program. These tests were run in bearing rigs as well as with complete SNAP 2 rotating packages. By and large, the tests have concentrated on a single diameter of 0.625 inch and have varied such dimensions as the following.

Length	0.312 to 0.450 inch
Clearance	0.0008 to 0.0022 inch
Orifice size (diameter)	0.020 to 0.078 inch
Number of orifices	1 or 3 per pad
Supply pad size	None, or 1/4-inch axial x 1.8-inch circumferential, by 0.030 inch deep
Degree of alignment	Up to 0.001-inch misalignment over the bearing length

The test conditions were also varied and included:

1) Overall performance - go or no-go type tests

2) Basic parametric studies of the bearing only

3) Influence of rotor dynamics on bearing performance in both bearing rigs and SNAP 2 rotating packages

4) Bearing length optimization tests

5) Misalignment capability

6) Hot and cold (lubricant and turbine air temperature) parametric studies

7) Endurance testing

8) Effect of high rotating loads on bearing performance

9) Influence of orifice compensation versus inherent compensation both by orifice size control and by control of flow and pressure to each of the three sectors of the bearing

A schematic of the three-sector bearing is shown in Figure 1. Initial analysis and development was conducted on a three-sector bearing which had three orifices per sector and no recessed supply pad, as shown in Figure 2. Figure 3 shows the modified version in which the three supply orifices were replaced by a single 0.078-inch orifice surrounded by a recessed supply pad.

TABLE 1

SNAP 2 BEARING TEST SUMMARY

Bearing Type	Test Number
Annular	BCR 1; FRR 4, 4-1, 5, 5-1
Plain with Hole	BCR 2
Axial Pad with Tangential Feed	FRR 2, 3, 4, 4-1
Load Pad	FRR 6, 7, 8, 9
*Plain with Axial Pads	BCR 3; MDBTR 1, 2; FRR 1, 1-1, 2, 3, 10, 11; BETR 4, 4A, 4B
*Tilting-Pad	MDBTF 1-0, 1-1, II-1, II-1A, II-1B, II-2, II-2A, II-2B, II-2C, III-1, III-2, III-2A, III-3
*Three-Sector	FRR 11, 12, 12A, 12B, 12B-1, 13, 13A, 14, 14-1, 15, 16, 17, 17-1, 18, 19, 19-1, 20, 21, 21-1, 22-1, 23, 24, 25, 26, 27, 28, 28-1, 29, 30; BETR 1, 2, 3; TFR 1, 2; DBTR 1, 1A; AI Pump; DBTR 5, 5A, 5C, 6, 6A, 6C; CRU II-1, II-2, II-2A, II-2B, II-3
*Three-Pad	DBTR 2, 3, 3A, 4, 4A, 4H, 4M; BETR 5, 5E
Thrust Step Land	PTR 1, 2
*Spiral-Groove Thrust	DBTR 4-1, 4-2, 4-3

BCR = Bearing Concept Rig
BETR = Bearing Endurance Test Rig
DBTR = Dual Bearing Test Rig
FRR = Free Running Rig
CRU = Combined Rotating Unit
MDBTR = Modified Dual Bearing Test Rig
MBTR = Modified Bearing Test Rig
PTR = Pocket Thrust Rig
TFR = Transparent Flow Rig

* Only these bearing types are reviewed in this report. The data from the underlined test numbers are used to present performance.

HOLE FED JOURNAL BEARING

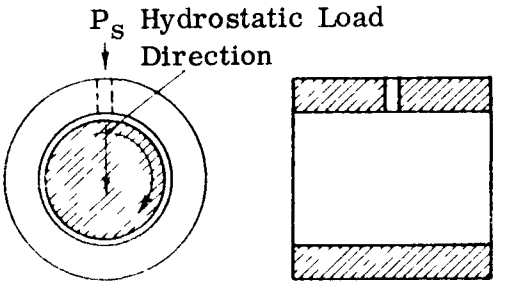

AXIAL GROOVE JOURNAL BEARING

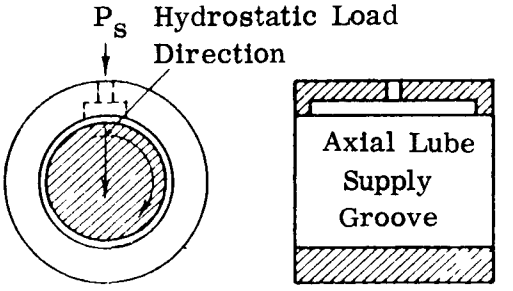

TANGENTIAL INLET JOURNAL BEARING

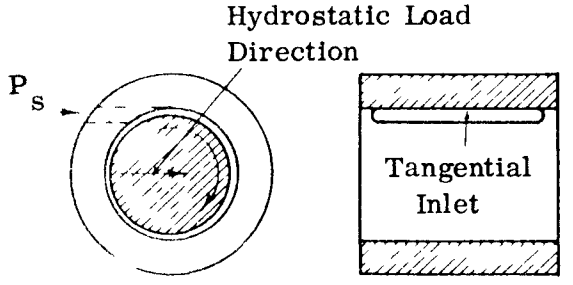

ANNULAR GROOVE BEARING

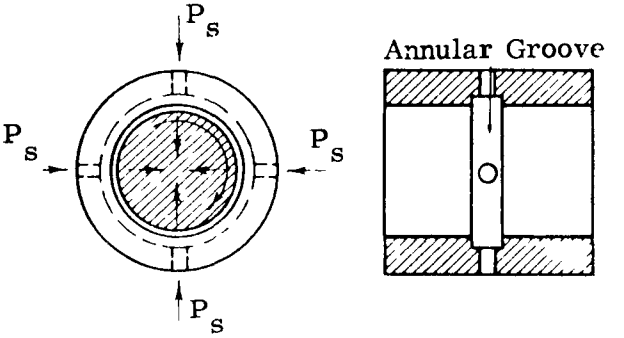

LOAD-PAD TYPE JOURNAL BEARING

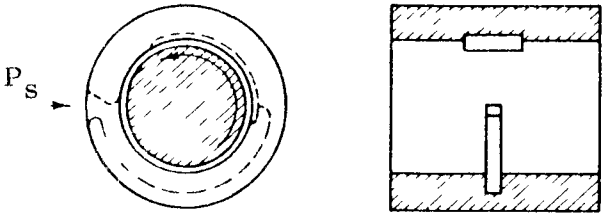

THREE-SECTOR JOURNAL BEARING

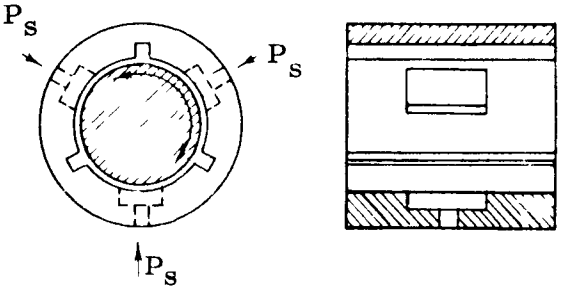

THREE-PAD JOURNAL BEARING

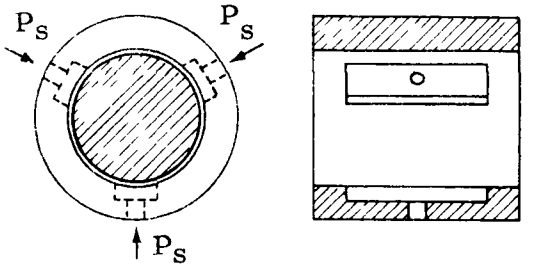

TILTING-PAD BEARING

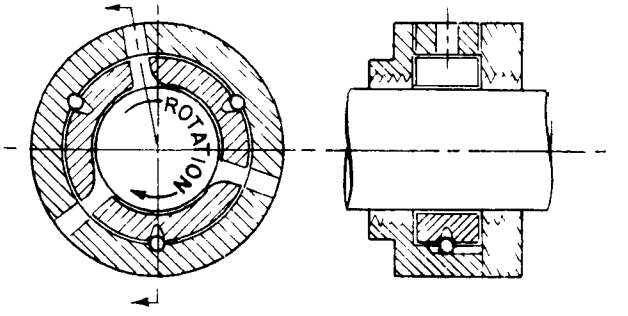

Figure 1. Typical Journal Bearing Geometries

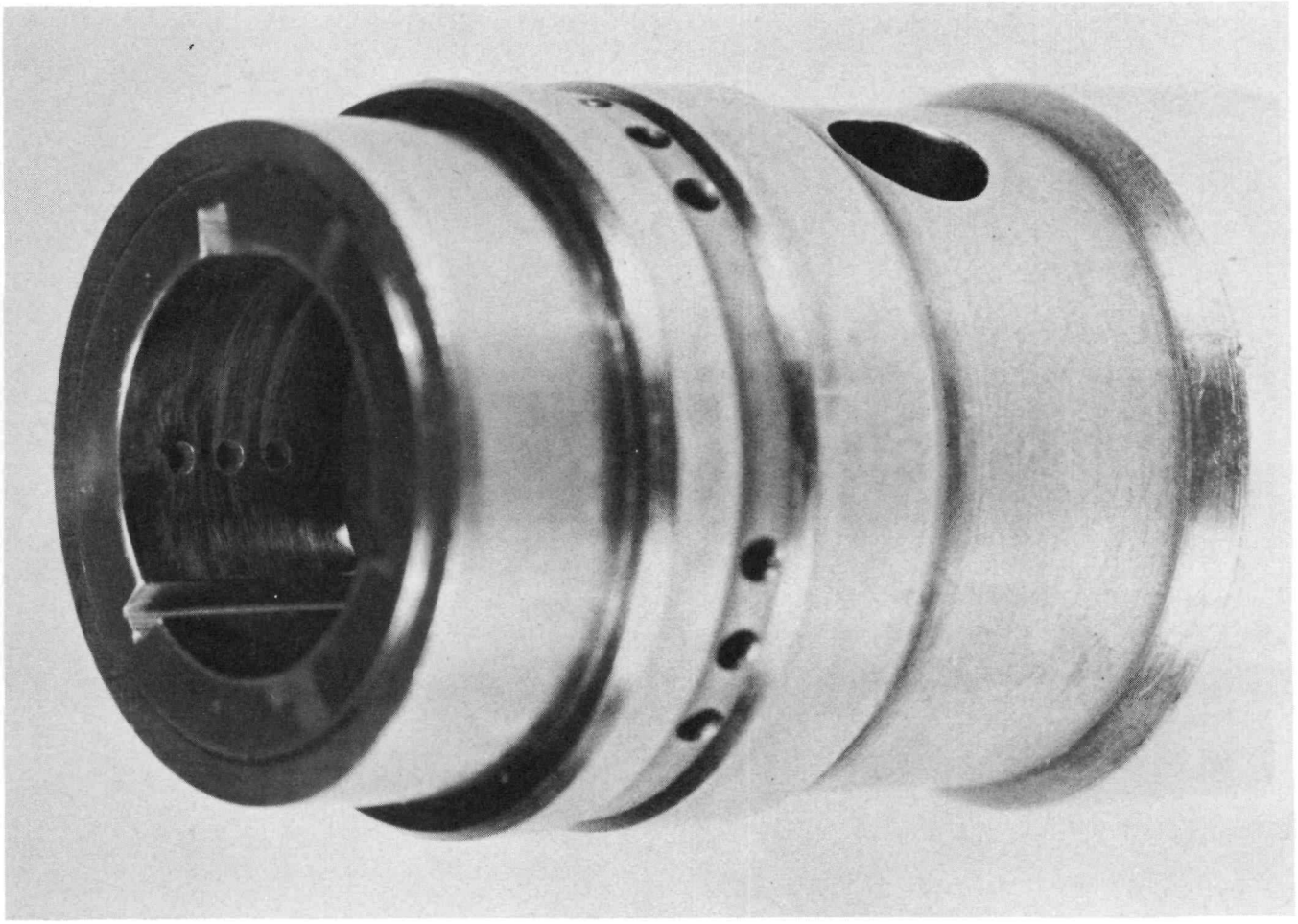

Figure 2. Three-Sector Bearing Without Recessed Supply Pad

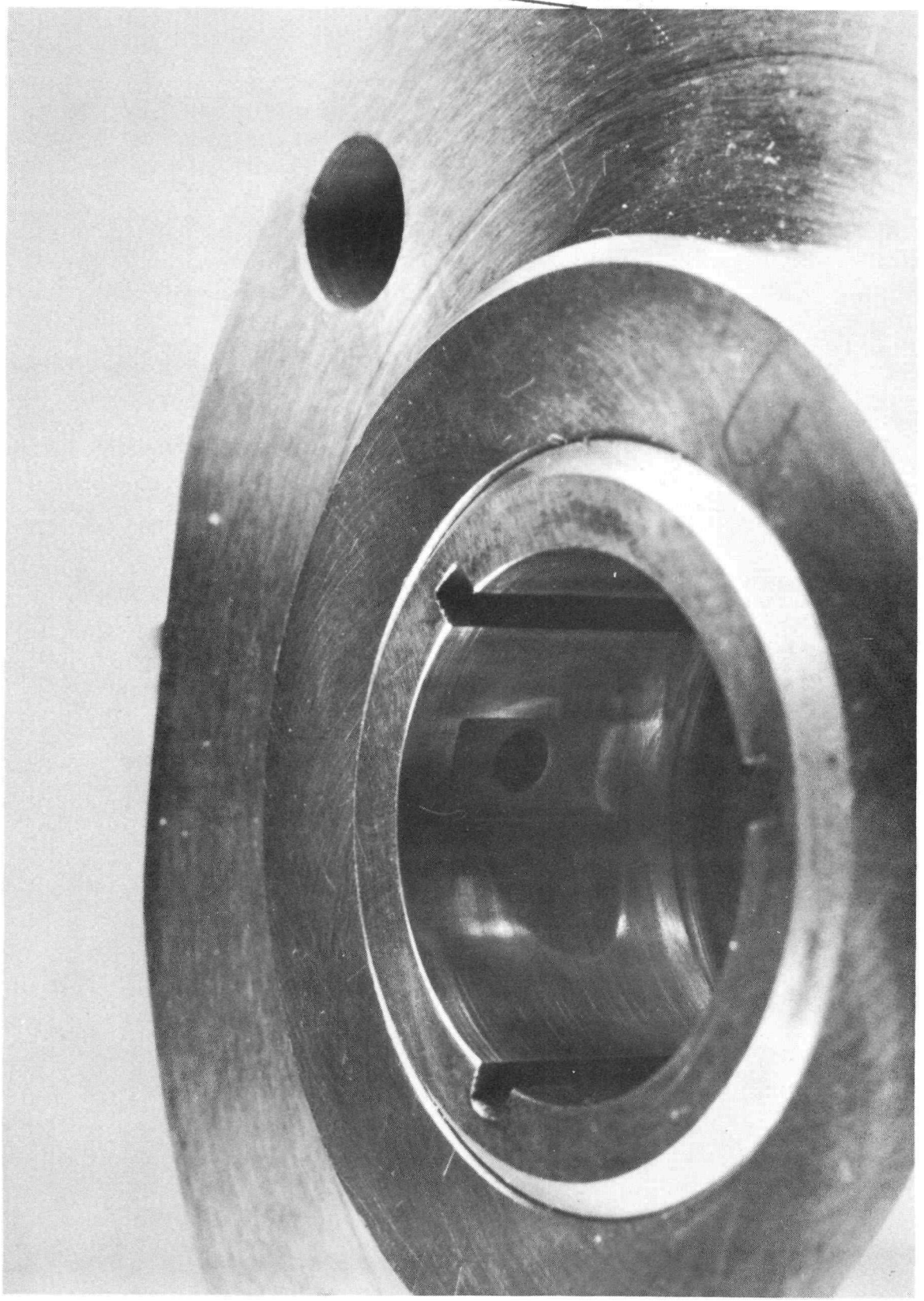

Figure 3. Three-Sector Bearing With Recessed Supply Pad

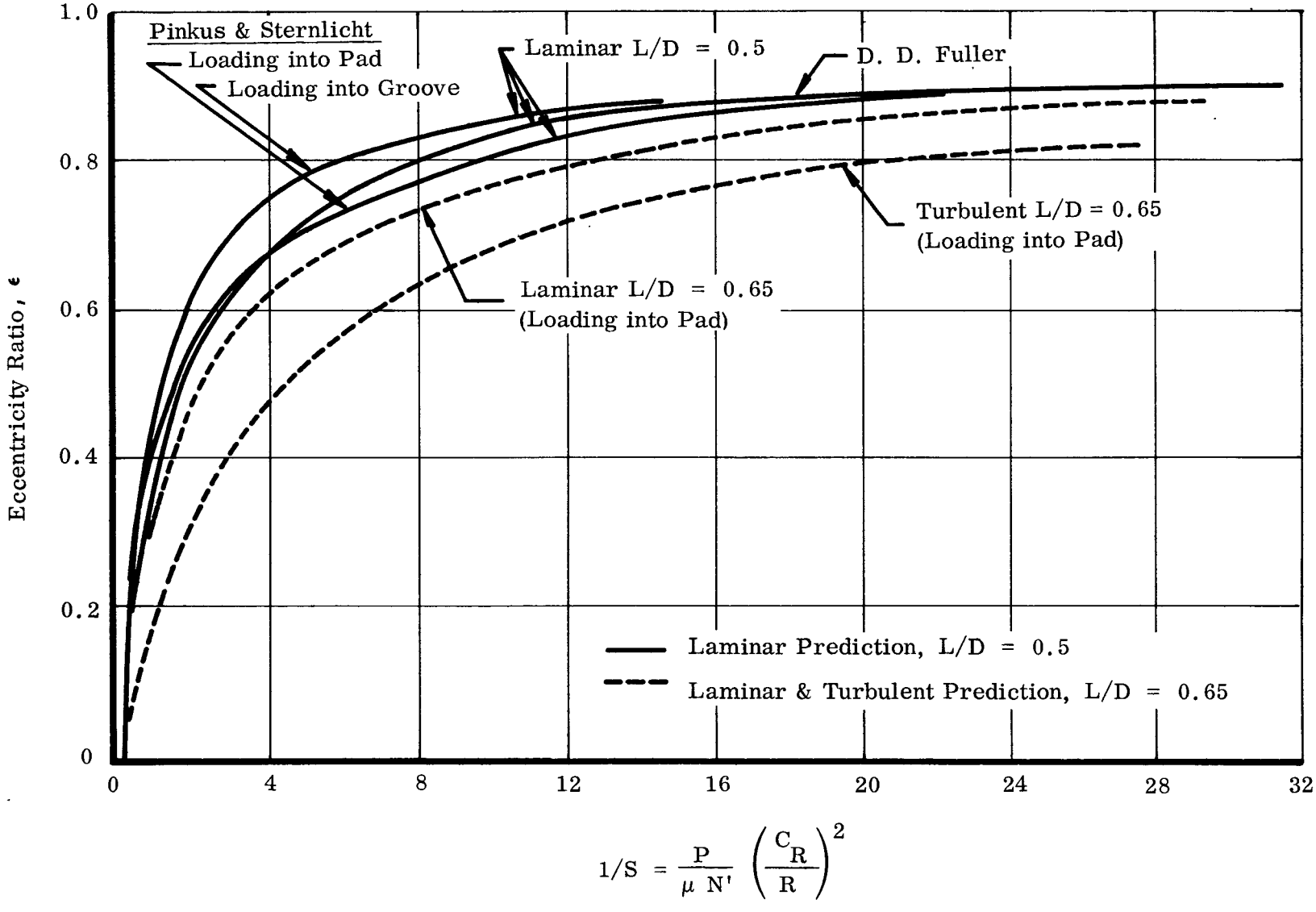

Figure 4. Generalized Laminar and Turbulent Performance Characteristics of Three-Sector Bearings (L/D = 0.5, 0.65)

CONFIDENTIAL

The three-sector bearing is essentially a plain journal bearing with three equally sized and spaced axial drain slots or grooves. These axial drain grooves break up the hydrodynamic action of the bearing and improve stability since it is the hydrodynamic forces that generally contribute to half-frequency whirl instability. Combined with the high supply pressures and the recessed supply pad,this bearing then becomes partially a hydrostatic bearing and partially a hydrodynamic bearing, i.e., a "hybrid" bearing, under rotating conditions. For zero speed the bearing is purely hydrostatic.

The following discussion will be limited to presenting some of the highlights of the three-sector bearing development program since it is impossible to make a detailed review of all the tests shown in Table 1 in one report. This section will present predicted performance based on the analytical approach discussed in Volume I and then compare it to the results of the following test programs:

1) Program I. Three-sector uncompensated test series, which include limited parametric tests, influence of length, misalignment, rotating load and clearance, and leads to endurance tests

2) Program II. Individually fed three-sector bearing tests in which each supply pad is fed separately

3) Program III. Partially orifice-compensated three-sector bearing tests including the influence of rotating load on performance

4) Program IV. Fully orifice-compensated three-sector bearings including the influence of clearance and rotating load on performance

A. PREDICTED PERFORMANCE

Volume I, Paragraph III-C-3 presented the analytical technique selected for predicting the performance of the three-sector bearing. Although the influence of turbulence and load direction was considered, no allowance was made for the hydrostatic influence on the over-all performance of this hybrid bearing. The hydrostatic contribution was considered as an added safety margin for load capacity and half-frequency whirl threshold.

1. Load Capacity

The predicted performance for the three-sector bearing, considered laminar and turbulent flow, is shown in a generalized form in Figure 4. Following the procedure outlined in Volume I, the laminar performance based on D. D. Fuller (Ref 14) is presented for L/D of 0.5. Following the suggested technique by Pinkus and Sternlicht (Ref 16), the performance of a three-sector bearing loading into a groove and into a pad was established for the laminar case. Appendix G summarizes the analytical technique developed at TRW Inc. The results of this analysis are shown in Figure 4. Loading into a pad using the Fuller approach (Ref 14) and the Pinkus and Sternlicht approach (Ref 16) shows slight deviation because Fuller assumes that the two unloaded sections have no influence on performance. The small contribution of the unloaded sections is

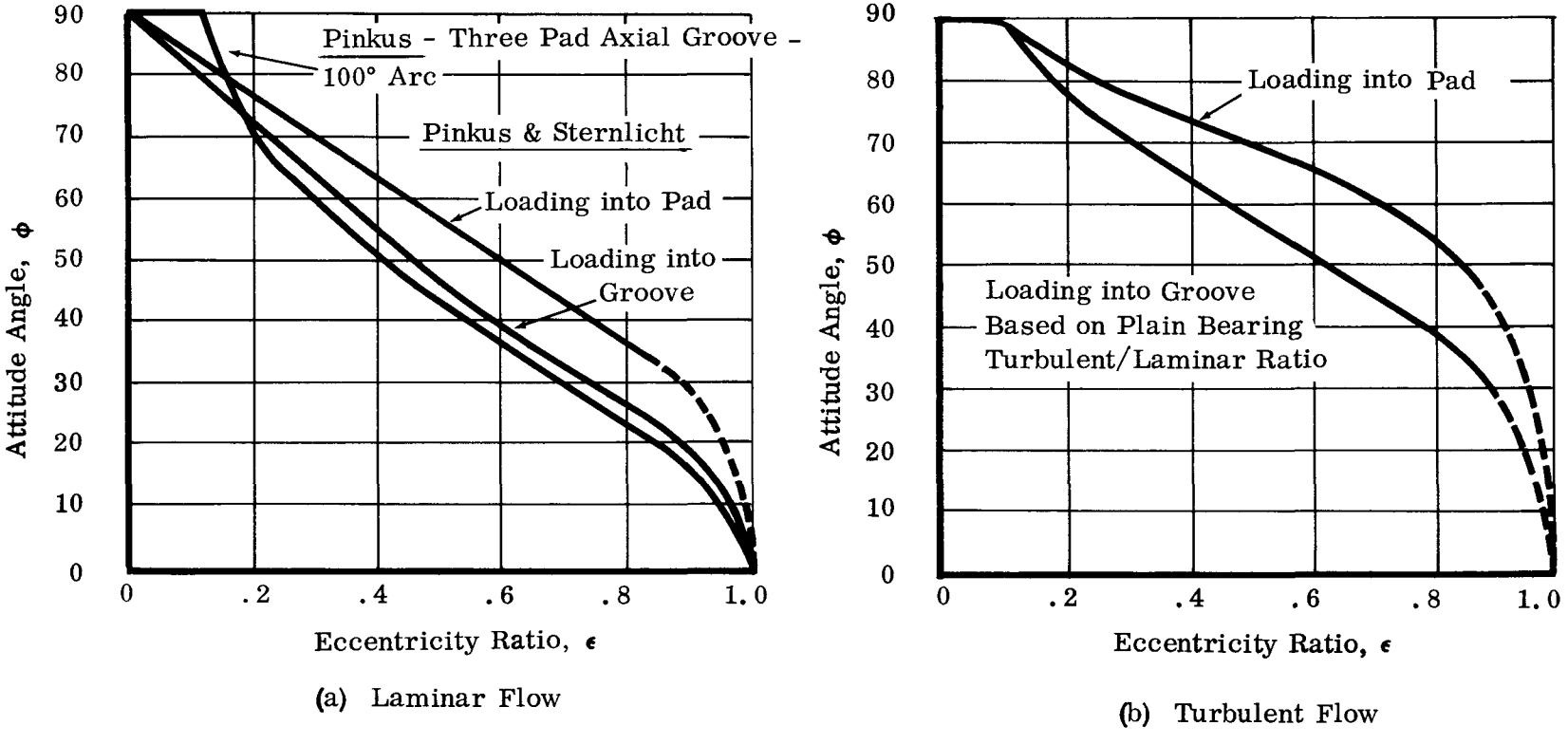

(a) Laminar Flow

(b) Turbulent Flow

Figure 5. Attitude Angle as a Function of Eccentricity Ratio For Three-Sector Bearings

verified in Figure 4. However, loading into an axial groove shows a sizable variation, being weaker, as expected, when the load vector is in that direction. In applications where large, unidirectional loads are present, it is therefore important to orient this type of bearing to achieve best performance. In the SNAP 2 application, orientation is not so critical since small unidirectional loads are anticipated, resulting in small eccentricity ratios where the difference in capacity is not great. Since the largest loads can be due to magnetic unbalance which results in rotating loads, there is no preferred orientation.

Since the three-sector bearing considered for application has a length of 0.407 inch and a diameter of 0.625 inch, Figure 4 shows the performance prediction of the L/D = 0.65 three-sector. This analysis is based on Ref. 14 (Fuller) and assumes load direction into the pad. The performance for the turbulent flow, L/D = 0.65, three-sector bearing has been estimated by making the same assumption for end leakage as was made for the plain bearing. From Volume I the turbulent performance is given by the following relationship:

$$\frac{1}{S_{turbulent}} = \frac{1}{S_{laminar}} \times \frac{1}{\eta_{(L/D=1)_{laminar}}} \quad \ldots 1$$

End leakage factors (η for L/D = 1) are obtained from Fuller (Ref 14). The predicted performance, however, is established for hydrodynamic operation only, and does not include the effect of high lubricant inlet pressures. This assumption is based on the axial slots operating at drain pressure and the fact that the net effect of the supply pressure was felt to be small without some form of orifice compensation. Figure 4 shows the estimated turbulent performance for an L/D = 0.65 loading into a pad. The end leakage correction results in a load-capacity approximating that of a three-sector bearing with an L/D of 0.8. The above prediction should prove to be conservative if a sizable hydrostatic component is present, for instance, for orifice compensation.

2. Attitude-Eccentricity Locus

The laminar and turbulent attitude-eccentricity loci for the three-sector bearing are shown in Figure 5. The estimated attitude angle also varies depending on the direction of the load line. Since the variation of the attitude angle for different L/D ratios is very small in the case of the three-sector bearing, Figure 5 can be used with sufficient accuracy for a range of L/D ratios from 0.5 to 1.5. Figure 6 shows the small variation in attitude angle with L/D ratio. For the preliminary analysis a turbulent locus was not available, and, consequently, the plain journal bearing laminar locus was used. This was justifiable on the basis that the larger plain bearing locus would compensate for turbulence in the three-sector bearing.

To include the influence of turbulence, i.e., moving the journal center further in the direction of motion, the ratio of measured turbulent to laminar predicted attitude angle

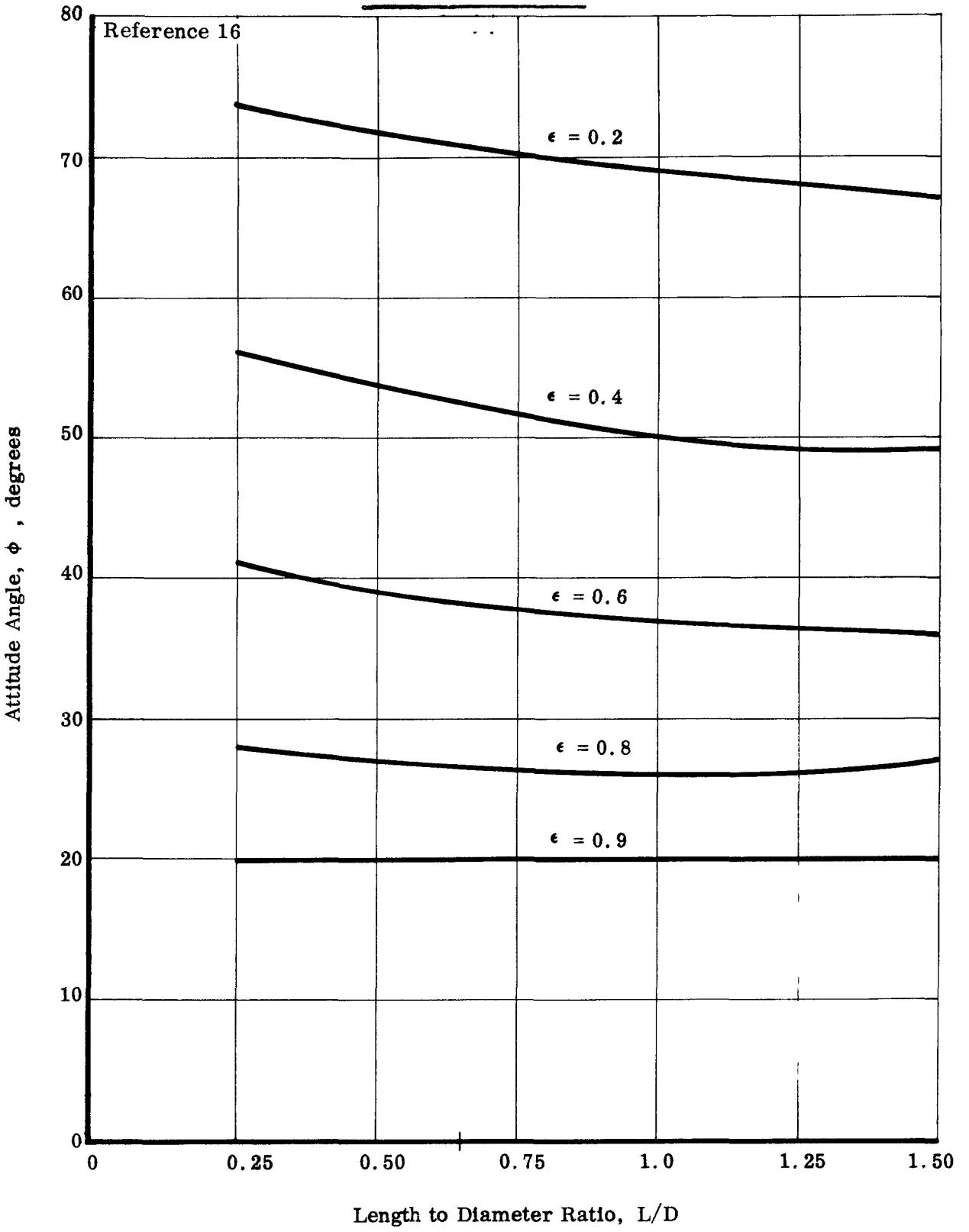

Figure 6. Laminar Attitude Angle vs Eccentricity Ratio For Three-Sector Bearing

for the plain bearing was applied to the three-sector bearing. Figure 5b therefore shows the turbulent locus for loading both into the pad and into the axial groove based on this approach. Similar to load-capacity the load direction has a considerable influence on the attitude-eccentricity locus. Loading into a pad will tend to result in a less stable condition because of the larger attitude angle and the resultant tangential force which causes instability.

3. Fluid Film Stiffness

As indicated in Volume I the fluid film stiffness can be obtained from the slope of the generalized curve 1/S vs ϵ (Figure 4) for any operating speed and for any clearance modulus ($m = C_D/D$). Predicted stiffness will be established later for comparison with specific bearing geometries.

4. Stability (Half-Frequency Whirl)

To establish the onset of instability, or stable and unstable regions for a particular bearing, the procedure outlined in Volume I, Paragraph III-C-5 is followed. The radial film stiffness (K_R) is obtained from the slope of the generalized plot of $1/S \cos \phi$ vs ϵ. From Figures 4 and 5b, Figure 7 is obtained. The method developed at TRW for predicting the stable and unstable operating regions for a specific bearing and rotor mass, using the equations for radial stiffness K_R and threshold speed ω_c as presented in Volume I, is as follows:

Given a three-sector bearing with a diameter of 0.625 inch, a length of 0.407 inch, and a diametral clearance of 0.001 inch and 0.0016 inch and using mercury at 100°F as the lubricant:

1) Establish slope of $1/S \cos \phi$ vs ϵ (Figure 7) for values of ϵ from 0 to 0.8.

2) Calculate radial stiffness (K_R) from the equation

$$K_R = \text{slope} \times \left(\frac{D}{C_D}\right)^3 \frac{\mu NL}{30} \qquad \ldots 2$$

for N = 20,000; 30,000; and 40,000 rpm (i.e., cover operating region).

3) Establish threshold speed N_c from equation

$$N_c = \frac{2 \times 60}{2\pi} \sqrt{\frac{K_R}{M}} \qquad \ldots 3$$

for each speed (20,000; 30,000; and 40,000 rpm) as a function of eccentricity ratio (ϵ).

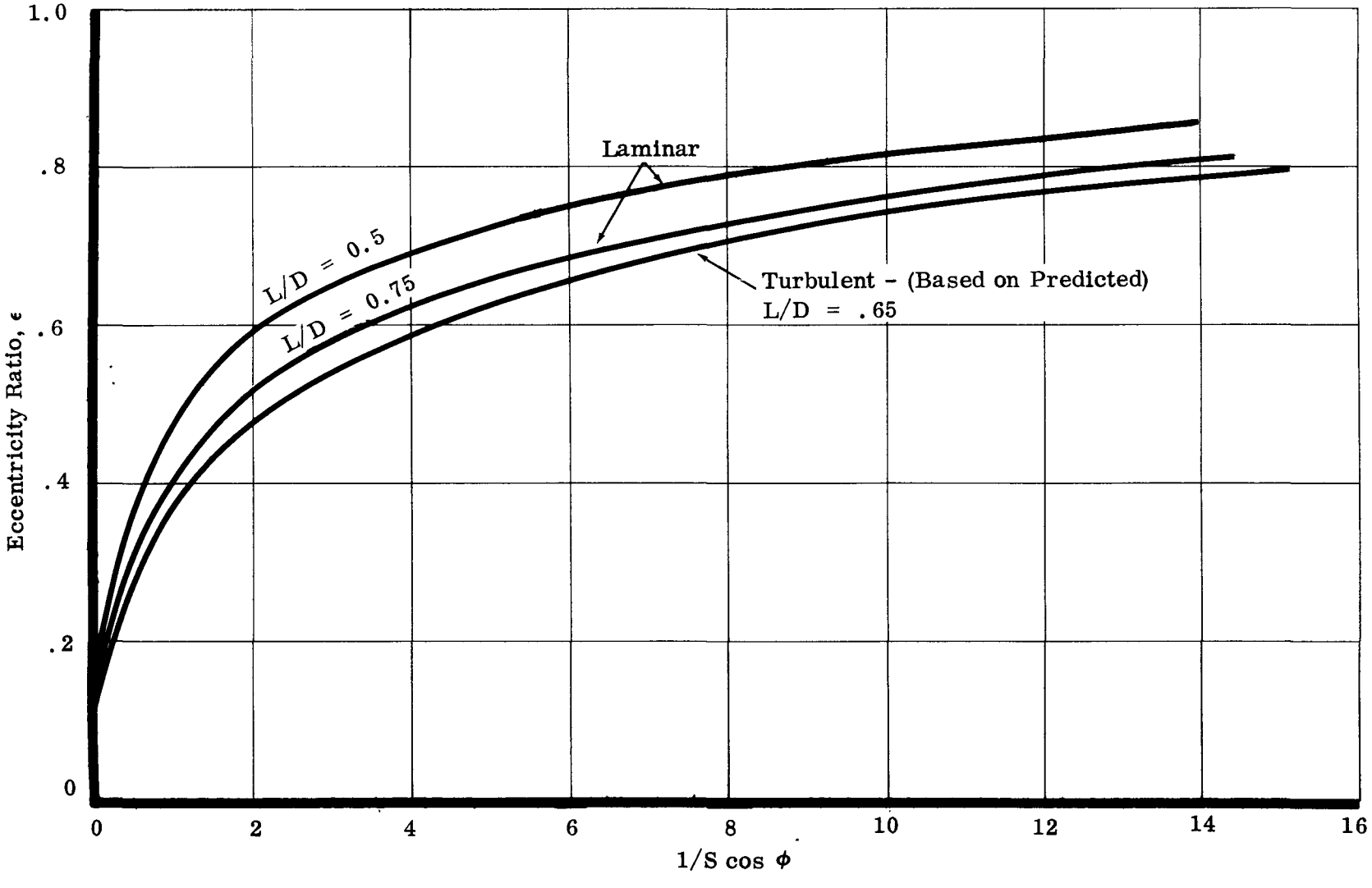

Figure 7. Predicted Radial Stiffness Characteristics for Three-Sector Bearing

4) Plot curve of threshold speed N_c vs eccentricity ratio (ϵ) for each speed. The result for the given bearing is Figure 8.

5) From Figure 8 establish the threshold locus of the bearing in question by the points where the operating speed (N) corresponds to the threshold speed (N_c).

6) Obtain stable performance by operation to the right of this locus, and unstable performance by operation to the left of this locus.

7) Establish the operating eccentricity ratio and refer to Figure 8 to determine if a given bearing will encounter instability under certain load and speed conditions.

8) Establish the minimum loads required to assure stable operation at all speeds by combining Figures 8 and 4. For the three-sector bearing used in this example the predicted loads required to suppress half-frequency whirl are shown in Figure 9. As anticipated the smaller clearance bearing (C_D = 0.001) has greater stability, requiring less load to suppress whirl, than the larger clearance bearing (C_D = 0.0016).

The above procedure is summarized in Figure 10.

5. Power Loss

As indicated in Volume I, Paragraph III-C-3, power loss was predicted using the semi-empirical relationship for turbulent flow established experimentally by Smith and Fuller (Ref 6). Since each three-sector bearing size and clearance has a varying power loss with speed, predicted performance shown in Figure 11 is for standard size; i.e., D = 0.625 inch, L = 0.407 inch at clearances of 0.001, 0.0015, and 0.002 inch. Performance for different lengths or clearances can be found in specific sections dealing with the experimental performance.

A large number of tests were conducted on three-sector bearings with different clearances, orifice sizes, lengths, and alignment. The complete list is presented in Table 1. Only the more significant tests underlined in Table 1 are included in this report.

B. PROGRAM I - THREE-SECTOR UNCOMPENSATED ORIFICE TEST SERIES

The three-sector bearing was selected for evaluation and development to overcome several serious shortcomings inherent in the plain (cylindrical) journal bearing. These included:

1) Unstable operation - susceptibility to large amplitude, half-frequency whirl

2) Flow-pressure problems - caused by limited pump supply pressure

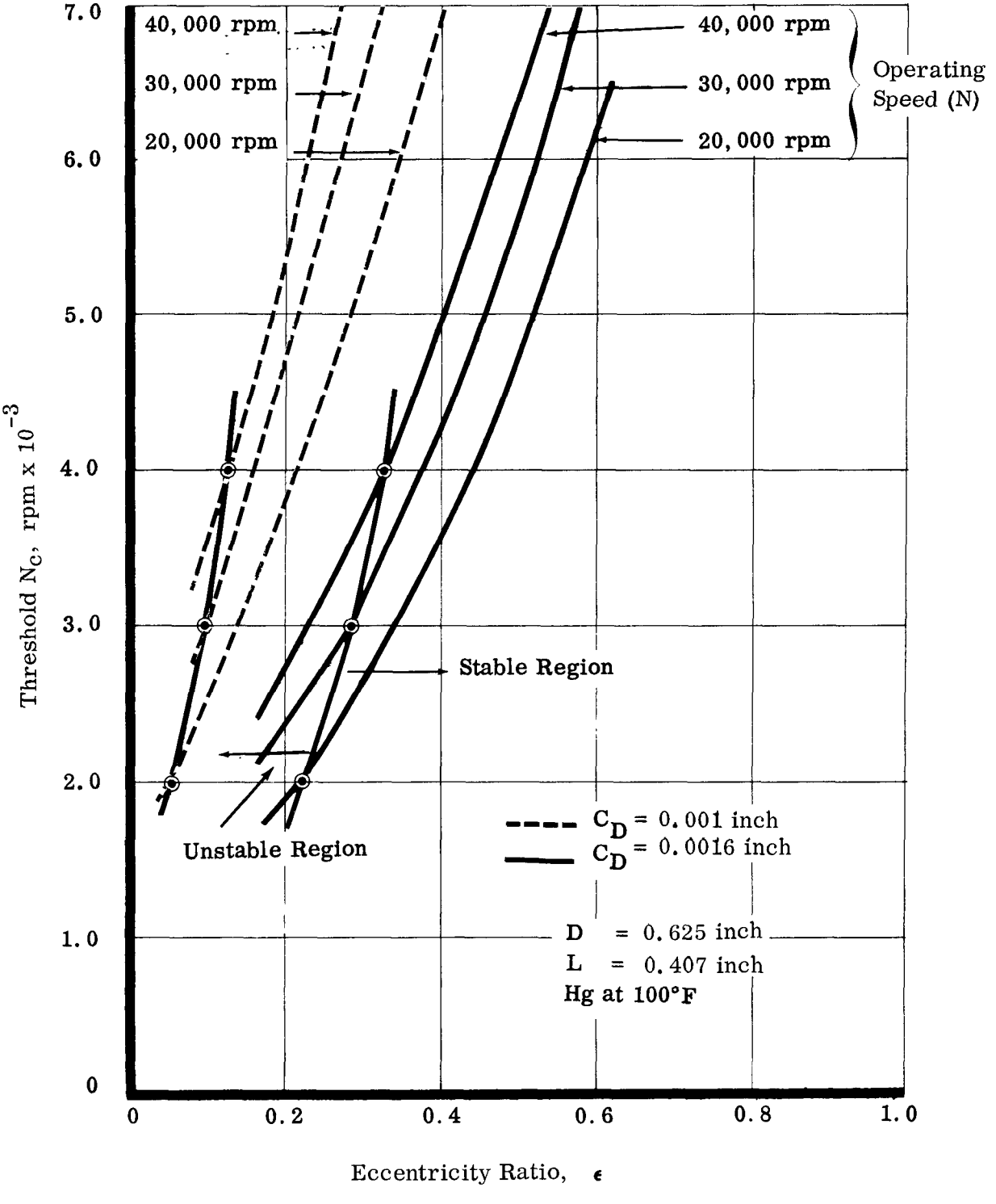

Figure 8. Predicted Half-Frequency Whirl Threshold for Three-Sector Bearing

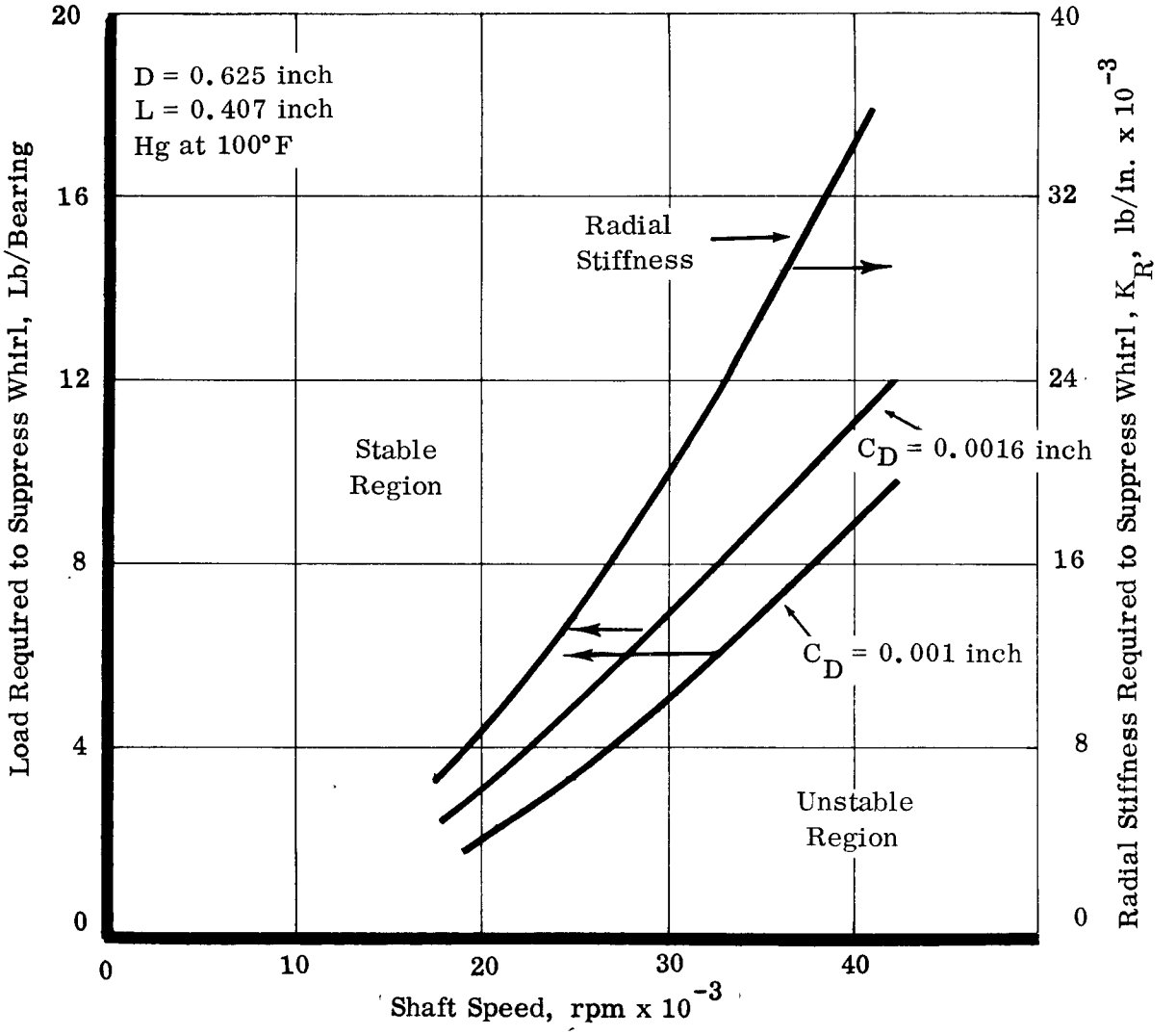

Figure 9. Stability Requirements for Three-Sector Bearing

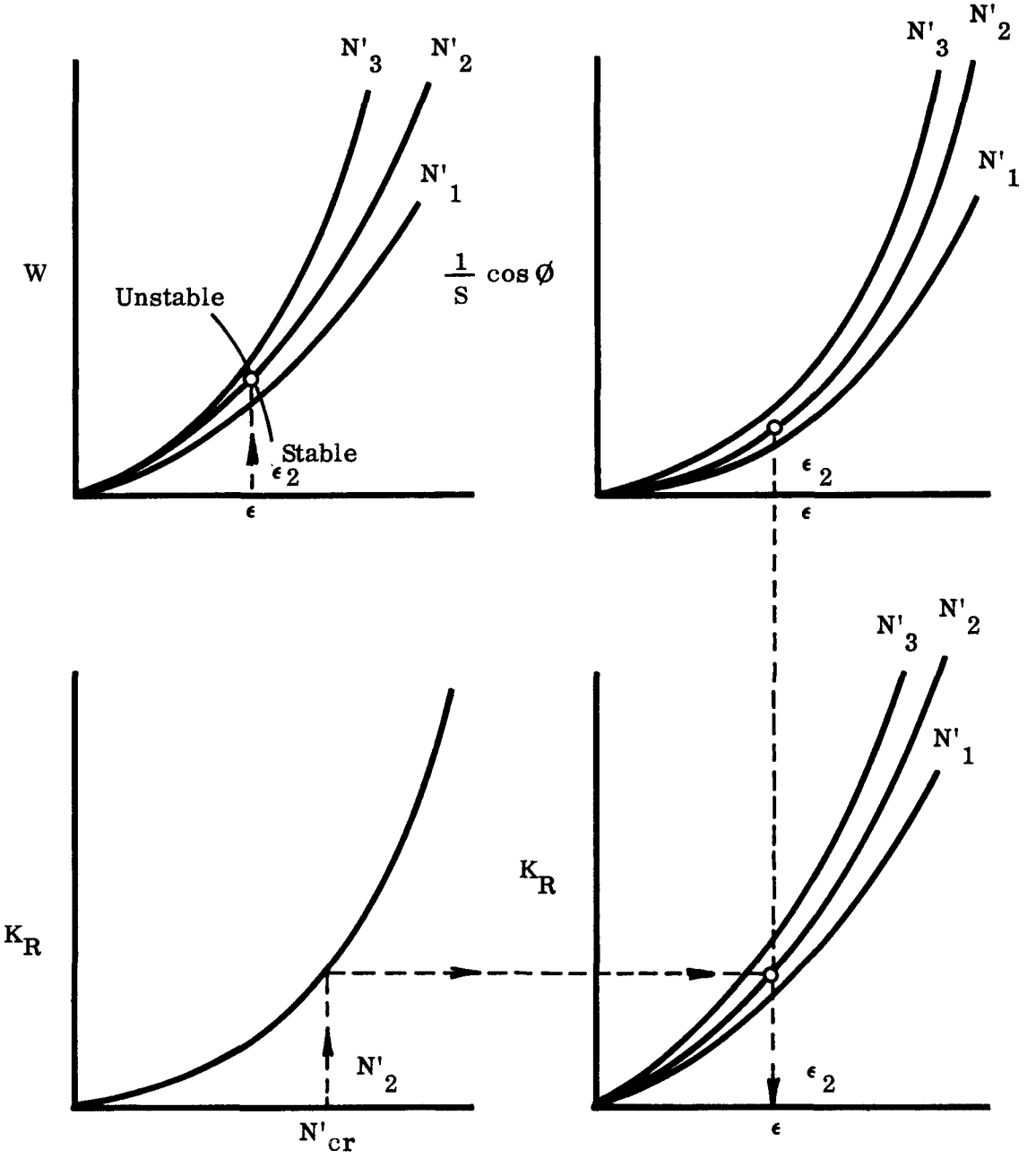

Figure 10. Stable and Unstable Operating Regions

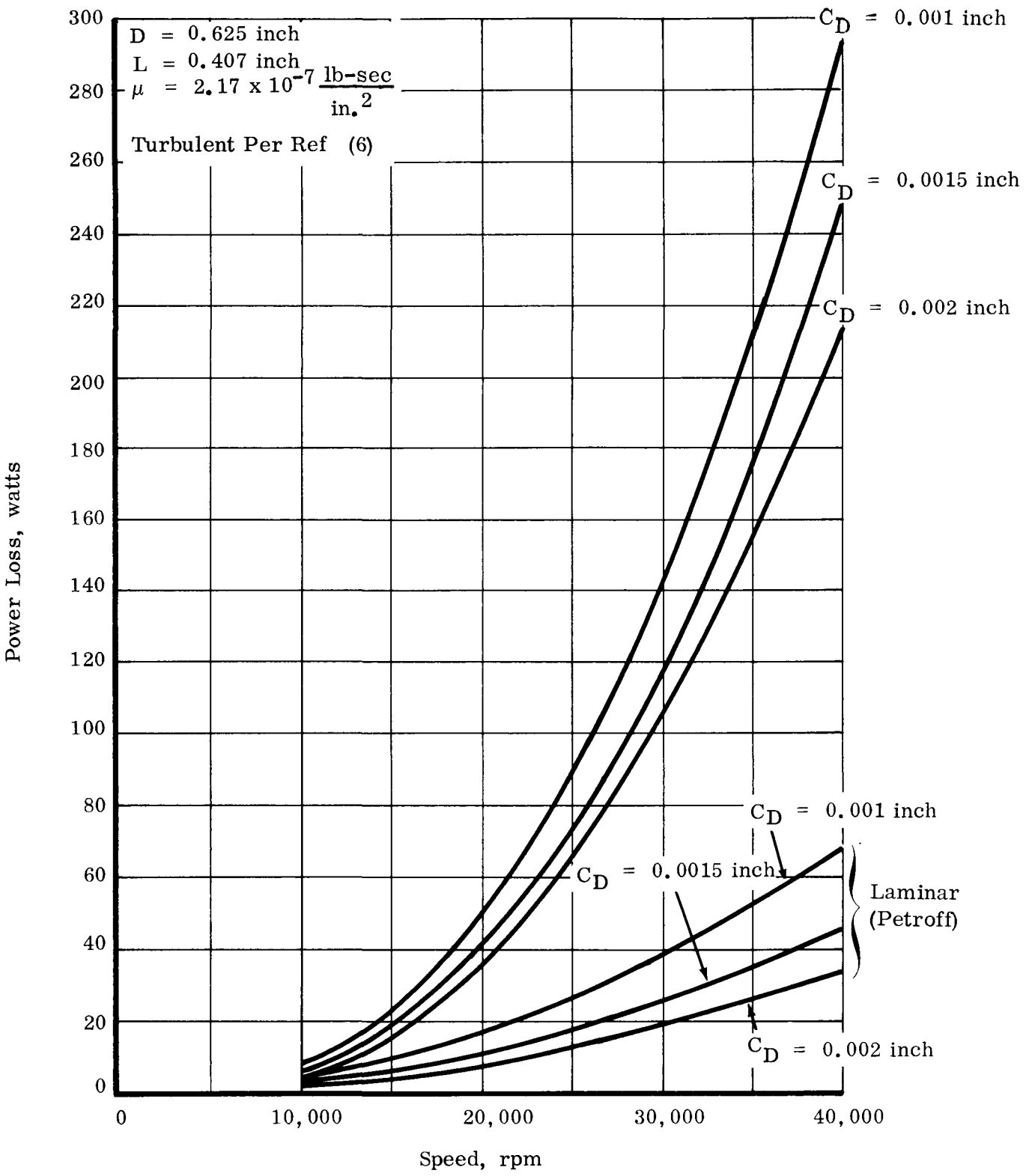

Figure 11. Predicted Power Loss vs Speed for a Three-Sector Bearing

TABLE 2

PROGRAM I TEST SUMMARY

Test Designation	Bearing Configuration (All Bearing Dimensions in Inches)	Test Duration (Hrs)	Remarks and Objectives
*FRR 11	Three-sector, C_D = 0.0016 9 holes with 0.050 diameter	2.2	Flow calibration of first three-sector whirl threshold
FRR 17	Three-sector, C_D = 0.002 Three holes per brg. with supply pad 1/4 x 1/8 x 0.025 deep	6.1	Flow calibration, whirl threshold
FRR 28, 29, 30	Three-sector, C_D= 0 001 for 28 } single C_D= 0.0012 for 29 } supply C_D= 0 0015 for 30 } pads/per sector	17	Flow calibration, load test whirl threshold.
FRR 19	Three-sector, C_D= 0.002	4.8	Influence of 30 lb/bearing rotating load at 40,000 rpm.
FRR 21, 24, 25, 27	Three-sector, C_D= 0 0016/0 0017 alignment =0 for 21 =0.0004 for 24 =0 0007 for 25 =0.001 for 27	25	Influence of misalignment on performance (flow and stability).
FRR 21, 22, 23, 26	Three-sector, C_D= 0 0016/0 0017 Length (axial) = 0 407 for 21 = 0 447 for 22 = 0 350 for 23 = 0 314 for 26	22	Influence of axial length on performance (flow and stability).
**BETR 1	Three-sector, C_D= 0 0017 Length (axial) = 0 407	17 9	Check-out of improved test fixture incorporating instrumentation for measuring attitude-eccentricity locus and film thickness, high temperature lubrication operation includes shaft-mounted pump to supply bearings
BETR 2A	Three-sector, C_D = 0 022		Parametric test prior to entrance
FRR 18	Three-sector, C_D = 0 002 Axial length = 0.407	100	Endurance test at 40,000 rpm, including influence of 10 lb/ bearing rotating load.
BETR 2E	Three-sector, C_D= 0 0022 Axial length 0.407	875 5	Endurance test at 40 000 rpm at elevated temperature of 350 - 400°F

* Free Running Rig
** Bearing Endurance Test Rig

3) Limited life - caused by presence of cavitation-erosion damage.

4) Metal-to-metal contact during start-up and shut-down - due to hydrodynamic characteristics of the bearing

Experience with axial groove bearings, similar to the three-sector, indicated that improved stability could be accomplished as a result of the hydrostatic contribution and breaking up the hydrodynamic forces; that lower pressures would be required to circulate lubricant through the bearing because of its three separate supply sources; that life would be improved since the axial drain grooves would permit vapor bubbles to be swept out of the bearing without collapsing in the clearance space; and that the hydrostatic component in the bearing would prevent metal-to-metal contact during start and stop cycles.

The initial tests were essentially go or no-go tests while attempting to establish if the three-sector bearing was indeed superior to the plain bearing and the other bearings tested to date. General performance rather than detailed parametric data was obtained. The instrumentation available prevented generation of data such as load-deflection and attitude angle, and was only capable of establishing:

1) Magnitude of load applied and net result on performance, i.e., could the bearings support this load

2) Flow-pressure-speed data as influenced by load and stability

3) Stability or instability performance, i.e., half-frequency whirl threshold as influenced by varying supply pressures and loads

4) Power loss as a function of speed

5) Endurance capability

The following section will summarize these limited tests, with the major variables being diametral clearance, bearing length, degree of misalignment, and magnitude of applied rotating loads. Table 2 shows the tests conducted in this series.

1. Free Running Rig Test 11

This represented the initial test on the uncompensated three-sector bearing shown in Figure 2. The bearings had a diameter (D) of 0.625 inch, an axial length (L) of 0.407 inch, and a diametral clearance (C_D) of 0.0016 inch. Each sector included three supply orifices with 0.050-inch diameters. The bearings had an axial drain groove on top and were made of 18-4-1 tool steel, hardened to Rc-63. The journal sleeves were of BG-41 modified 440C, hardened to Rc-58.

The free-running test fixture consists of a terry turbine-driven shaft supported by two test journal bearings. A double-acting thrust bearing (spiral groove for all tests) is located on the "A" or alternator end of the fixture. The other end is defined as the "B" or turbine end. The journal bearings are consequently referred to as the alternator and turbine bearings. The test fixture schematic is shown in Figure 12.

For this initial test, a plain journal bearing with an axial groove was installed in the "A" end and a three-sector bearing was installed in the "B" end. Speed was limited to 30,000 rpm during this initial test because half-frequency whirl was encountered at 20,000 rpm. A single capacitance probe was used to monitor shaft motion. Flow-pressure characteristics and stability data were obtained.

a. Stability

The plain journal bearing (C_D = 0.002 inch) appeared to initiate unstable operation since application of unidirectional load and increased supply pressure to this bearing suppressed the instability. However, application of load to the three-sector bearing had no noticeable effect on the shaft instability.

The plain bearing required unidirectional load and supply pressures of 5 lb and 130 psi at 20,000 rpm and 15 lb and 209 psi at 30,000 rpm to achieve stability. At 20,000 rpm this agrees well with the stability data shown in Figure 9, but at 30,000 rpm it is slightly high.

Maximum load applied was 30 lb total (15 lb/bearing).

b. Flow

Figure 13 shows the calibration curve for the three-sector bearing. Since improved flow-pressure characteristics is one of the three-sector bearing requirements, flow in Figure 13 is compared with the axial groove plain bearing with C_D = 0.002 inch. Statically, they are comparable. Dynamically, the slopes are somewhat changed and the pressure requirement for the nine 0.051-inch diameter hole three-sector bearings is less than that of the plain bearing. At high flows, however, the requirements appear to converge.

2. Free Running Rig Test 17

To further improve the flow-pressure characteristics of the three-sector bearing the three orifices in each sector were surrounded by a recessed groove which acted as a pressure pad. Uncompensated three-sector bearings at both the "A" and "B" ends were used with a diameter (D) of 0.625 inch, a length (L) of 0.407 inch, and a diametral clearance (C_D) of 0.002 inch. Each sector had three 0.069-inch diameter orifices surrounded by a pad 1/4-inch axial length x 1/8-inch circumferential length x 0.025-inch deep.

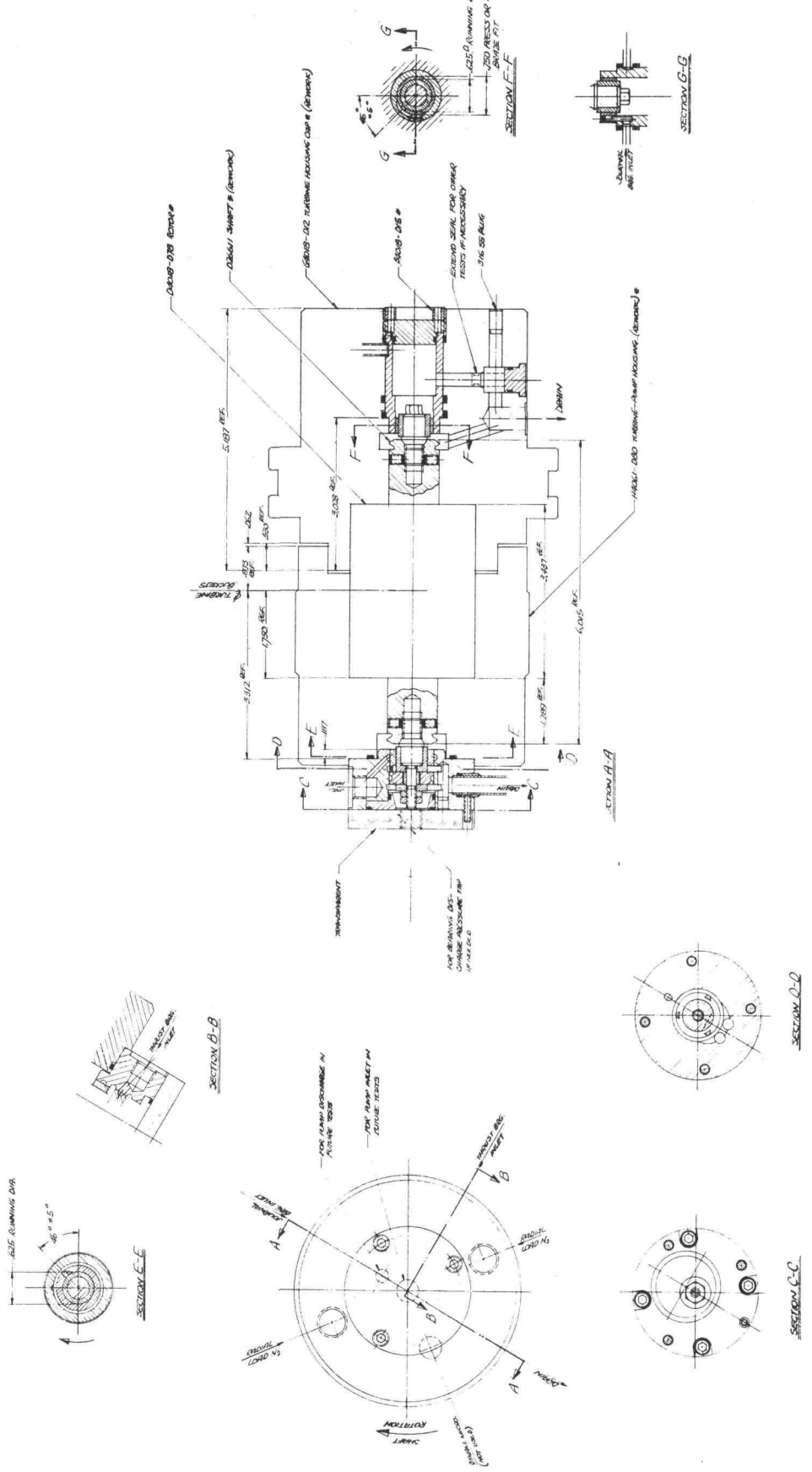

Figure 12. Layout - Simulated Shaft, Journal and Thrust Bearings FRR

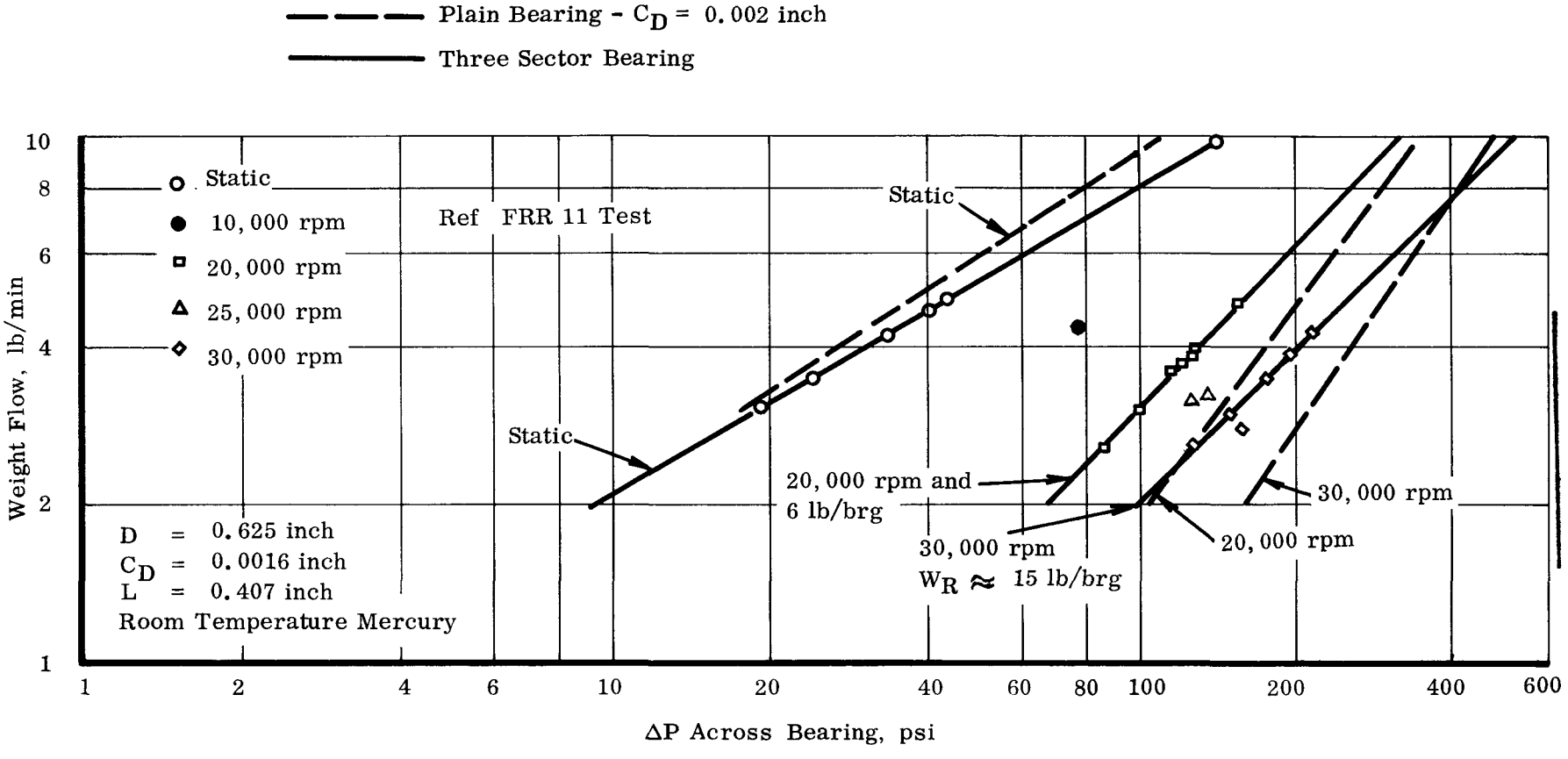

Figure 13. Flow Calibration of Three-Sector Journal Bearing

a. Stability

The threshold of half-frequency whirl for this large clearance bearing was reduced to 12,000 rpm. Loads required to assure stable operation at a supply pressure of 81 psig are summarized below.

Speed	Unidirectional Load
12,000 rpm	2.5 lb
20,000 rpm	6.0 lb
30,000 rpm	11.5 lb
40,000 rpm	19.3 lb

The large clearance to assure adequate flow has resulted in an inherently unstable bearing.

b. Flow

Figure 14 shows the influence of supply pad modification and large clearance on the flow-pressure characteristics. For comparison, the 30,000 rpm flow line from FRR 11 is shown.

3. Free Running Rig Test 28, 29, and 30

This series of tests was conducted to establish the influence of clearance on flow-pressure characteristics and half-frequency whirl instability. The uncompensated three-sector bearing used for this series is shown in Figure 3. The three orifices per sector were replaced by a single 0.078-inch diameter orifice surrounded by the 1/4-inch x 1/8-inch x 0.030-inch supply pad. The diameter and length remained unchanged at 0.625 inch and 0.407 inch, respectively.

The diametral clearance was varied as follows:

FRR 28	0.001 inch
FRR 29	0.0012 inch
FRR 30	0.0015 inch

An analysis prior to selecting the clearance for the FRR 28 test indicated that considering hydrodynamic, laminar theory and a stiff shaft, a reduction in diametral clearance would increase the threshold of half-frequency whirl. The uncompensated three-sector bearing (D = 0.625 inch, L = 0.407 inch) was analyzed ignoring the hydrostatic contribution. Selection of laminar analysis, therefore, compensated to some degree for ignoring the hydrostatic influence in establishing stability trends. Two clearances were selected for the analysis, C_D = 0.001 inch and = 0.0017 inch, and shaft weight (2.5 lb/brg)

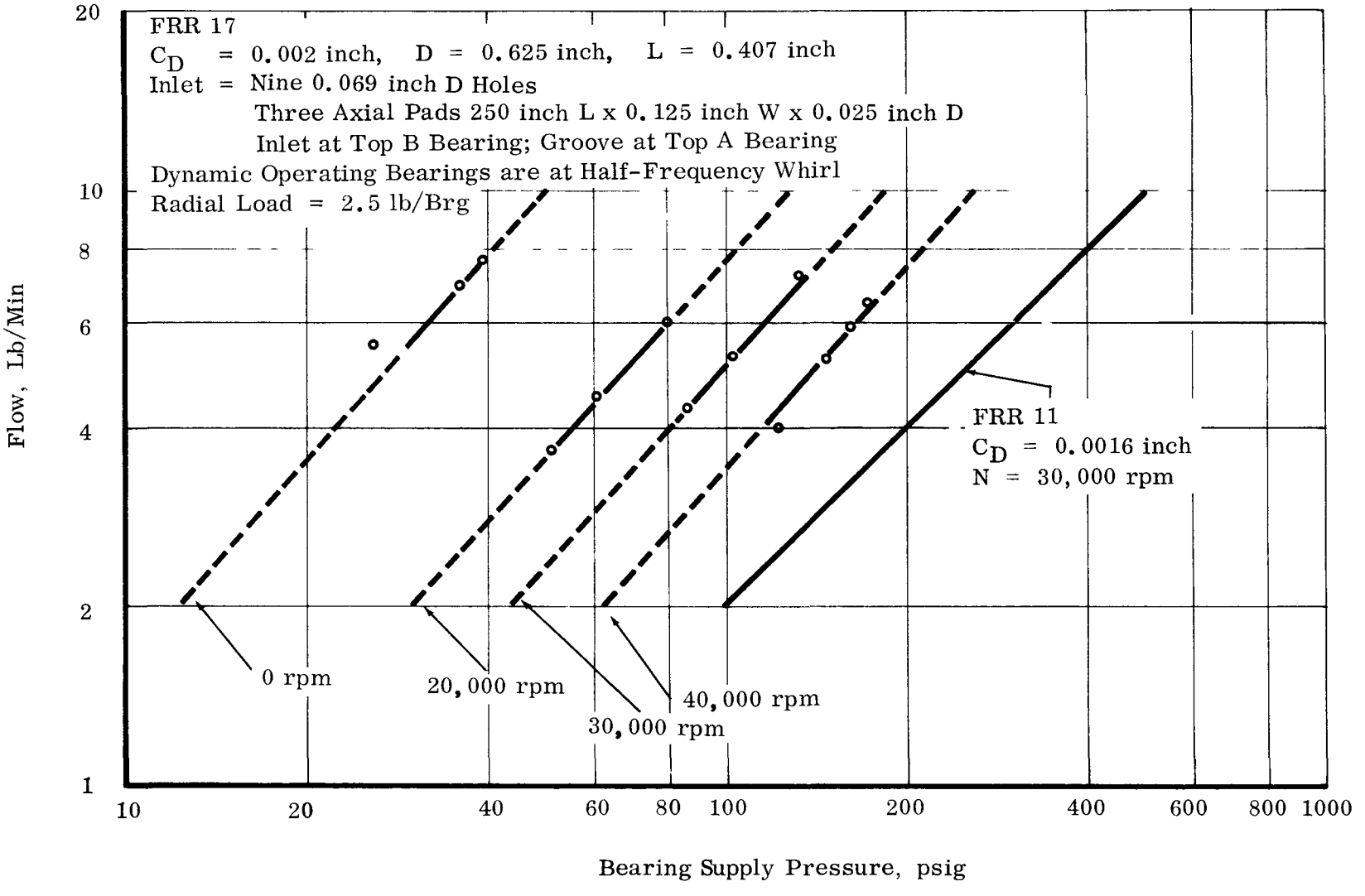

Figure 14. Flow Calibration of Three-Sector Alternator Bearing

only was assumed acting on the bearing. This resulted in eccentricity ratio (ϵ) of 0.1 for C_D = 0.001 inch and 0.2 for C_D = 0.0017 inch at 40,000 rpm. The radial film stiffnesses (K_R) were obtained from the slope of the radial force ($F_R = W\cos\phi$) curves versus eccentricity ratio (ϵ). This is shown in Figures 15 and 16. Applying

$$f_w = \frac{2 \times 60}{2} \sqrt{\frac{K_R \times 386}{2.5}} \quad \text{rpm} \qquad \ldots 4$$

resulted in whirl thresholds as follows:

$$C_D = 0.0017 - f_w = 28,100 \text{ rpm}$$
$$C_D = 0.001 - f_w = 48,700 \text{ rpm}$$

The above analysis points out that for the assumptions made the 0.0017-inch clearance bearing tends to become unstable below 40,000 rpm while the 0.001-inch clearance bearing has a threshold of instability above 40,000 rpm (design speed).

To verify the analysis, establish onset of half-frequency whirl, and develop a stable bearing, the clearances listed above were selected and tested.

a. Stability Characteristics

As predicted the 0.001-inch clearance bearing remained stable at all speeds tested. The maximum speed reached was 44,280 rpm. Unidirectional loads were zero (shaft supported simulating zero g) or equivalent to shaft weight only. Figures 17a and 17b represent the dynamic shaft motion at 40,000 rpm. Run-out of 0.0005 to 0.0006 inch between probe and journal surfaces represents the major portion of the amplitude shown. However, fairly large vibration levels at synchronous speed were picked up by a combination of accelerometers and wave analyzers, indicating fairly large rotating loads (or residual unbalance).

At approximately 23,000 rpm a slight trace fluctuation was observed. This may have been due to the shaft trying to become unstable or to a possible critical. Figure 17c shows the condition. In any case, the wave analysis of the vibration pickups indicated no measurable half-frequency component at rotating speeds of 20,000; 23,280; 30,000; and 40,000 rpm.

Vibration levels monitored indicated a gradually increasing amplitude with speed as shown below:

Speed	Alternator End	Turbine End
20,000	0.14	0.14
23,280	0.11	0.169
30,000	0.62	0.45
40,000	0.76	0.635

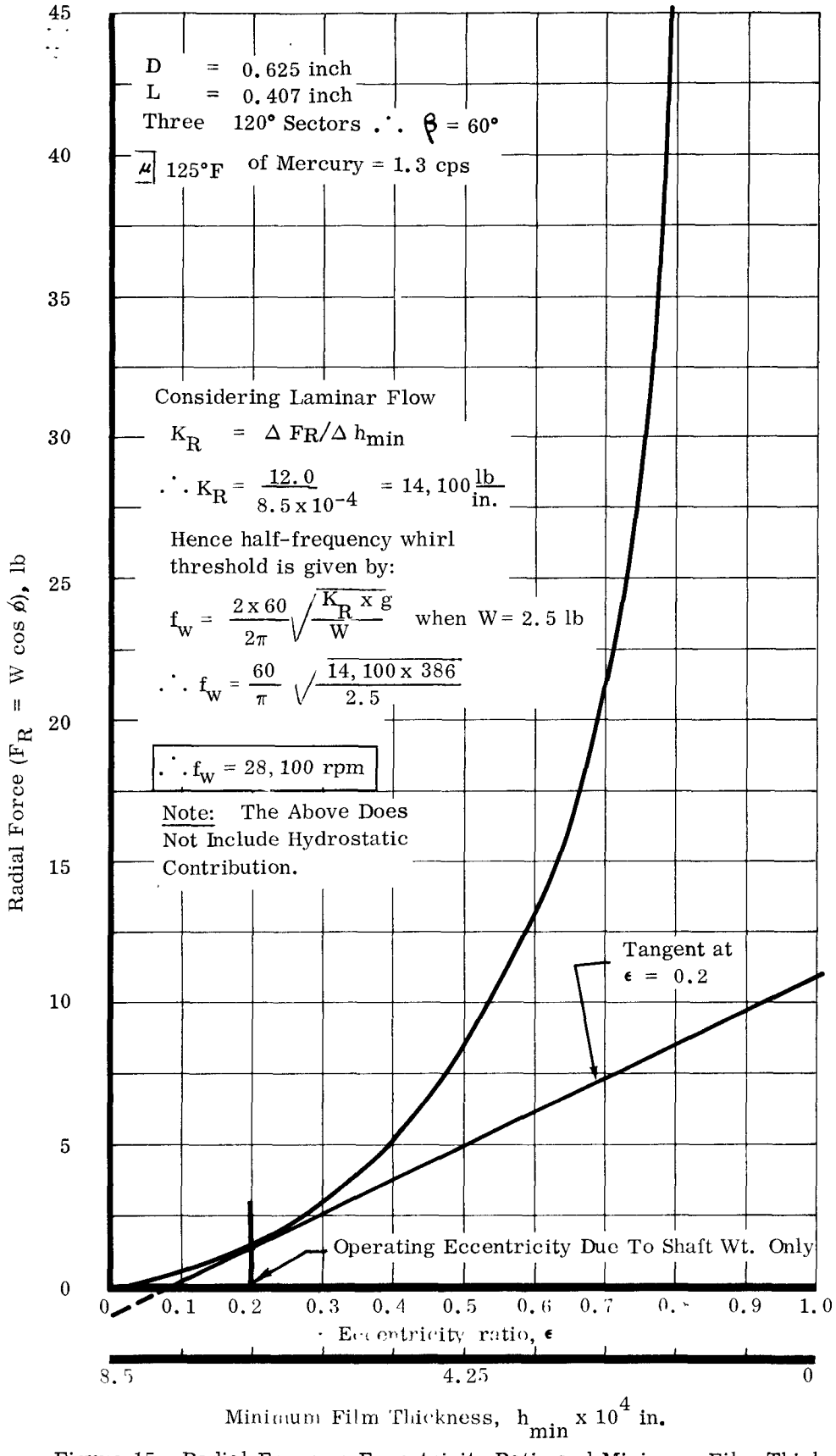

Figure 15. Radial Force vs Eccentricity Ratio and Minimum Film Thickness For a Three-Sector Bearing at 40,000 rpm and C_D = 0.0017 Inch

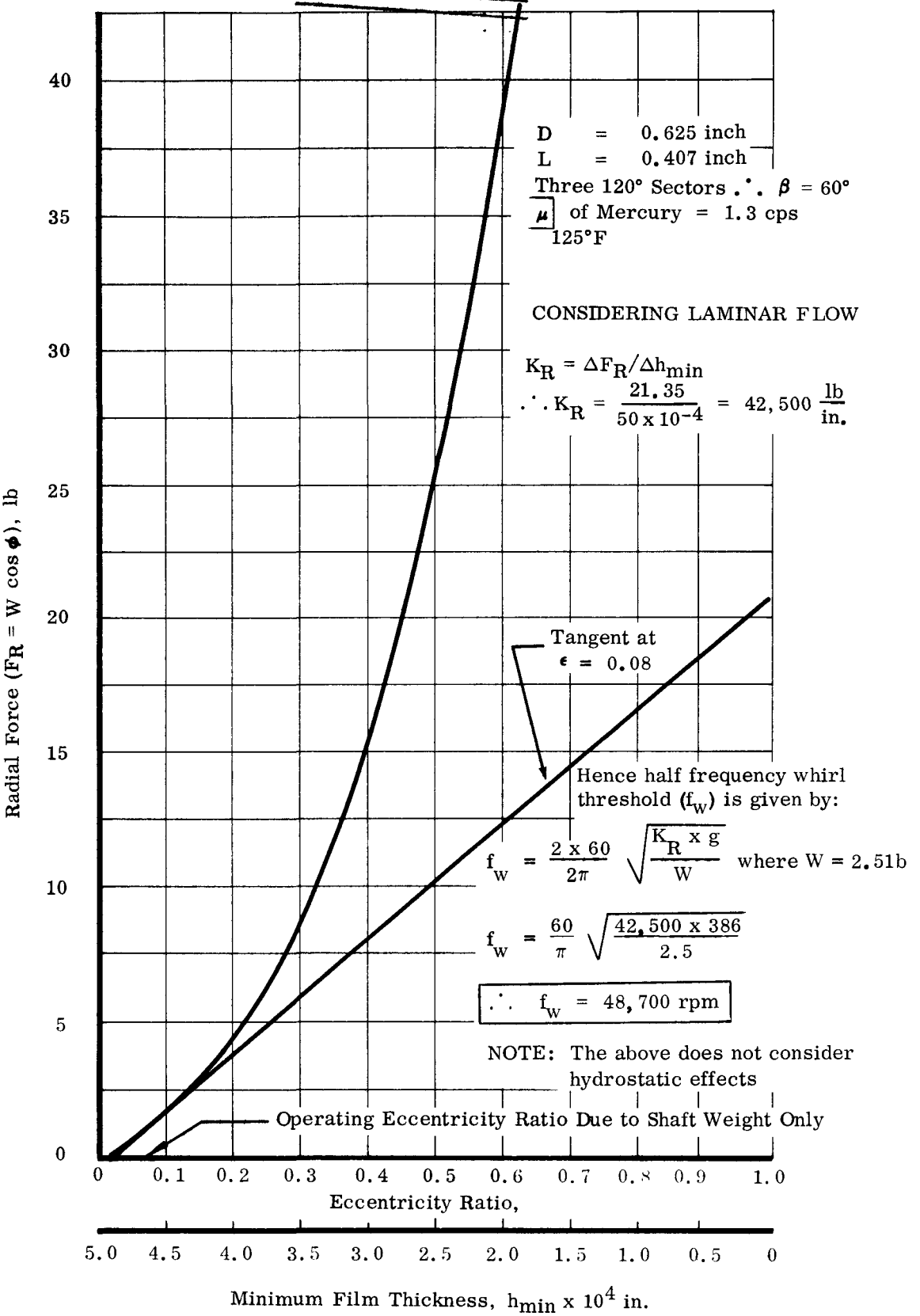

Figure 16. Radial Force vs Eccentricity Ratio and Minimum Film Thickness for a Three-Sector Bearing at 40,000 rpm and C_D = 0.001 Inch

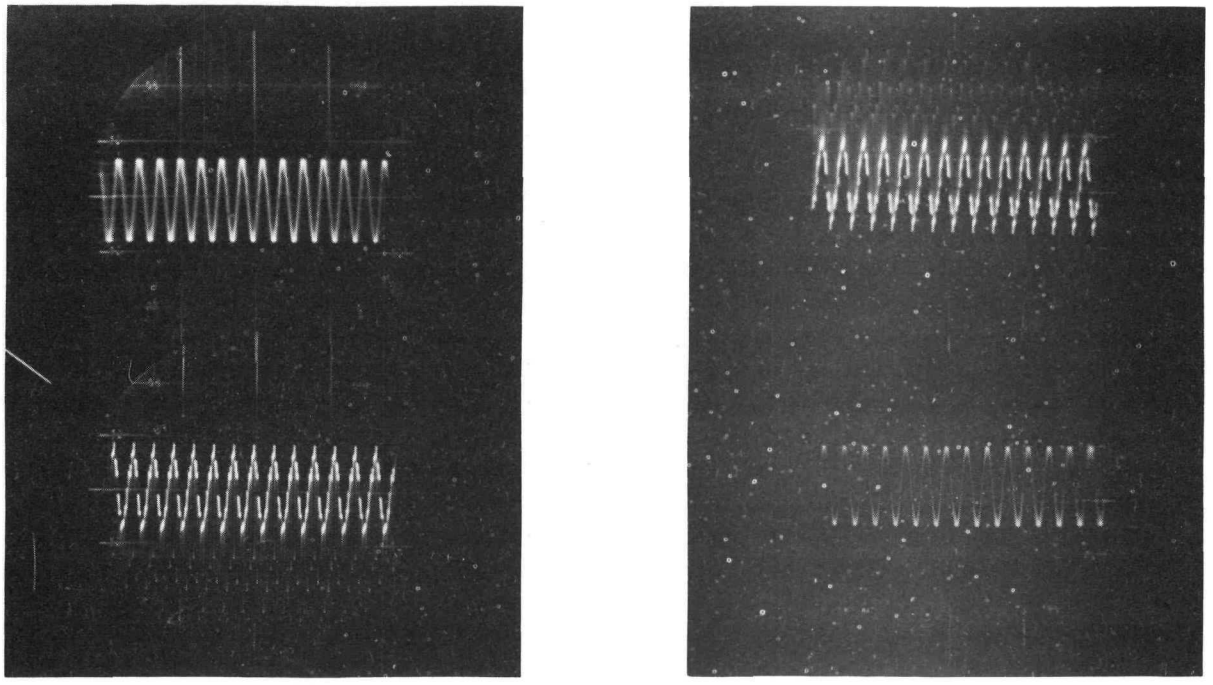

(a) (b)

(a) 40,000 rpm - Stable
Simulated Zero 'g'
(P_S = 175 psi)

(b) 40,000 rpm - Stable -
with Shaft Weight Only
(P_S = 175 psi)

(c) 23,280 rpm - Stable
(Tendency for Instability)
Simulated Zero 'g'
(P_S = 200 psi)

FRR - 28
3-Sector
D = 0.625 inch
L = 0.407 inch
C_D = 0.001 inch

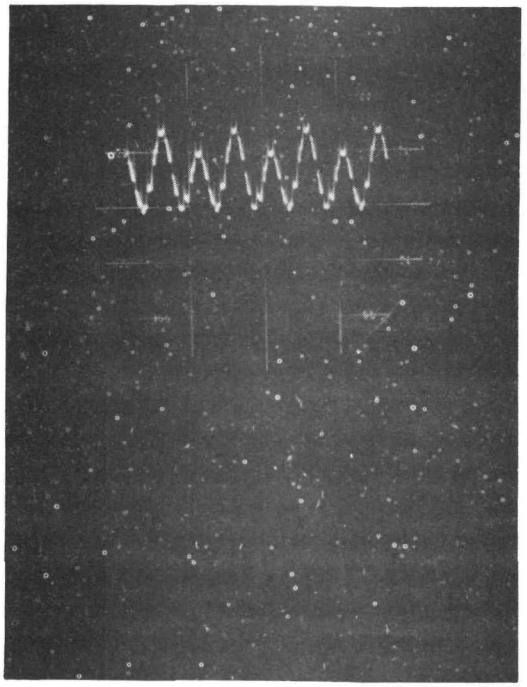

(c)

Figure 17. Stability Characteristics of a Three-Sector Bearing (FRR-28)

This trend indicates that at 40,000 rpm the rotor was operating close it its first mode critical speed. Based on predicted stiffness for the 0.001-inch bearing, the lowest critical speed of the rotor bearing system (inversion speed) is approximately 45,000 rpm.

The 0.0012-inch clearance bearing encountered small amplitudes of half-frequency whirl below the design speed of 40,000 rpm. With shaft weight acting and neutralized, indications of half-frequency whirl existed at 20,000 and 30,000 rpm.

At 40,000 rpm the shaft was stable for both load conditions. The application of increased supply pressure was generally adequate to eliminate the tendency toward instability. Figure 18 shows the various dynamic traces and the instability tendencies. A vibration survey revealed a peak amplitude at approximately 35,000 rpm which began decreasing at 40,000 rpm. Based on predicted fluid film stiffness, this corresponds to the first mode rotor-bearing critical speed.

Figure 19 summarizes the vibration survey of the 0.001- and 0.0012-inch clearance three-sector bearing. Threshold of half-frequency whirl was approximately 19,500 rpm for the 0.0015-inch clearance bearing. Rig limitations prevented whirl suppression with lube supply pressure above 20,000 rpm. Figure 20 presents the stability characteristics of this larger clearance bearing. Table 3 below indicates that peak instability occurs around 30,000 rpm for the 0.0015-inch clearance three-sector bearing.

TABLE 3

STABILITY CHARACTERISTICS FOR THE 0.0015-INCH DIAMETRAL CLEARANCE THREE-SECTOR BEARING

Speed, rpm	Pressure, psig	Load = applied + shaft weight, lb
19,500	101	2.5
20,100	81	4.1
29,800	81	7.2
35,100	81	5.5
39,800	81	4.4
42,100	81	2.5

b. Flow-Pressure Characteristics

Summarizes of flow data at shaft weight generated during this test series are presented in Figures 21 through 24 for static; 20,000; 30,000; and 40,000 rpm as functions of clearance. Two additional tests, FRR 21 and BETR (reference Paragraphs B-5, B-8, and B-10), are included. These curves were obtained for mercury at 80°F. Considerable extrapolation was necessary because of rig limitations on flow and pressure.

Since the bearings are not orifice-compensated, flow-pressure characteristics are influenced by magnitude of applied load (eccentricity ratio) and stability (both half-frequency and synchronous whirl). Small variations in orifice or pad size also have an appreciable influence. Consequently, the calibration curves must be used with care in estimating the flow-pressure characteristics of the three-sector bearing.

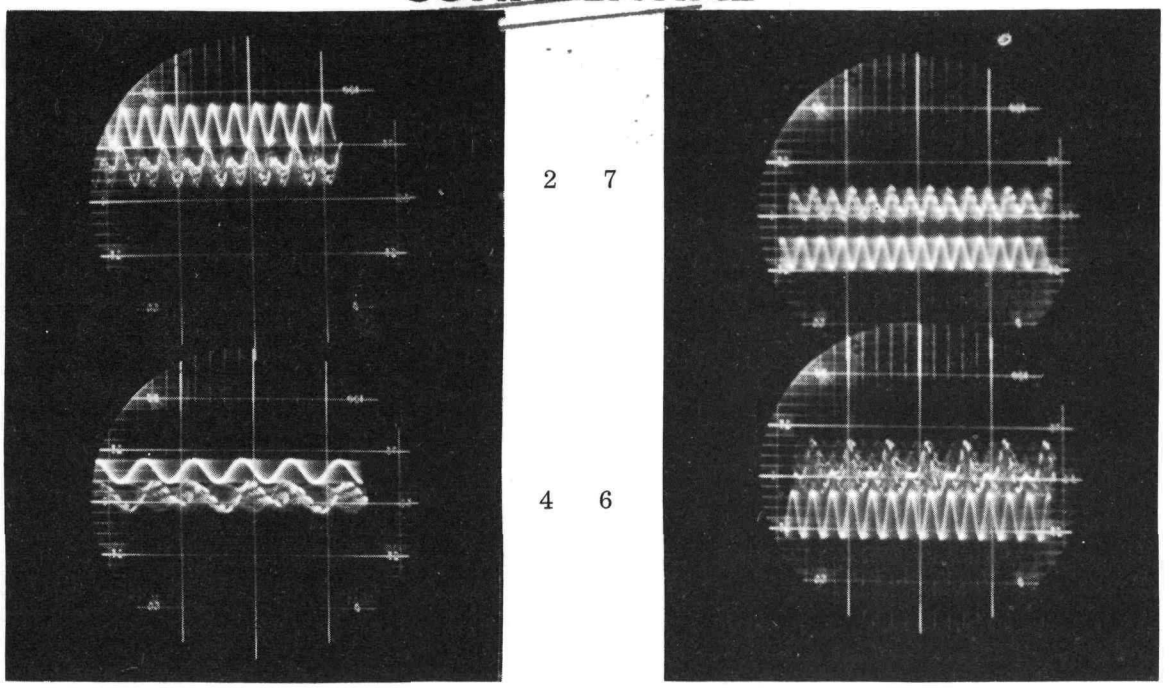

(a) (b)

(a-2) 16,620 rpm - Stable
Tendency for Instability
Simulated Zero "g"
P_S = 86 psi

(a-4) 18,190 rpm - Stable
Simulated Zero "g"
P_S = 98 psi

(b-6) 20,000 rpm Instability
Tendency
Simulated Zero "g"
P_S = 78 psi

(b-7) 20,000 rpm Stable
Simulated Zero "g"
P_S = 131 psi

(c-14) 30,000 rpm Instability
Tendency
Simulated Zero "g"
P_S = 91 psi

(c-15) 30,000 rpm Stable
Simulated Zero "g"
P_S = 101 psi

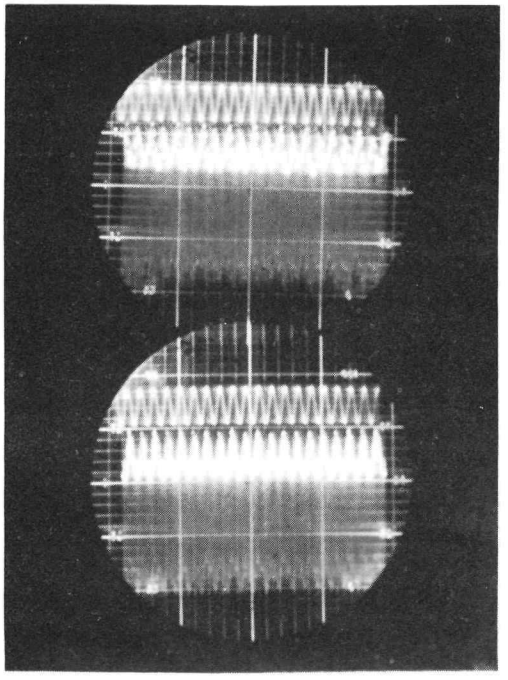

(c)

FRR 29, Three-Sector, 0.0625 inch, L = 0.407 inch, C_D = 0.0012 inch

Figure 18. Stability Characteristics of a Three-Sector Bearing

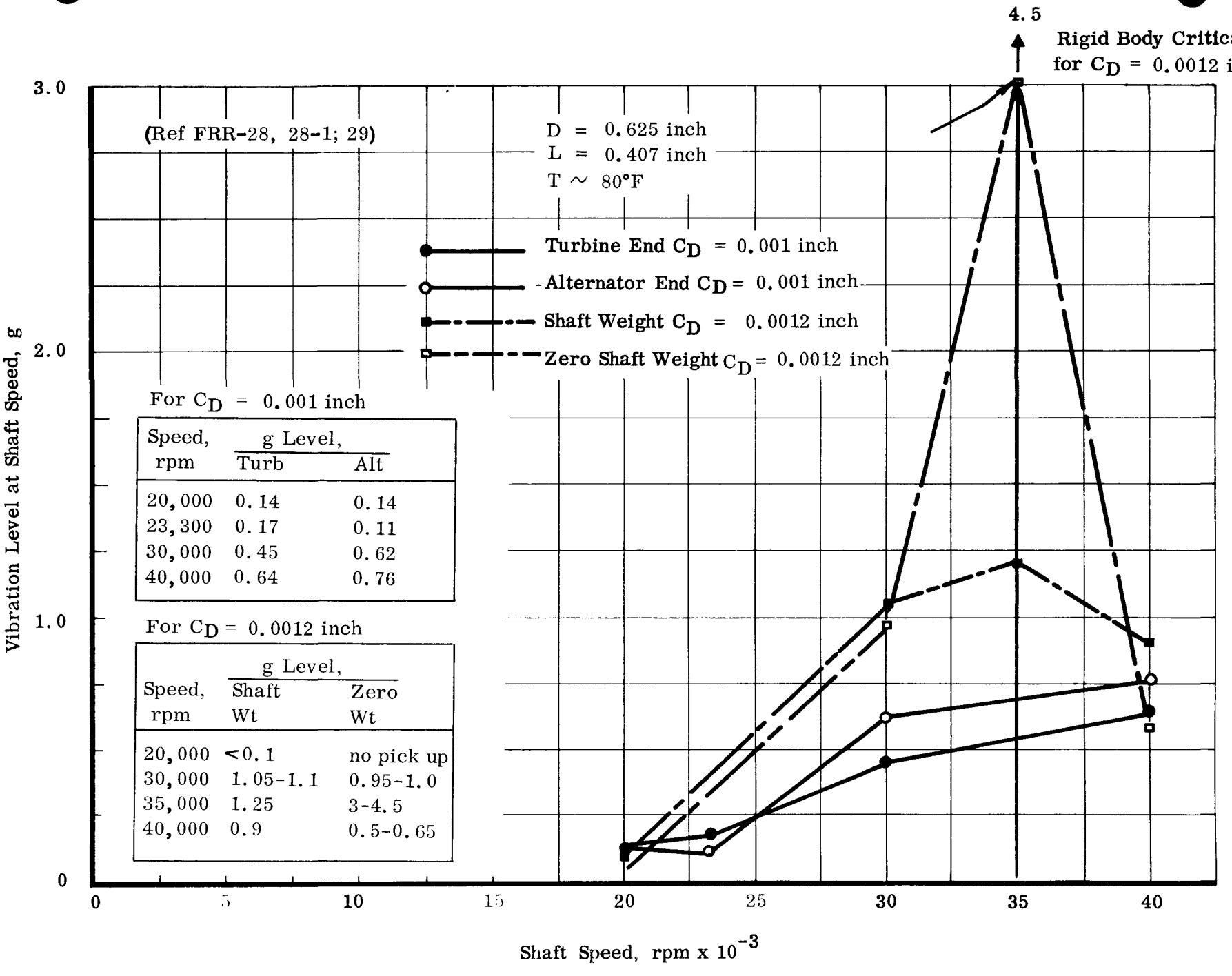

For C_D = 0.001 inch

Speed, rpm	g Level, Turb	g Level, Alt
20,000	0.14	0.14
23,300	0.17	0.11
30,000	0.45	0.62
40,000	0.64	0.76

For C_D = 0.0012 inch

Speed, rpm	g Level, Shaft Wt	g Level, Zero Wt
20,000	<0.1	no pick up
30,000	1.05-1.1	0.95-1.0
35,000	1.25	3-4.5
40,000	0.9	0.5-0.65

Figure 19. Vibration Survey of Three-Sector Bearing g Load vs Shaft Speed

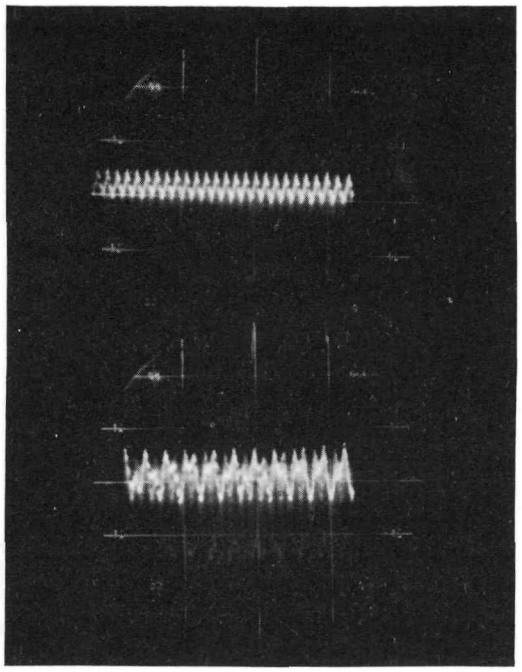

58

56

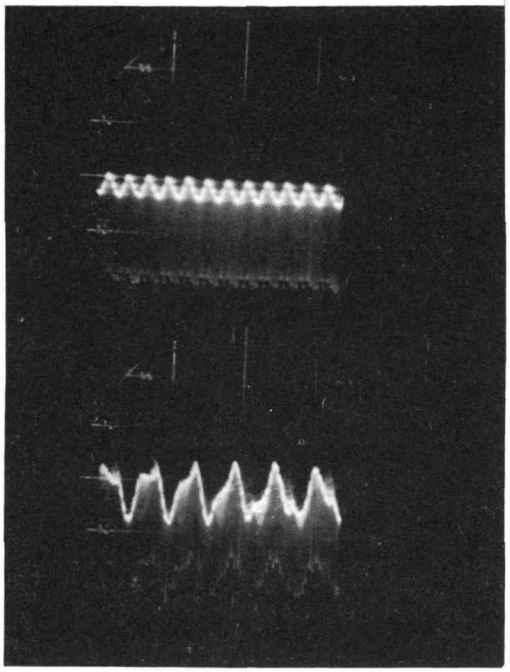

43

40

(a)

(b)

(a-56) 40,000 rpm Unstable
With Shaft Weight Only
P_S = 81 psi

(a-58) 40,000 rpm Stable
With Shaft Weight +
4.7 lb/brg
Unidirectional Load
P_S = 96 psi

(b-40) 20,000 rpm Unstable
With Shaft Weight Only
P_S = 81 psi

(b-43) 20,000 rpm Stable
With Shaft Weight Only
P_S = 111 psi

FRR 30
Three Sector
D = 0.625 inch
L = 0.407 inch
C_D = 0.0015 inch

Figure 20. Stability Characteristics of a Three-Sector Bearing

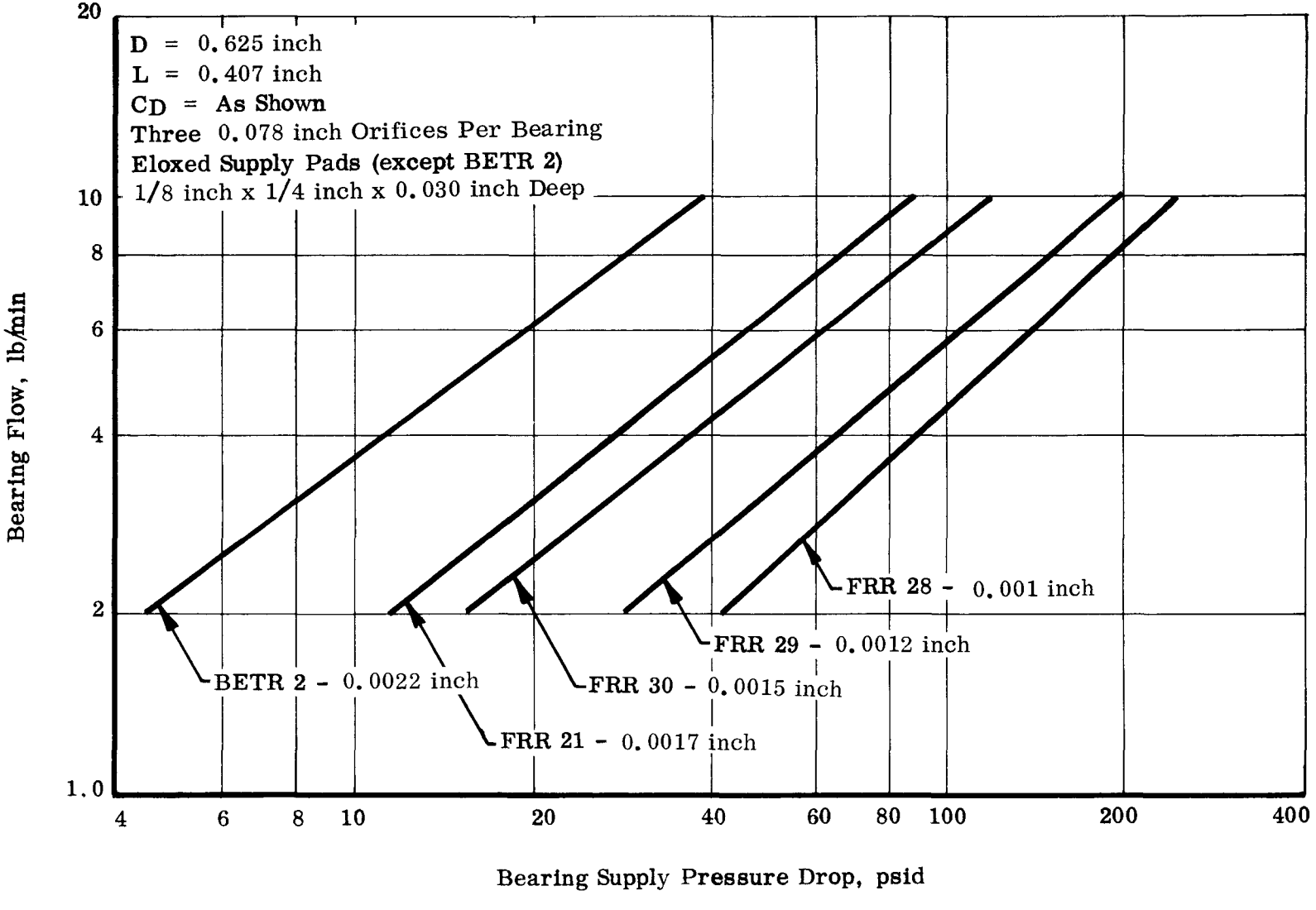

Figure 21. Flow-Pressure Relationship for Three-Sector Bearings at Zero Speed (Liquid Mercury at 80°F)

CONFIDENTIAL

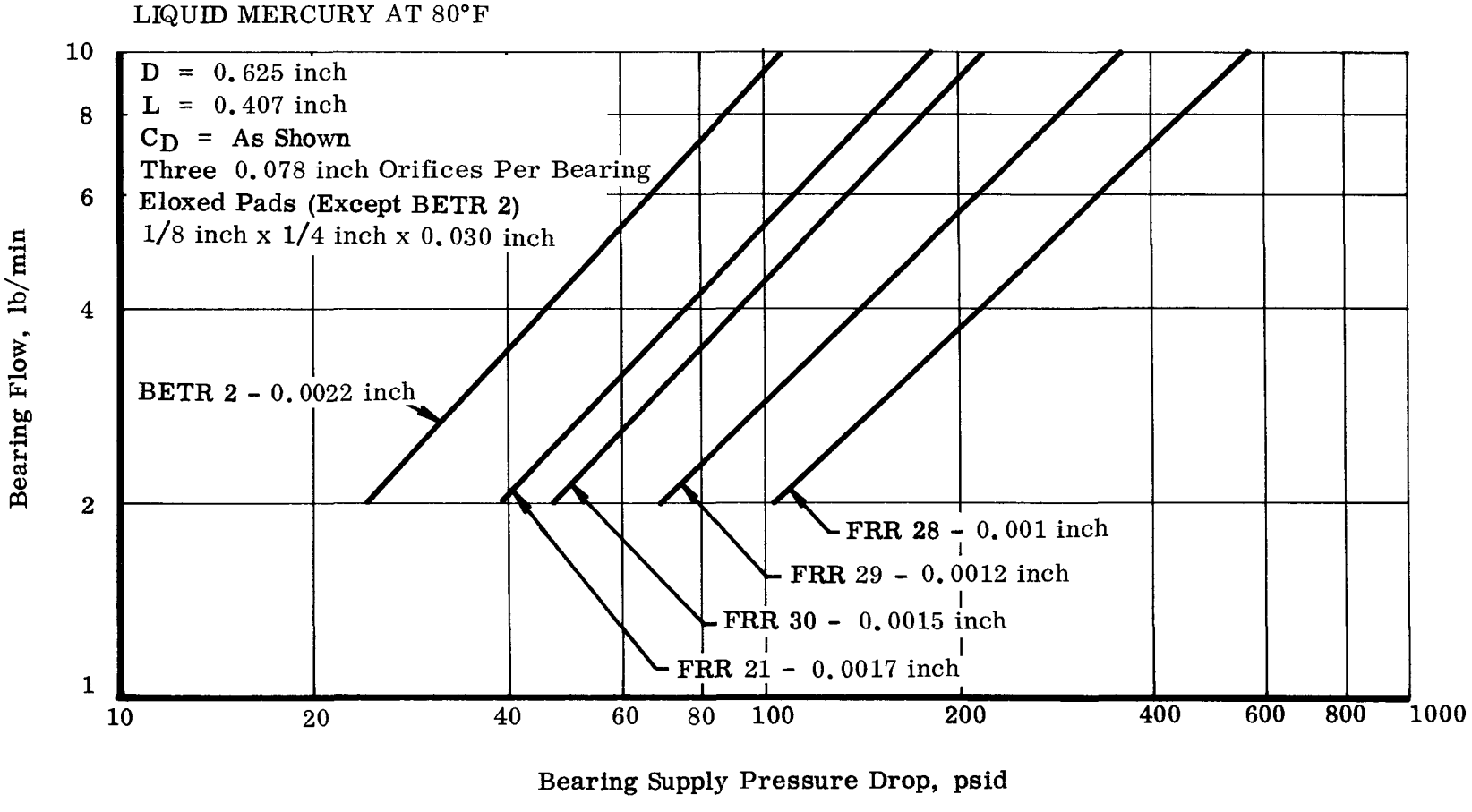

Figure 22. Flow-Pressure Relationships for Three-Sector Bearings at 20,000 rpm

LIQUID MERCURY AT 80°F

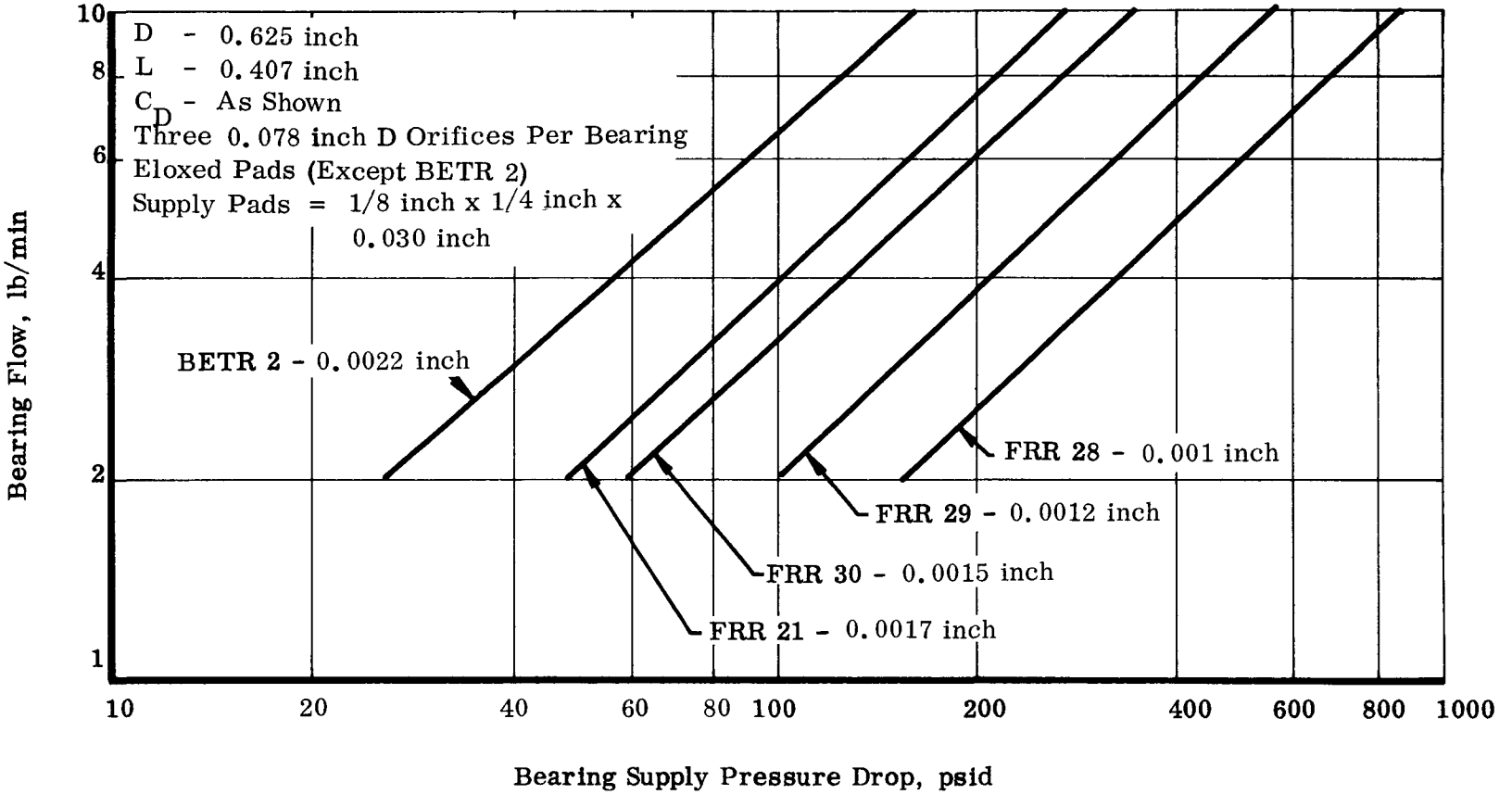

Figure 23. Flow-Pressure Relationships for Three-Sector Bearings at 30,000 rpm

CONFIDENTIAL

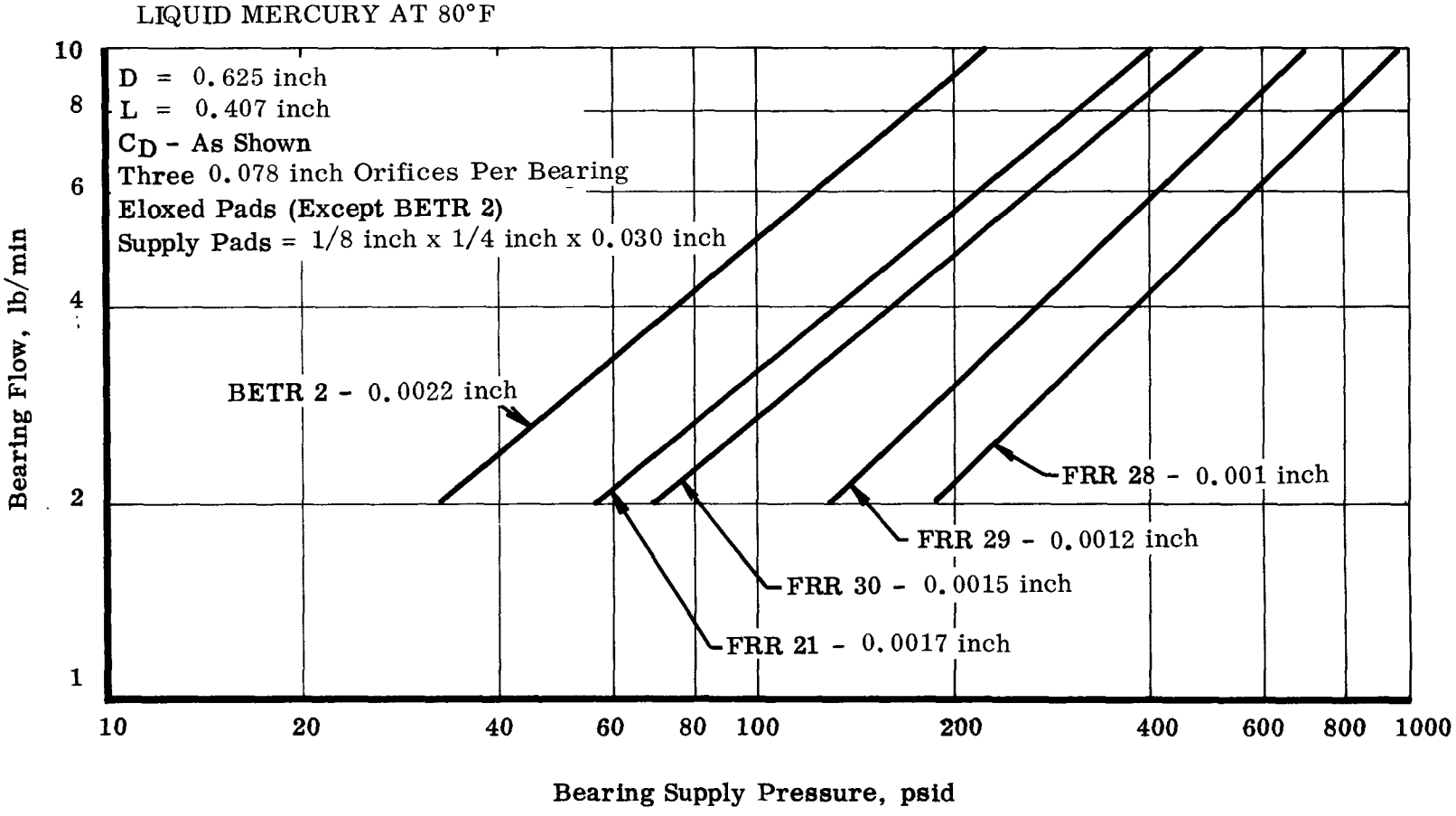

Figure 24. Flow-Pressure Relationships for Three-Sector Bearings at 40,000 rpm

To include the influence of lubricant temperature,a simple Reynolds number correction is applied. Since volume flow Q is a function of $1/\mu$, as temperature increases, the value of Q increases proportionally all other factors being equal) as follows:

$$Q_{T_2} = Q_{T_1} \times \frac{\mu_{T_1}}{\mu_{T_2}} \quad \ldots 5$$

But weight flow $Q_w = Q \times \rho$, where ρ = density.

As temperature increases density decreases, i.e., lowers mass flow. The net result is the correction factor shown below.

$$Q_{T_2} = Q_{T_1} \times \frac{\mu_{T_1}}{\mu_{T_2}} \times \frac{\rho_{T_2}}{\rho_{T_1}} \quad \ldots 6$$

Using Figure 25, Table 4 is derived.

TABLE 4

FLOW CORRECTION FACTORS FOR VARYING TEMPERATURES

T_2 Temp. (°F) (1)	2 Density (lb/ft^3) (2)	μ_2 Viscosity (lb-sec/in.^{2}) (3)	Density Correction ρ_2 / ρ_1 (4)	Viscosity Correction μ_1 / μ_2 (5)	Correction Factor (4 x 5) (6)
80	841	2.075×10^{-7}	1.0	1.0	1.0
100	840	2.0×10^{-7}	0.9988	1.0375	1.0363
200	832	1.725×10^{-7}	0.9893	1.2029	1.1900
300	824	1.550×10^{-7}	0.9798	1.3387	1.3117
400	816	1.425×10^{-7}	0.9703	1.4561	1.4129
500	808	1.34×10^{-7}	0.9606	1.5485	1.4875
where ρ_1 and μ_1 are considered at T_1 = 80°F					

The net result of this Reynolds number correction is shown in Table 5.

TABLE 5

FLOW CORRECTIONS AT DIFFERENT TEMPERATURES

Flow, lb/min

80°F	200°F	300°F	400°F
3.0	3.57	3.94	4.24
4.0	4.76	5.25	5.65
6.0	7.14	7.87	8.48
8.0	9.52	10.50	11.30

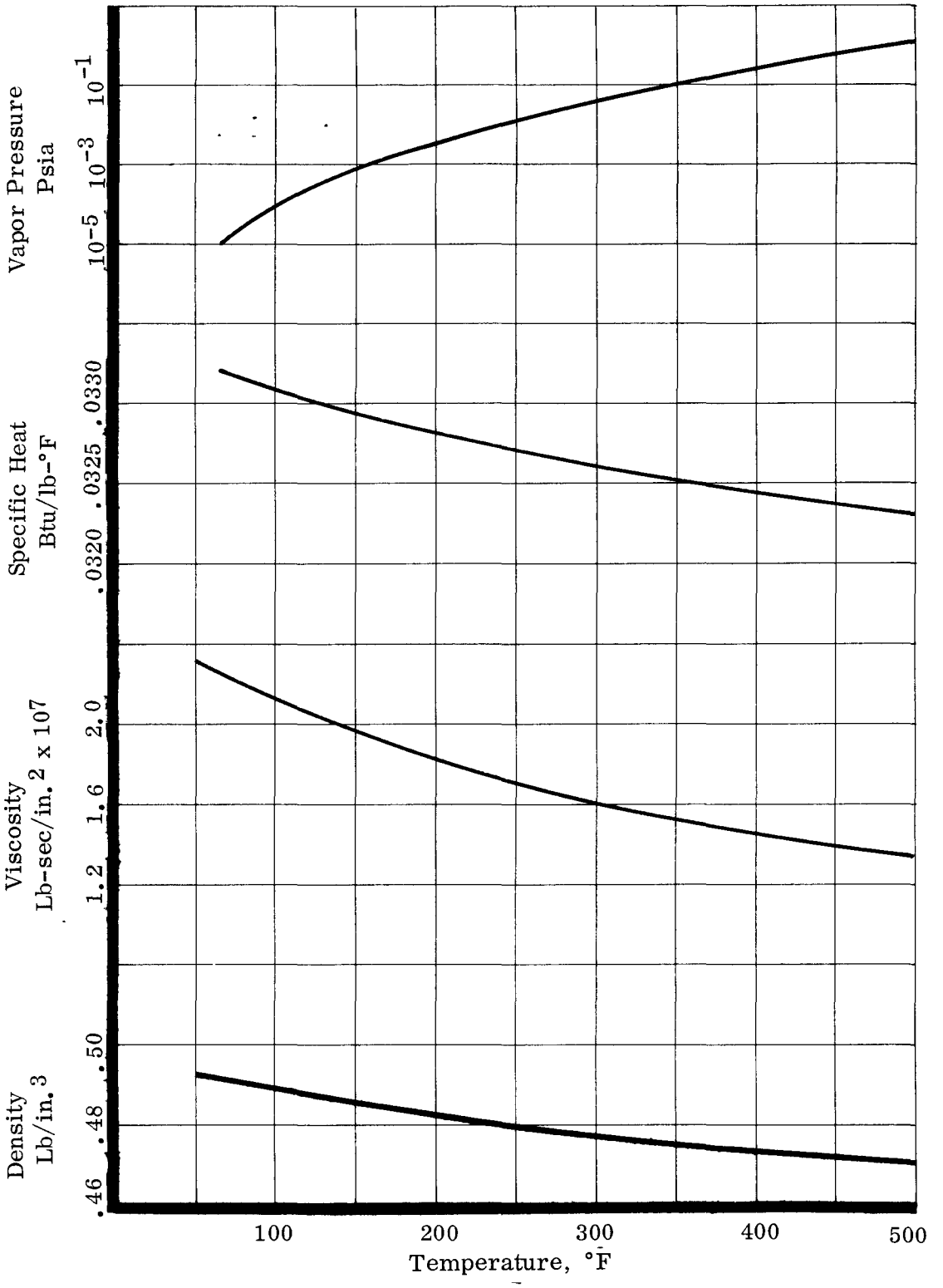

Figure 25. Properties of Liquid Mercury

The correction factor for flow is valid only if clearance of the bearing does not vary with lube temperature. However, given flow, pressure, lube temperature, and speed, the bearing clearance is established. Given the cold clearance and operating temperature, pressure, flow, and speed permits estimation of the running clearance.

For the range of clearances and the operating speed, Figures 26 and 27 show the static and dynamic flow characteristics of the uncompensated three-sector bearing. For the static case, the flow is given as:

$$Q = 3.12 \times 10^4 \left(\frac{C_D}{D}\right)^{1.95} \left(P_s\right)^{0.81} \quad \ldots 7$$

For the dynamic case the flow is given as

$$Q = 3.24 \times 10^6 \left(\frac{C_D}{D}\right)^{1.97} \times \left(P_s\right)^{0.95} \times (N)^{-0.845} \quad \ldots 8$$

These are useful equations which include pressure drop, clearance modulus (C_D/D), and speed as variables. All the data collected fall quite close to the final line for which equations have been established. Data spread for the static case is shown in Figure 26. Maximum deviation of actual data from the final line showing dynamic characteristics is less than 15%. This is acceptable since data have been obtained for speeds of 10,000 to 40,000 rpm over a large clearance range (0.001 to 0.0022 inch), and because of variation of flow as a function of stability, applied load, and operating eccentricity ratio.

c. Power Loss

Although power loss was not specifically measured for this series of tests by the speed-decay method, the turbine flow requirements indicated little variation in power consumption as a function of clearance changes. A measurement of lube temperature rise through the 0.001-inch clearance bearing and the assumption that all the heat generated due to viscous shear is transferred to the lubricant permitted the following analysis.

$$\text{Heat generated} = \text{Heat removed}$$

$$\therefore\ Q' \times \Delta T \times c = FHP \quad \ldots 9$$

Where:

Q' = flow, lb/sec

ΔT = temperature rise of lube, °F

c = specific heat of liquid Hg, $\frac{\text{Btu}}{\text{lb°-F}}$

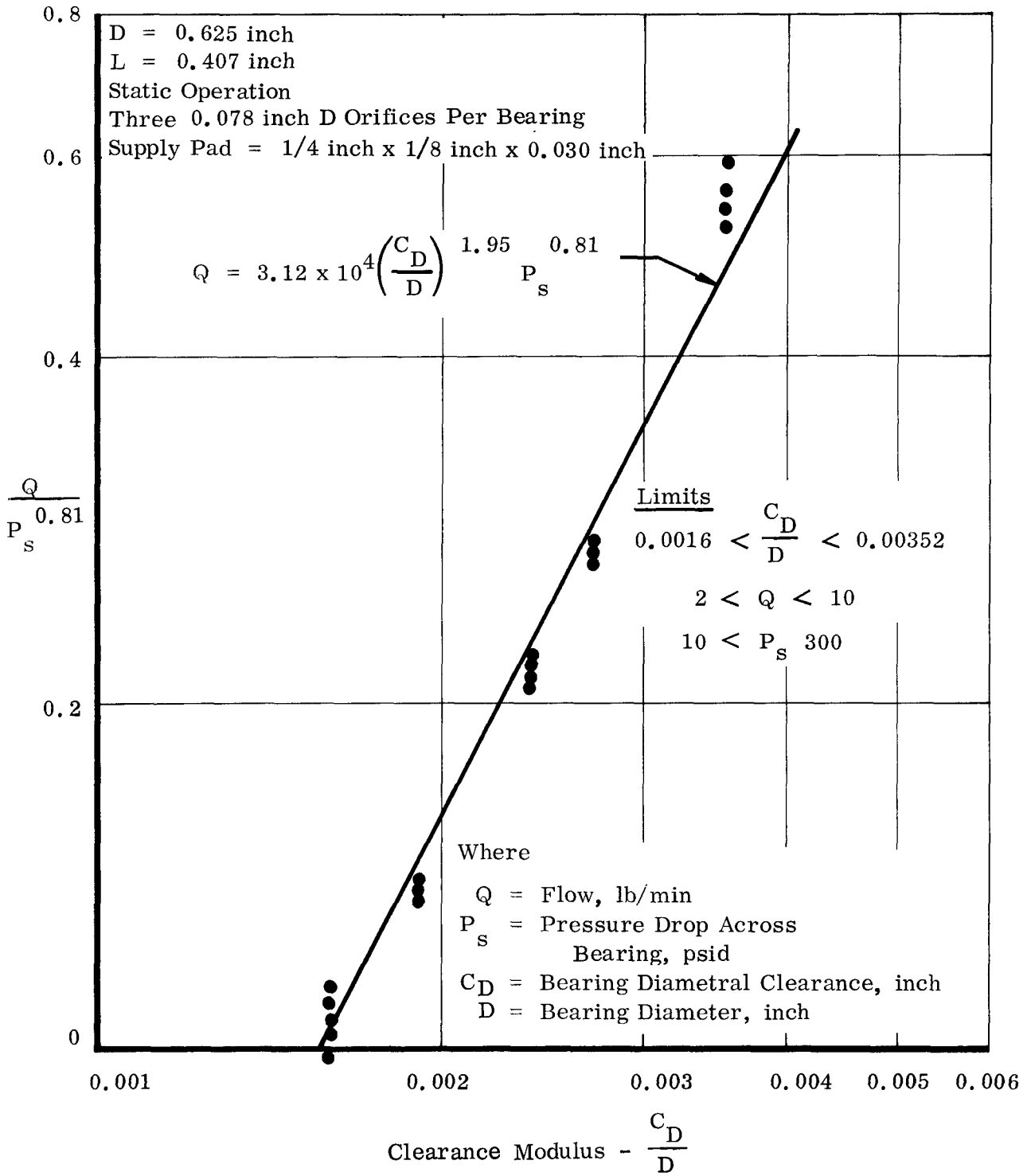

Figure 26. Static Flow Characteristics of the Uncompensated Three-Sector Bearing Liquid Mercury at 80°F

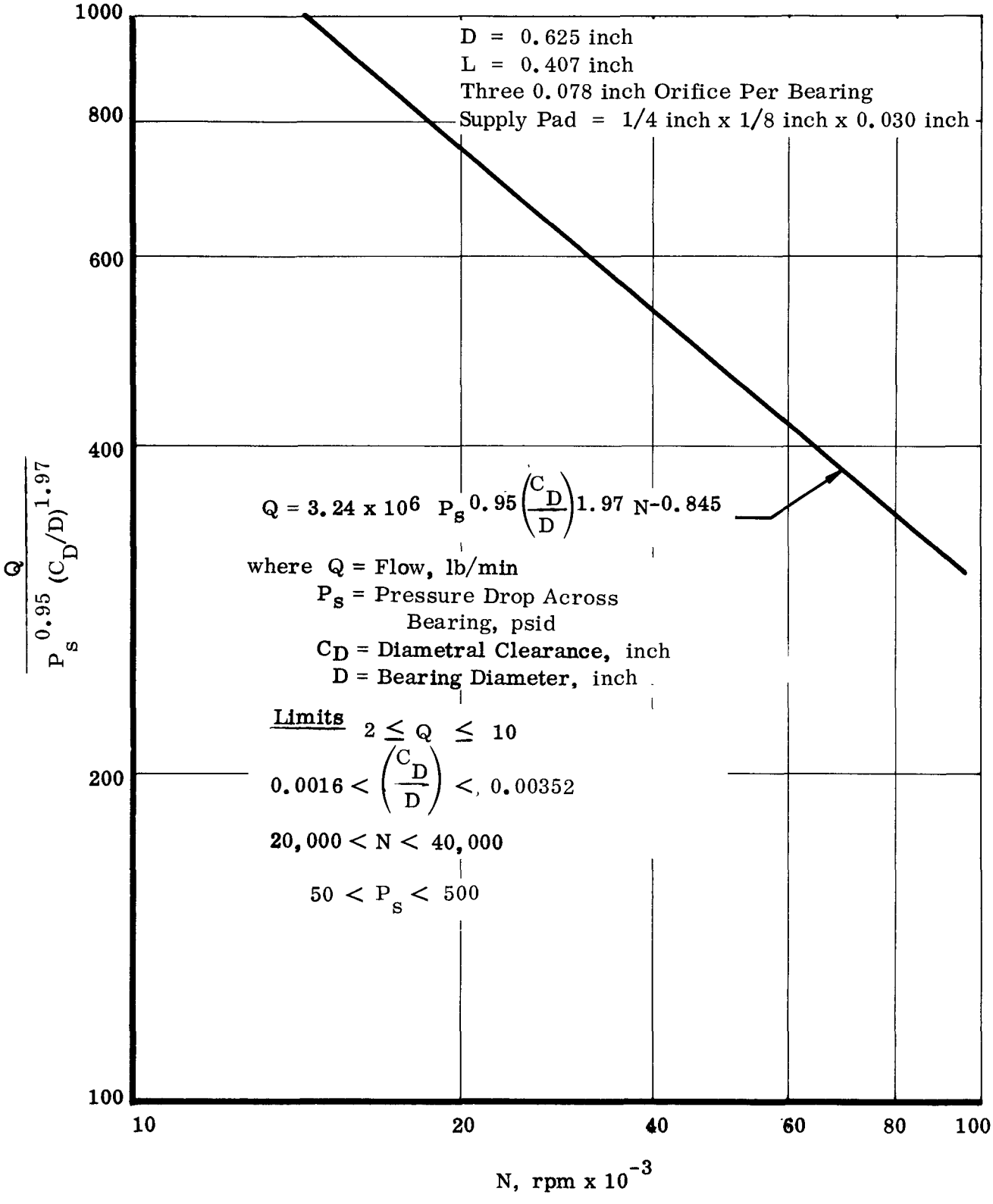

Figure 27. Dynamic Flow Characteristics of the Uncompensated Three-Sector Bearing, Liquid Mercury at 80°F

For $\Delta T = 100°F$ measured and 2 lb/min flow at 40,000 rpm, friction loss per journal bearing is 115 watts. This is a conservative estimate because the cool bearing housings absorb heat which is not reflected in the mean temperature rise, the peak temperatures are not recorded, and the cool turbine air is removing heat. However, it is the same magnitude as predicted using the equation listed in Volume I.

d. Conclusions on Test Series

These initial tests on the three-sector, uncompensated bearing revealed the following:

1) Freedom from half-frequency whirl could be achieved but only by going to small clearances ($C_D < 0.0012$ inch) or by maintaining high supply pressures. (Unidirectional loads could also be used, but, since these were unpredictable and unreliable in space, they were not considered.)

2) For the small clearance three-sector bearing, flow-pressure requirements were beyond the system pump capability as then designed. Consequently, flow was insufficient to remove the heat absorbed in and generated by the bearings.

3) First mode rotor-bearing critical speeds are a function of clearance (bearing stiffness). For the 0.001-inch bearing it is $> 40,000$ rpm; For the 0.0012-inch bearing it is $\approx 35,000$ rpm; and for the 0.0015-inch bearing it is $\approx 25,000$ rpm.

4) No cavitation-erosion type damage, similar to that suffered by the plain journal bearings, was detected in the three-sector bearings.

4. Free Running Rig Test 19

This test was conducted to establish the influence of rotating load on the performance, especially stability, of the three-sector bearing. Previous tests had demonstrated the susceptibility of the bearing to half-frequency whirl. Since whirl had been suppressed by the addition of rotating loads in laminar flow, compressible bearings, and since a rotating unbalance could be incorporated into the rotor assembly, this approach, if successful, could be utilized in the final application to eliminate half-frequency whirl. Bearing dimensions were identical to previous tests with a diametral clearance of 0.002 inch. Three 0.069-inch diameter orifices, each surrounded by a pad, supplied flow to each sector. The rotor was unbalanced to an equivalent rotating load of 30 lb/bearing at 40,000 rpm.

a. Stability

The addition of unbalanced loads increased the instability of the bearing at speeds above 30,000 rpm. Beyond 35,000 rpm, the rig limitation prevented whirl suppression by the application of unidirectional load or lube supply pressure. For these conditions, an

estimated 57.5 lb unidirectional load is required to suppress whirl at 40,000 rpm. As with the plain journal bearing the addition of a 30 lb/bearing rotating load was detrimental. Figure 28 represents a summary of the stability characteristics of the three-sector uncompensated bearing as a function of clearance and rotating load for various tests. Estimated load to suppress half-frequency whirl for the 0.0016-inch three-sector bearing is superimposed in Figure 28. (Data are obtained from Figure 9.) Agreement is reasonably good at this clearance, indicating justification for the following procedures:

1) Turbulent end leakage correction factor to establish load capacity

2) Turbulent correction factor to attitude angle based on plain bearing performance

3) Minor hydrostatic contribution of the uncompensated bearing toward suppressing half-frequency whirl

4) Analytical procedure to predict whirl threshold

Figure 28 clearly demonstrates the influence of clearance on half-frequency whirl threshold. A small clearance change below C_D = 0.0016 inch decreases load required to suppress whirl, thus increasing stability. Figure 29 shows stability data plotted as a function of diametral clearance. The trend for stable operation as clearance decreases is evident. Extrapolating the curves to zero radial load indicates that a diametral clearance of approximately 0.0012 inch is required for a fully stable bearing to speeds of 40,000 rpm. This verifies the stability search made during the FRR 28, 29, and 30 test series.

b. Flow-Pressure Characteristics

Reasonable agreement was achieved at low speeds where the influence of rotating load is not significant. However, above 30,000 rpm flow increased for a given pressure in the unbalanced case because of the combination of larger apparent operating clearances and lack of orifice compensation.

c. Load Capacity

A combined load of 37 lb/bearing and 30 lb/bearing rotating load was successfully supported by this bearing at 40,000 rpm. The current rig limit was 37 lb. The high loads and large journal motion in the bearing did not cause any of the noticeable cavitation-erosion damage that had occurred in the plain bearing.

5. Free Running Rig Test 21, 24, 25, and 27

This test series was designed to establish the influence of misalignment on bearing performance. Load capacity, flow, and stability were again of primary interest. The three-sector bearing selected for this test series had the standard configuration with a diam-

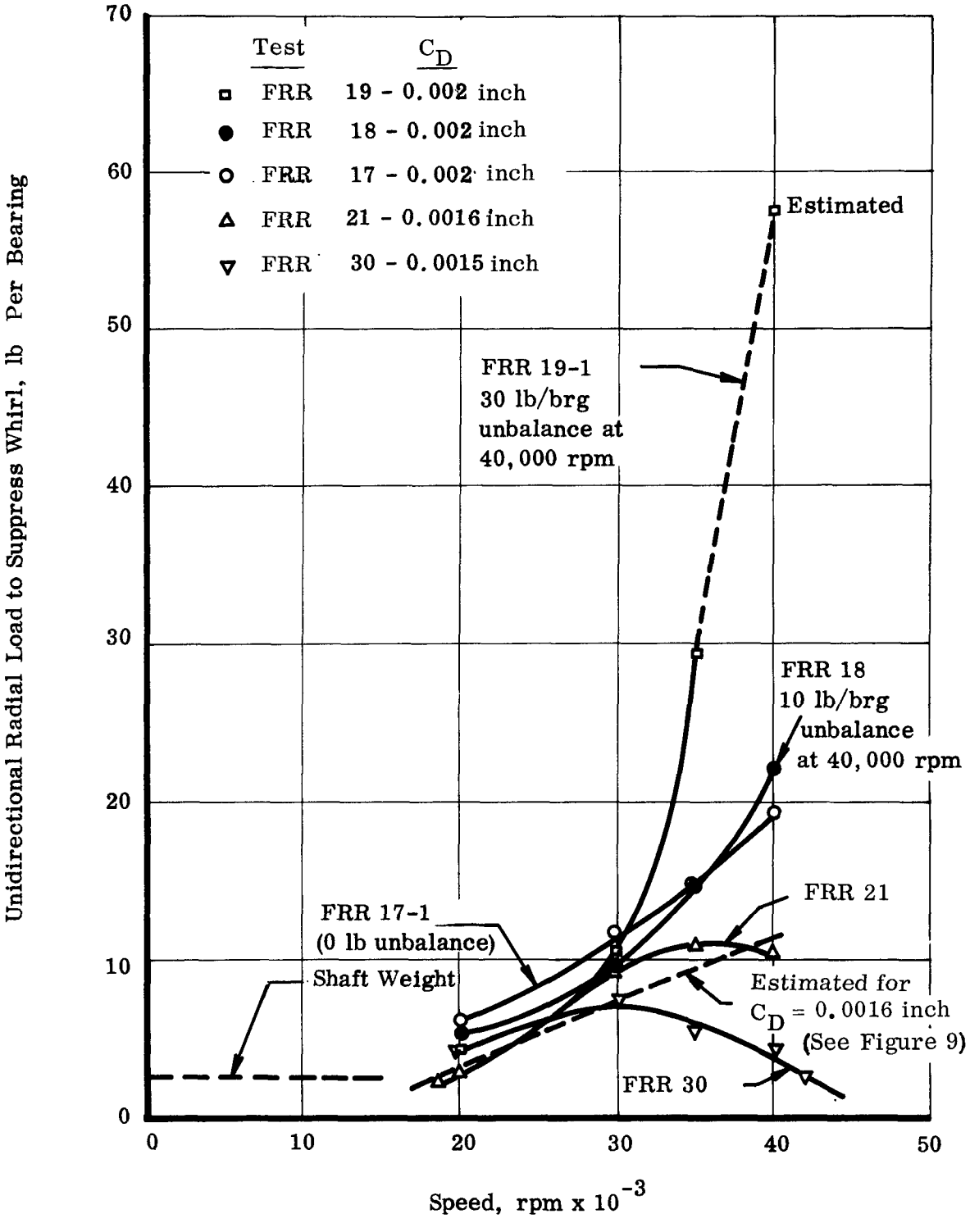

Figure 28. Radial Load to Suppress Whirl in Three-Sector Bearing

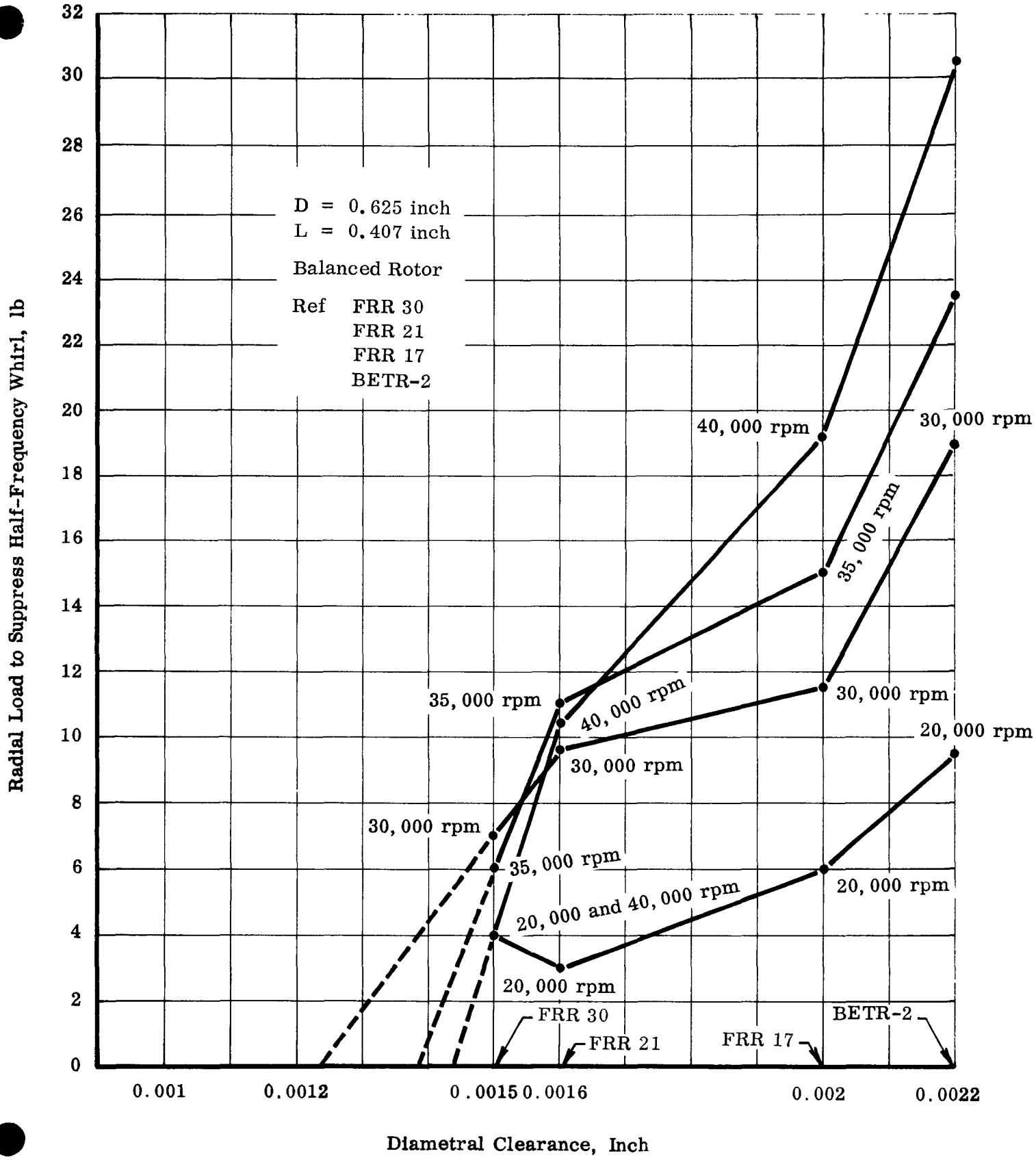

Figure 29. Stability Characteristics of Three-Sector Bearing

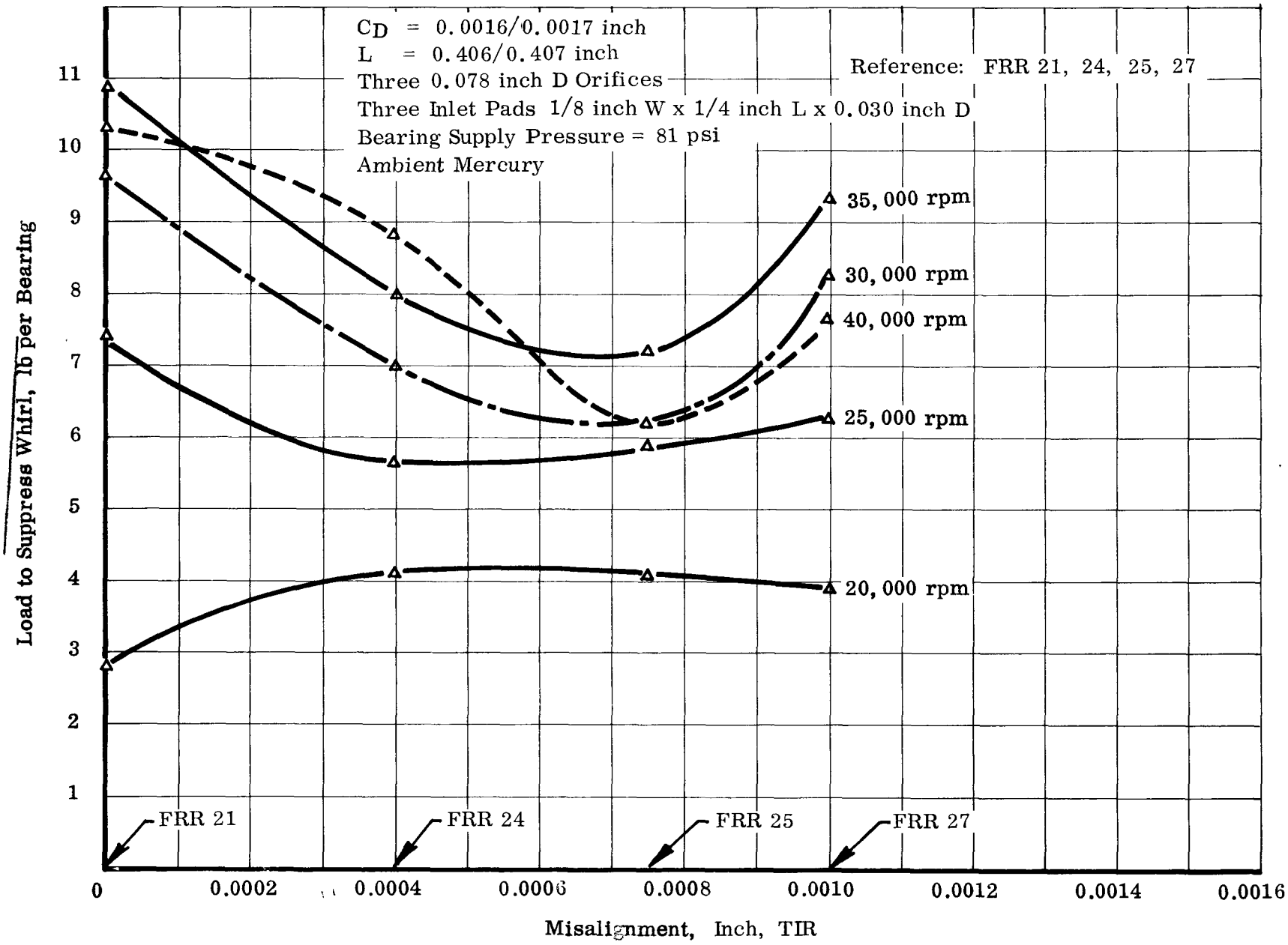

Figure 30. Stability Characteristics of Misaligned Three-Sector Bearings

eter (D) of 0.625 inch, a length (L) of 0.407 inch, and a diametral clearance (C_D) of 0.0016 to 0.0017 inch. Each sector had a single 0.78-inch diameter orifice surrounded by a 1/4-inch x 1/8-inch x 0.030-inch supply pad. The degree of misalignment built in at one end only ("A" bearing) was as follows:

FRR 21	aligned
FRR 24	0.0004-inch TIR* misaligned
FRR 25	0.00075-inch TIR misaligned
FRR 27	0.001-inch TIR misaligned

* Total Indicator Reading

a. Stability

The influence of misalignment on stability is summarized in Figures 30 and 31. Onset of whirl remained unchanged with misalignment, but the loads required to suppress the whirl show a possible optimum misalignment of approximately 0.0007 inch at speeds above 20,000 rpm. Figure 30 demonstrates that approximately 35,000 rpm represents the most unstable speed of this bearing type. This phenomenon and the optimum misalignment (from a stability point of view) are explainable in the following terms. As misalignment is increased the operating eccentricity for a given load increases and a more favorable operating attitude angle results. Consequently, the rate of change of $F_R = W\cos\emptyset$ is increased. The net result is increased stability. Beyond this optimum misalignment, the operating ratio increases but the load capacity decreases more rapidly. The net result is decreased stability.

b. Flow Characteristics

The influence of misalignment on flow was statically quite small as shown in Figure 32. Variation was $\pm$ 0.5 lb/min at 20,000 rpm for a constant inlet pressure of 81 psig. Under dynamic conditions, flow remained constant with misalignment. This is significant since it demonstrates that flow is not influenced by misalignment but only by load, speed, and ΔP across the bearing.

c. Load Capacity

The misaligned bearings supported the load of 37 lb/bearing which was the maximum due to rig limitations.

d. Conclusions on Test Series

The major conclusion derived from this series of tests was that the 0.0016- to 0.0017-inch clearance uncompensated three-sector bearing was capable of supporting the specified loads with a maximum misalignment of 0.001-inch TIR.

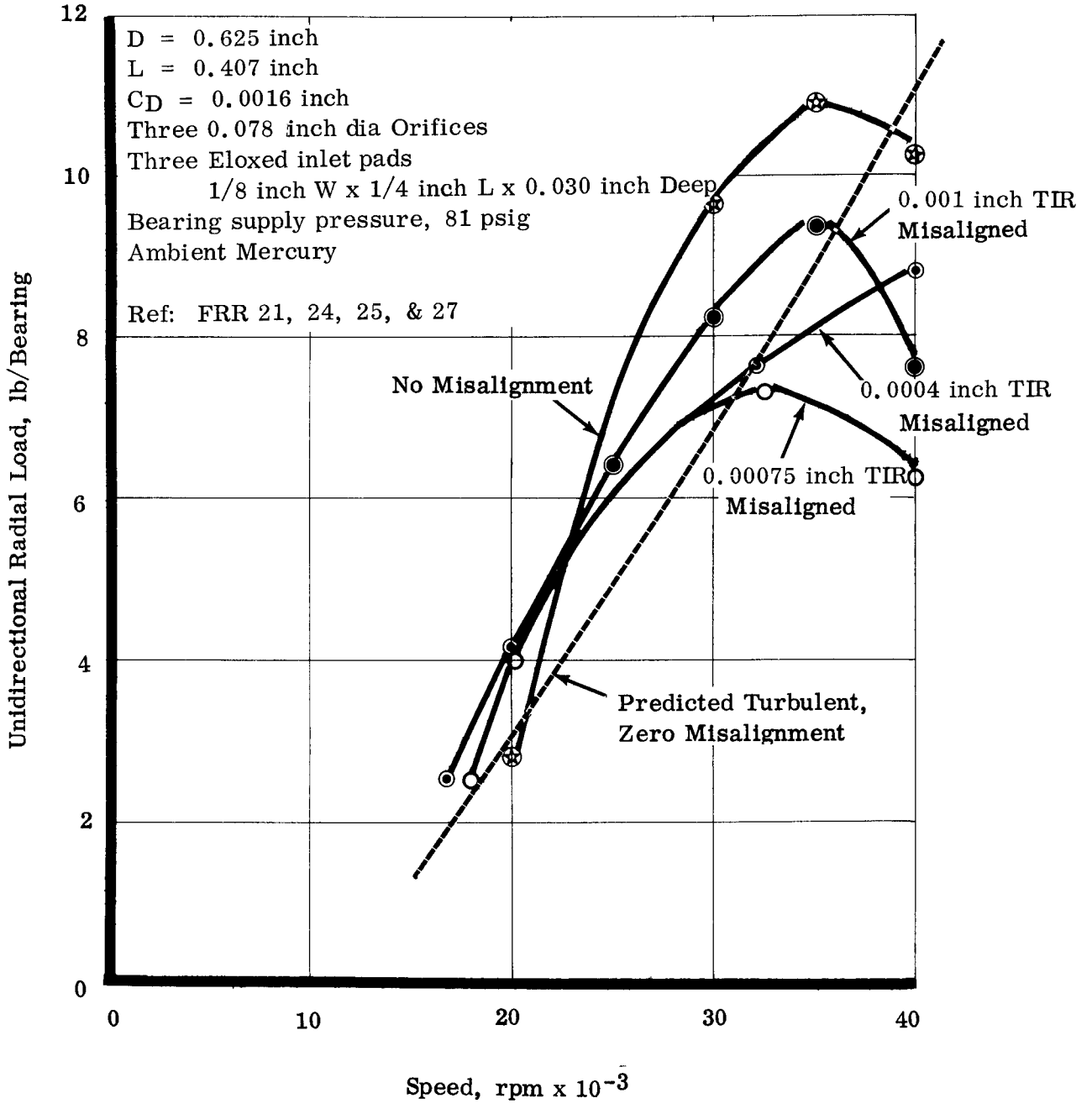

Figure 31. Unidirectional Load Required to Suppress Half-Frequency Whirl for Different Misaligned Three-Sector Bearings

References

FRR 24 - 0.0004 inch TIR Misaligned
FRR 27 - 0.0017 inch TIR Misaligned
FRR 25 - 0.00075 inch TIR Misaligned
FRR 21 - 0

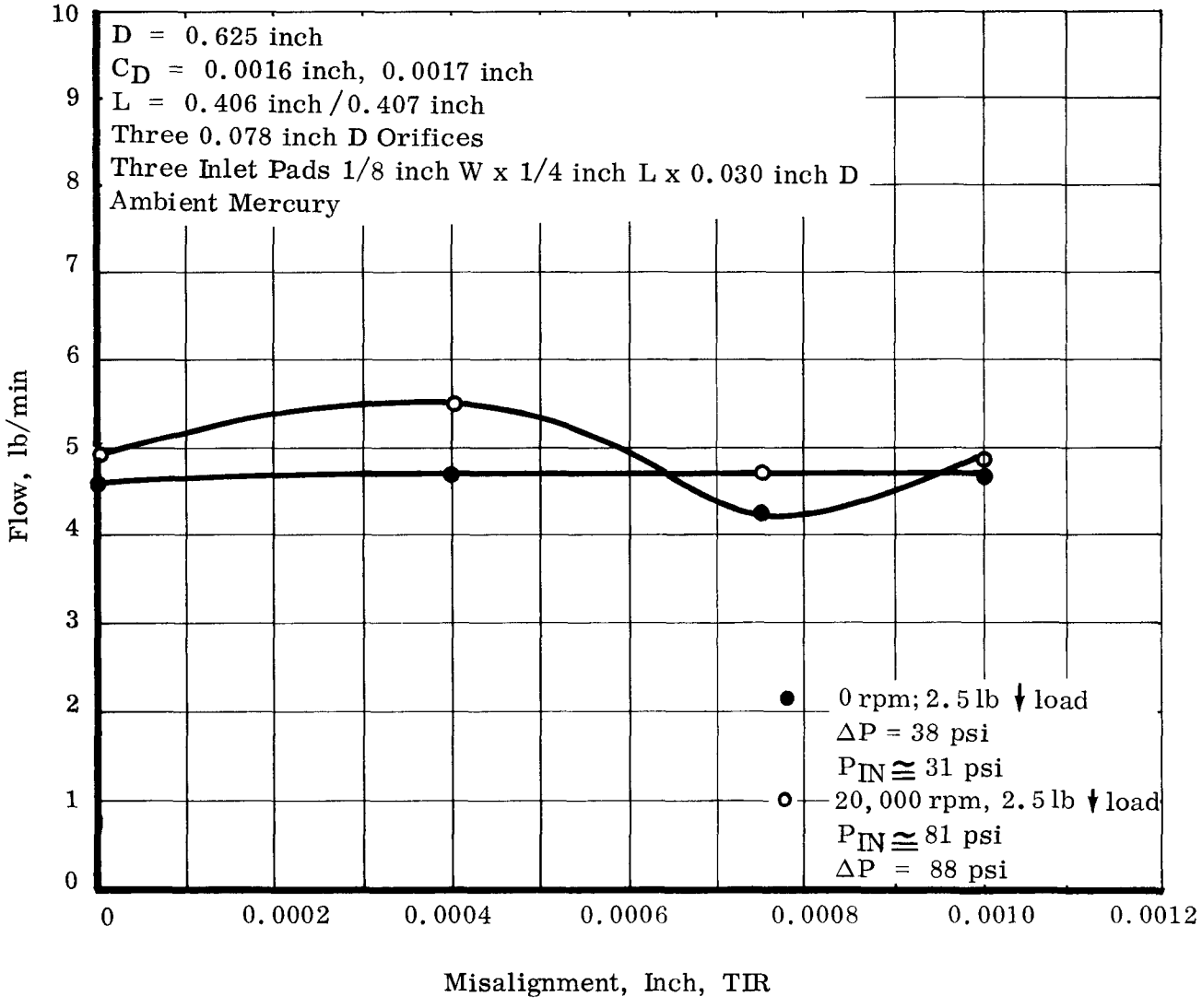

Figure 32. Flow vs Misalignment in a Three-Sector Turbine Bearing

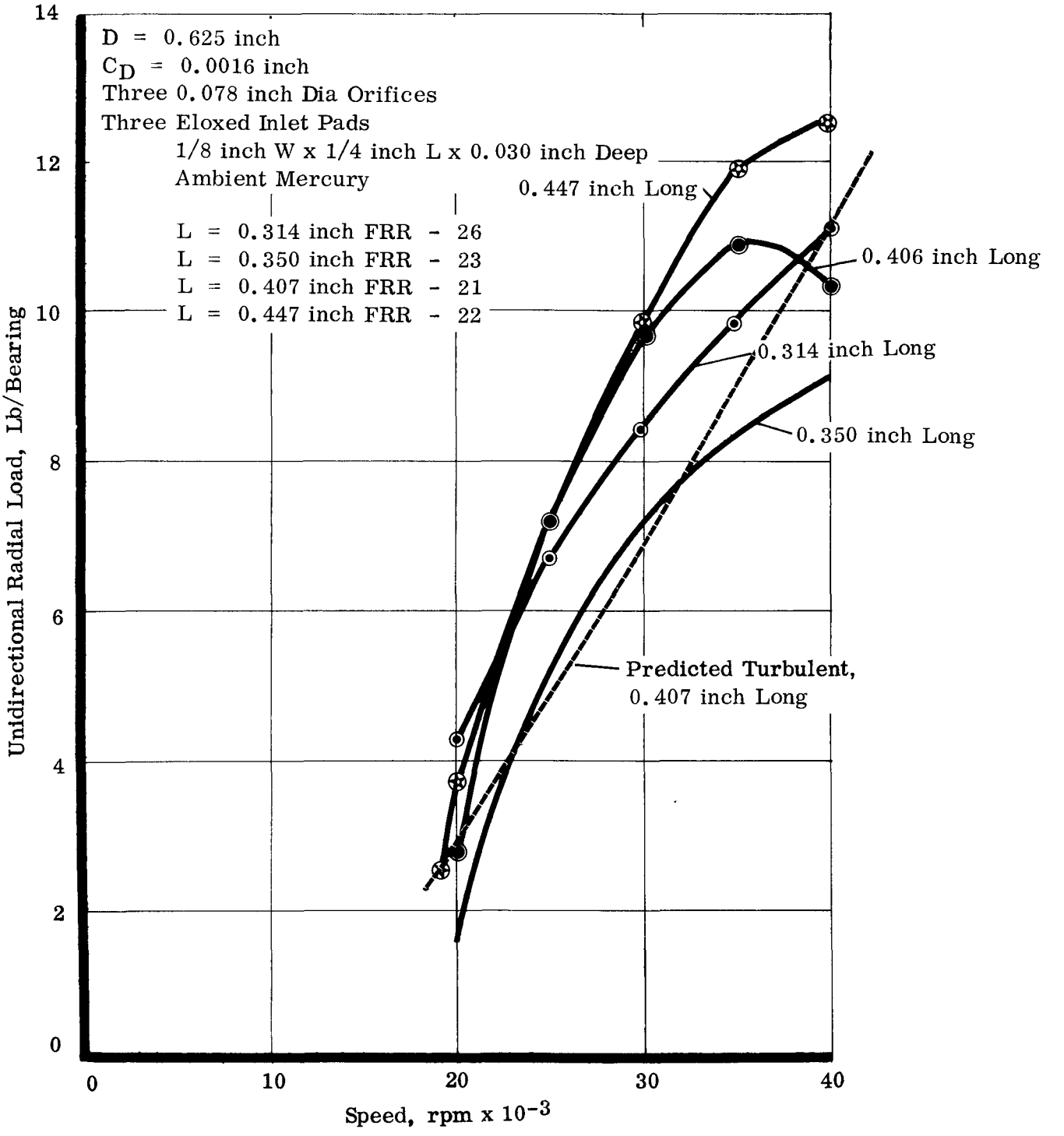

Figure 33. Unidirectional Load Required to Suppress Half-Frequency Whirl for Different Length Three-Sector Bearings

6. Free Running Rig Test 21, 22, 23, and 26

The effect of varying axial length on the flow and stability performance of the uncompensated three-sector bearing was established in this series of tests. Length, like diametral clearance and supply configuration, represents an easily changed basic bearing dimension. From the point of misalignment capability, axial length should be minimum. Similarly for maximum flow the axial length should be small. However, from a load capacity both hydrostatic and hydrodynamic, the length for a given diameter should be maximum.

The three-sector bearing dimensions were identical to the configuration evaluated in the misalignment tests, except that they were aligned and the length was varied as follows:

FRR 21	0.407 inch (standard)
FRR 22	0.447 inch
FRR 23	0.350 inch
FRR 26	0.314 inch (same as plain bearing length)

a. Stability

The influence of axial length on load required to suppress half-frequency whirl is summarized in Figures 33 and 34. Load required to suppress whirl increases with speed except for the 0.406-inch bearing. However, there is an axial length which requires the minimum load to suppress whirl. The optimum length for stability is 0.35 inch or L/D = 0.56. Figure 33 shows that the 0.447-inch bearing is the most unstable, requiring greatest suppression loads. As in the case of the optimum misalignment, the 0.35-inch bearing permits operation at an eccentricity ratio and attitude angle which result in the largest radial stiffness at shaft weight. As the bearing gets larger the eccentricity ratio is smaller and the attitude angle larger, resulting in the rate of change of the radial force $\frac{df_R}{de} = \frac{d(W\cos\phi)}{de}$ being smaller.

b. Flow Characteristics

The flow characteristics are presented in Figures 35 through 38. Statistically, flow decreases slightly with the initial increase in length (from 0.314 inch to 0.350 inch), and then remains constant. This is to be expected since the majority of the flow is axial out of the supply pad area and, consequently, insensitive to axial length. Dynamically, there is a decreasing trend in flow with increasing length. This is also to be expected since at speeds above 10,000 rpm the flow which is no longer laminar, becomes predominantly circumferential and is swept out ot the axial drain slots. As the L/D ratio increases, the end leakage decreases. The sensitivity of flow-pressure characteristics on unidirectional load (shaft position) is shown in Figure 38. The constant pressure lines should be as smooth at 40,000 rpm as they are at 20,000 and 30,000 rpm. Loading downward for the 0.314-inch, 0.406-inch and 0.447-inch bearings has increased the flow for a given pressure.

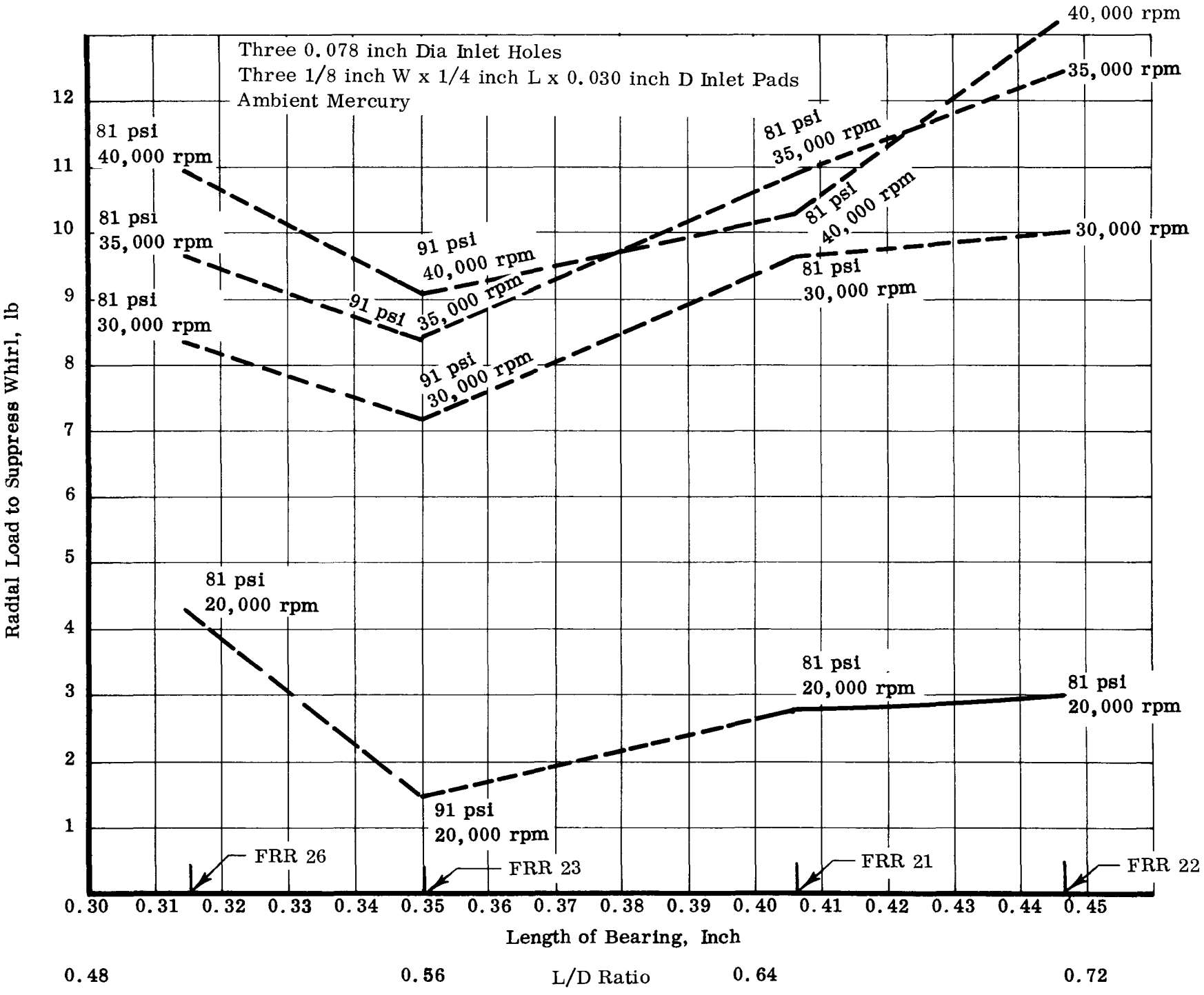

Figure 34. Radial Load to Suppress Whirl vs Length of Bearing in a Three-Sector Bearing

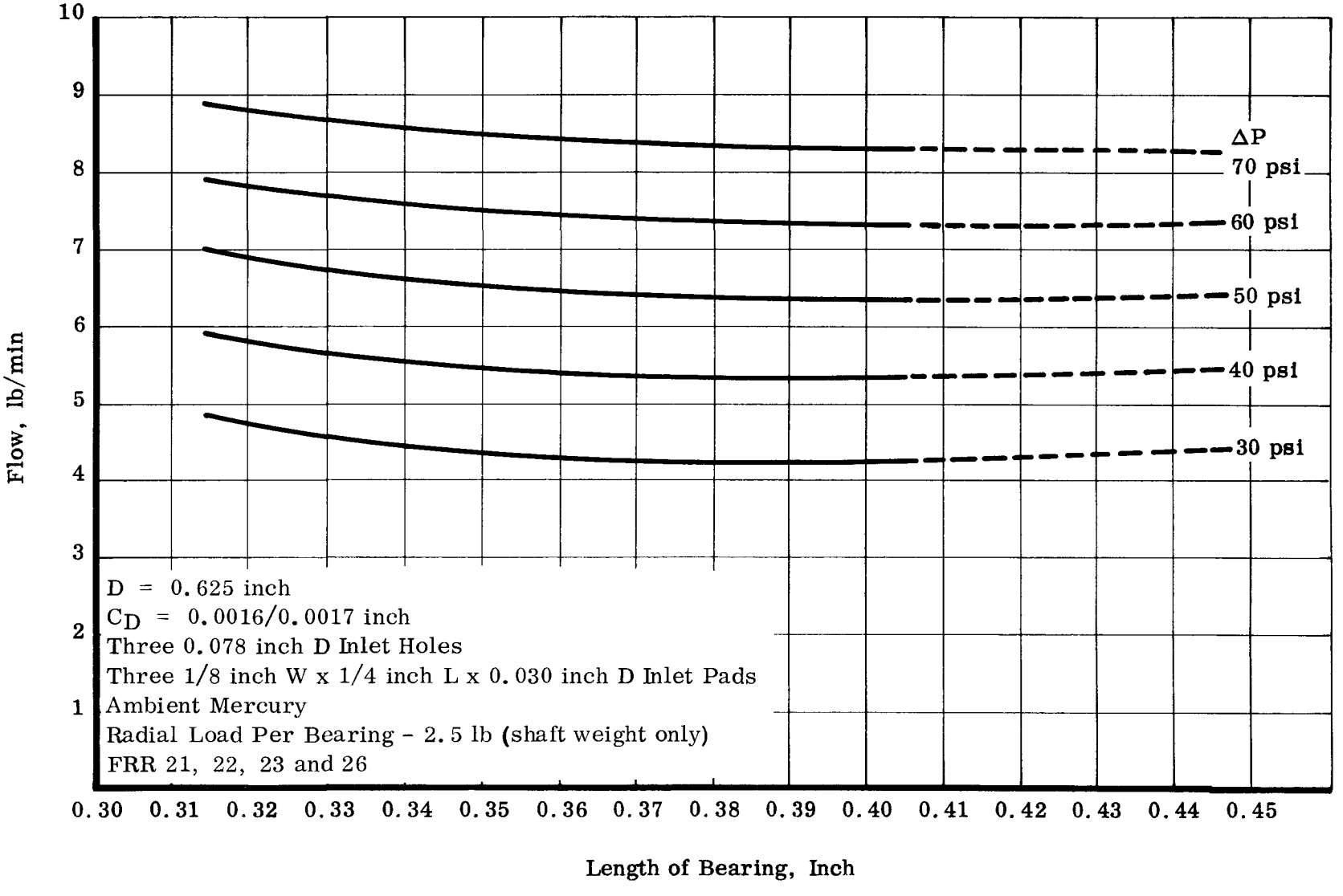

Figure 35. Static Flow vs Bearing Length for a Three-Sector Bearing

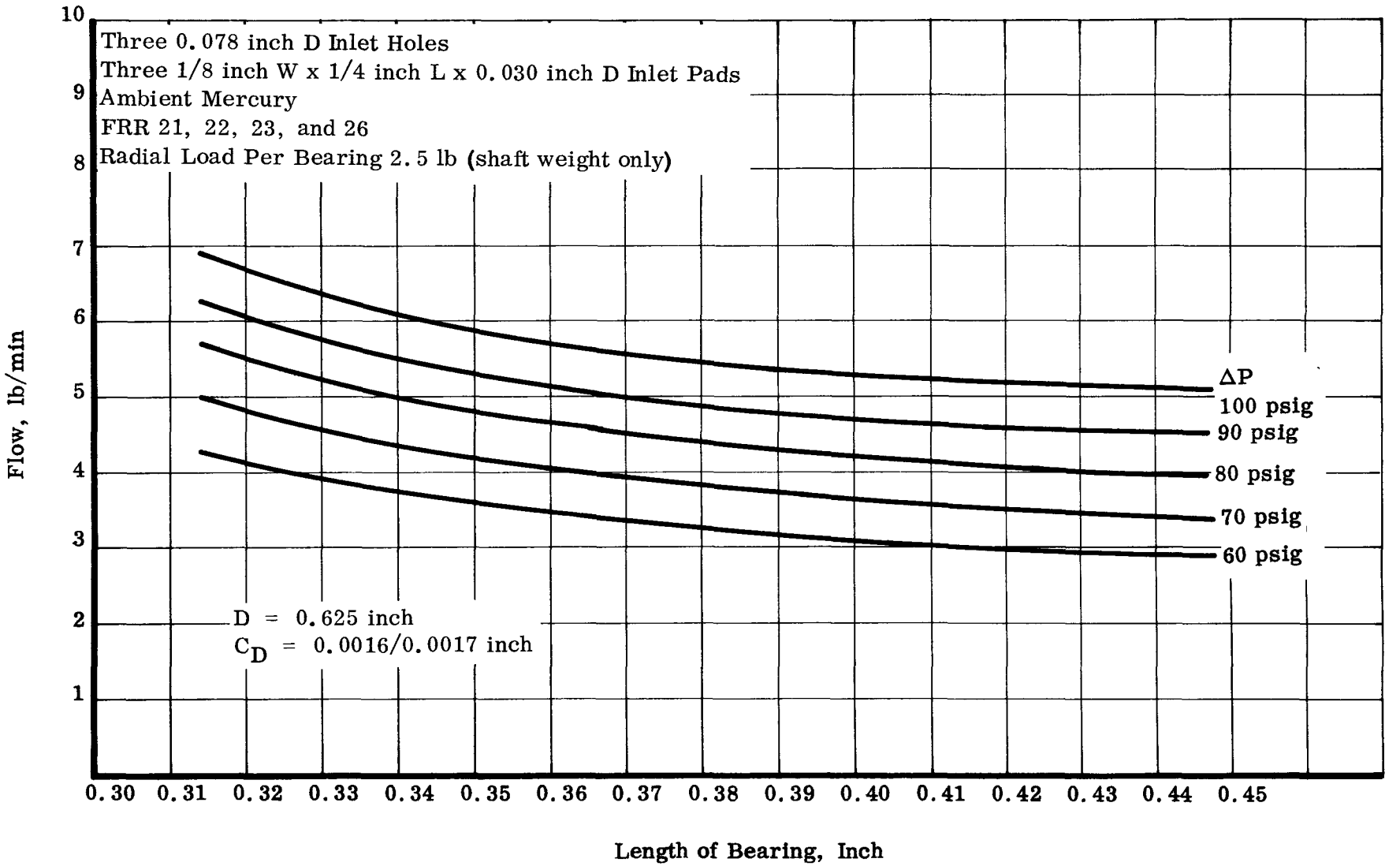

Figure 36. Flow vs Bearing Length for a Three-Sector Bearing at 20,000 rpm

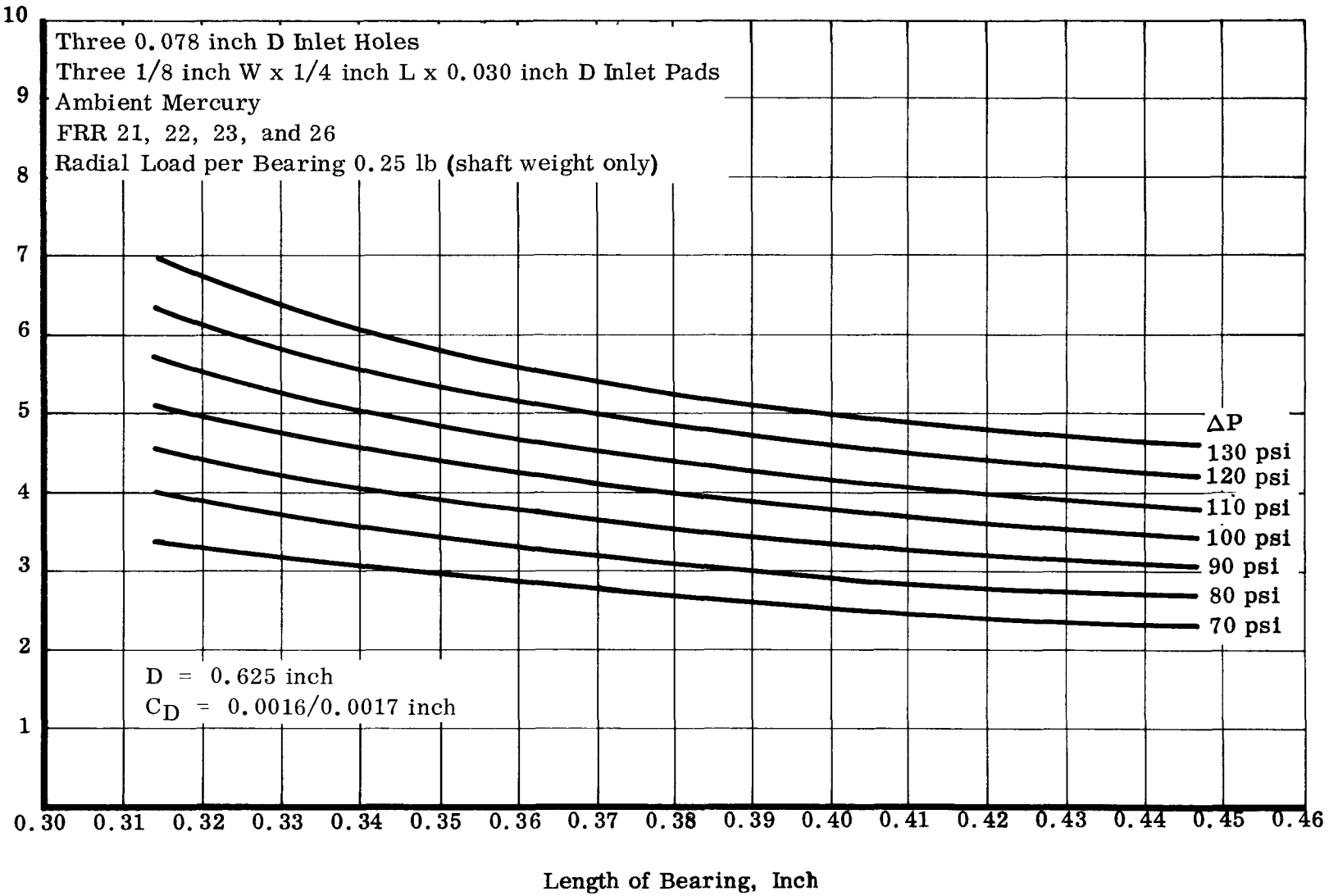

Figure 37. Flow vs Bearing Length for a Three-Sector Bearing at 30,000 rpm

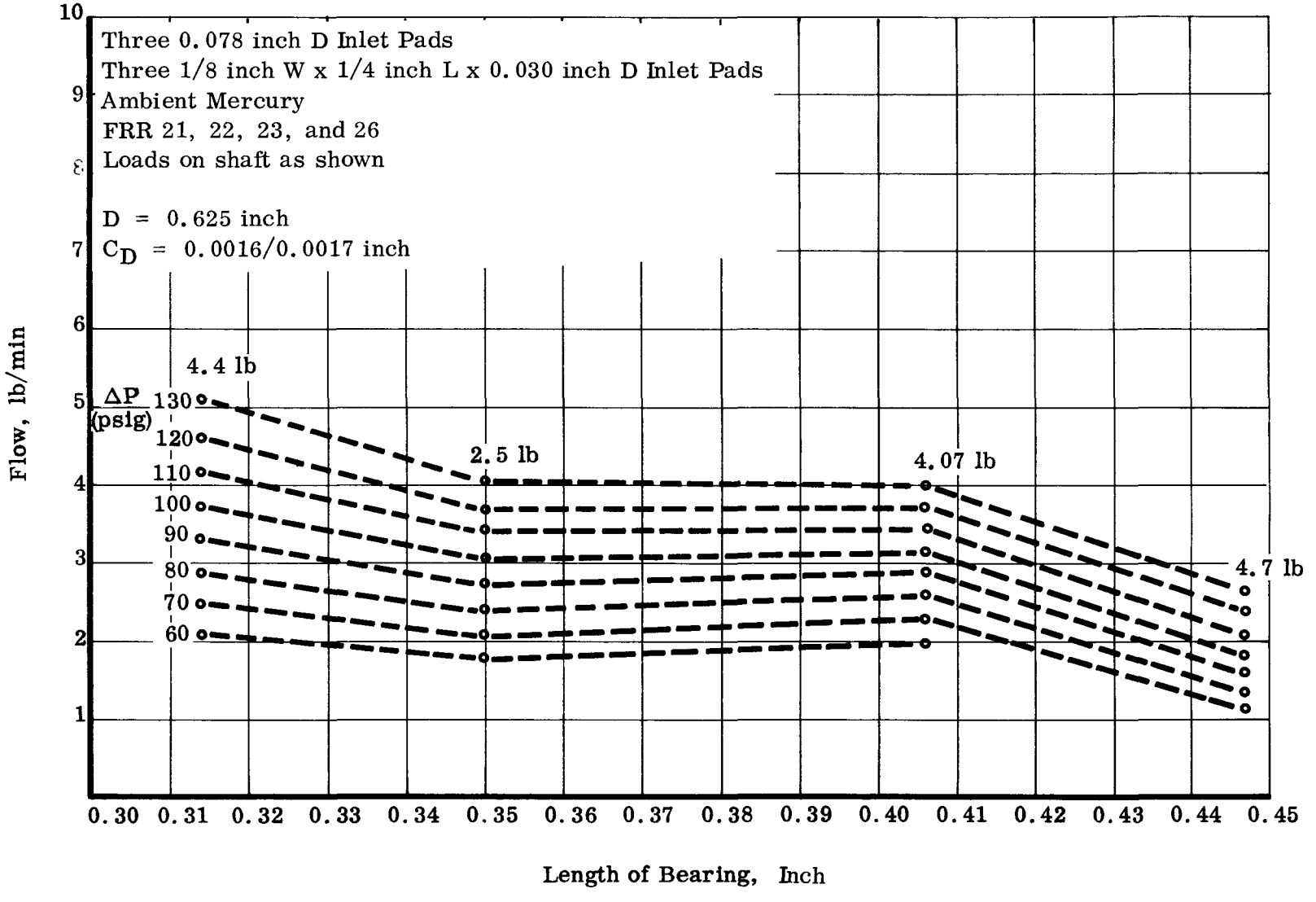

Figure 38. Flow vs Bearing Length for a Three-Sector Bearing at 40,000 rpm

The application of a 4.07-lb load to the 0.406-inch bearing results in the same flow as the 0.350-inch bearing which is loaded by a 2.5-lb shaft weight only.

c. Conclusions on FRR Test Series

With the completion of FRR test 30, sufficient data on flow-pressure, stability, and overall load capability was available to indicate that the three-sector bearing overcame three of the major drawbacks suffered by the plain journal bearing. These were: flow limitation due to pump performance, absence of cavitation-erosion damage and consequent long life, and metal-to-metal start up problems. Instability (half-frequency whirl) below the design speed of 40,000 rpm was not eliminated with the uncompensated bearing at a clearance which would permit adequate flow. To establish more detailed performance characteristics on load-deflection, minimum film thickness, attitude angles, power loss, and endurance capability; a new test fixture was designed and built. This test fixture, designated BETR (Bearing Endurance Test Rig), included improved instrumentation, increased flow-pressure and load capability, and a shaft-mounted pump to provide closer shaft simulation with actual CRU's and greater lubricant flow flexibility. Figure 39 shows a schematic of this fixture. A single parametric test on an uncompensated three-sector bearing was run prior to establishing long term life capability.

7. BETR 1

This test represented a rig and fixture checkout test and, consequently, resulted in a minimum quantity of parametric information. However, secondary objectives were to obtain flow-pressure characteristics, stability data, and measurement of attitude-eccentricity locus.

The three-sector bearing installed in the fixture had a diameter (D) of 0.625 inch, a length (L) of 0.407 inch, and a diametral clearance (C_D) of 0.0016 to 0.00175 inch. It contained three 0.078-inch diameter orifices and three 1/4-inch x 1/8-inch x 0.025-inch axial pads. Capacitance probes shown as radial proximity transducers in Figure 39 were utilized to monitor shaft motion. Two probes located in the same plane, 90 degrees apart, provided X and Y displacement of the shaft center which by the use of an oscilloscope was then converted to the locus.

a. Load Capacity

Load deflection tests at zero; 20,000; 30,000; and 40,000 rpm were run simultaneously with stability performance. Unfortunately, zero shift due to thermal effects prevented determination of accurate deflection, eccentricity ratio, and attitude angle. Consequently, the load-deflection curves show trends only and do not represent actual values of film thickness (or eccentricity ratio) for a given applied load. Figure 40 shows these trends for zero; 20,000; 30,000; and 40,000 rpm. Theoretically at zero load (simulating zero g) the shaft and bearing centers should coincide. Figure 40 shows that this assumption is not correct, even at zero speed where zero shift is negligible. The uncompensated orifices and unbalanced hydrostatic forces acting on the shaft are responsible for this shift.

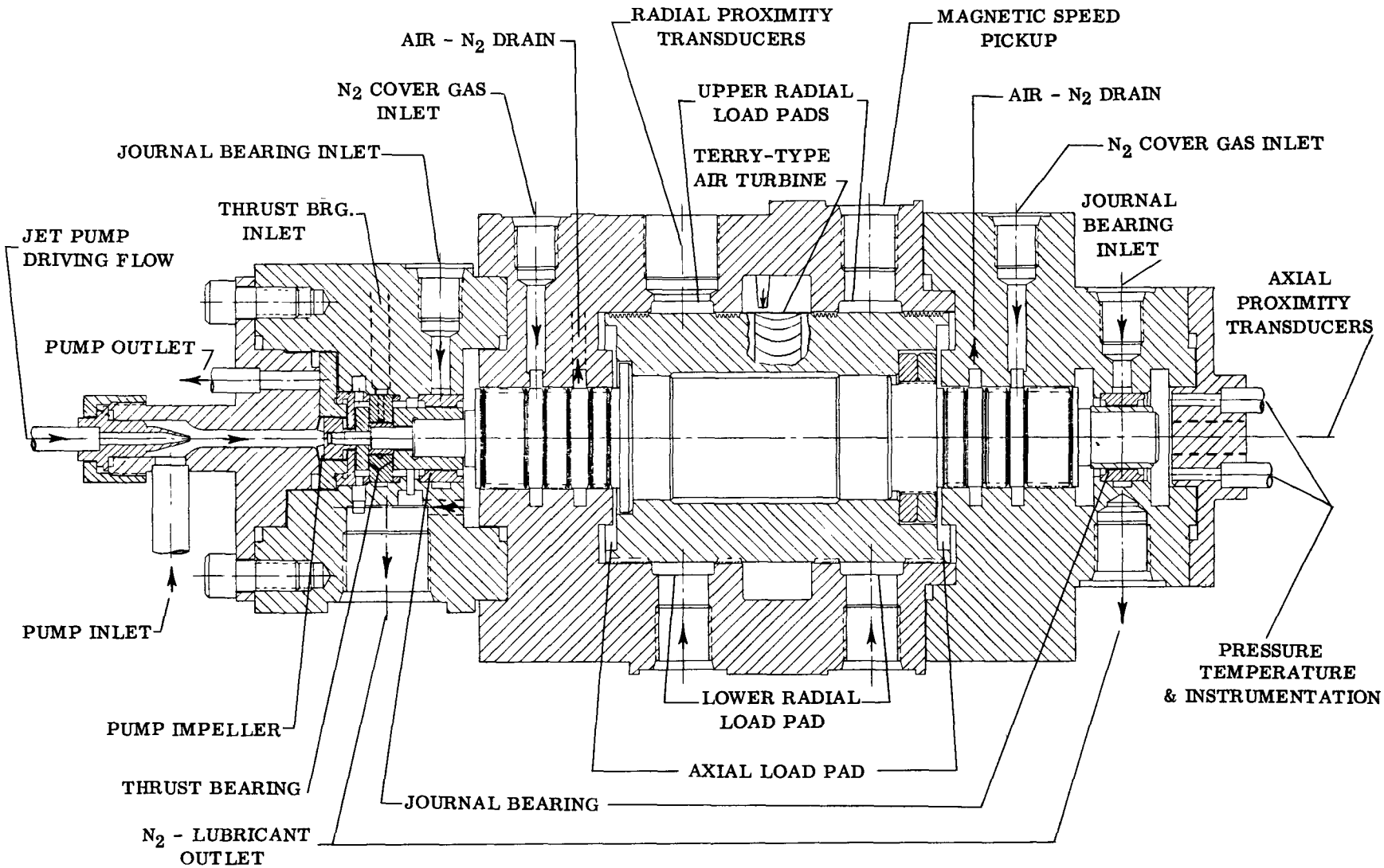

Figure 39. High Temperature Bearing Pump Test Rig
(Bearing Endurance Test Rig, BETR)

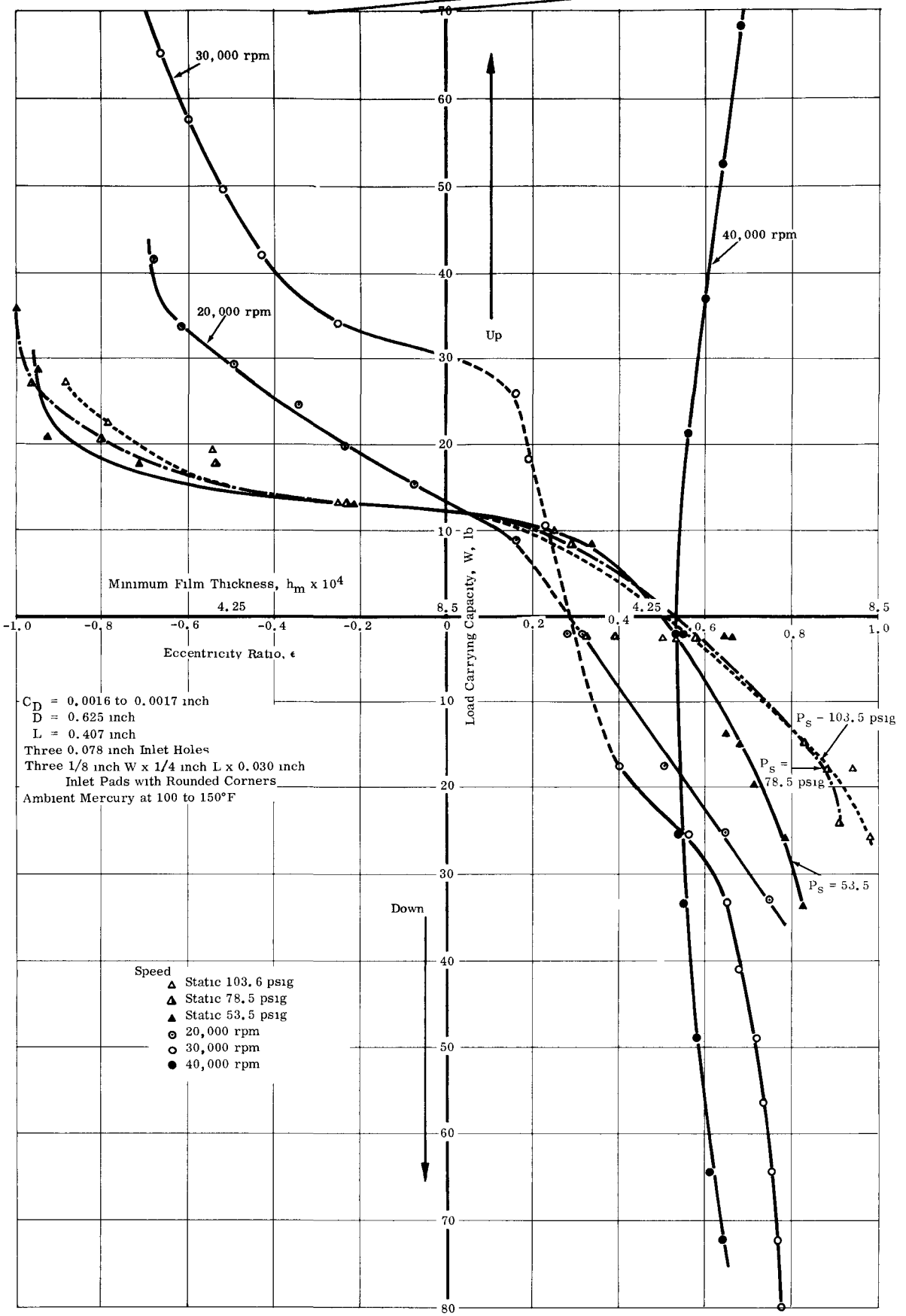

Figure 40. Load Deflection Characteristics for Three-Sector Bearing With Axial Groove on Top

BETR 1 Test Series

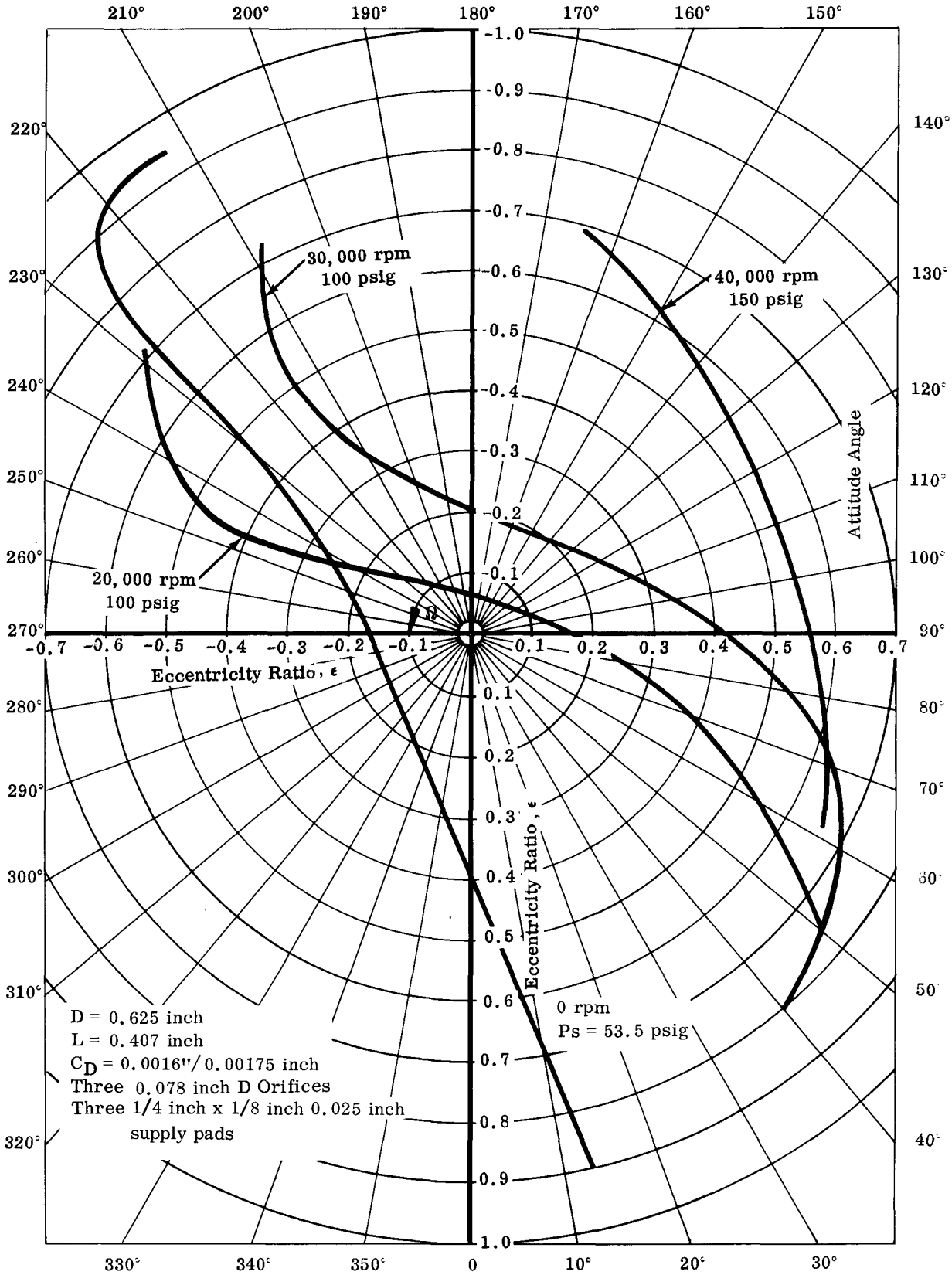

Figure 41. Attitude-Eccentricity Locus Curves of Three-Sector Bearing

BETR 1 Test Series

This factor plus the probe drift caused by temperatures accounts for the unusual load-deflection characteristics observed. No adjustments are possible since zero shift corrections were not made during the test. However, the change in deflection as a result of applied loads, vertically up and down, are accurate even though the absolute value of eccentricity ratio is incorrect.

The locus of the shaft center, due to loads applied up and down at zero; 20,000; and 30,000 rpm, discussed below has the standard "S" shape even if slightly displaced due to zero shift. At small loads ($\epsilon \rightarrow 0$) the actual location was difficult to establish because of rotor instability. At 40,000 rpm, the deflection curve did not follow the anticipated trend. A combination of probe drift and uneven pressure forces, caused by hydrodynamic action and unbalanced hydrostatic forces due to uncompensated orifices, are responsible for this large shift to the "right" in Figure 40.

A relatively large rotor unbalance resulting in a sizable locus made definition of actual eccentricity ratio difficult. The static load curve in Figure 40 demonstrates the hydrostatic capability of the uncompensated three-sector bearing. Loads in excess of 30 lb were supported. Since hydrodynamic action is absent and probe drift is negligible at zero speed, the static load curve clearly shows the shift due to uneven hydrostatic pressure forces within the uncompensated bearing. The three-sector bearing, or any odd number pad or sector type, has unequal load capacity loading up and down. With uncompensated orifices located at an angle to the applied load, flow is throttled at the point of minimum film thickness as the shaft is displaced and, consequently, increases rapidly 180 degrees away where the large clearance exists (unloaded side). The net result is a large, uneven pressure distribution which is reflected in the deflection curve, i.e., Figure 40. The hydrodynamic pressure forces superimposed on the hydrostatic forces increase and contribute further to the uneven pressure distribution, resulting in the deflection curves for the 20,000; 30,000; and 40,000 rpm speeds. Loads in excess of 70 lb were successfully supported by the bearings at 30,000 and 40,000 rpm. No attempt to correlate with predictions was made because of the unresolved probe drift problem.

b. Attitude-Eccentricity Locus

The locus for the different speeds is summarized in Figure 41. The upward drift (to the "right") with speed is evident in this figure. As mentioned above, the displacement of the locus is partially due to uneven pressure forces which result in a negative attitude for zero load and partially to the zero shift of the capacitance probes caused by temperature variations.

c. Film Stiffness

At 20,000 and 30,000 rpm under certain load conditions, the rotor indicated a critical speed (or synchronous whirl or inversion speed as some investigators define the lowest bearing-rotor critical speed). Applying:

$$f_{cr} = \frac{60}{2\pi} \sqrt{\frac{K \times 386}{W}} \qquad \ldots 10$$

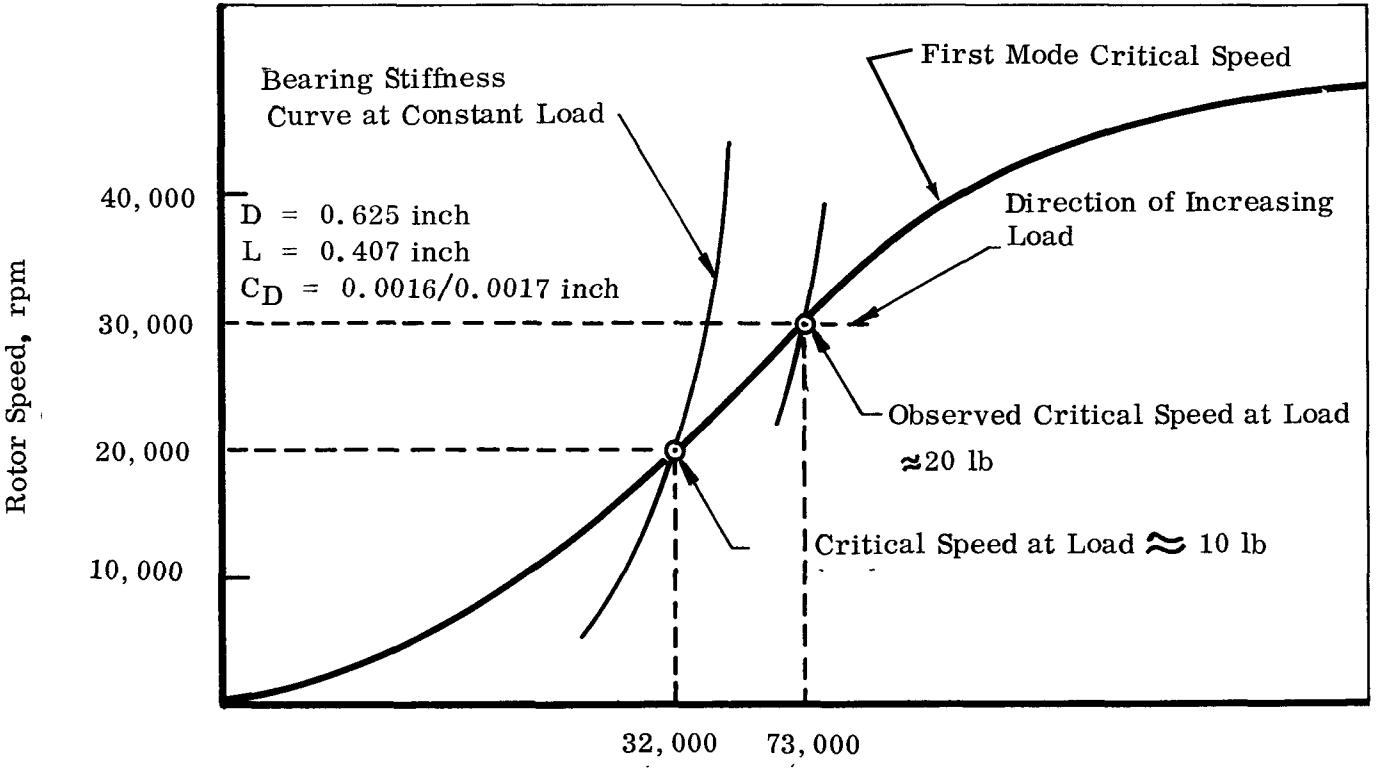

Figure 42. Critical Speed Characteristics of the Three-Sector Bearings BETR 1 Test Series

CONFIDENTIAL

Where:

K = fluid film stiffness, lb/in.

W = rotor weight acting on the bearing, lb

data points 16, 17 and 18 at 20,000 rpm and the photographs taken at these points of shaft dynamics revealed the presence of a resonance. From Figure 40 the slope of the load-deflection curve at the applied loads results in a fluid film stiffness (dW/de) of 32,000 lb/in. Applied to Equation 10, f_{cr} = 20,000 rpm, which verifies the presence of the first mode critical and the method for predicting the actual frequency.

While investigating bearing performance at 30,000 rpm, reading 26 also indicated a critical speed. The calculated fluid film stiffness at this point from the slope of the load-deflection curve was 73,000 lb/in. This resulted in a critical speed of 30,900 rpm which verified the observation.

Probe drift will not affect these calculations since analysis depends on ΔW and Δe. Absolute values are consequently not important. The presence of first mode bearing-rotor critical speeds is significant but readily explainable. The hybrid three-sector bearing has a controllable fluid film stiffness by virtue of its supply pressure. This or any bearing has a variable fluid film stiffness depending on the applied load and resultant deflection. The occurrence of two critical speeds is explained in Figure 42 for this particular bearing. At 20,000 rpm for a load of approximately 10 lb, the resultant bearing film stiffness of 32,000 lb/in. coincided with the stiffness required to satisfy the critical speed equation. Increasing speed at that load condition would have resulted in the curve indicated and no further critical speed. But at 30,000 rpm the speed was held constant while the load was varied, resulting in a horizontal displacement in the direction shown. The first mode critical speed, consequently, was encountered at a load of approximately 20 lb, resulting in a fluid film stiffness of 73,000 lb/in.

At 40,000 rpm no critical speed was encountered. The load-deflection curve indicates that the slope is too steep to result in a fluid film stiffness which satisfies the critical speed equation.

d. Stability

Half-frequency whirl was encountered at 20,000 rpm with shaft weight and 50 psig. The stability characteristics are shown in Figure 43. The stability characteristics established during the FRR 21 test are superimposed. The trends are identical, showing peak instability between 30,000 and 40,000 rpm. Figure 43 shows the considerable hysteresis area between stable and unstable operation. A stable shaft will remain stable at pressures (and loads) well below the level required to make an unstable shaft become stable. The generation of the attitude-eccentricity locus verifies the early assumption for the peak instability between 30,000 and 40,000 rpm. The attitude angle and subsequent restoring force for shaft weight is small in that speed range, while at 20,000 and 40,000 rpm the angle results in a larger restoring force.

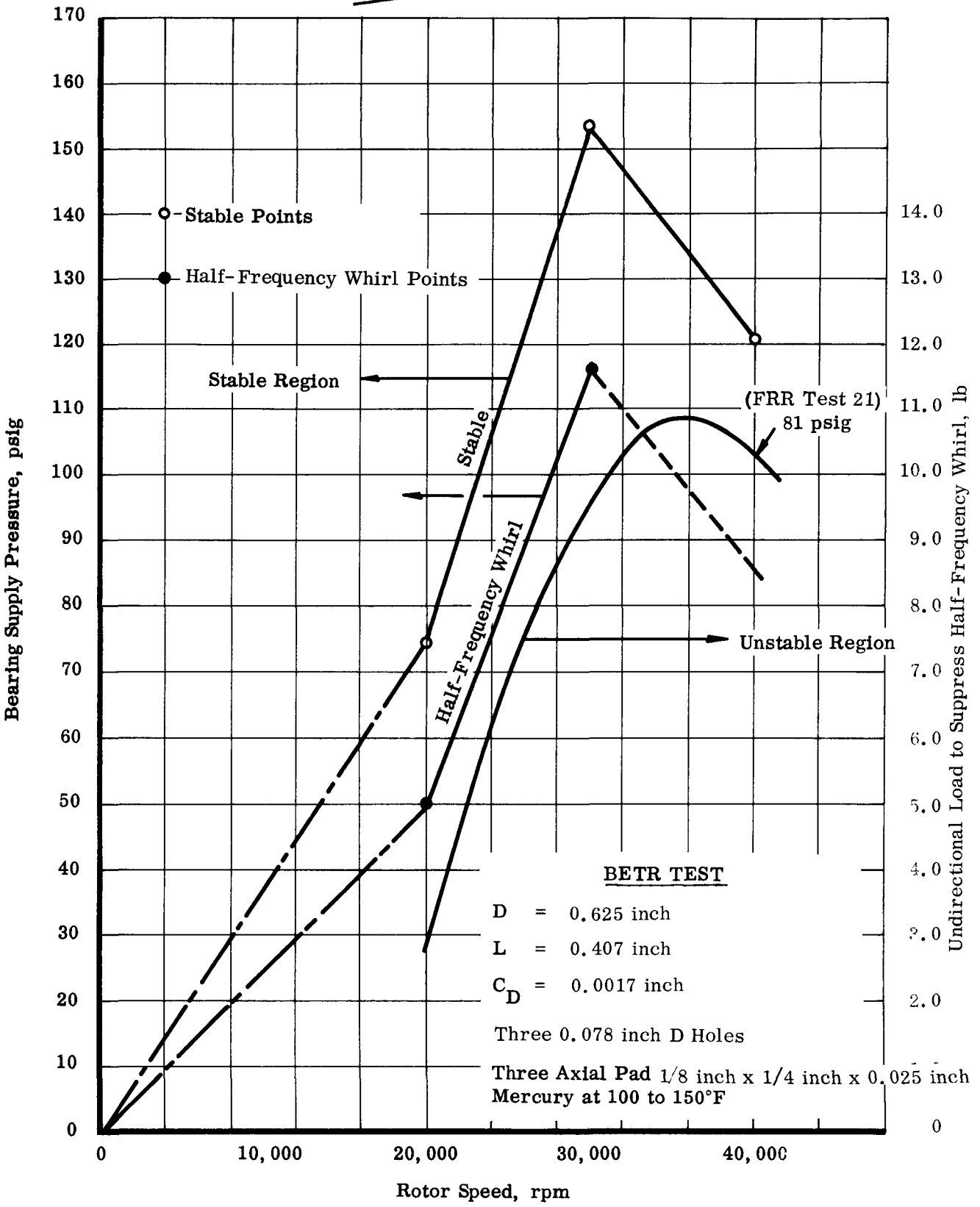

Figure 43. Stable and Unstable Operating Regions of Three-Sector Bearing as a Function of Bearing Supply Pressure and Unidirectional Load to Suppress Half-Frequency Whirl

e. Flow Characteristics

Previous flow data obtained for this clearance bearing were verified.

f. Conclusions on Test Series

The BETR 1 test objectives were successfully accomplished. The bearings were also supplied by the shaft-mounted pump at temperatures of 350 to 400°F. The capability of the new improved test fixture permitted larger unidirectional loads and determination of film thickness, attitude angle, flow-pressure, and power loss data. Improvements and temperature corrections to the shaft deflection measuring techniques must still be developed so that final data are accurate, useful, and descriptive of what is happening to the rotor and the bearing at all conditions. The three-sector bearing demonstrated a load capacity in excess of 70 lb.

8. BETR 2A

This performance test was conducted prior to a planned 1000 hour endurance run on the three-sector bearing used in BETR 1 but with a diametral clearance of 0.0022 inch.

a. Load Capacity

The load-deflection characteristics of this clearance bearing were reduced and compared with the 0.0016-inch bearing and predicted performance. Figure 44 shows the generalized performance of 0.0016-inch and 0.0022-inch clearance, uncompensated three-sector bearings compared to the predicted values.

For the 0.0016-inch clearance, bearing performance at 20,000 and 30,000 rpm (equivalent to Reynolds number of 3,250 and 4,900, respectively) is not significantly affected by Reynolds number in the manner predicted by Tao. In fact, at higher eccentricity ratios where hydrodynamic action predominates, it approaches the predicted turbulent performance based on the Smith and Fuller prediction. At lower eccentricity ratios, however, load capacity is greater than turbulent correction predicts, due to the hydrostatic contribution. At 40,000 rpm the effect of the higher Reynolds number, i.e., 6,500, is becoming apparent with the observed increased capacity. If the assumption is made that hydrostatic contribution is independent of speed (and for the uncompensated bearing this is a reasonable assumption), then the generalized results indicate that at sufficiently high speeds and Reynolds numbers, Tao's approach for plain bearings can be used with adequate modification for three-sector bearings.

For the 0.0022-inch clearance bearing, the Reynolds number and hydrostatic effects are clearer. For 20,000 rpm, i.e., Re = 4,500, the bearing performance correlates almost perfectly with laminar predictions. (Assumed viscosity for the predicted performance may have been too high to account for small variation at $\epsilon \rightarrow 0.7$.) A smaller hydrostatic component due to the large clearance and incomplete turbulent film at large eccentricity ratios explains this performance even though the Reynolds number is 4,500 (based on $\epsilon = 0$). For 30,000 and 40,000 rpm, i.e., Re = 6750 and 9000 respectively, the effect of Reynolds number is evidenced by the rapid increase in load capacity.

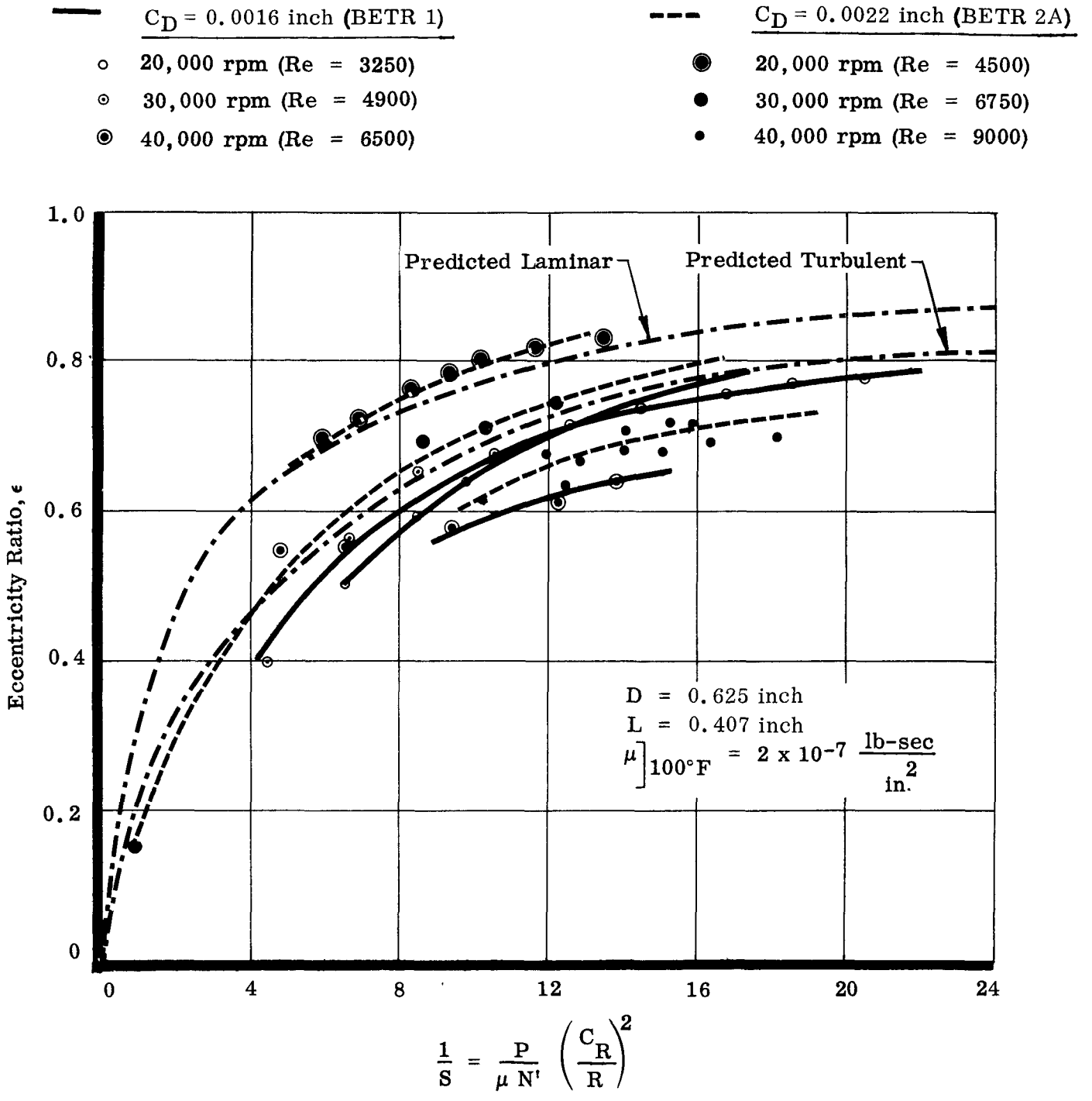

Figure 44. Generalized Experimental Performance Characteristics of Uncompensated Three-Sector Bearing

From Figure 44 the effect of the hydrostatic contribution on performance can be established. Tao's approach for a particular turbulent flow bearing results in a separate performance curve for each Reynolds number. For different bearings, so long as the combination of speed, diametral clearance, etc. results in the same Reynolds number, the predicted performance should be identical. Figure 44 shows that for the pressurized three-sector bearing this is not the case even though individual bearings are affected by Reynolds number. The difference in performance of equal Reynolds number is due to the hydrostatic contribution. For example, at 20,000 rpm the 0.002-inch clearance bearing has a Reynolds number of 4500 while at 30,000 rpm the 0.0016-inch clearance bearing has a Reynolds number of 4900, yet the capacity of the 0.0016-inch clearance bearing is considerably greater than that of the 0.0022-inch clearance bearing. The hydrostatic contribution increases with decreasing clearance expected.

b. Attitude-Eccentricity Locus

Figure 45 summarizes the attitude angle data generated during this test. Few data points were obtained at small eccentricity ratios because of the presence of half-frequency whirl. At 20,000 rpm the influence of pressure on increasing hydrostatic forces is shown for loading up. As pressure increases, the attitude angle becomes smaller. At 30,000 and 40,000 rpm this factor is not predominant since the hydrodynamic forces exceed the hydrostatic contribution. Much of the 40,000 rpm locus is estimated because of the lack of data at small eccentricity ratios. Figure 45 clearly demonstrates the larger locus loading up than down, indicating poor stability characteristics in the upward direction. (The bearing orientation in the rig is such that a supply pad exists 40 degrees from top dead center in the direction of rotation.)

c. Stability

The unidirectional loads required to suppress half-frequency whirl, loading both up and down, are shown in Figure 46. Loads required to suppress whirl loading up are much larger than those required when loading down. This verifies the statement above about the less favorable attitude angle in the upper quadrant. Stability characteristics of the 0.002-inch and 0.0017-inch clearance bearings are superimposed for comparison. Slightly lower unidirectional loads are required to suppress whirl for the 0.0022-inch bearing than are required for the 0.002-inch bearing, but considerably more unidirectional loads are required for the 0.0022-inch bearing than are required for the 0.0017-inch bearing.

d. Flow

Characteristics for this bearing were summarized and presented in Section II-Paragraph B-3.

9. Free Running Rig Test 18

This was the initial endurance test conducted on the three-sector uncompensated bearing. The primary objectives were to run "cold" for 100 hours and determine if the

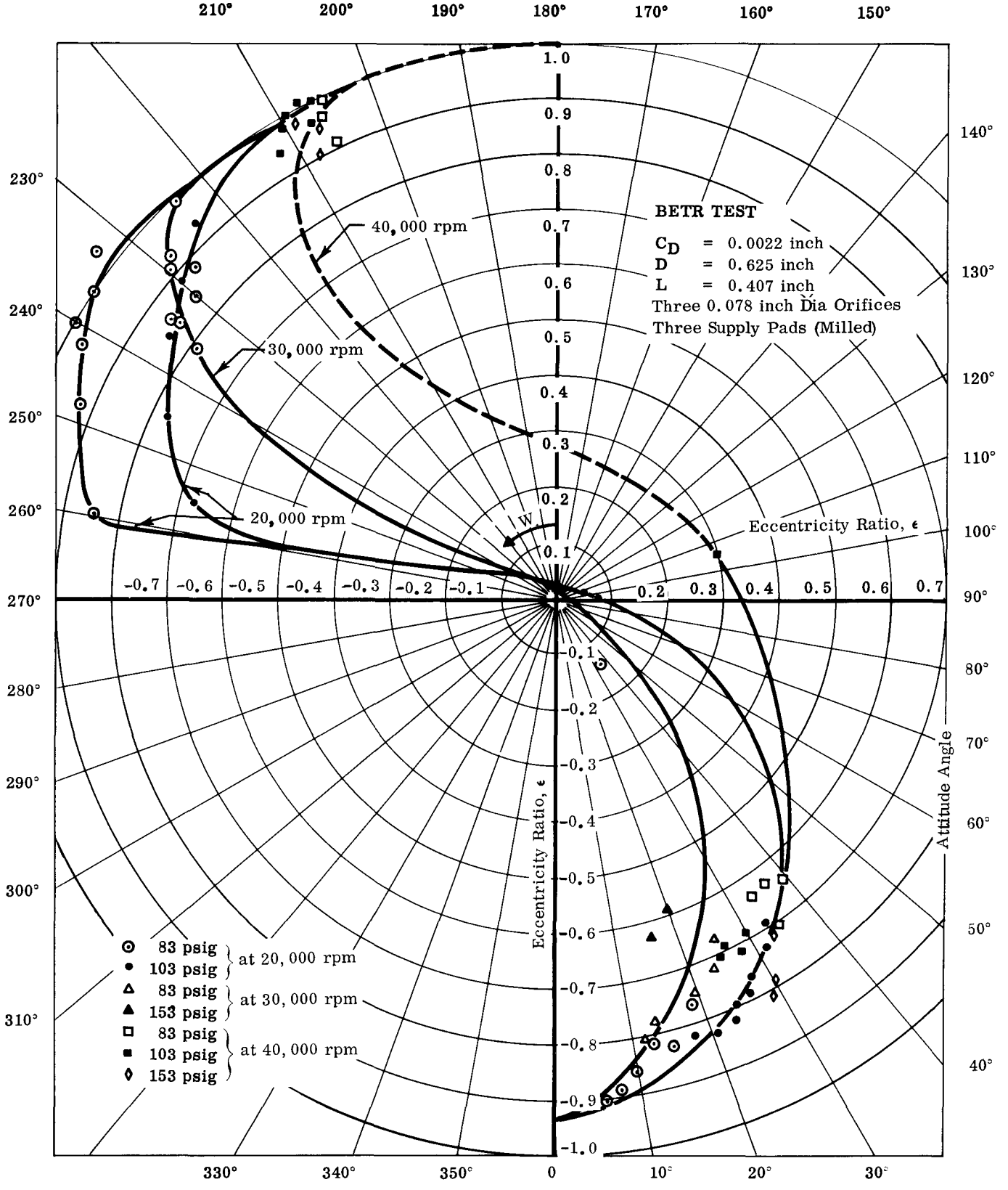

Figure 45. Attitude Eccentricity Locus for Three-Sector (120°) Bearing at 20, 30, and 40 Krpm BETR 2A Test Series

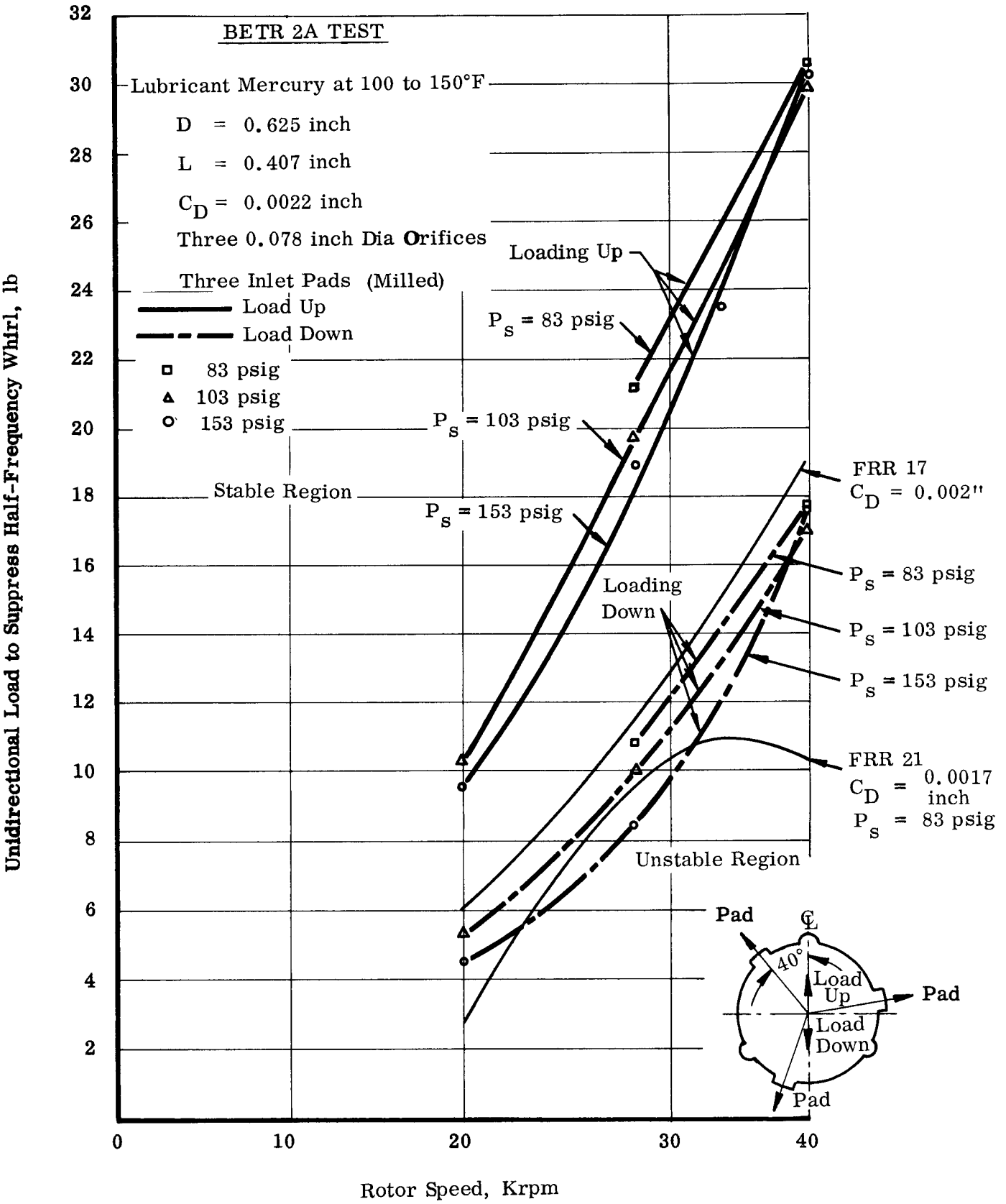

Figure 46. Unidirectional Load to Suppress Half-Frequency Whirl vs Rotor Speed for a Three-Sector Bearing at Supply Pressures of 83, 103 and 153 psig

three-sector bearing eliminated the problem of cavitation-erosion damage suffered by the plain journal bearing. The bearing had a diameter (D) of 0.625 inch, a length (L) of 0.407 inch, and a diametral clearance (C_D) of 0.002 inch. It contained nine 0.069-inch diameter inlet orifices and three 1/4-inch x 1/8-inch x 0.025-inch supply pads.

Initial requirements were to operate at rig maximum total unidirectional load of 35 lb/bearing plus 10 lb/bearing rotating load at 40,000 rpm. Consequently test conditions were:

Loads	
Unidirectional	35 lb/bearing
Rotational	10 lb/bearing
Speed	40,000 rpm
Lube temperature	cold (ambient)
Scheduled duration	100 hours

During the first five hours of the test, these conditions were maintained. This permitted stable operation at 40,000 rpm.

After five hours, the applied load was removed for the remaining 95 hours. Removal of the load resulted in unstable operation under the influence of shaft weight and a rotating load of 10 lb/bearing only.

The 100-hour objective was successfully achieved. Post-test flow calibration revealed no change in bearing characteristics, and the bearings themselves looked exceptionally clean.

10. BETR 2E

The primary objective of this endurance test was to obtain 1000 hours of operation on the uncompensated three-sector bearings at a lubricant supply temperature of 350°F. This test was a continuation of BETR 2A, which established the parametric performance. Dimensions remained unchanged, with the clearance at 0.0022 inch. The bearing material was BG-41 (modified 440C). A secondary objective was to establish the endurance performance of a package type jet-centrifugal pump combination which supplied bearing flow throughout the test. Radial and axial loads of 16.5 lb/bearing and 20 lb/bearing were imposed on the journal and thrust bearings, respectively, to simulate actual CRU loads.

It is important to recognize that only temperatures and loads were being simulated. It was not feasible to simulate such things as thermal gradients, a hermetically-sealed unit, or shaft dynamics. Consequently, final results are general and must be utilized with care, especially since nitrogen cover gas and air for the turbine drive were used.

The endurance test was terminated after accumulating 875 hours and 26 minutes. Of this time, 803 hours were continuous with a lubricant temperature of approximately 350°F. The premature termination was caused by a failed turbine bearing which was subsequently positively traced to lubricant starvation caused by the pump cavitating and losing prime. Pump cavitation and loss of prime were traced to an air leak in the sub-atmospheric jet pump inlet line.

Throughout the test the bearings were whirling at large, half-frequency amplitudes. Figure 46 shows that application of 16.5 lb/bearing radial load was marginal for stability. However, variation of 10 to 30°F in lubricant and turbine air inlet temperature was sufficient to result in stable operation. The thermal gradients and resultant decrease in radial clearance combined with the radial load was responsible for the stable operation during these temperature variations.

At times lack of nitrogen necessitated the use of air for cover gas. Failure of the vacuum drain pump during a portion of the test also resulted in flooded and atmospheric drains. Flow and pressures to the bearings and pump were maintained as follows:

Turbine bearing	6 to 8 lb/min at 75 to 100 psig
Alternator bearing	2 to 4 lb/min at 75 to 150 psig
Thrust bearing	4 to 10 lb/min at 75 to 100 psig
Pump flow	$\approx$ 40 lb/min at 350 to 375 psig

Temperatures were maintained as follows:

Lubricant inlet	350 $\pm$ 25°F
Alternator bearing surface	375 to 400°F
Turbine bearing surface	400 to 425°F
Alternator bearing housing	325 to 350°F
Turbine bearing housing	$\approx$ 350°F

For all intents and purposes, the package was at isothermal conditions. After 14 days the 20 lb axial load was removed when severe pump cavitation resulted in momentary loss in flow and an apparent rub on the thrust bearing.

The condition of the hardware after the test is shown in Figures 47 through 53. The alternator and turbine bearings were metallurgically inspected. Appendix H (Volume I) presents these findings. The endurance test and the rapid stop (seizure resulted in deceleration from 40,500 to 0 rpm in less than five seconds) left the alternator bearing in excellent condition. Some scratch marks are evident on the journal sleeves, but they are not significant enough to affect performance. Some corrosion product deposition (crud) was found in the supply pads, but it was also insignificant. The remainder of the bearing surface was free from this deposition, although some evidence of pitting upstream of

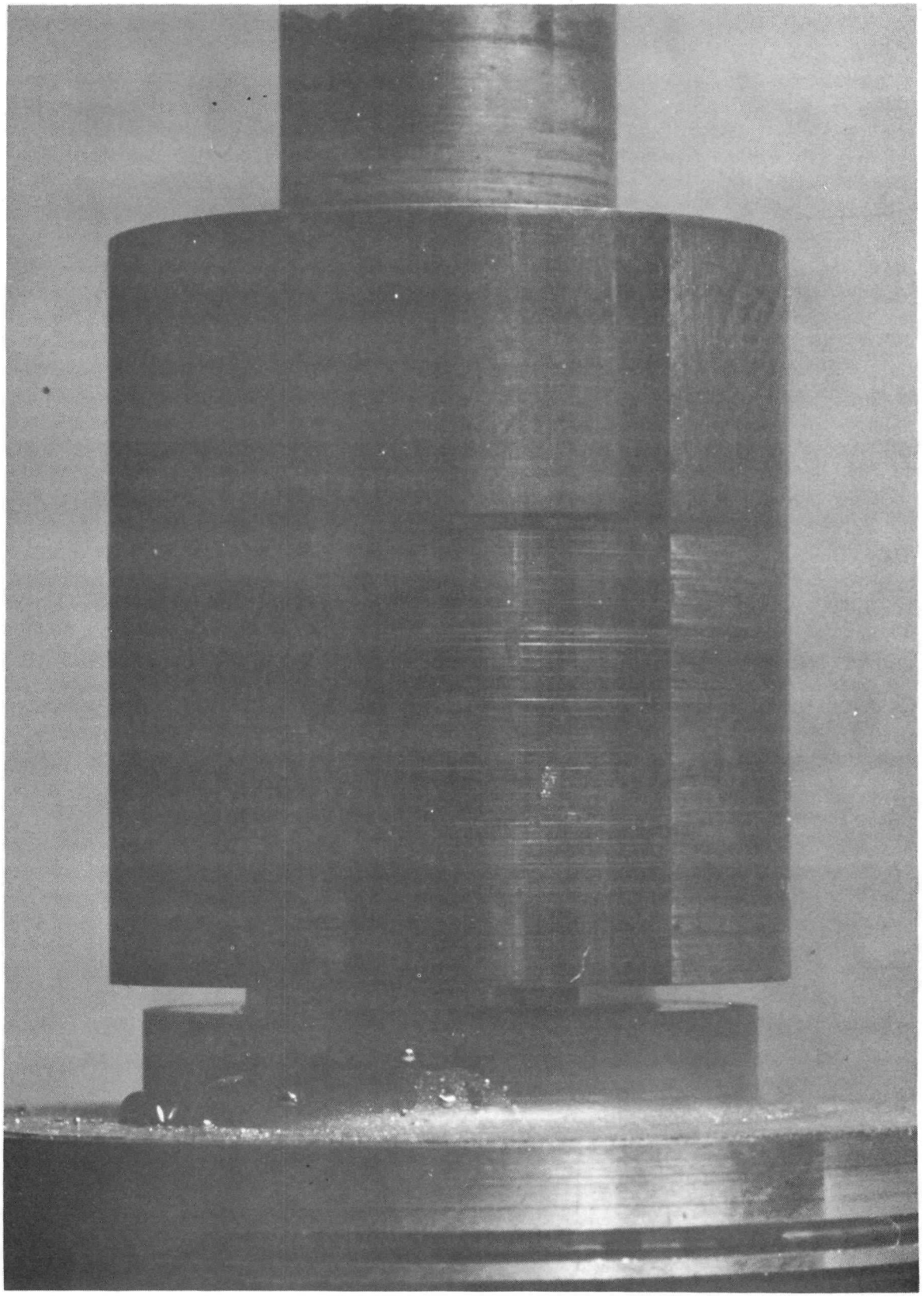

Figure 47. Three-Sector Alternator Journal Bearing After 875 Hours BETR 2E Test Series

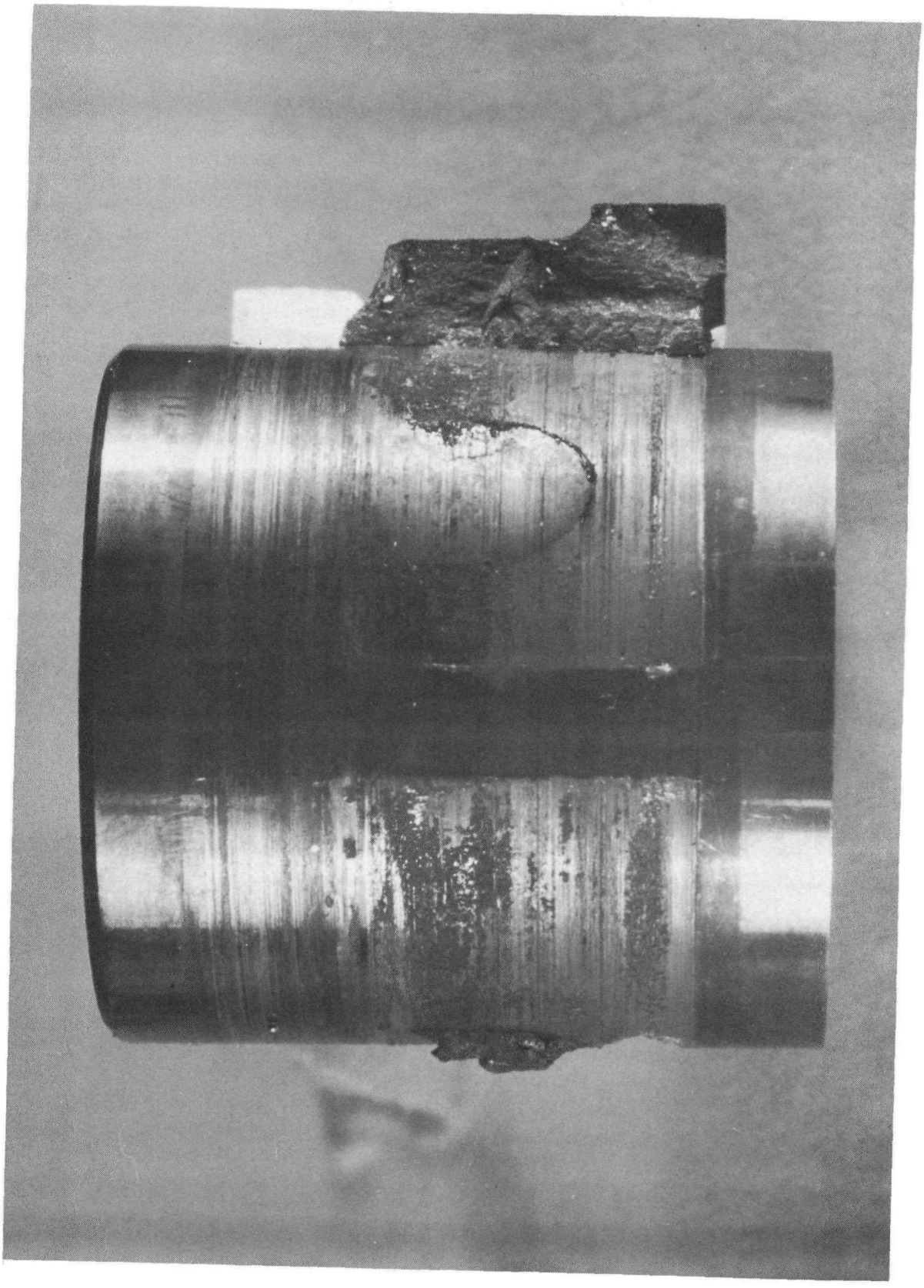

Figure 48. Three-Sector Turbine Bearing After 875 Hours BETR 2E Test Series

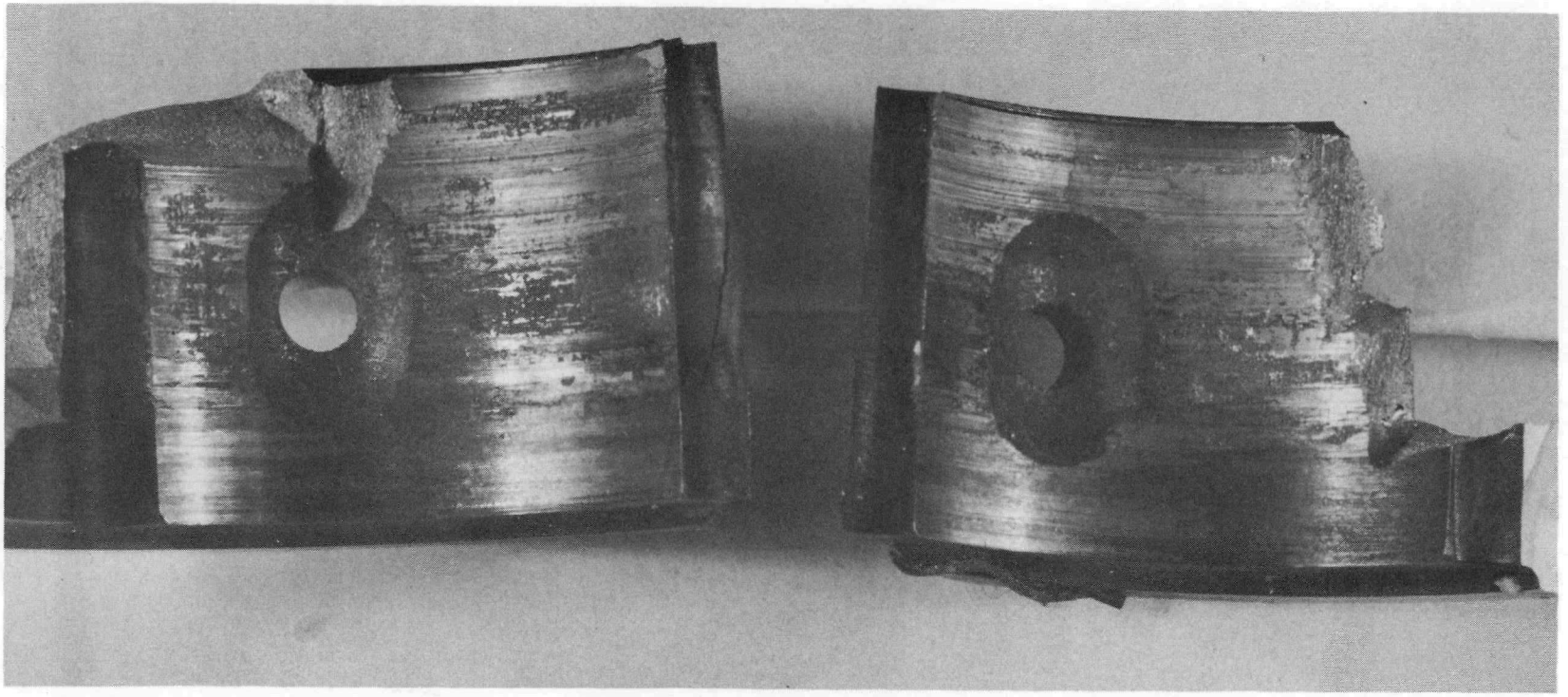

Figure 49. Three-Sector Turbine Bearing Bushing After 875 Hours

BETR 2E Test Series

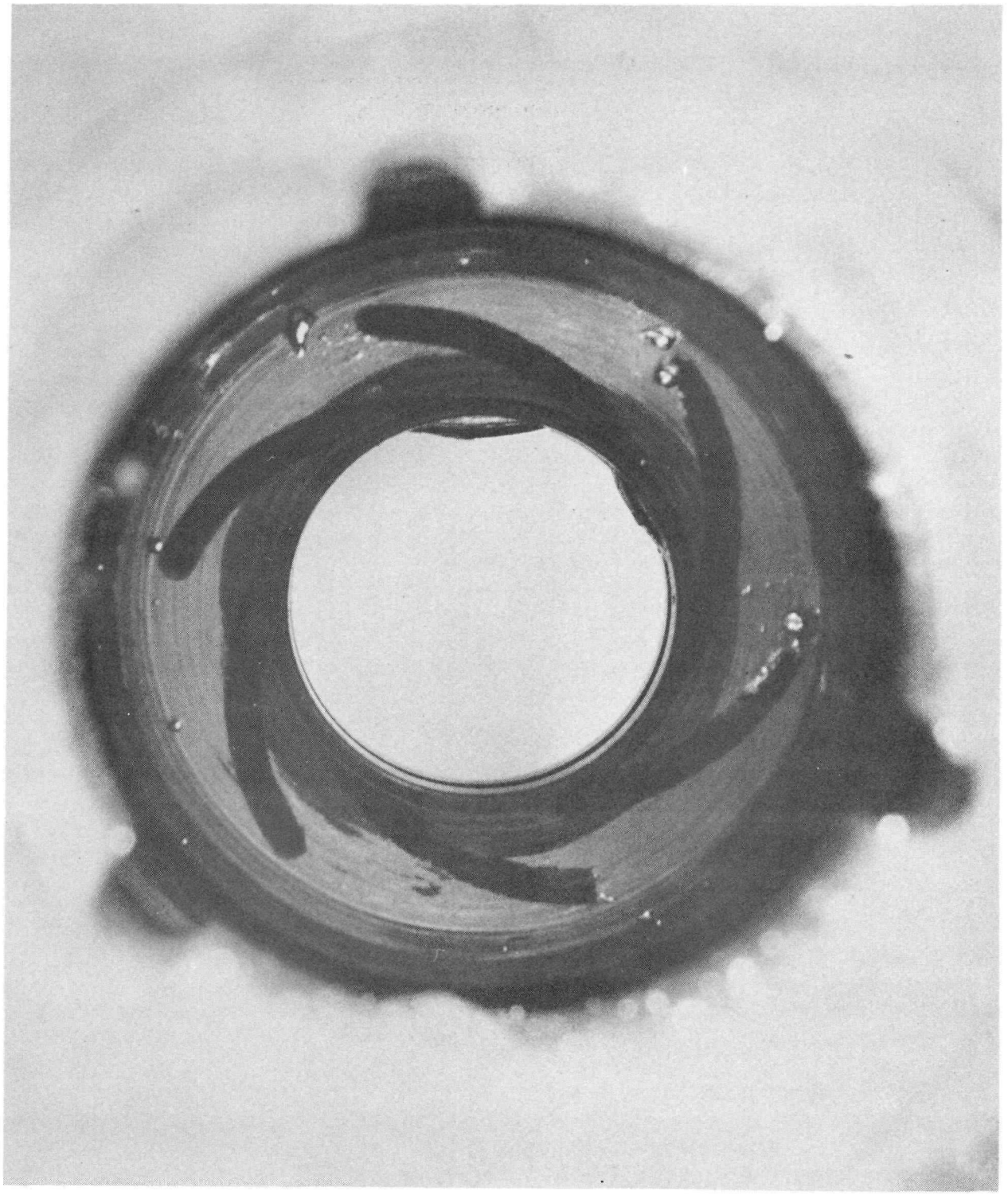

Figure 50. Spiral Groove Thrust Bearing After 875 Hours
BETR 2E Test Series

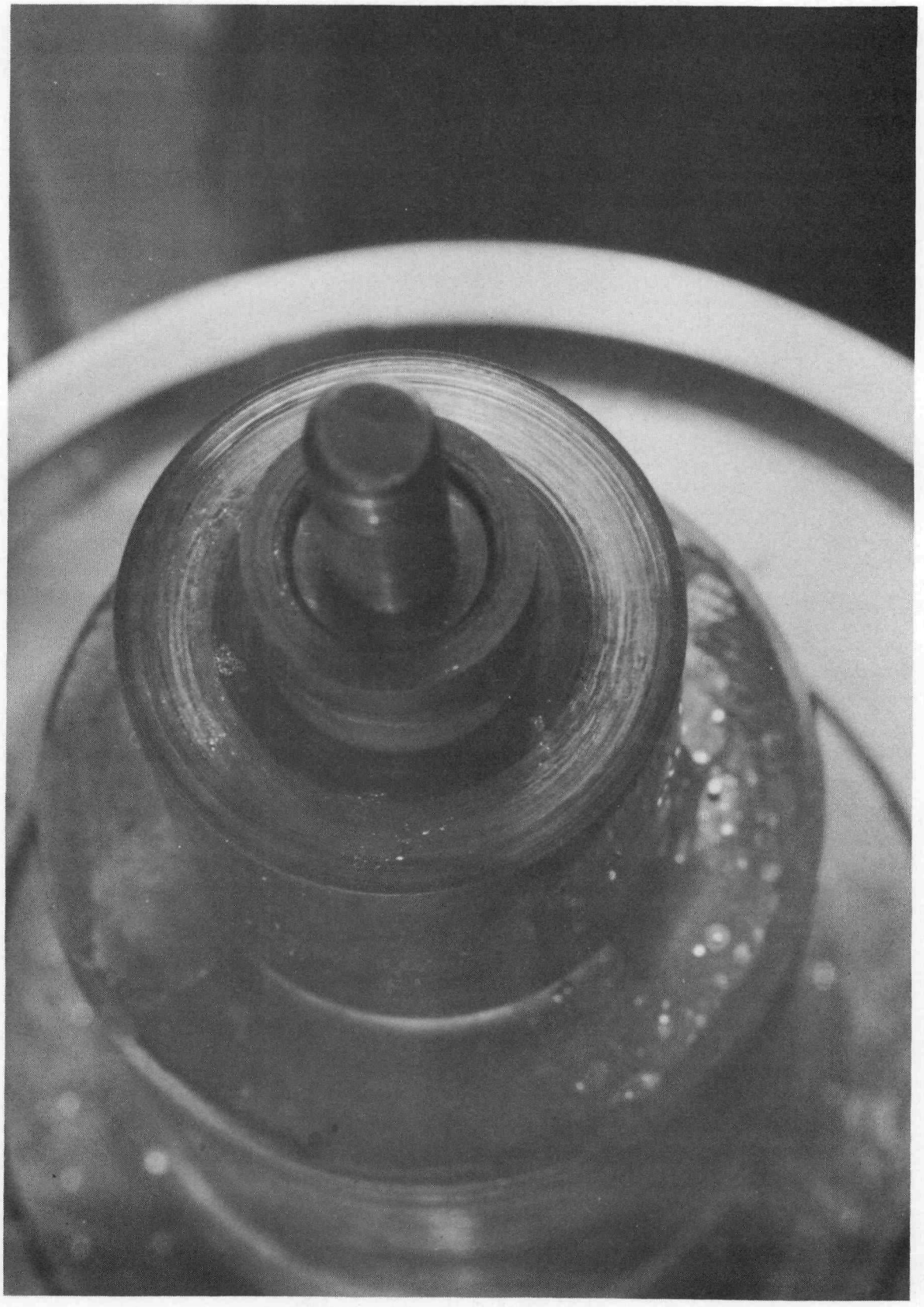

Figure 51. Thrust Bearing Surface After 875 Hours

BETR 2E Test Series

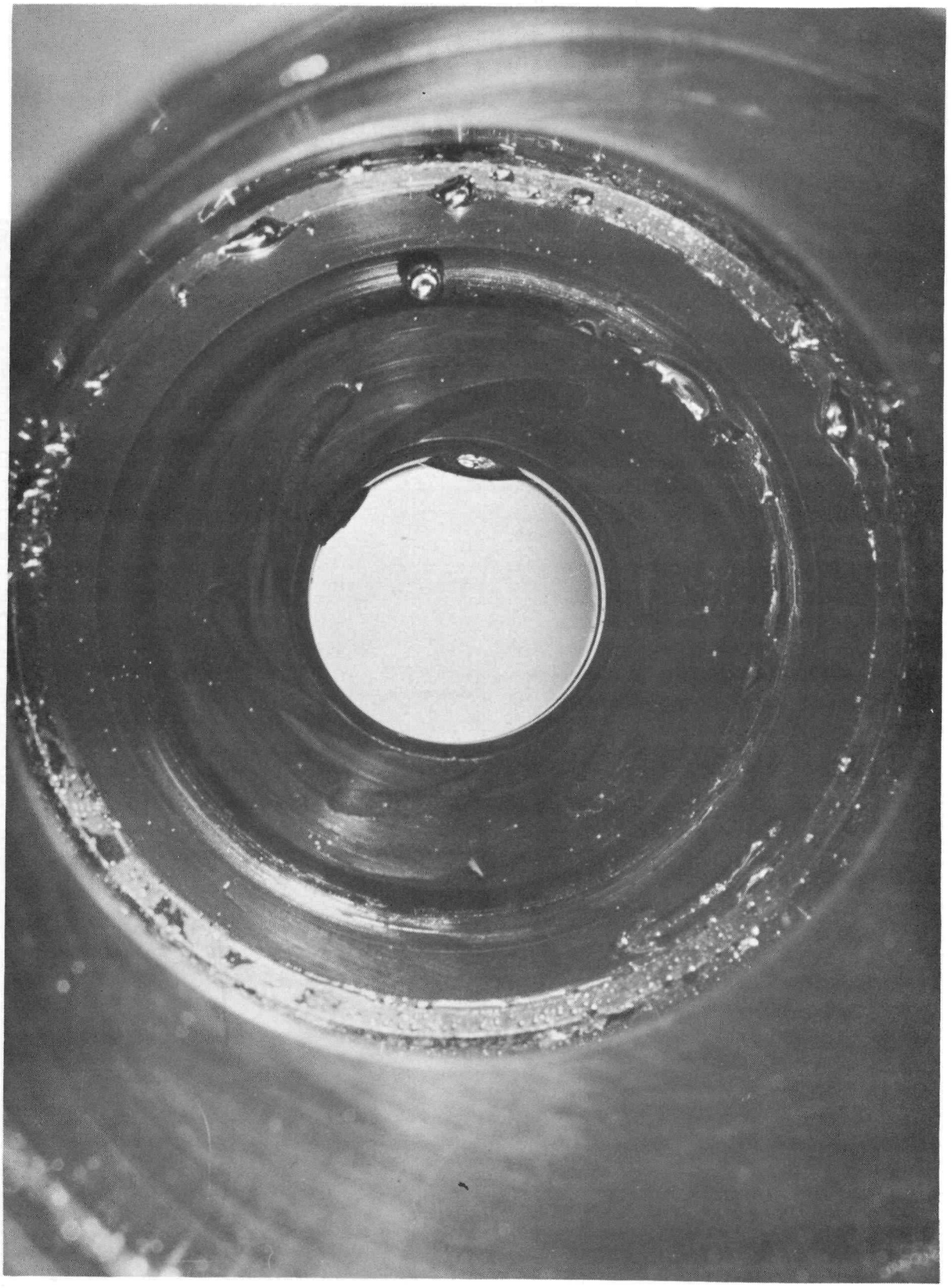

Figure 52. Spiral Groove Thrust Bearing After 875 Hours (Unloaded Side) BETR 2E Test Series

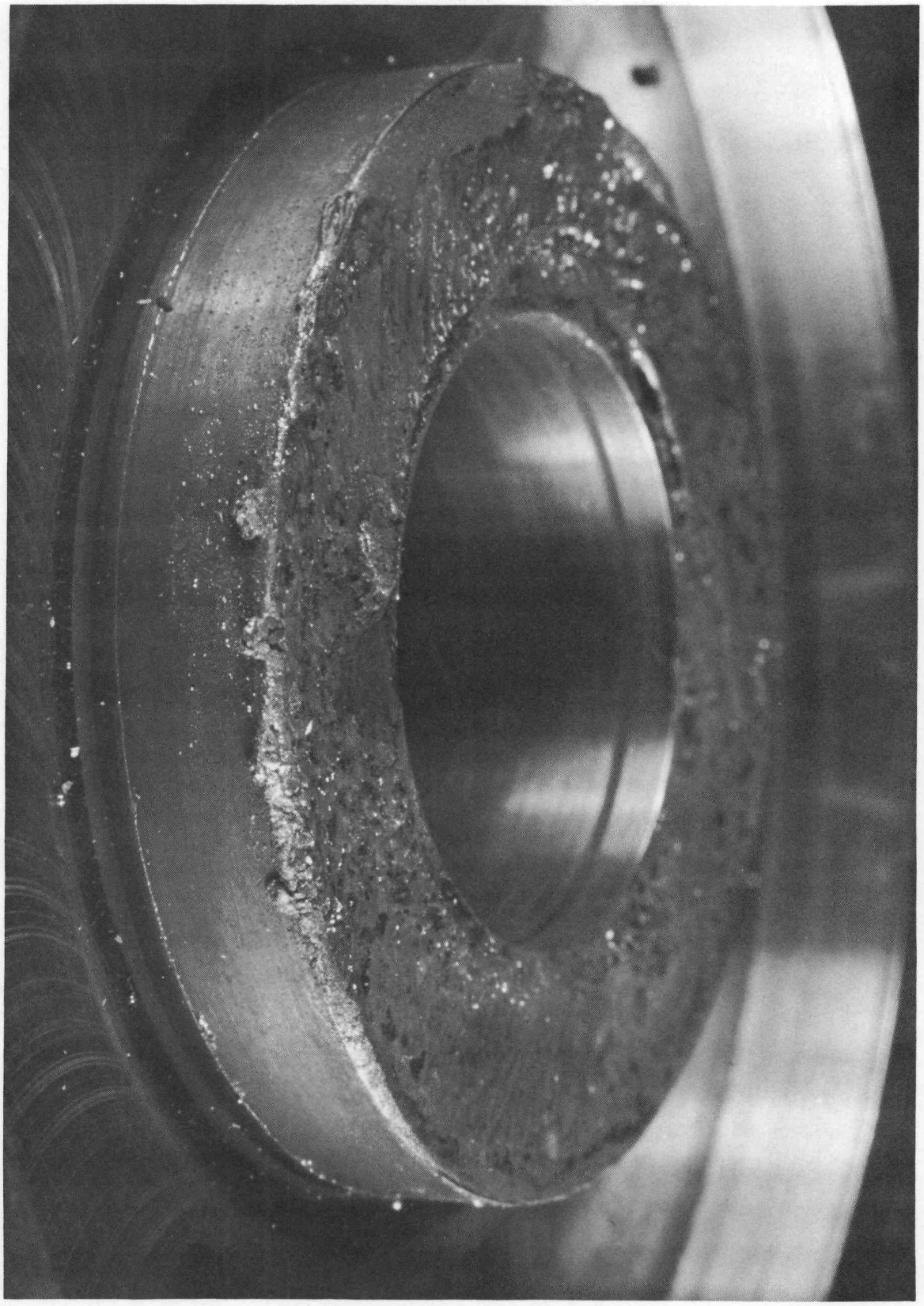

Figure 53. Corrosion Product Deposition on Turbine Housing (Pump End) After 875 Hours BETR 2E Test Series

the supply pads existed. No serious cavitation-erosion damage was discovered. Metallurigical inspection resulted in the conclusion that the bearing was capable of further operation in excess of 1000 hours without influencing performance.

Figures 48 and 49 show the typical welding between sleeve and bearing, respectively, that accompanies a seizure while operating at high speeds. The relatively large contact area is typical of the damage that occurs under the influence of lubrication starvation and high radial loads.

The scored (rubbed) thrust bearing surface is shown in Figures 50 and 51. Wear was only measurable in terms of tenths of thousandths as the remaining spiral grooves (originally 0.0005 to 0.001 inch deep) indicated. Wear is fairly even, indicating remaining load capacity as well as good alignment. The damage suffered on the loaded side verifies the suspicions originating during the test when flow was momentarily interrupted. The undamaged (unloaded) side of the thrust bearing is shown in Figure 52. The edges are sharp and the surface is generally good. No large deposits of crud (corrosion products) were noted.

Figure 53 shows a considerable quantity of corrosion products deposited in a stagnant or "dead" area of the fixture. This brittle-hard deposit had to be chipped off since it adhered tenaciously to the surface. The air leaks and the nitrogen and air used during this test are probably due to this accelerated crud formation.

Conclusions on Test Series

Although the 1000-hour objective was not achieved, some positive conclusions could be made as a result of the abbreviated test.

1. The three-sector bearing is capable of mercury operation in excess of 1000 hours at elevated temperatures (350°F) with half-frequency whirl present.

2. Isothermal conditions with a 0.0022-inch clearance bearing will lead to half-frequency whirl; without unidirectional loads, the whirl amplitude may exceed safe limits for satisfactory bearing operation.

3. Cavitation-erosion damage was not evident even though the conditions (large amplitudes of shaft motion in the bearing due to whirl) were present.

C. PROGRAM II - INDIVIDUALLY FED THREE-SECTOR BEARING (BETR 3)

The previous test series demonstrated the capability of the uncompensated three-sector bearing in meeting the CRU requirements, except for stability. Stability could be achieved by using a clearance modulus $m = C_D/D = 0.0016$ in./in. This represents a relatively large clearance for laminar flow bearings where m is usually 0.001 in./in. However, because of the turbulent conditions in the bearing clearance space, it was difficult to force sufficient lubricant through the 0.001-inch clearance bearing at the

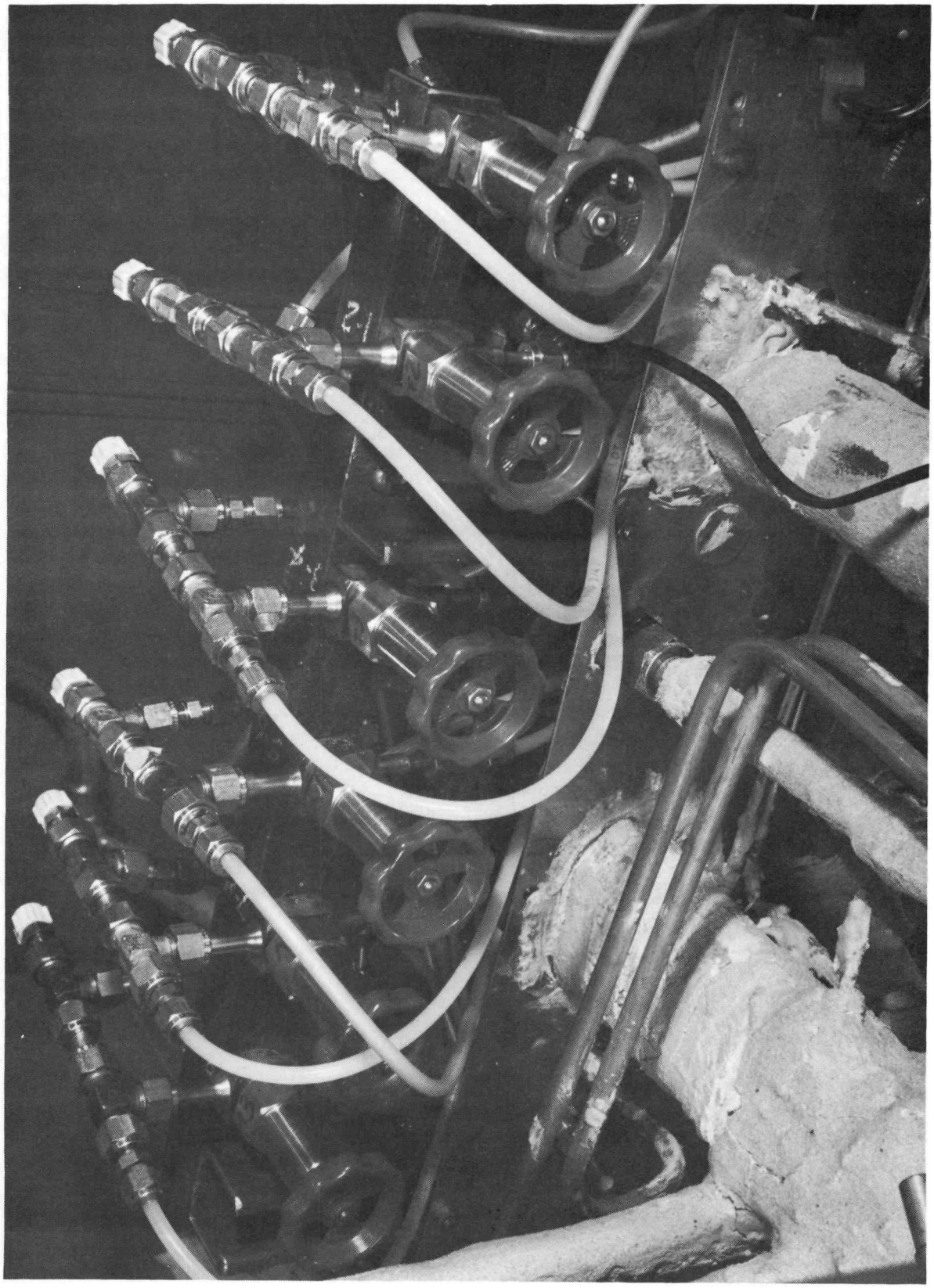

Figure 54. Flow Control Arrangement for BETR 3 Test Series

available pressures. In addition, the flow through the uncompensated bearing was sensitive to shaft position, indicating that flow starvation was possible if the shaft was displaced to a large eccentricity ratio.

The following test was conducted to establish the flow division between the three supply pads as a function of shaft position; to establish bearing performance,keeping supply pressure constant to each pad but letting flow vary; and to establish bearing performance,keeping flow constant to each pad while letting pressure vary. It was designated as the "individually fed bearing" since flow and pressure could be individually controlled to each of the three-sectors for both journal bearings. The flow control arrangement, individual flow regulation to each sector by manual valves, is shown in Figure 54. This bearing had a diameter of 0.625 inch, a length of 0.407 inch,and a diametral clearance of 0.001 inch. It contained one 0.078-inch diameter orifice and one 1/4-inch x 1/8-inch x 0.030-inch deep supply pad per sector.

The test program was conducted in two separate phases. The first phase maintained constant pressure to each sector while letting flow vary. The second phase maintained constant flow to each sector by adjusting supply pressures as required. In addition,the experimental program was divided into two parts: static and dynamic performance determinations. A summary of the test is shown below:

1) Static

Transfer pump mercury supply

a) Flow calibration constant flow, each pad of 1, 1.5, 2, and 2.5 lb/min

b) Flow calibration, constant pressure, each pad of 50, 75, 100, 125, 150, 175, 200, 225, 250, and 275 psig

c) Spring rate, constant pressure, each pad of 100, 150,and 200 psig

d) Spring rate constant flow, each pad of 0.75, 1, and 1.5 lb/min

2) Dynamic

Transfer pump mercury supply

a) Spring rate, constant flow, each pad of 0.75, 1, and 1.5 lb/min at 20,000 rpm; 0.75, 1, and 1.25 lb/min at 30,000 and 35,000 rpm

b) Spring rate constant pressure, each pad of 150, 200, and 300 psig at 20,000 rpm; 250, 300, and 350 psig at 30,000 and 35,000 rpm (plus 475 psig at 35,000 rpm)

c) Speed decay constant pressure of 530 psig from 36,000 rpm

d) Flow calibration, lapp pump supply constant pressure at 20,000, 30,000; 35,000; and 40,000 rpm

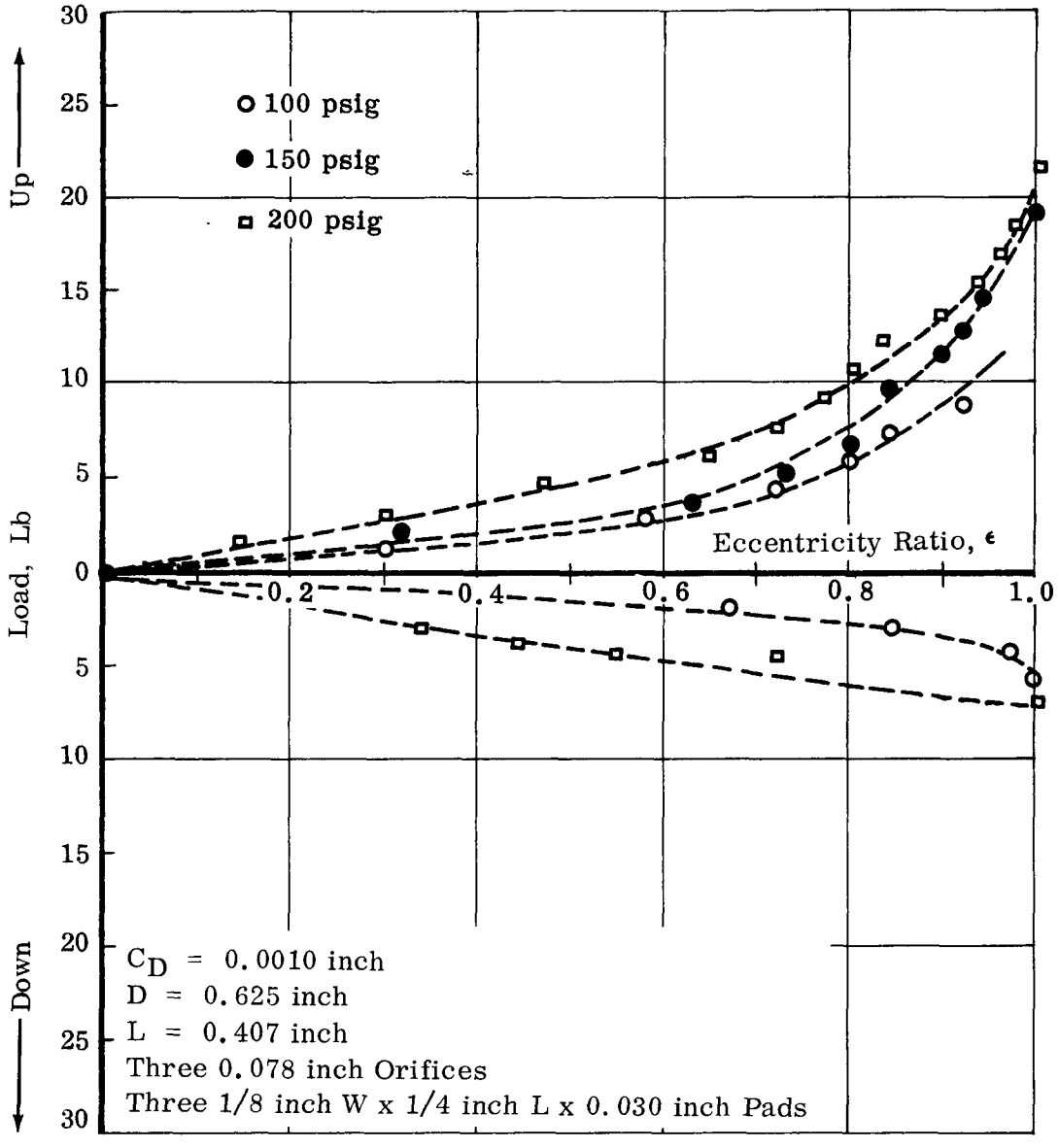

Figure 55. Static Load Deflection Characteristics at Constant Pressure (Flow Variable)

BETR 3 Test Series

Load-deflection data from which spring rate performance is established could not be obtained at 40,000 rpm because of rig flow-pressure limitation. Attitude-eccentricity data were obtained at all of the above points as well as flow pressure characteristics as influenced by applied unidirectional load.

1. Load-Deflection Characteristics

Figures 55, 56, and 57, show load capacity at zero; 20,000; and 30,000 rpm, respectively, for constant pressure to each supply pad, letting flow vary at will. Dynamically and at large deflections, the decreased load capacity loading up into an axial groove is evident from these figures. Since the bearing is predominantly hydrodynamic at large eccentricity ratios (see below) this is to be expected. Figure 58 presents a composite of the above data. At constant pressure the pressurized three-sector bearing behaves predominantly like a hydrodynamic bearing with a weak hydrostatic influence at eccentricity ratios below 0.5. Increasing supply pressure does not improve load capacity appreciably, but this is typical of an uncompensated bearing. Figure 59 presents the performance summarized in Figure 58 in generalized 1/S vs ϵ form. At constant supply pressure, the load capacity agrees well with that predicted by laminar hydrodynamic theory over the entire range of speeds and loads evaluated. This is significant since it verifies the assumptions made in the initial analysis (which neglected hydrostatic influence) and the work of Smith and Fuller on plain journal bearings. At 20,000 and 30,000 rpm, the Reynolds numbers are approximately 2,030 and 3,050, respectively, which is generally considered well into the turbulent regime for pipe flow. However, at constant pressure the performance of the 0.001-inch clearance bearing was not affected by Reynolds number nor did it behave as Tao's analysis predicted. Just as Smith and Fuller established that performance of a plain bearing can be predicted satisfactorily by laminar methods up to speeds of five times the value at which laminar shear flow becomes unstable, so it appears the performance of a three-sector bearing with pressurized inlet can be predicted as long as it is uncompensated and the Reynolds number is below 3,000. At larger Reynolds numbers, i.e., higher speeds or larger clearances or with orifice compensation, this assumption may not be valid.

Figures 60, 61, and 62 show the load capacity at zero; 20,000; and 30,000 rpm, respectively, while maintaining flow constant to each sector and adjusting the supply pressure to maintain these conditions. The predominantly hydrostatic characteristics of this bearing (see below) at low speeds and small eccentricity ratio are verified by the almost equal load capacity regardless of applied load direction. Figure 63 presents a composite of the above data. These figures show clearly that for constant flow the performance approaches that of a hydrostatic bearing. The method used to maintain flow constant from each pad simulates the condition of perfect compensation, so this behavior is to be expected. Load capacity varies linearly with displacement and increases with supply pressure (in this case, increased flow to each sector) as in the hydrostatic bearings. As the speed increases and larger loads are applied, hydrodynamic action increases which in part explains the increased load capacity for constant flow and the smaller spread between deflection characteristics at a fixed speed as flow is increased. The three-sector uncompensated bearing under these conditions becomes

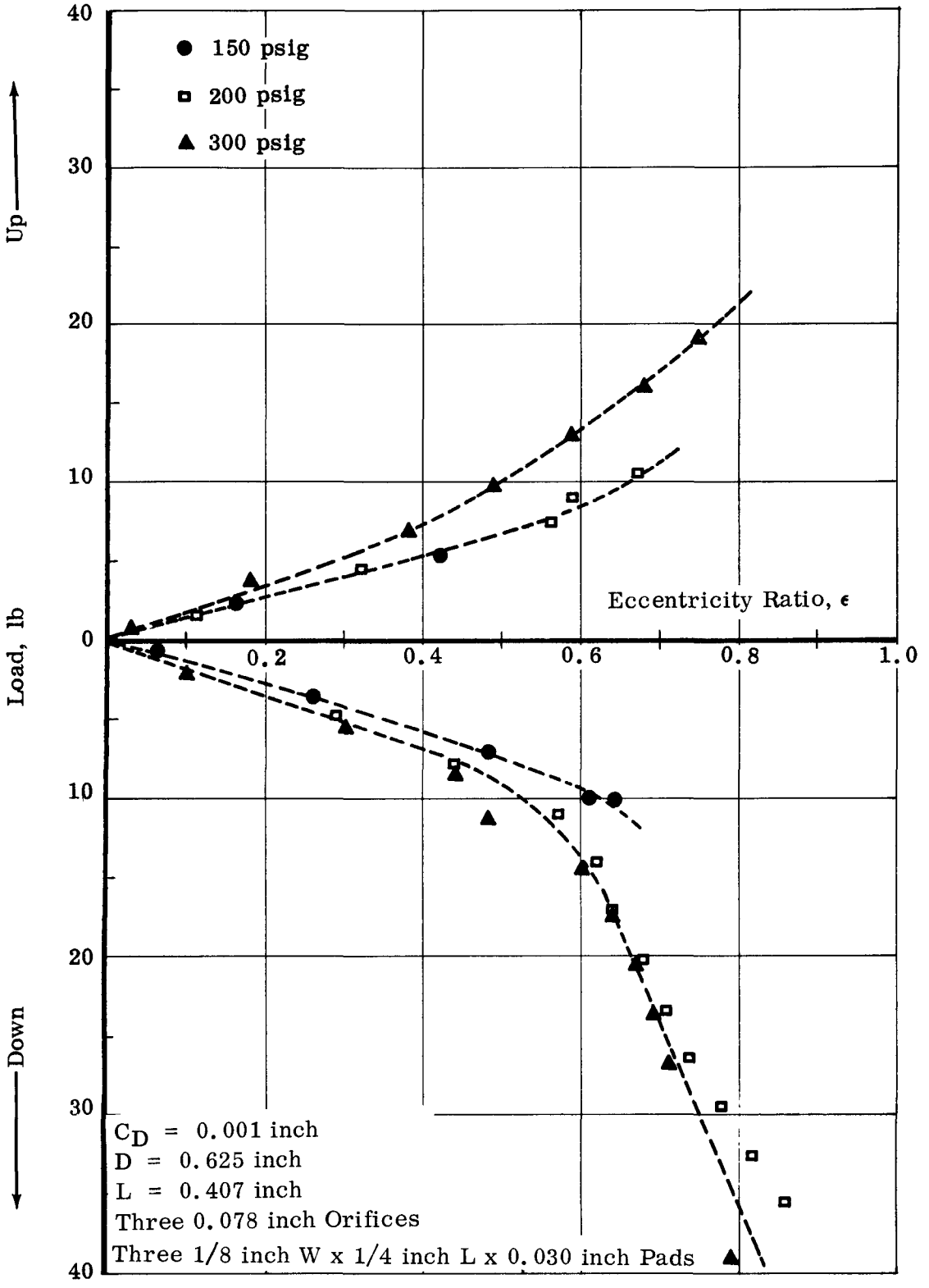

Figure 56. Dynamic Load Deflection Characteristics at 20,000 rpm and Constant Pressure (Flow Variable)

BETR 3 Test Series

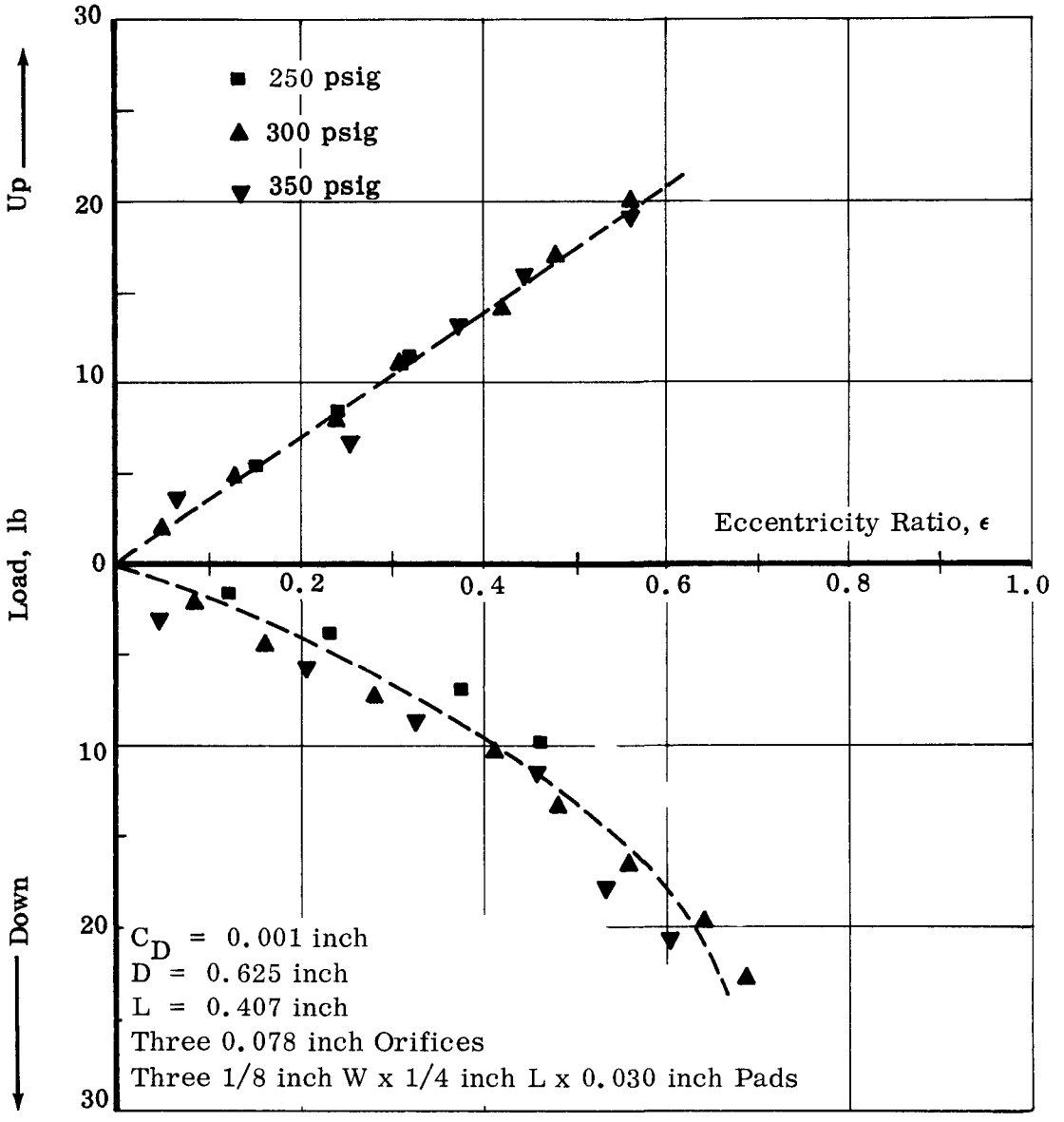

Figure 57. Dynamic Load Deflection Characteristics at 30,000 rpm and Constant Pressure (Flow Variable)

BETR 3 Test Series

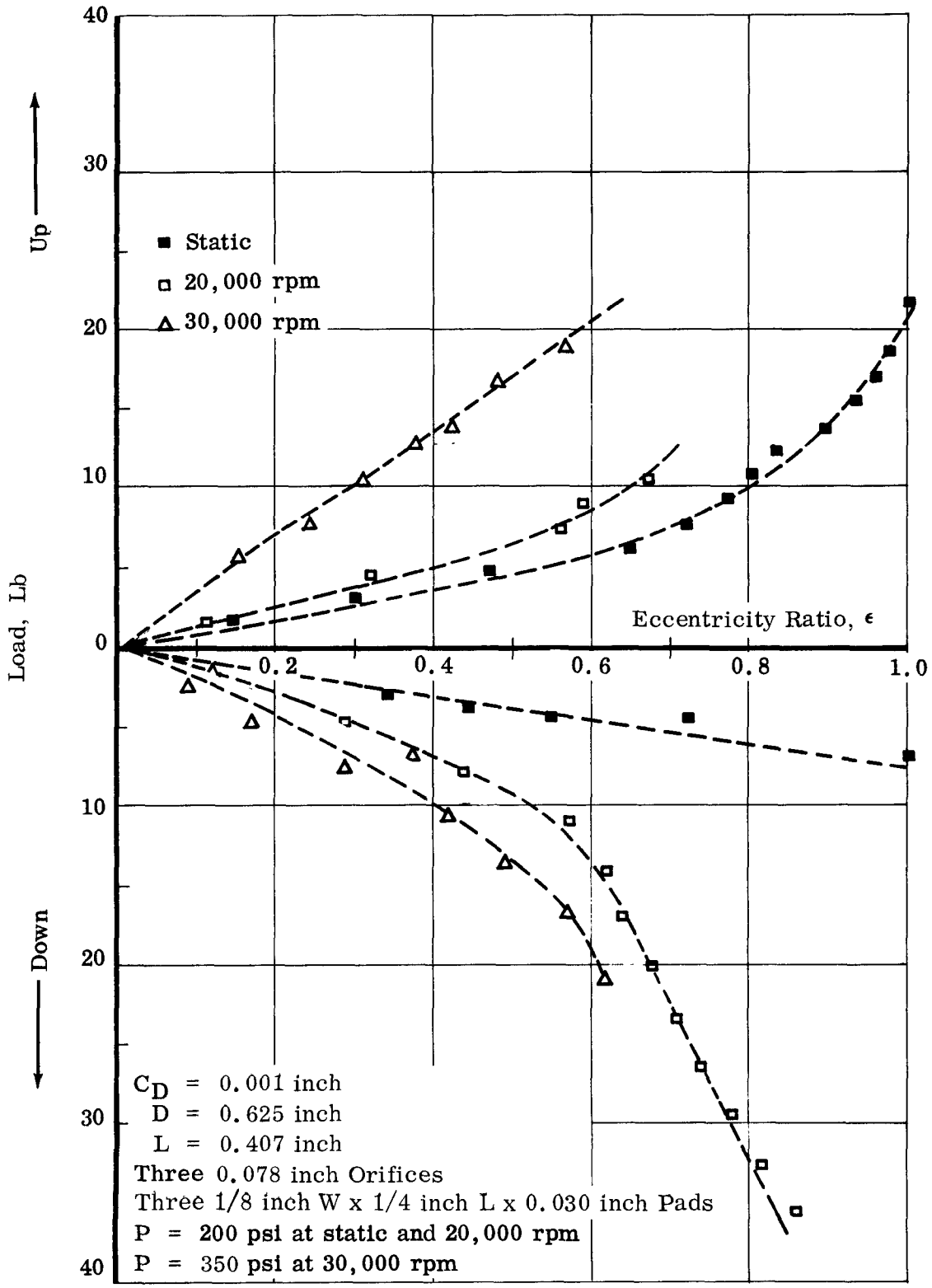

Figure 58. Static and Dynamic Load Deflection Characteristics with Variable Flow

BETR 3 Test Series

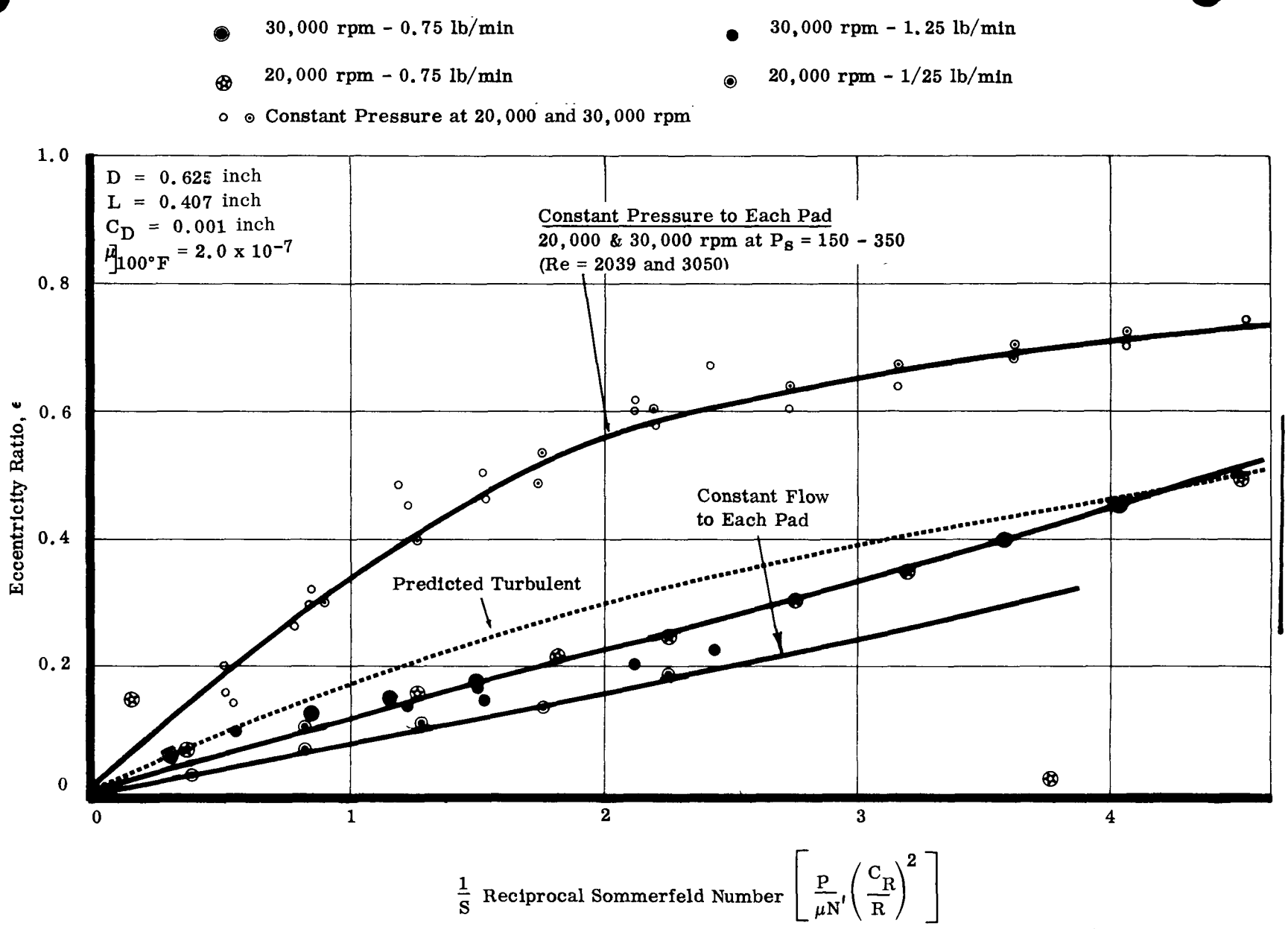

Figure 59. Experimental Results Compared to Predicted Performance for Three-Sector Bearing (L/D = 0.65)

BETR 3 Test Series

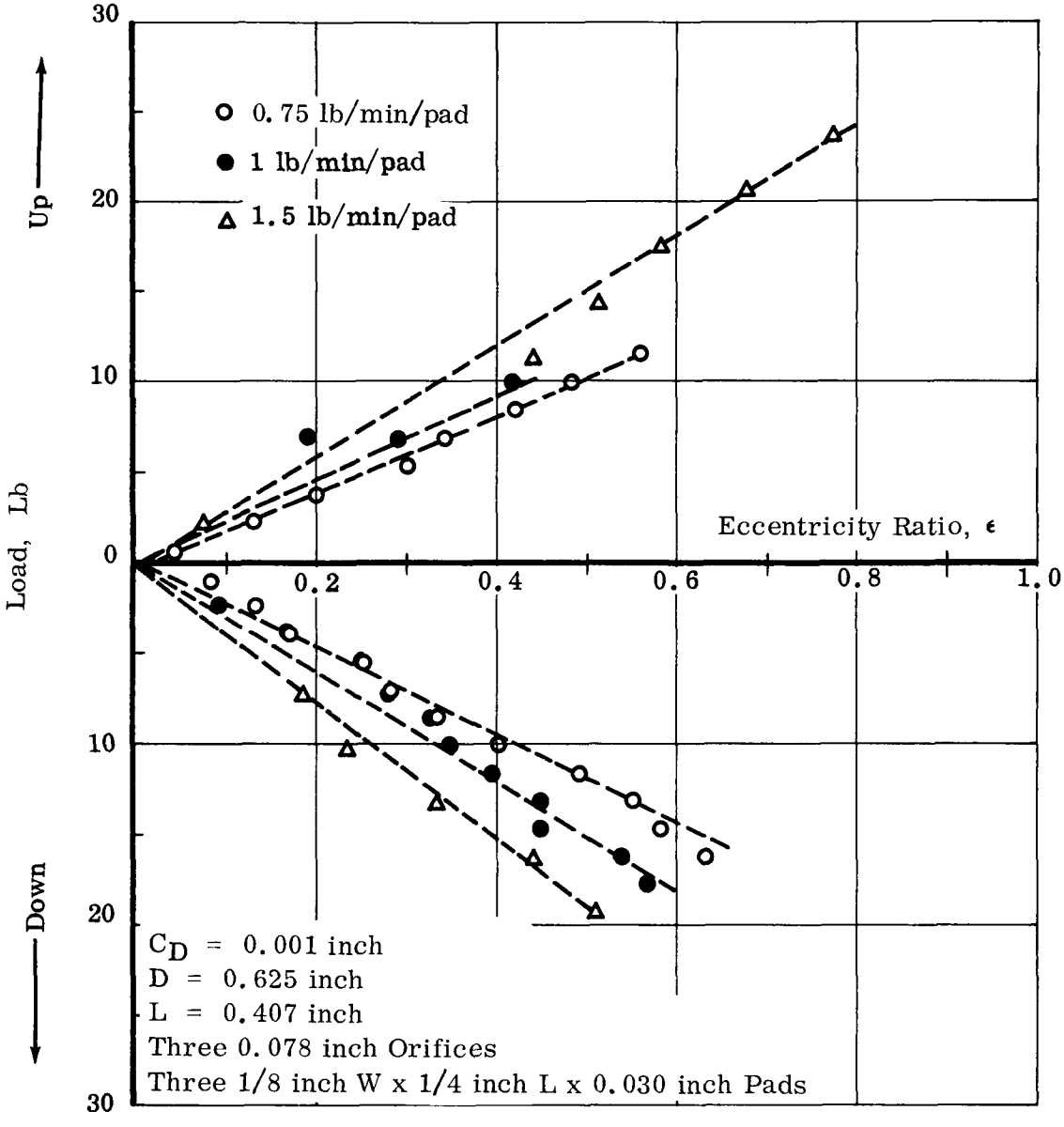

Figure 60. Static Load Deflection Characteristics at Constant Flow (Pressure Variable)

BETR 3 Test Series

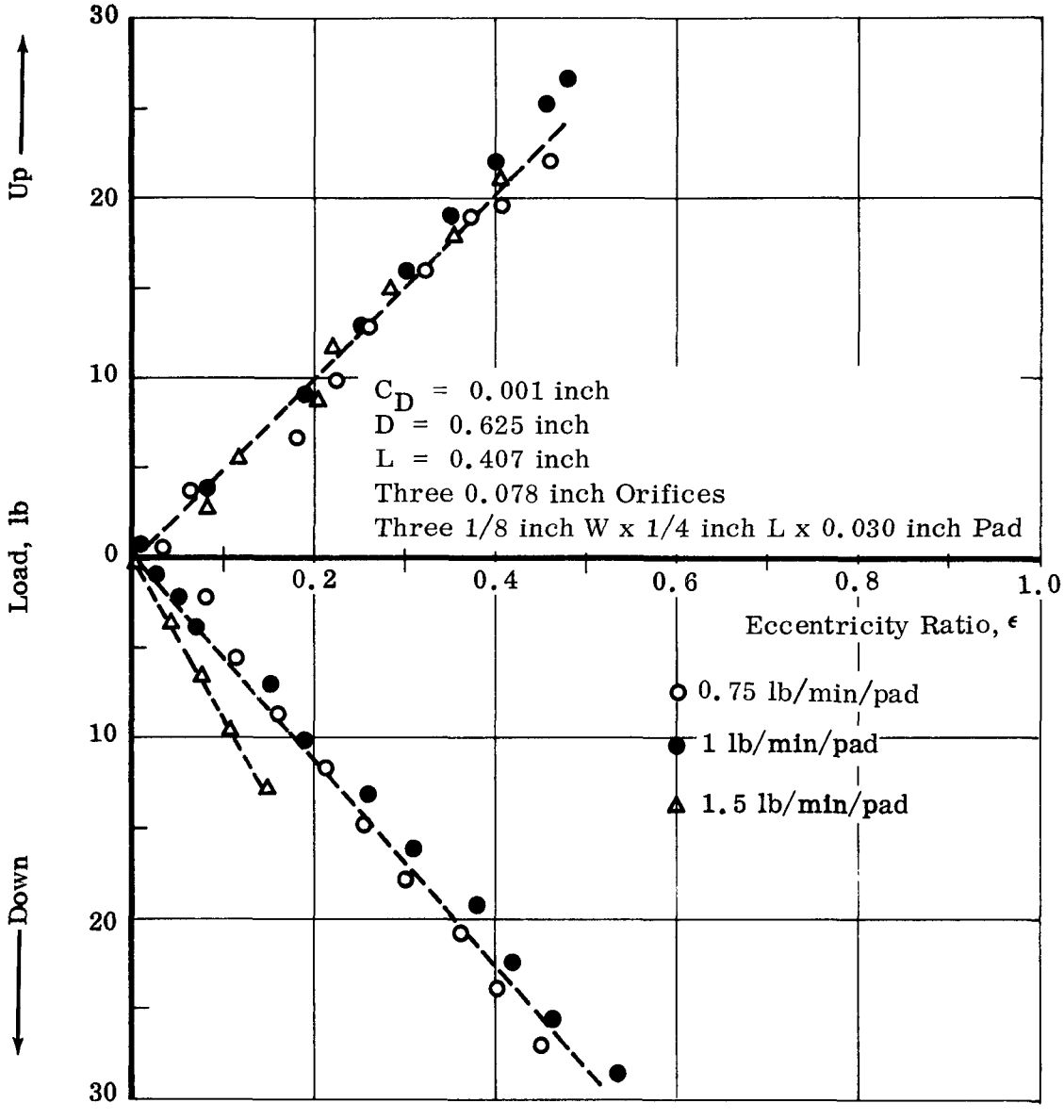

Figure 61. Dynamic Load Deflection Characteristics at 20,000 rpm and Constant Flow (Pressure Variable)

BETR 3 Test Series

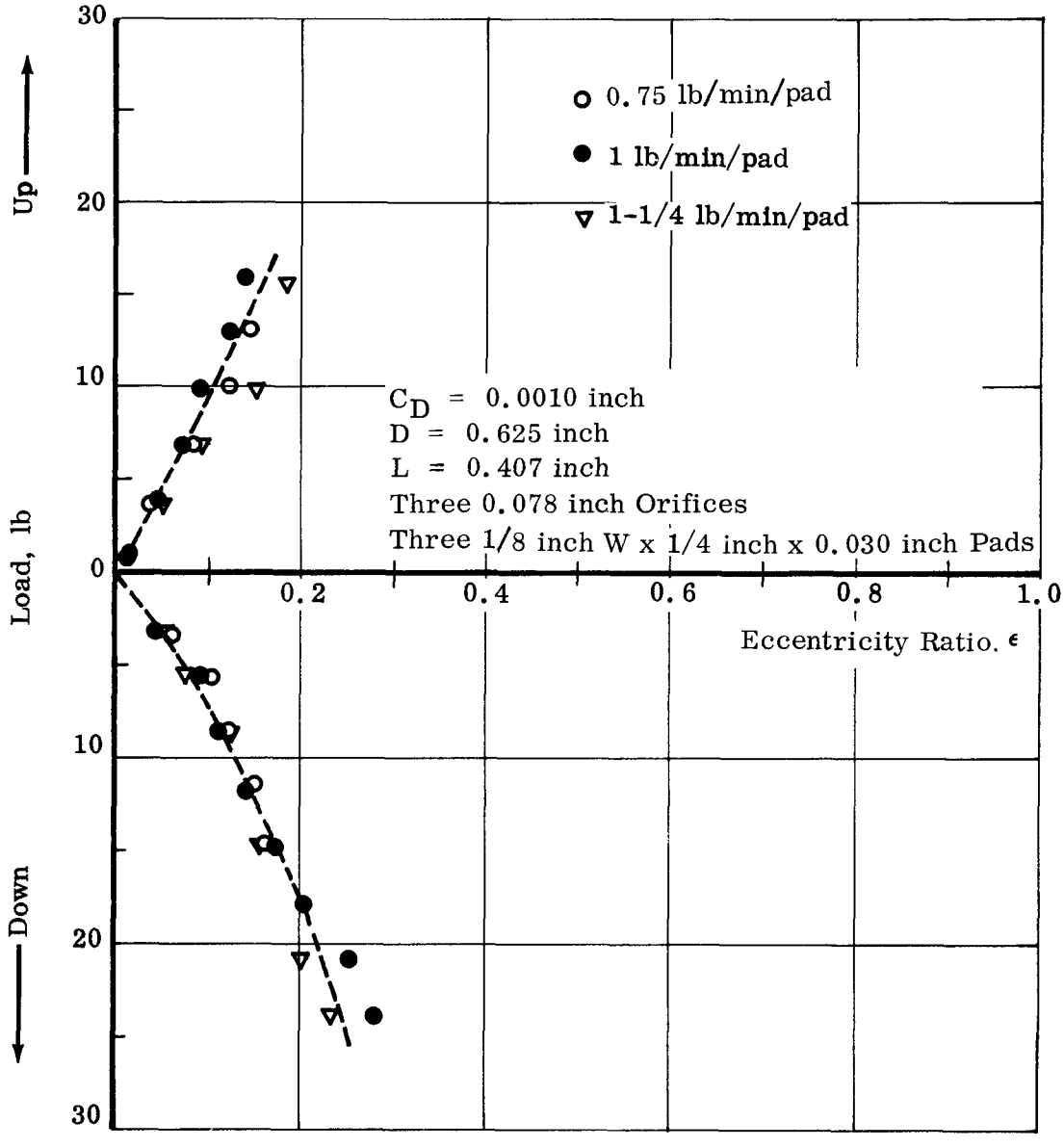

Figure 62. Dynamic Load Deflection Characteristics at 30,000 rpm and Constant Flow (Pressure Variable) BETR 3 Test Series

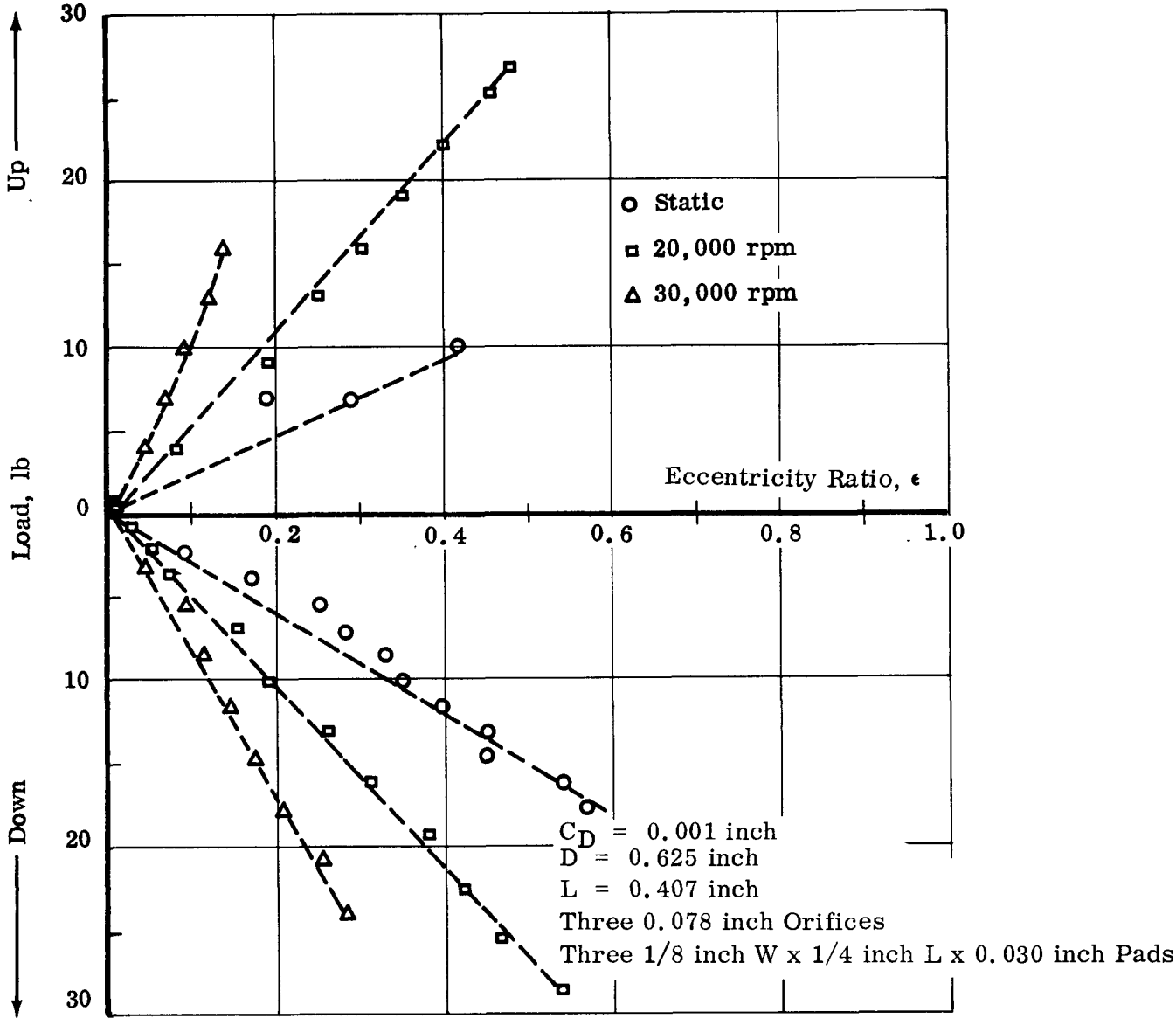

Figure 63. Static and Dynamic Load Deflection Characteristics and 1 lb/min/pad Flow and Variable Pressure

BETR 3 Test Series

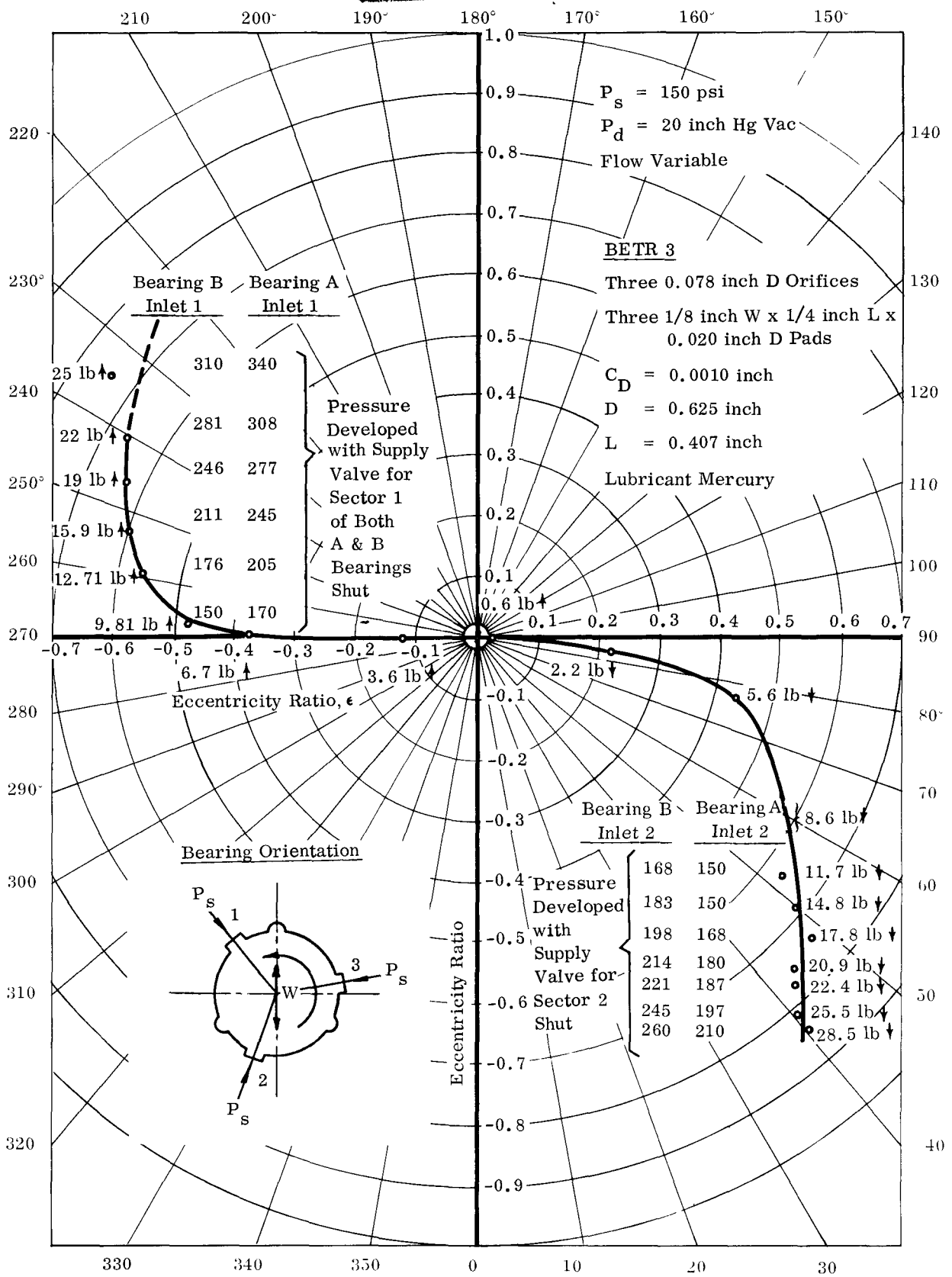

Figure 64. Attitude-Eccentricity Locus for a Three-Sector Bearing with Individually Fed Pads at 20,000 rpm

a true hybrid bearing. Load capacity may also increase as speed increases, while maintaining flow constant, because the pressure increases. To maintain flow constant as speed increases requires greater supply pressure. This greater pressure, is then in part responsible for the additional load capacity.

On the generalized plot of 1/S vs ϵ, Figure 59, the hydrostatic performance at constant flow is also indicated. Capacity of this type of bearing can no longer be adequately predicted by hydrodynamic theory or turbulent flow corrections even though the turbulent corrections come closer to actual performance. Figure 59 verifies that at constant pressure no Reynolds number effect exists for this bearing to speeds of 30,000 rpm. For constant flow of 0.75 lb/min,the generalized data at 20,000 rpm coincides closely with that at 30,000 rpm to give a single curve. The same holds true at 1.25 lb/min flow. At this flow,the hydrostatic forces are greater than those for the 0.75 lb/min case because of the increased pressure. The results from the constant pressure and constant flow tests indicate that load capacity and fluid film stiffness derived from load capacity may be predicted with good accuracy by laminar hydrodynamic theory for uncompensated and by hydrostatic theory for compensated three-sector bearings,respectively,even though speeds correspond to $Re > 1000$.

2. Fluid Film Stiffness

The slopes of the load-deflection characteristics vary considerably depending on whether flow or pressure is held constant. Stiffness will be independent of eccentricity ratio for a pure hydrostatic bearing. This is true for constant flow to eccentricity ratios of 0.5 to 0.6, for the hybrid bearing stiffness tends to increase with speed to account for the increasing hydrodynamic contribution. Figures 60 through 63 again verify this trend for constant flow. The relatively large constant stiffness from $\epsilon = 0$ to $\epsilon = 0.5$ or 0.6 is one advantage of the hybrid bearing (constant flow case) in predicting critical speed. Variations in fluid film stiffness from zero to 30,000 rpm at flows from 0.75 lb/min to 1.5 lb/min per pad, for $0 < \epsilon < 0.6$, were from 42,000 lb/in. to 174,000 lb/in.

For the predominantly hydrodynamic case when pressure is maintained constant, the bearing stiffness is dependent on applied load and resultant eccentricity ratio. For the hydrodynamic case stiffness increases with load and speed as indicated by the slopes of Figures 55 through 58. This is somewhat of a disadvantage since doubtful repeatability in critical speed may result between rotating packages which have different applied loads. Assuming that unidirectional loads are zero at zero g (in space), the stiffness variation was from a low of 5,000 lb/in. at 100 psig and zero speed to a high of 64,000 lb/in. at 250 psig and 30,000 rpm.

3. Hydrodynamic-Hydrostatic Effects

Figures 64, 65, and 66 indicate that without inherent orifice compensation, at constant supply pressure,the bearing is partially hydrostatic and partially hydrodynamic for small eccentricity ratios and is completely hydrodynamic at large eccentricity

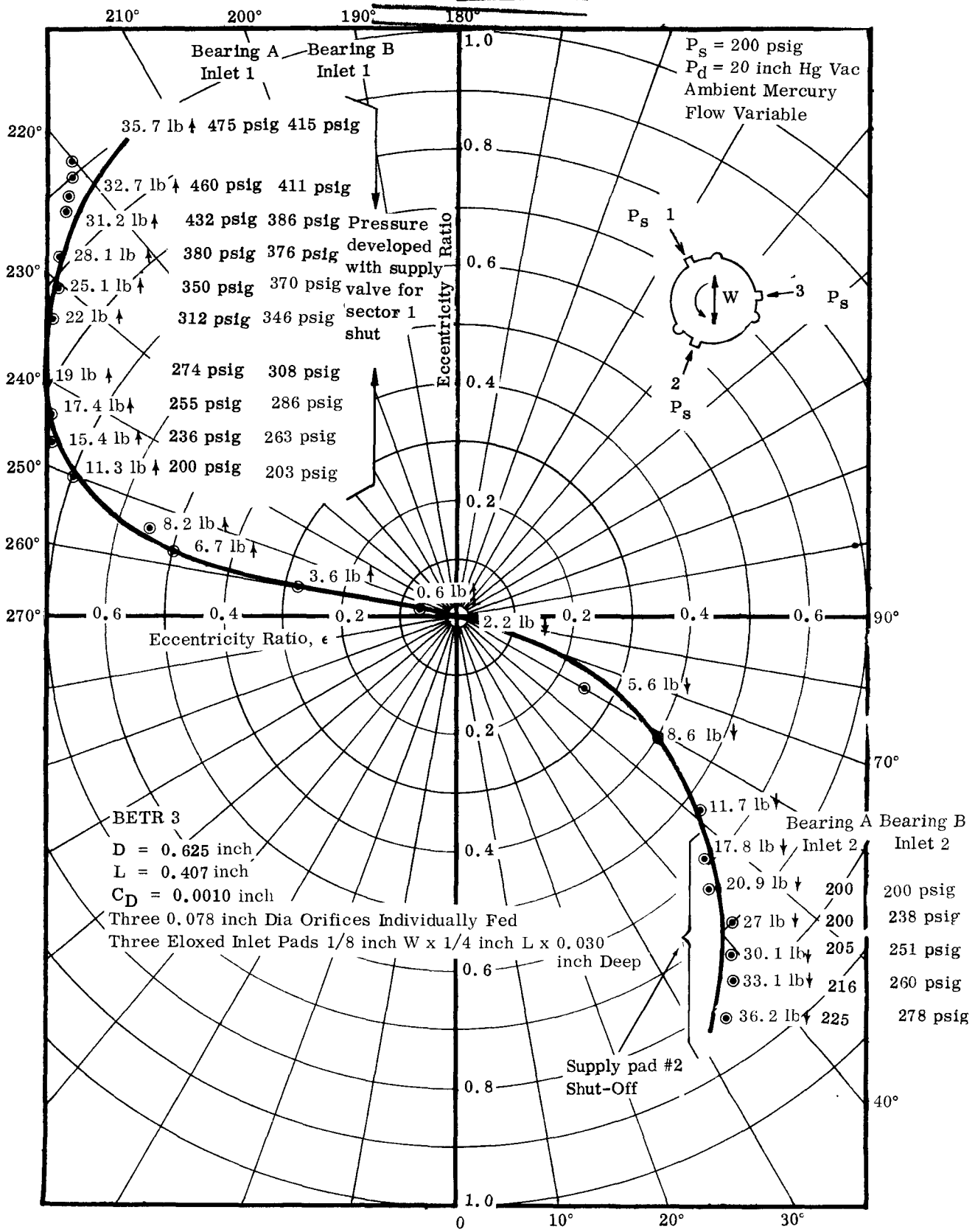

Figure 65. Attitude-Eccentricity Locus for a Three-Sector Bearing at 20,000 rpm

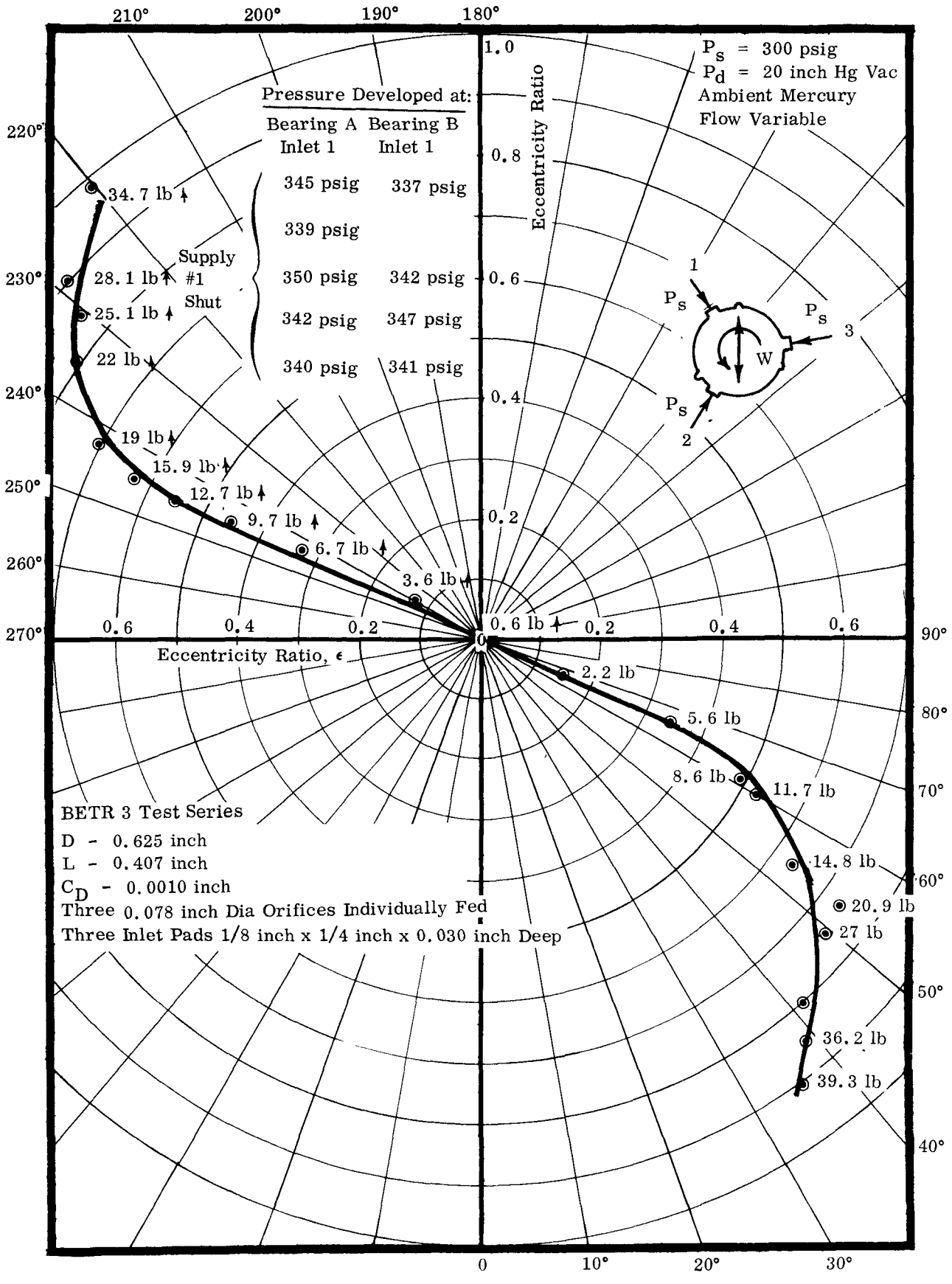

Figure 66. Attitude-Eccentricity Locus for a Three-Sector Bearing at 20,000 rpm and 300 psig

ratios. The figures show the locus of the shaft center and the magnitude and direction of the applied unidirectional loads (into an axial groove loading up and into a pad loading down). The hydrodynamic pressures generated at the loaded supply pad for zero flow are also shown.

Figure 64 shows the shaft locus at 20,000 rpm with supply pressure to each pad held constant at 150 psi. Loading up with 9.8 lb results in an operating eccentricity ratio of 0.48. At this displacement the hydrodynamic pressure generated in the loaded section of the bearing results in a pressure in the supply pad which is equal to the 150 psi supply pressure. The result is zero flow from the loaded supply pad and a fully closed flow control valve. As the load is further increased, the corresponding pressure increase is measured by a gauge located between the pad and the shut flow valve. Loading down, 11.7 lb is required before the resulting eccentricity ratio of 0.6 develops a hydrodynamic pressure equal to the supply pressures. This verifies the analysis which indicates that loading into a pad results in a greater load capacity than loading into an axial groove.

Figure 65 indicates that an upward load of 11.3 lb and a corresponding eccentricity ratio of 0.7 are required before the hydrodynamic pressure forces exceed a supply pressure of 200 psi. Loading down requires 20.9 lb and an eccentricity ratio of 0.65 before accomplishing the same phenomenon.

Figure 66 shows the need for an upward load of 22 lb and a corresponding eccentricity ratio of 0.8 before balancing the supply pressure of 300 psi and throttling all flow out at the loaded pad. Loading down, the hydrodynamic pressure forces as a result of a displacement caused by 39.3 lb were insufficient to overcome the supply pressure.

The load-deflection characteristic curves combined with Figures 64, 65, and 66 indicate that the hydrodynamic pressure forces generated at eccentricity ratios above 0.6 rise rapidly as $\epsilon \rightarrow 1.0$. Two important factors emerge from these data; they are general and apply to this type of combined hydrostatic-hydrodynamic (or "hybrid") bearing, but are not necessarily confined to mercury lubricated bearings:

1) Without orifice compensation, large unidirectional loads readily throttle off all the flow to the loaded sector (except that which is swept into the loaded region from the previous sector).

2) The "hybrid" three-sector bearing has a larger capacity when loaded into the sector and, consequently, can have a preferential orientation.

When the hydrodynamic pressure forces exceed those of the supply pressure, lubricant from the preceding or "upstream" sector must be "dragged" or pumped into the loaded sector or the film will rupture. To accomplish this with this type bearing, the lubricant must be carried around by the shaft or splashed across the axial groove which acts as the drain slot. Well-rounded corners are essential to permit this to happen when the drain groove is not operating flooded. Figures 64, 65, and 66 show that

lubricant is pumped this way since the flow to the loaded sector was stopped completely by closing the supply valve after the supply recess was pressurized above the supply pressure. Backward flow under those conditions is also possible with the shaft acting as the impeller of a pump and the orifice functioning as a discharge port. The above conditions are not desirable for large unidirectional or rotating loads since the reliability of maintaining lubricant in the loaded region of the bearing is dependent on feeding across a drain groove. Lubricant starvation and its disastrous effects can easily occur for low total flow rates.

Orifice compensation under the conditions discussed above is extremely advantageous if high supply pressures cannot be maintained. (When a higher supply pressure is available, larger eccentricity ratios are possible before the hydrodynamic pressure forces exceed the supply pressure. Figure 66 shows that for constant supply of 300 psi an eccentricity ratio of 0.8 must be attained to throttle off all flow from the loaded pad.)

In the uncompensated case the situation becomes critical when total flow to the bearing is constant. (This is not the same as maintaining constant flow to each sector.) Under constant total flow all the flow can be dumped into the unloaded region and be drained from the axial grooves before it has a chance to be forced into the loaded sector. Orifice compensation will improve the flow distribution to this type of bearing in addition to improving stability characteristics (see later discussion on orifice-compensated three-sector bearing test). For constant flow to each sector, which represents perfect compensation, the load-deflection curves, Figures 60 through 63, illustrate the typical increased load capacity, stiffness and shaft center motion of a hydrostatic bearing.

The contribution of the hydrostatic forces was neglected in the analysis, and the above results indicate that this approach is satisfactory, if somewhat conservative, for the uncompensated case at low eccentricity ratios. At larger eccentricity ratios, the high inlet pressure influence raises the level of the average pressure in the bearing, but because of the uncompensated situation and the presence of axial slots, hydrodynamic forces predominate so that hydrodynamic analysis will satisfactorily predict performance. For the compensated bearing, a hydrostatic analysis must be employed.

4. Attitude-Eccentricity Locus

The static locus at constant pressure is summarized in Figure 67. Lack of orifice compensation is responsible for the "S" shape of the curve. Figure 68 shows the dynamic locus for 20,000 and 30,000 rpm at constant pressure. The measured data agree quite well with the predicted locus considering hydrodynamic action only.

Figure 68 shows the typical attitude-eccentricity locus associated with hydrodynamic bearing operation. It indicates that loading into an axial groove results in a larger attitude angle for a given eccentricity ratio than loading into the middle of a sector. Consequently, the uncompensated three-sector bearing with the load applied into the middle of the sector has the following characteristics in relation to load applied into a groove:

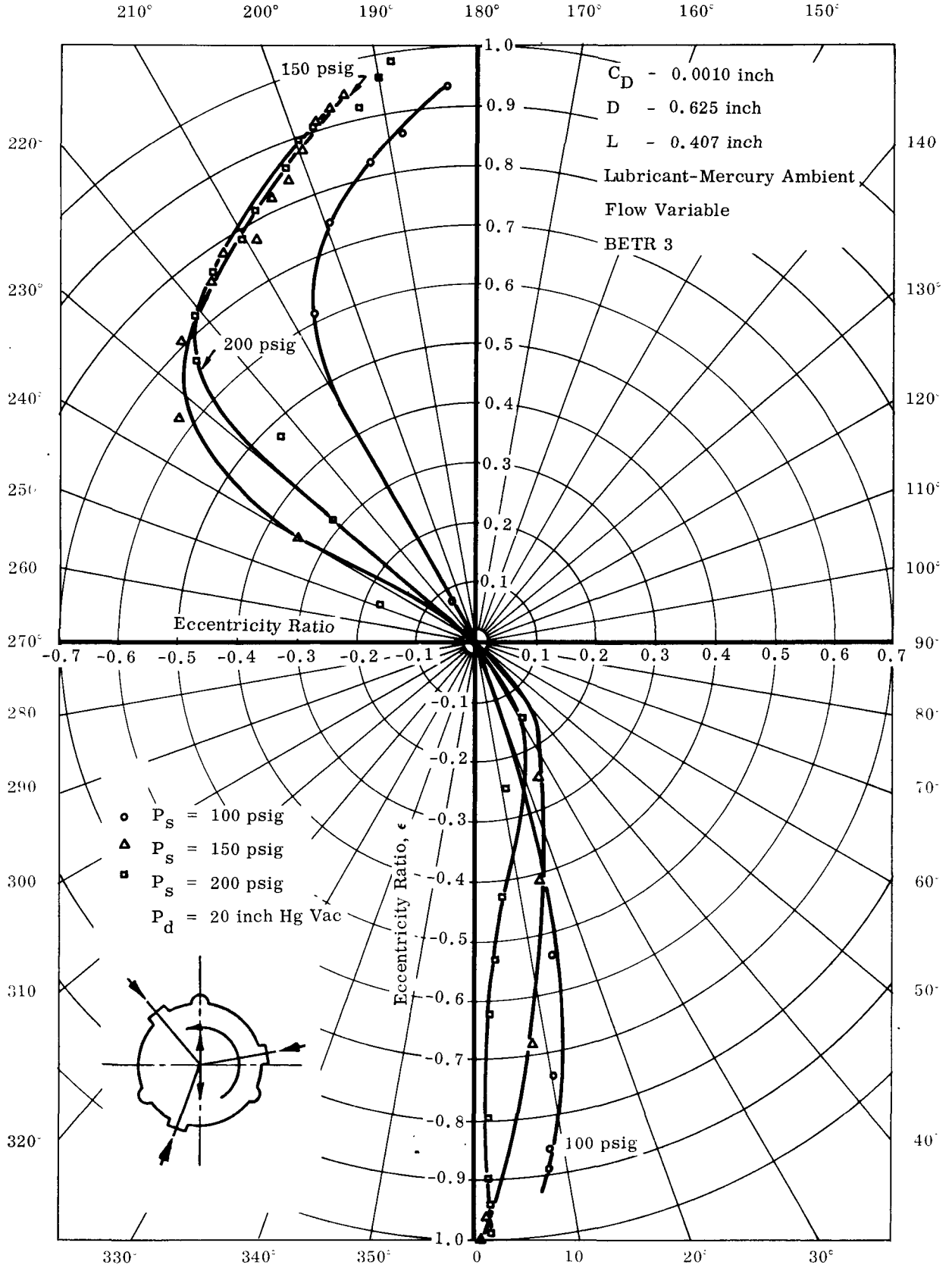

Figure 67. Static Attitude-Eccentricity Locus for a Three-Sector Bearing With Individual Feed to Each Pad

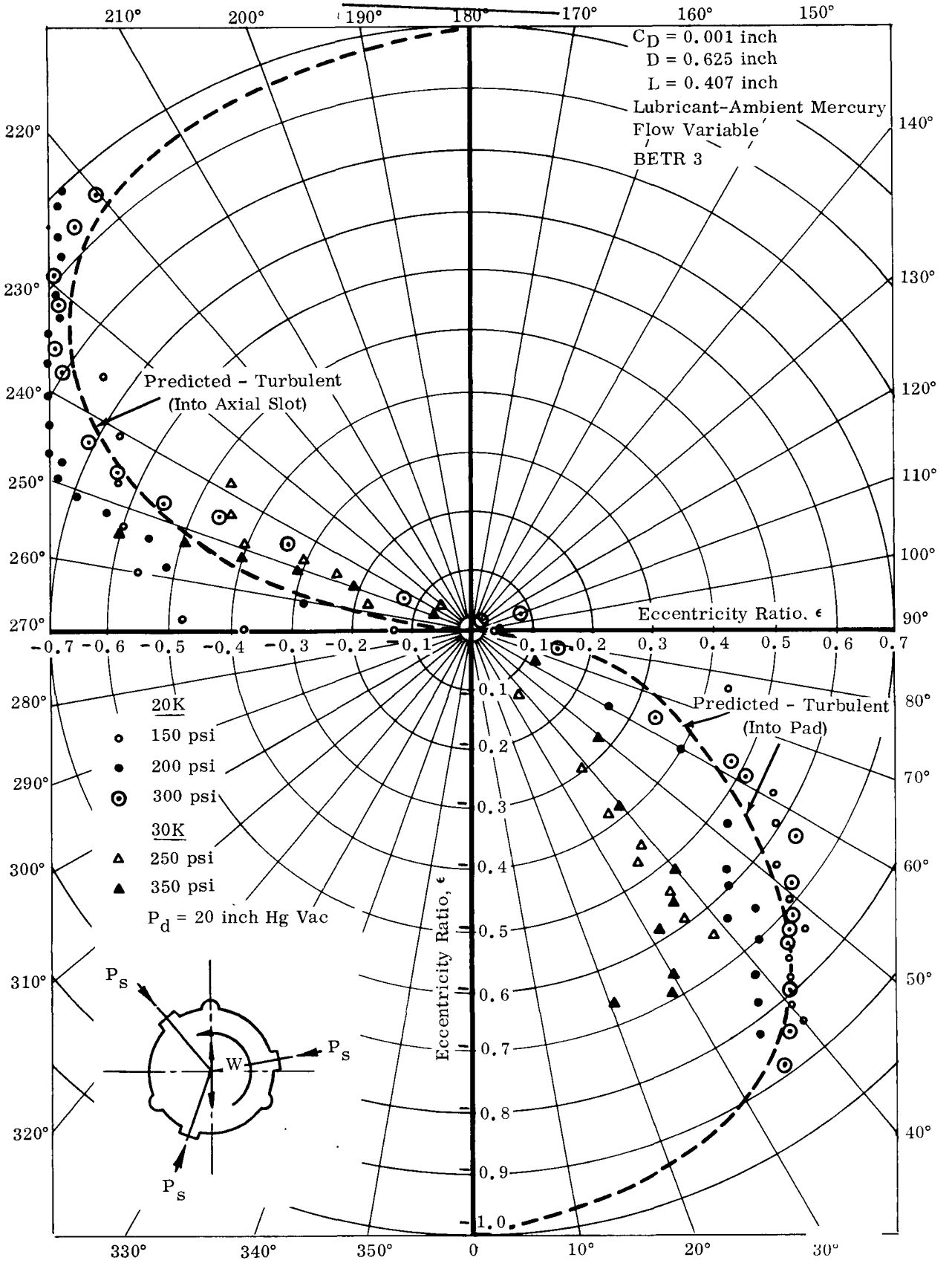

Figure 68. Experimental Attitude-Eccentricity Locus for Individually Fed Three-Sector Bearing at Constant Pressure

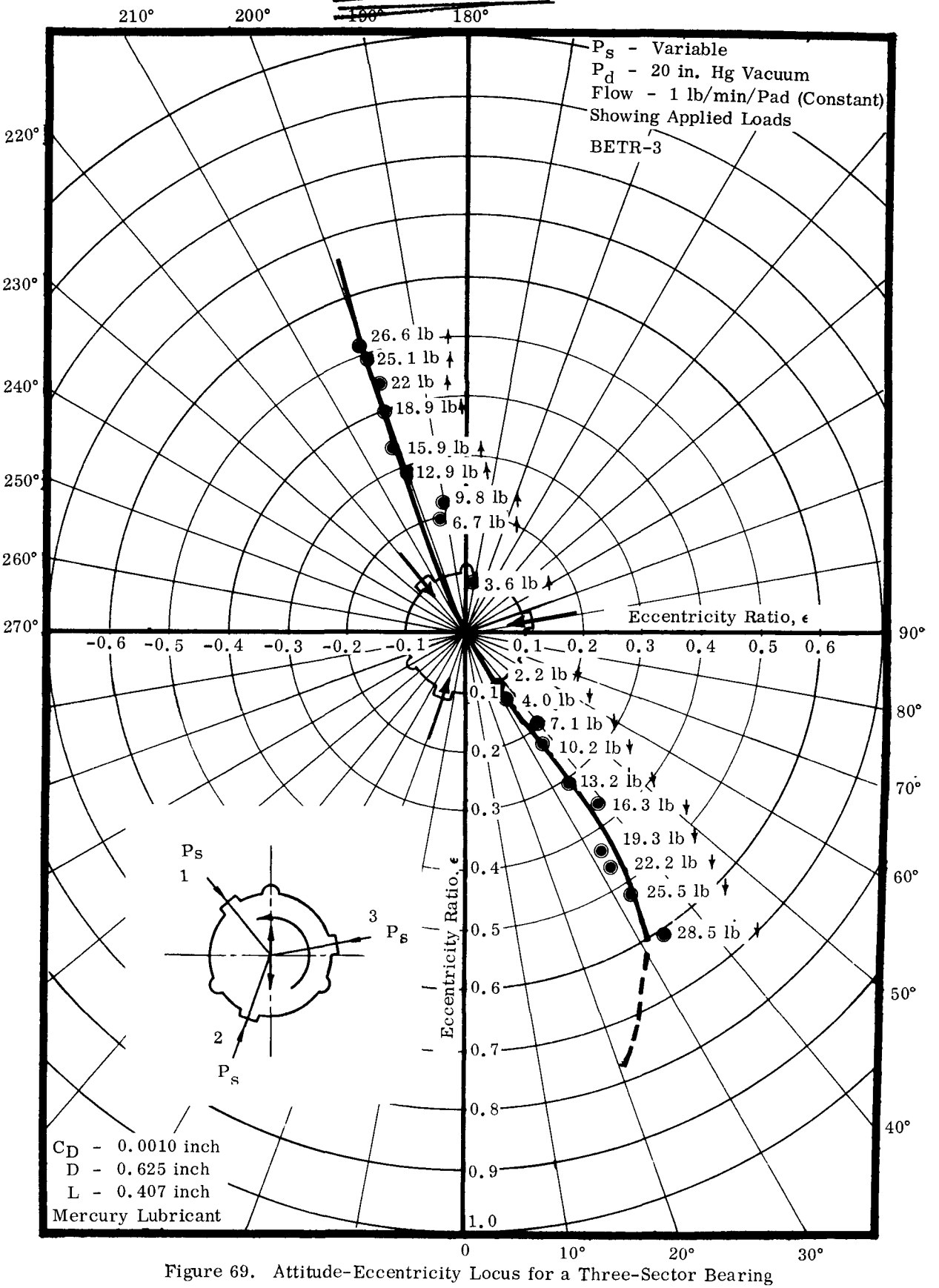

Figure 69. Attitude-Eccentricity Locus for a Three-Sector Bearing at 20,000 rpm and Variable Supply Pressure

1) Higher load capacity

2) Greater stiffness

3) Better stability

The effect of supply pressure level in Figure 68 is not readily distinguishable. This is to be expected since the hydrostatic contribution does not alter the load-deflection characteristic appreciably, and the higher pressure is not utilized because of the lack of compensation.

Maintaining the flow constant resulted in a locus for a typical hydrostatic bearing. The greater the flow, resulting in increased hydrostatic forces, the more vertical the shaft locus became, i.e., the more nearly the shaft displacement is in the direction of the applied load. The bearing, as indicated in the load deflection test, became extremely strong and stiff because of the constant flow (perfect compensation) provision. Figure 69 shows the locus as influenced by the hydrostatic operation. The marked difference between the hydrodynamic locus in Figure 68 and the hydrostatic locus in Figure 69 is obvious.

In Paragraph II-B-7 (BETR 1) the zero shift encountered in using capacitance displacement probes was mentioned. Similar problems were encountered in this test in measuring attitude-eccentricity (film thickness) at speeds of 30,000 rpm or greater. As speed increased, resulting in larger quantities of heat generated in the bearings, instrumentation calibration drift occurred. The displacement pickups, although water cooled, moved with the housing as the heat was transferred to it. The result was a zero drift with the change in initial "gap" setting. The gain calibration, however, was unchanged and remained linear to displacement. Correction for this drift was made by assuming that at zero load the shaft would be in the center of the bearing, i.e., $\epsilon = 0$. Justification and confidence in this approach was obtained from the flow and supply pressure versus unidirectional load data obtained during this individually fed bearing test discussed below. It was found that at zero load (static; 20,000; and 30,000 rpm) flow to each sector at constant supply pressure was equal. At zero load (static; 20,000; and 30,000 rpm) the supply pressure required to maintain flow constant to each sector was equal. Since this equality could only occur with the shaft located in the center of the bearing, i.e., at $\epsilon = 0$, it was assumed that at zero load, i.e., zero gravity, the shaft and bearing centers coincided. Attitude-eccentricity loci at 30,000 rpm and above were corrected accordingly for zero shift on this basis.

5. Stability Characteristics

Experimental results of the individually fed bearing test and observation of other uncompensated three-sector bearings operating at 0.001-inch clearance indicate stable operation at speeds up to 45,000 rpm with zero loads, i.e., simulating zero gravity. Figure 9 predicts that a unidirectional load of 9 lb/bearing will be required to accomplish stability at 40,000 rpm, based on hydrodynamic performance only. Consequently, it follows that the hydrostatic contribution, even though the bearing is

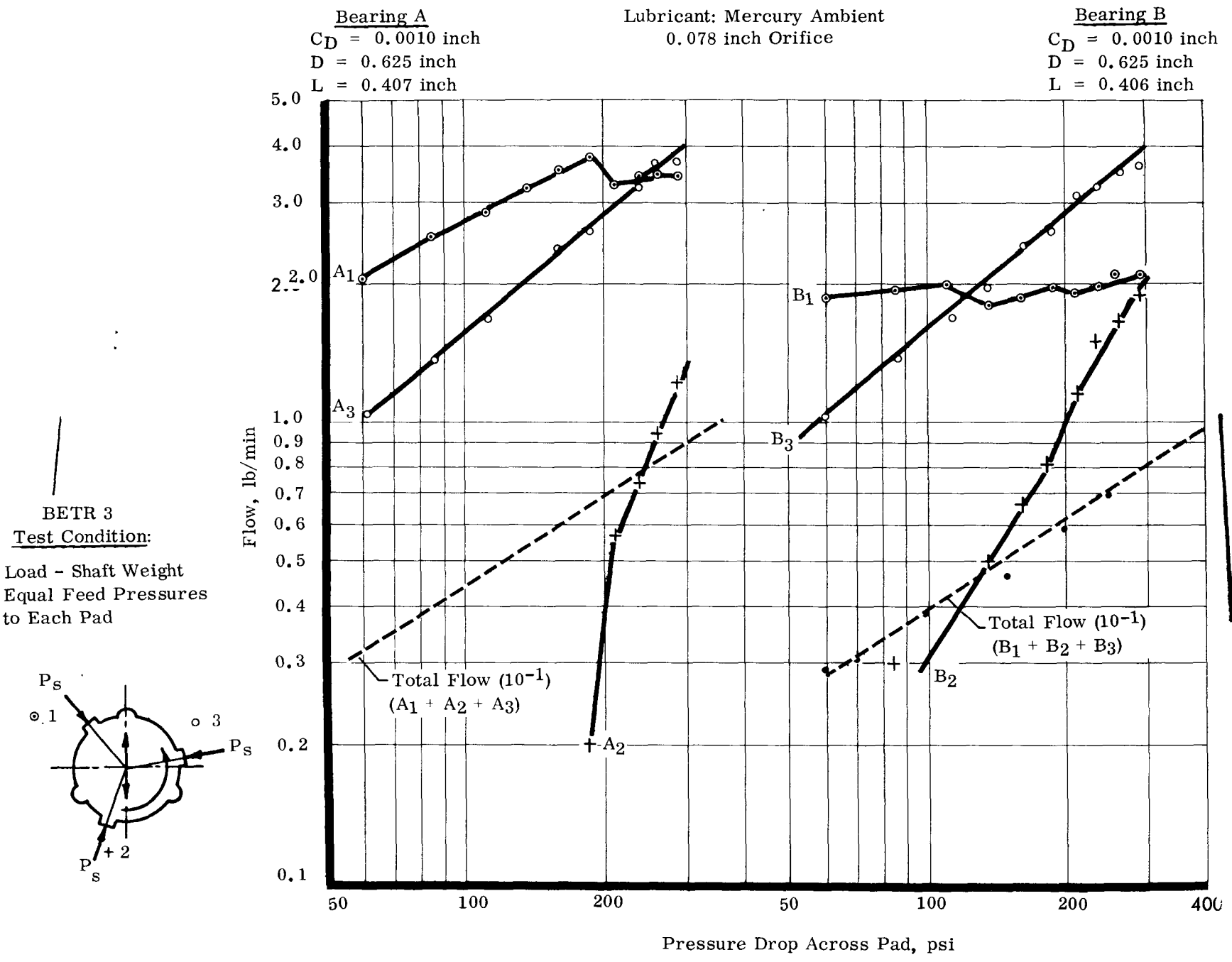

Figure 70. Static Flow Characteristics for Individually Fed Three-Sector Bearing

uncompensated, results in a radial stiffness curve that keeps the bearing stable at all speeds from 0 to 45,000 rpm. For other three-sector bearings with larger diametral clearances (see previous sections), the hydrostatic contribution is not as large and half-frequency whirl is encountered at relatively low speeds, i.e., approximately 20,000 rpm, without application of unidirectional loads.

6. Flow Characteristics

Static and dynamic flow characteristics are shown in Figures 70 and 71, respectively. Figure 70 shows the flow variation between the three different supply pads for both bearings, at zero speed, and load equivalent to the shaft weight only. As expected, the bottom supply pad is throttled by the shaft. It requires somewhere between 100 and 200 psi supply pressure to overcome the combined force of the shaft weight and the downward force due to the upper supply pads. Once the shaft moves off the pad, flow increases rapidly with increasing pressure. Superimposed on the individual pad flow is total flow (sum of three separate flows). This is what is normally measured. Figure 70 clearly shows that for the uncompensated bearing, merely measuring total flow does not represent a reasonable picture of what is happening inside the bearing. Tracing the flow variation gives a clear picture of the shaft locus in the bearings under the influence of increasing pressure (or hydrostatic forces).

Knowing the individual flow rates is essential in assigning the correct flow to each sector for purposes of working backward to establish pressure profile and, from that, load capacity for individual sectors. Assuming a third of the total flow to each sector for all eccentricity ratios other than zero results in gross errors under both static and dynamic conditions.

Figure 71 shows total flow at speeds up to 30,000 rpm. The total flow for each bearing is presented for shaft weight acting vertically downward. The small variations in flow between bearings are due to slight geometrical differences of clearance and supply pad configurations. As in the case of the plain bearing, flow-pressure relationships are speed dependent, and extremely high supply pressures are necessary to force adequate lubricant through the bearing under turbulent conditions. The axial grooves, however, permit larger flow rates since circumferential flow can be drained three times per revolution. The influence of load on total flow at constant pressure for static; 20,000; 30,000; and 35,000 rpm is shown in Figures 72 through 75.

Figures 76 and 77 show typical dynamic flow-pressure-load characteristics of the uncompensated three-sector bearing. A series of these curves was obtained both statically and dynamically to show the variation of flow with load, i.e., shaft position, for equal supply pressure to each pad and the variation of pressure with load for equal flow to each pad. These figures really present a pictorial explanation of how the shaft moves in the bearing under the influence of unidirectional loads. The attitude eccentricity locus does this directly so the above approach verifies the locus, provides separate sector flow data, provides confidence in the measured data, and shows that for zero load the shaft and bearing centers coincide very closely.

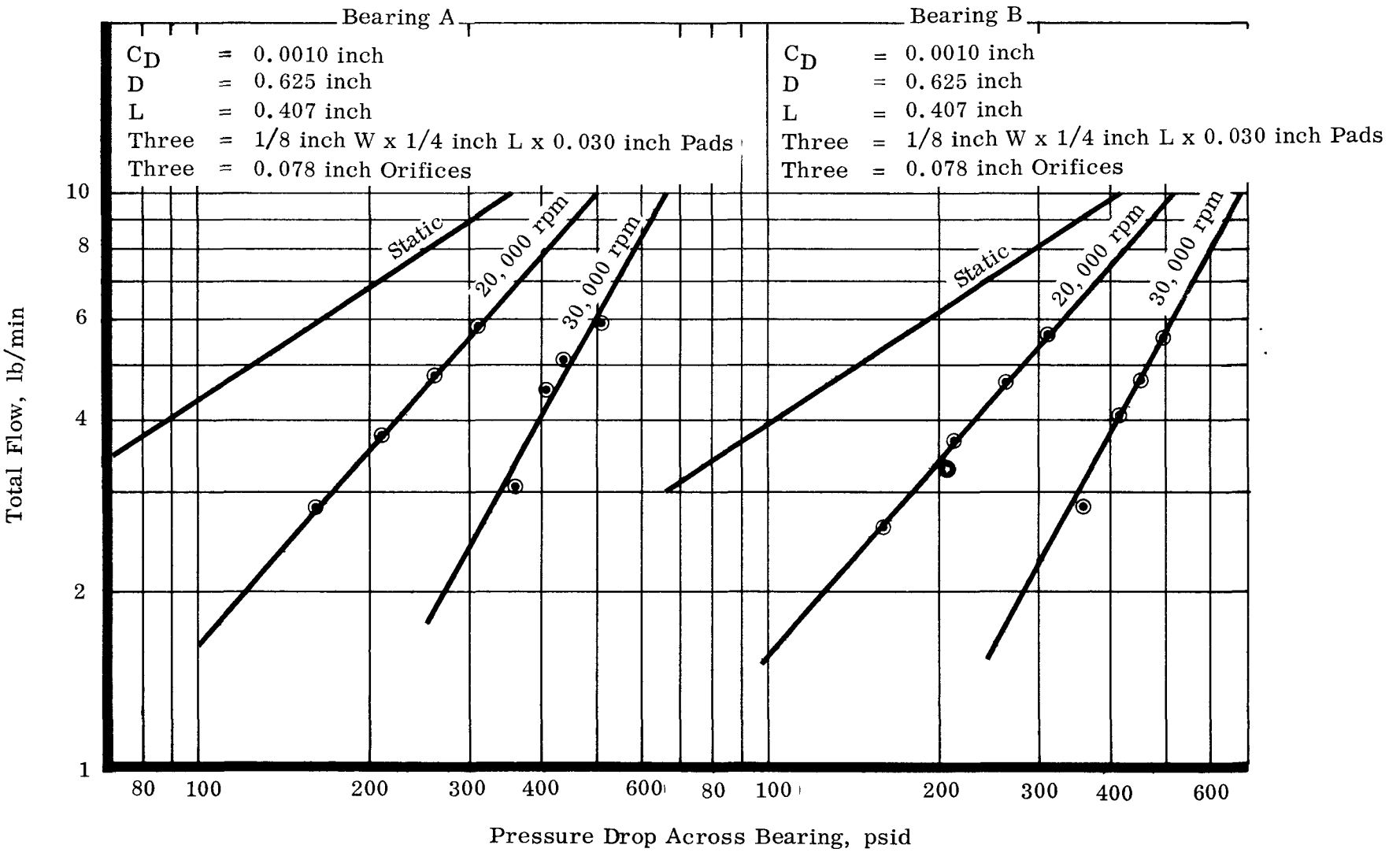

Figure 71. Dynamic Flow Characteristics for Individually Fed Three-Sector Bearing

BETR 3 Test Series

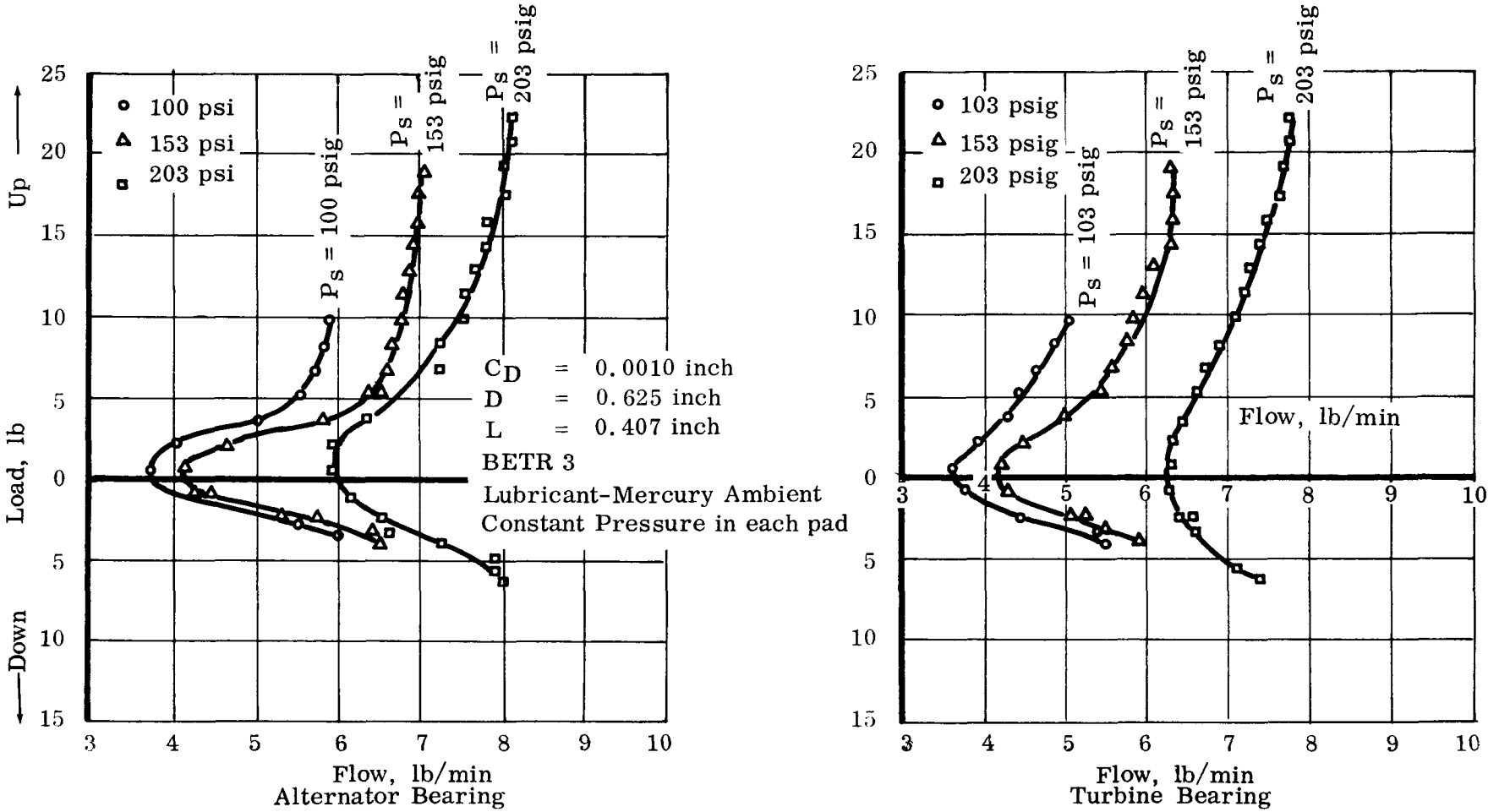

Figure 72. Static Load vs Total Flow for a Three-Sector Bearing With Individual Feed

CONFIDENTIAL

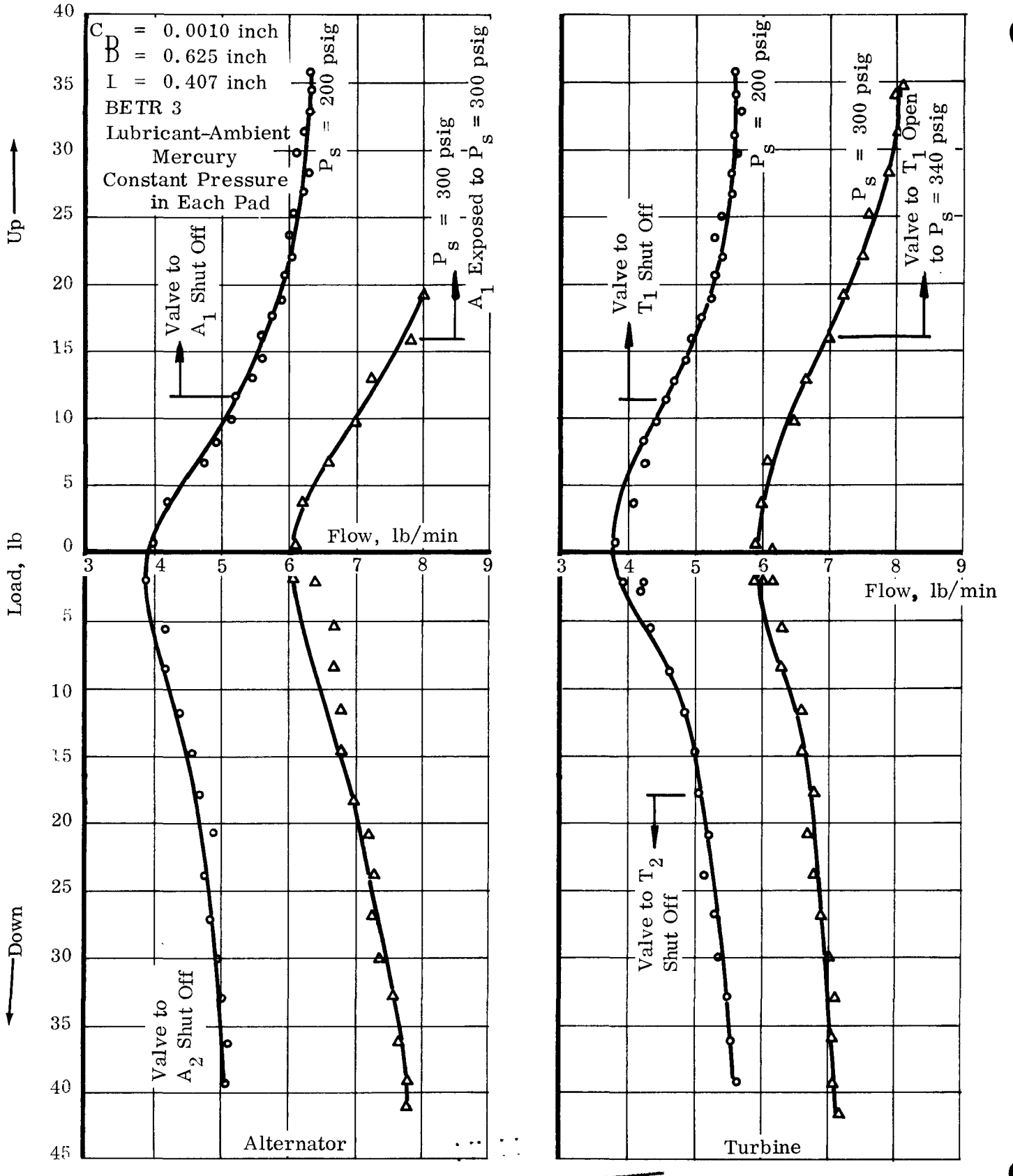

Figure 73. Load vs Total Flow for a Three-Sector Bearing With Individual Feed at 20,000 rpm

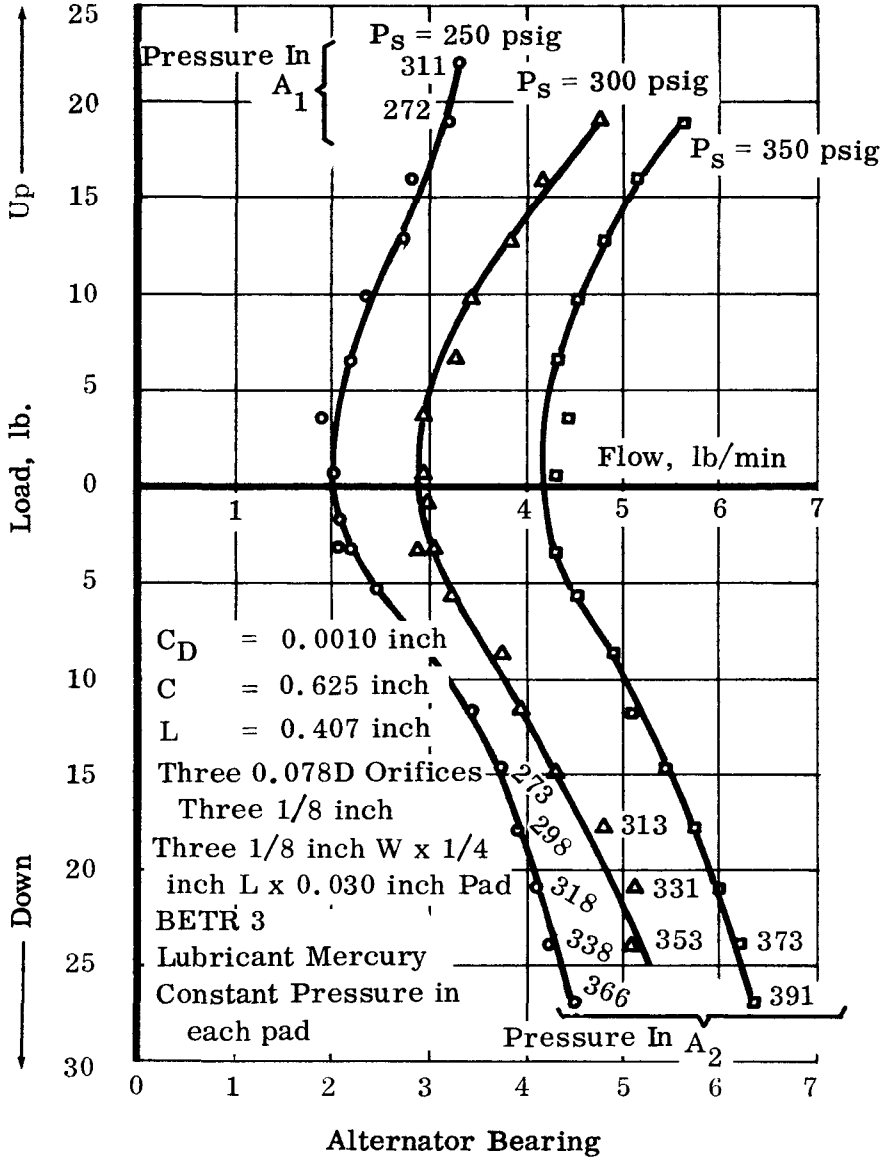

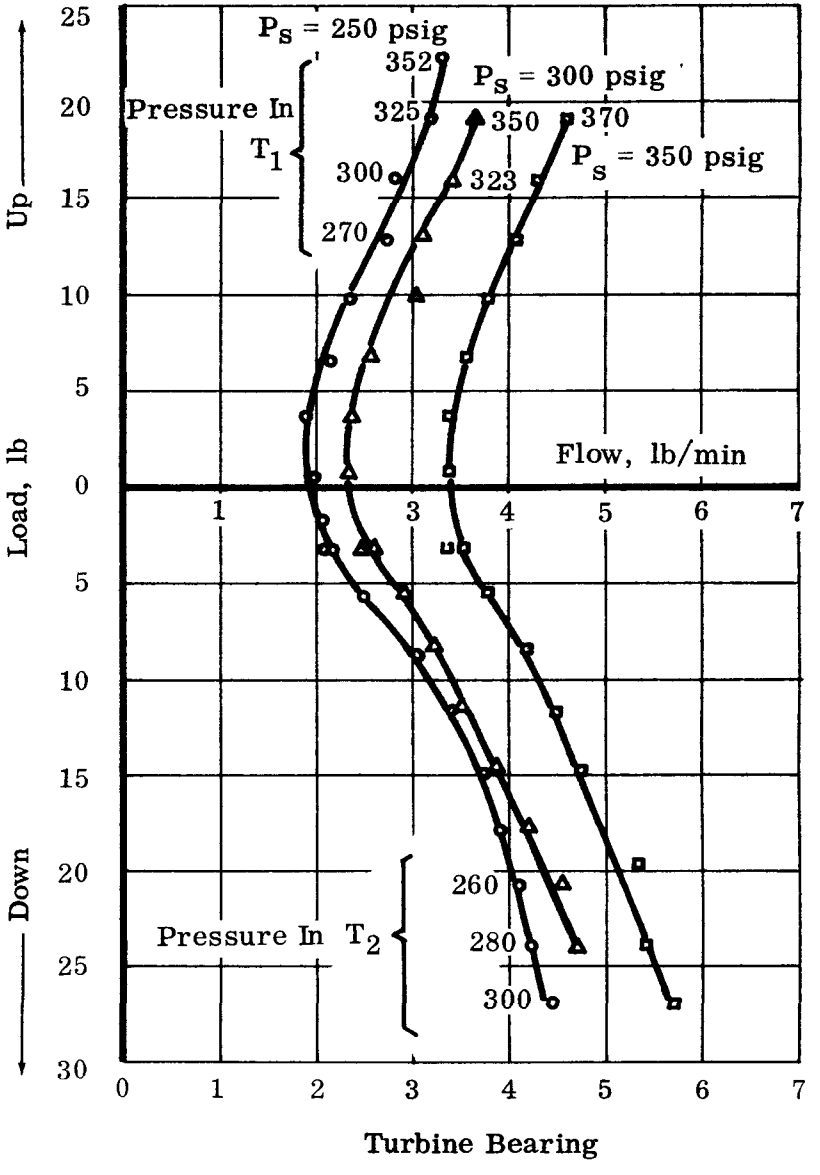

Figure 74. Load vs Total Flow for a Three-Sector Bearing With Individual Feed at 30,000 rpm

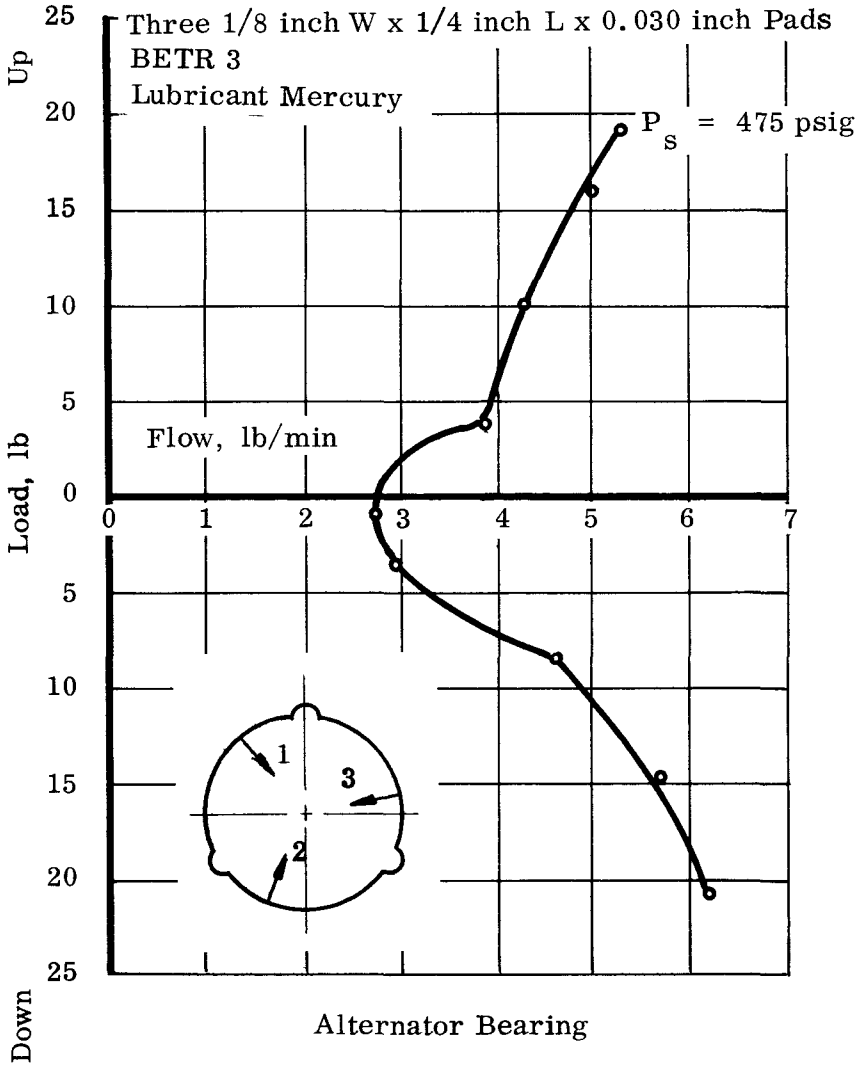

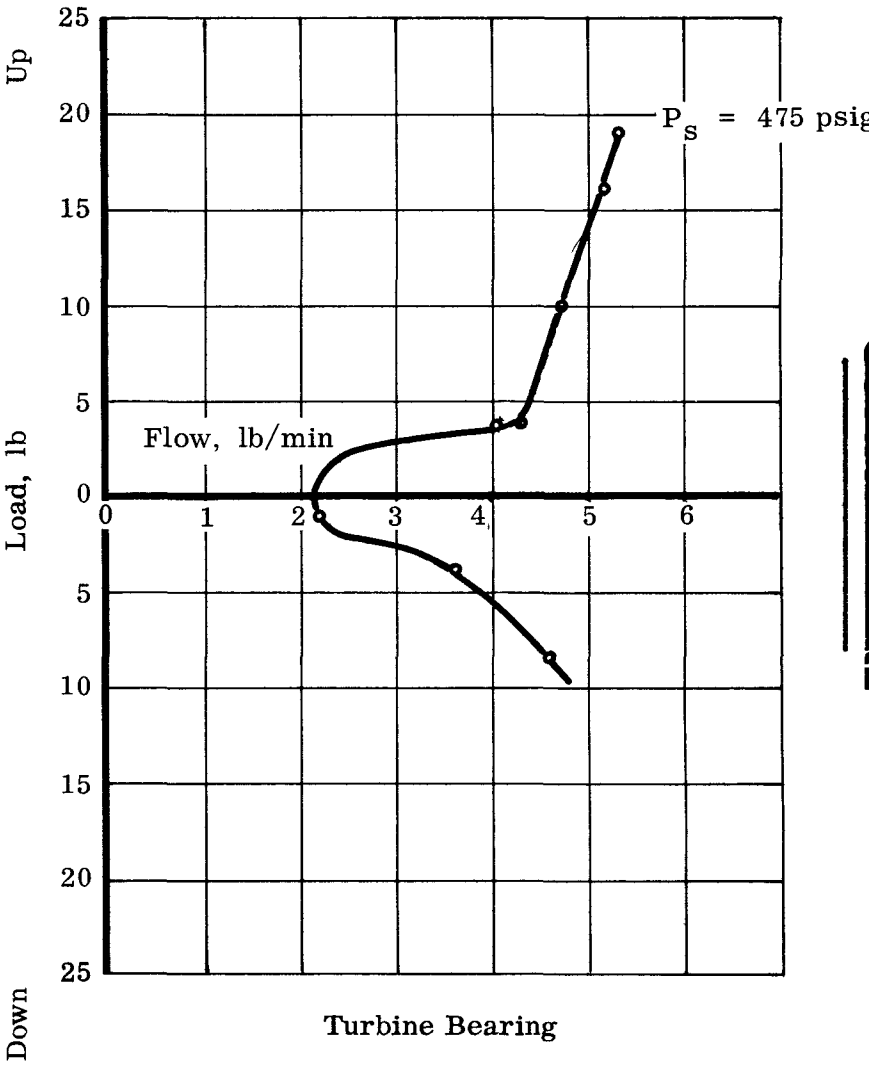

Figure 75. Load vs Total Flow for a Three-Sector Bearing with Individual Feed at 35,000 rpm

Figure 76. Load vs Total Flow in a Three-Sector Bearing at 20,000 rpm

BETR 3 Test Series

C_D = 0.001 inch
D = 0.625 inch
L = 0.407 inch

Three 0.078 inch Orifices
Three 1/8 inch W x 1/4 inch L x 0.030 inch Pads

Test Condition
200 psig supply to each pad except where noted

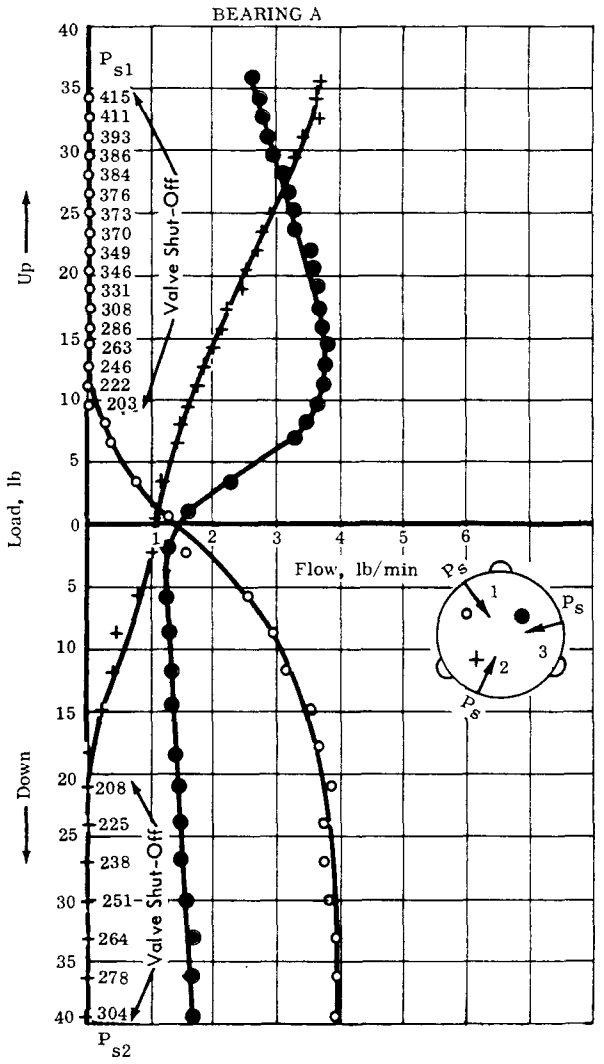

C_D = 0.0010 inch
D = 0.625 inch
L = 0.407 inch

Three 0.078 inch Orifices
Three 1/8 inch W x 1/4 inch L x 0.030 inch Pads

Test Condition
200 psig supply to each pad except where noted

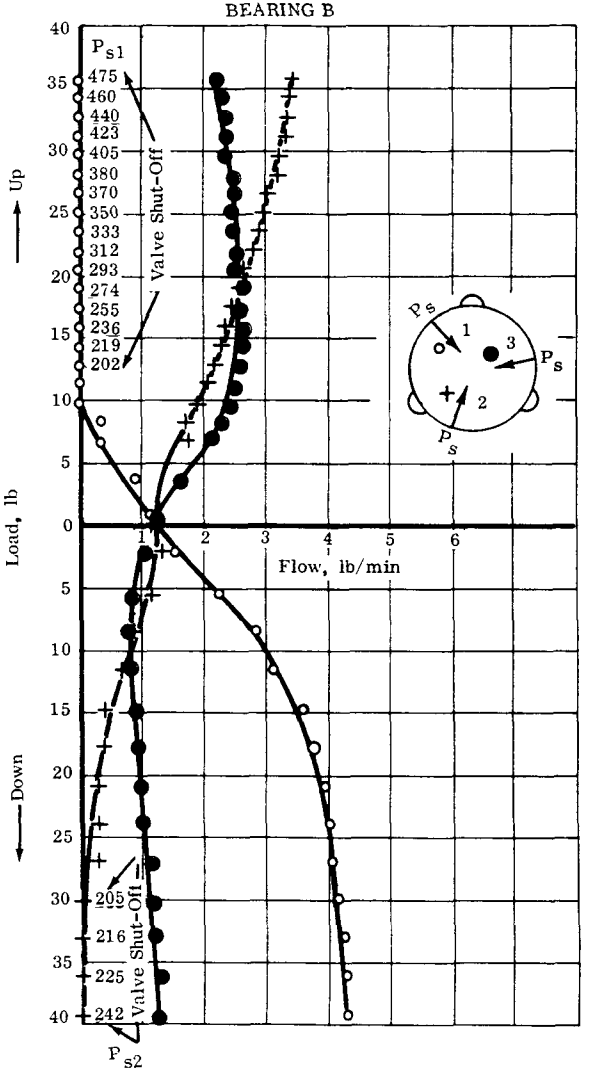

Figure 77. Load vs Pad Supply Pressure for a Three-Sector Bearing at 20,000 rpm and 1 lb/min to Each Pad
BETR 3 Test Series

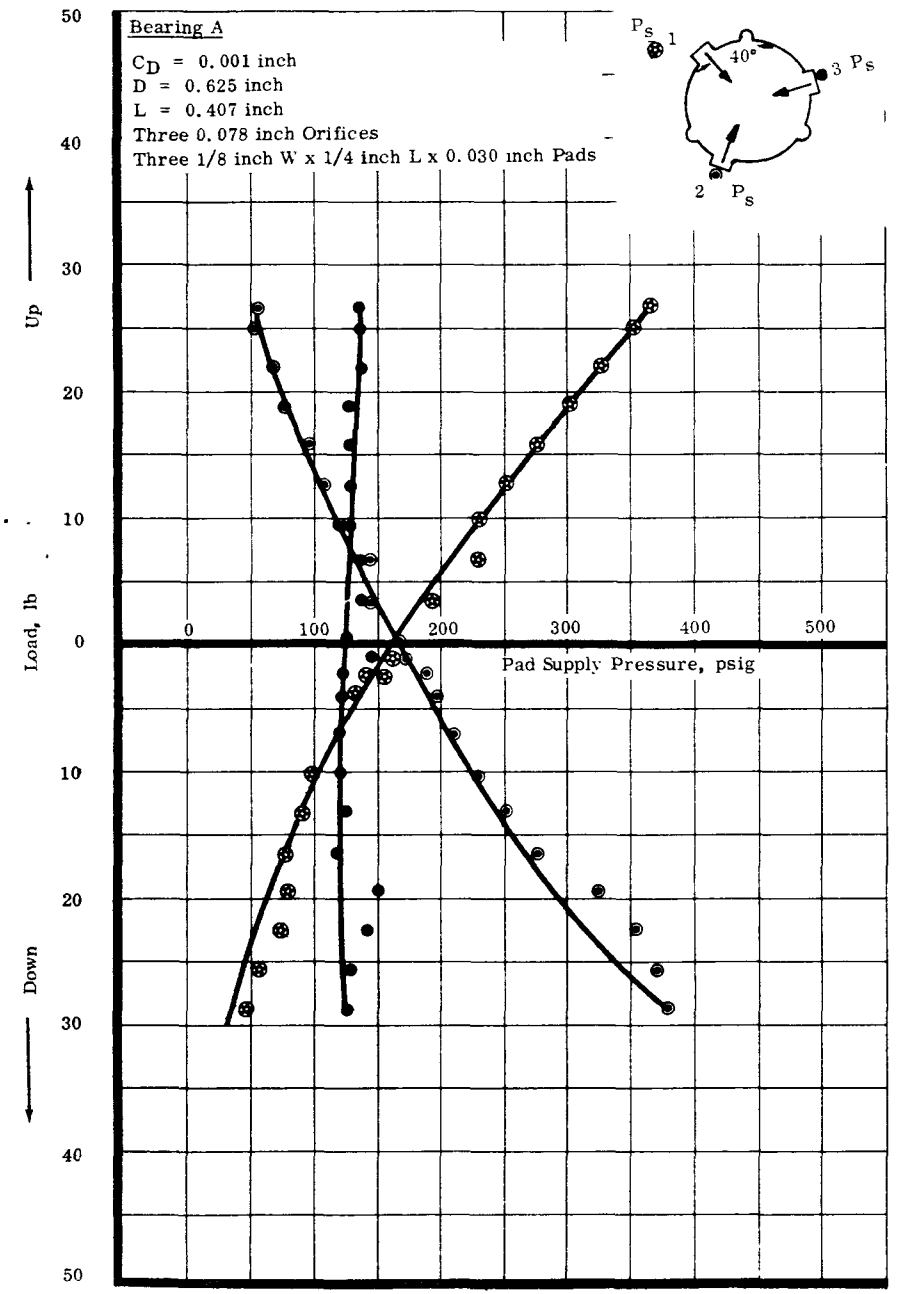

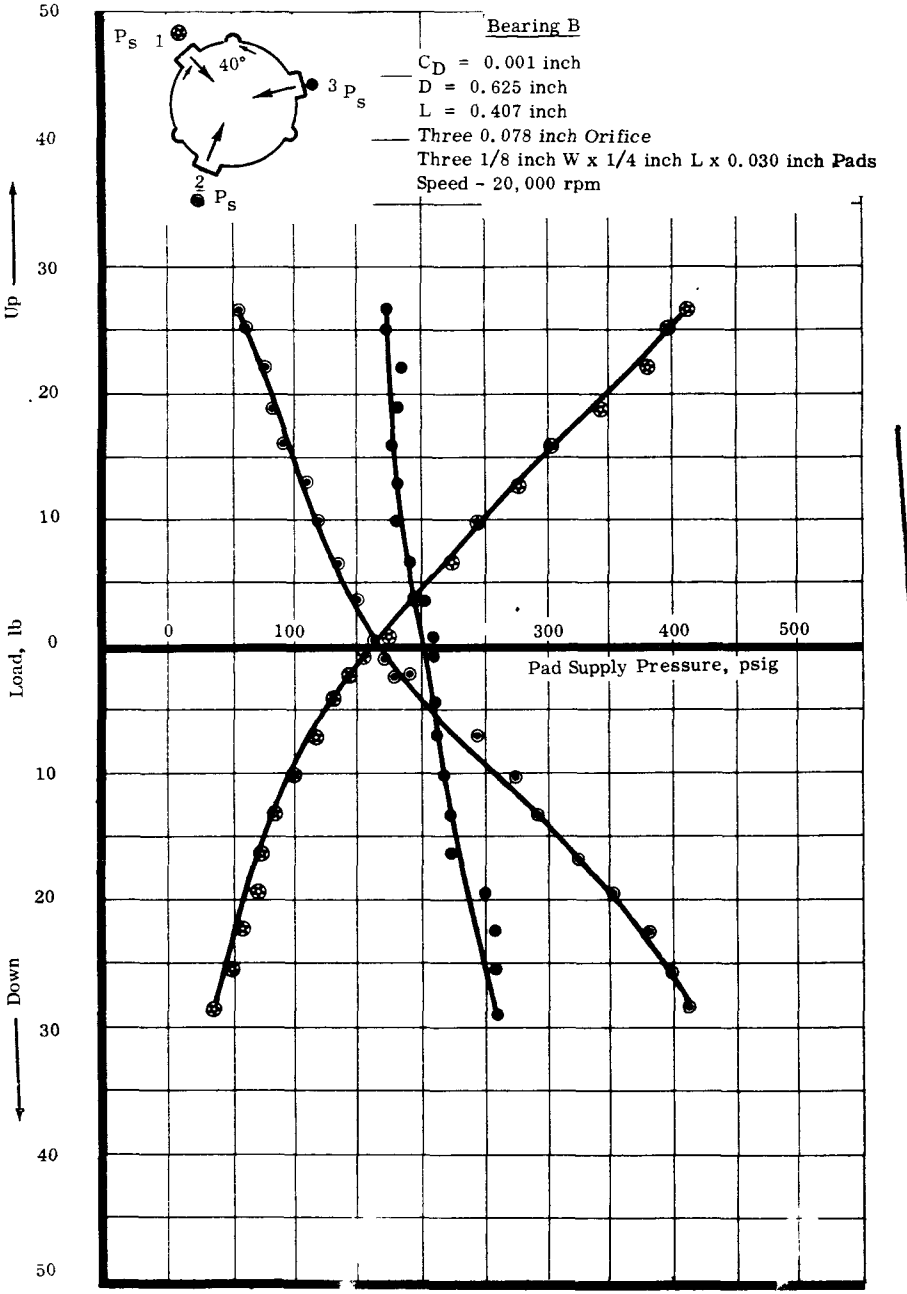

Figure 76 shows how flow varies with load to each sector at 20,000 rpm. It shows that, for loading down, flow from sector 1 increases, flow from sector 3 remains fairly constant, and flow from sector 2 is cut off for a load of approximately 20 pounds. For loading up, almost the reverse situation occurs, except that it only takes approximately 10 lb to throttle flow from sector 1. To accomplish this flow variation, the shaft must follow the locus presented in Figure 65. For zero load (this includes negating the effects of the shaft weight), the three separate flows agree within 0.5 lb/min, or better, with a supply pressure of 200 psi to each pad. Since the orifices are uncompensated and the minimum area the flow sees is the annulus formed by the supply pad and the bearing clearance space, it follows that at only one position can this condition be satisfied, i.e., where the shaft and bearing centers coincide. For loads as low as 10 lb/bearing, the shaft movement is great enough to cause flow variations between sectors of up to 3 lb/min.

From Figure 77 the same conclusions can be drawn. The slight variation of pressure required to flow 1 lb/min at zero load may be due to small differences in supply pad configurations and/or a misaligned condition whereby the rotating shaft is centrally located vertically, but cocked slightly horizontally. Figure 77 shows a very large pressure variation between sectors to maintain constant flow. For the same 10-lb load as much as 150 psi difference is necessary to assure constant flow to each pad. Figures 76 and 77 clearly point to the flow advantages of orifice compensation for the three-sector bearing. (Other advantages will be discussed later.) However, orifice compensation has some disadvantages in the SNAP 2 application. These include the need for high pressures to pass adequate flow through the bearing for cooling, and the potential problem associated with mercury contaminant build-up and erosion in small orifices.

7. Power Loss

Figure 78 shows the power loss measured by the speed decay method. From the total power loss (2 journals and a double acting thrust bearing), the individual journal bearing loss is obtained by assigning 180 watts to the thrust bearing at 40,000 rpm. The slope of the actual power loss is slightly different from the predicted performance. A 20 per cent variation exists at 40,000 rpm between measured and predicted using turbulent correction. Since the 0.001-inch clearance bearing did not exhibit the anticipated influence of turbulence on increased load capacity, it follows that the reduced influence of turbulence explains the discrepancy in power loss at higher speed.

8. Conclusions on Test Series

Although the test was terminated by a turbine bearing failure (caused by lubrication starvation when the clearance closed down at 42,000 rpm, resulting in insufficient pressure capacity to maintain adequate flow), and only limited parametric data above 30,000 rpm were obtained, many important conclusions could be made. In addition, a real insight and understanding of the hydrostatic and hydrodynamic forces which act on the shaft was achieved. The importance of orifice compensation; the need for

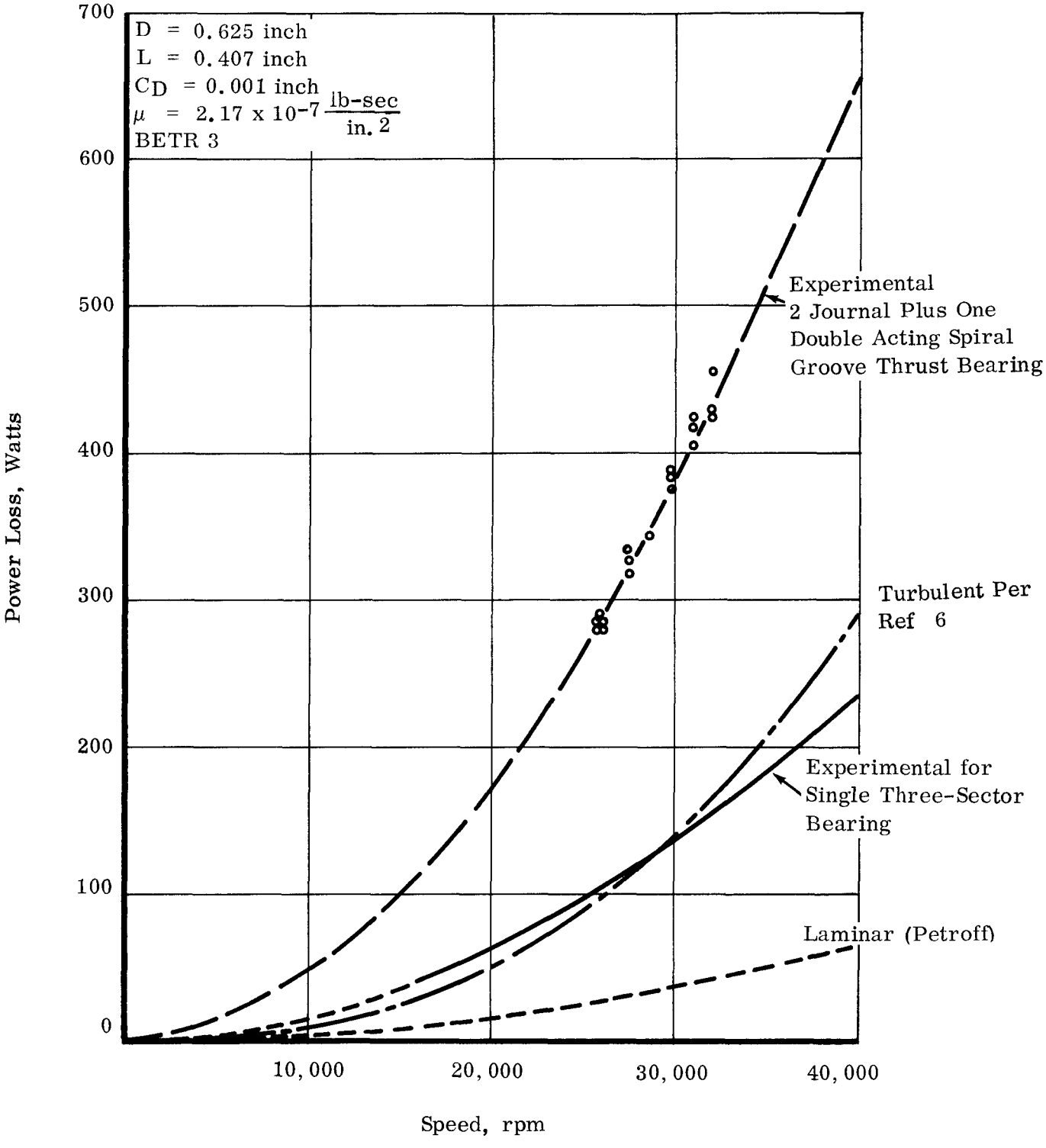

Figure 78. Power Loss vs Speed for a Three-Sector Bearing

well rounded axial slot and supply pads to assure lubrication to the loaded side; and the validity of the assumptions made to support the analytical solutions are some of the more important findings of this study.

Some of the other specific conclusions are:

1) Without orifice compensation the three-sector bearing behaves like a hydrodynamic bearing at large eccentricity ratios and high speeds.

2) Without orifice compensation it is possible to choke or throttle off all the flow out of the loaded pad.

3) With orifice compensation the bearing behaves predominantly like a hydrostatic bearing with some hydrodynamic influence at higher speeds and eccentricity ratios.

4) The tight clearance bearing has serious flow limitations at speeds of 40,000 rpm with existing system pressures.

5) No half-frequency whirl or critical speeds were detected up to 42,000 rpm.

Comparison of the experimental data with predicted performance indicated that for constant supply pressure the bearing behavior approached that of a hydrodynamic laminar flow bearing. For constant flow, perfect compensation seems to be approached and,as a result, performance is predominantly hydrostatic and not affected by Reynolds number or turbulence.

D. PROGRAM III - PARTIALLY ORIFICE-COMPENSATED THREE-SECTOR BEARING TESTS

The need for orifice compensation to improve the stability performance and flow dependability of the three-sector bearing was vividly demonstrated in the BETR 3 test on the individually fed three-sector bearing. The desirability of orifice compensation had actually been established prior to the BETR 3 test, but several factors had prevented the evaluation of such a bearing. The major ones were:

1) To provide full orifice compensation requiring orifices < 0.030 inch in diameter. There were considerable misgivings about plugging (by corrosion product deposition) based on some jet pump experiences.

2) Flow-pressure requirements without absorbing a further pressure drop through small orifices were already straining the system capacity.

3) The reduced pressure in the supply pad would weaken the bearings.

The importance of achieving stable operation, a continued improvement in elimination of crud deposition, adequate load capacity, the results of the BETR 3 test, and the

disappointing performance of the uncompensated three-sector bearing in the CRU III test series led to the initial series of tests of a partially orifice-compensated three-sector bearing.

The three-sector bearing was modified by replacing the 0.078-inch diameter orifice with a 0.028-inch orifice. The 0.025-inch orifice was selected because it represented the smallest jet pump diameter evaluated experimentally to that time. A comparison of the existing supply pad configuration and the orifice size indicated the following:

1) Area of orifice $= \frac{\pi}{4} d^2$

$$A_o = 0.00478 \text{ in.}^2$$

Where $d = 0.078$ inch

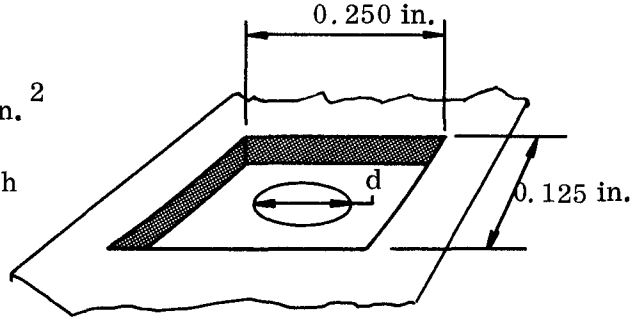

2) Area of supply pad annulus

If we consider radial clearance

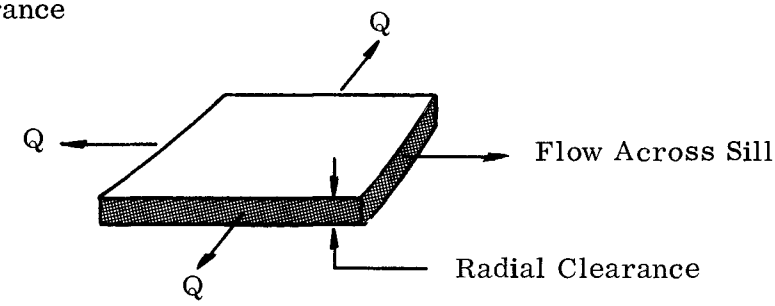

$$A_{S.P.} = \left[2 \times (0.25 + 0.125)\right] \times \frac{C_D}{2}$$

Where: $\frac{C_D}{2} = 0.0017$ inch

$$\therefore \quad A_{S.P.} = 0.000638 \text{ in.}^2$$

The above calculations show that the supply pad annulus represents the minimum area that the flow sees, and consequently the major pressure drop will occur across the sill formed by the supply pad and in the surrounding bearing annulus. This condition represents the inherently compensated case, where the entire pressure drop takes place inside the bearing clearance space.

If the bearing is considered as a resistance circuit

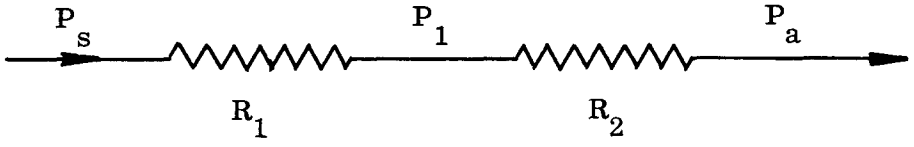

Where:

P_s = Supply pressure

P_1 = Pressure downstream of an inlet hole or orifice

P_a = Atmospheric or ambient pressure

and

R_1 = Resistance of hole or orifice

R_2 = Resistance in bearing annulus, i.e., of the lubricant film

For complete inherent compensation $R_1 \equiv 0$, and since P_s is constant, the same pressure drop will occur across R_2 regardless of the magnitude of R_2. This condition exists in the uncompensated three-sector bearing. There is no restoring force, i.e., build up in internal pressure, to counteract the shaft being displaced in the bearing. The only effect will be to throttle flow in the loaded area.

However, if $R_1 >> R_2$ then changes in R_2 will cause negligible changes in P_1. This represents the condition of complete orifice compensation where all the pressure drop occurs in the orifice and none in the lubricating film.

Since the maximum variation in P_1 is desired as the film thickness changes, it is apparent that some compensation is necessary and that it is essential to achieve an appropriate balance between R_1 and R_2. Under those circumstances, the maximum fluid film bearing stiffness, $K = dW/dh$, is achieved and the bearing tends to have maximum stability. Experience has revealed that maximum stiffness, and consequently maximum stability, is achieved if the minimum area that the flow sees exists in the orifice. To achieve the maximum stiffness, R_1 is made essentially equal to R_2. Consider a 1/4-inch x 1/8-inch supply pad and a total diametral clearance of 0.001 inch. (The clearance is purposely selected as the minimum under consideration to establish the value of the orifice diameter. Any increase in clearance will increase the orifice restriction portion of the overall bearing restriction.)

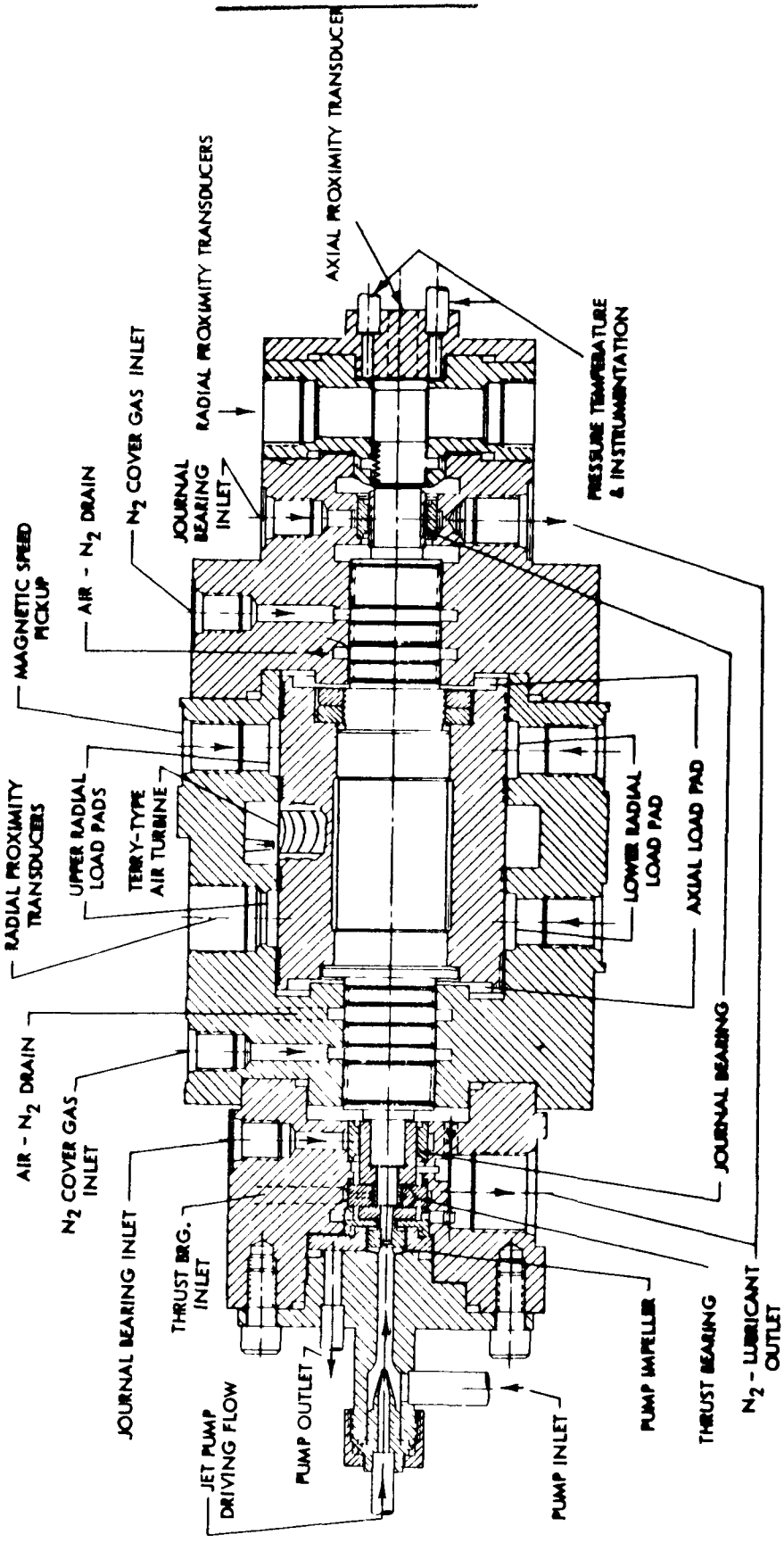

7636-0894

Figure 79. High Temperature Bearing Pump Test Rig Dual Bearing Test Fixture Schematic

Then since $R_1 = R_2$; i.e., resistance in orifice is equal to annulus restrictions

Area of orifice = Area of supply pad annulus

$$\therefore \frac{\pi}{4} d^2 = 2 \left[0.25 + 0.125 \right] \times \frac{0.001}{2}$$

where d = orifice diameter

$$\therefore \quad d \leq 0.0218 \text{ inch}$$

The following test series, DBTR 1 and 1A*, was conducted to establish the influence of partial orifice compensation, i.e., $R_1 < R_2$, but not $R_1 << R_2$ as in the previous tests, on the performance of the three-sector bearing. Of particular interest was the influence on stability.

1. DBTR 1 Test Series

The dual bearing test fixture was a new test fixture with improved instrumentation. It was the basic BETR design but included a shaft extension on the "B" bearing end to permit another plane of radial proximity probe (two, 90° apart) and an axial probe for thrust bearing measurement. Figure 79 shows the schematic, and Figure 80 shows the assembled fixture with instrumentation.

The three-sector journal bearings installed in DBTR 1 had a 0.625-inch diameter, 0.407-inch length, and 0.0016-inch diametral clearance. There were three 0.025-inch diameter orifices (one per sector) surrounded by a 1/4-inch x 1/8-inch x 0.030-inch deep supply pad.

The standard test procedure was followed, whereby load capacity, film thickness, attitude angles, and flow characteristics were established over a speed range of 0 to 40,000 rpm. A balanced rotor was initially used, but toward the end of the test there were some indications that mercury was trapped in the rotor creating some 9 lb/bearing unbalance.

a. Load Capacity

Figures 81 through 85 show the load deflection characteristics at zero; 15,000; 20,000; 30,000; and 40,000 rpm. The influence of partial orifice compensation is evident at the zero speed and at speeds up to 20,000 rpm. The increase in load capacity as a result of increased supply pressure is more clearly shown in Figure 81. At the higher speeds, the increased hydrodynamic forces overshadow the hydrostatic component so that changes in supply pressure have little influence on increasing load capacity.

*Dual Bearing Test Rig

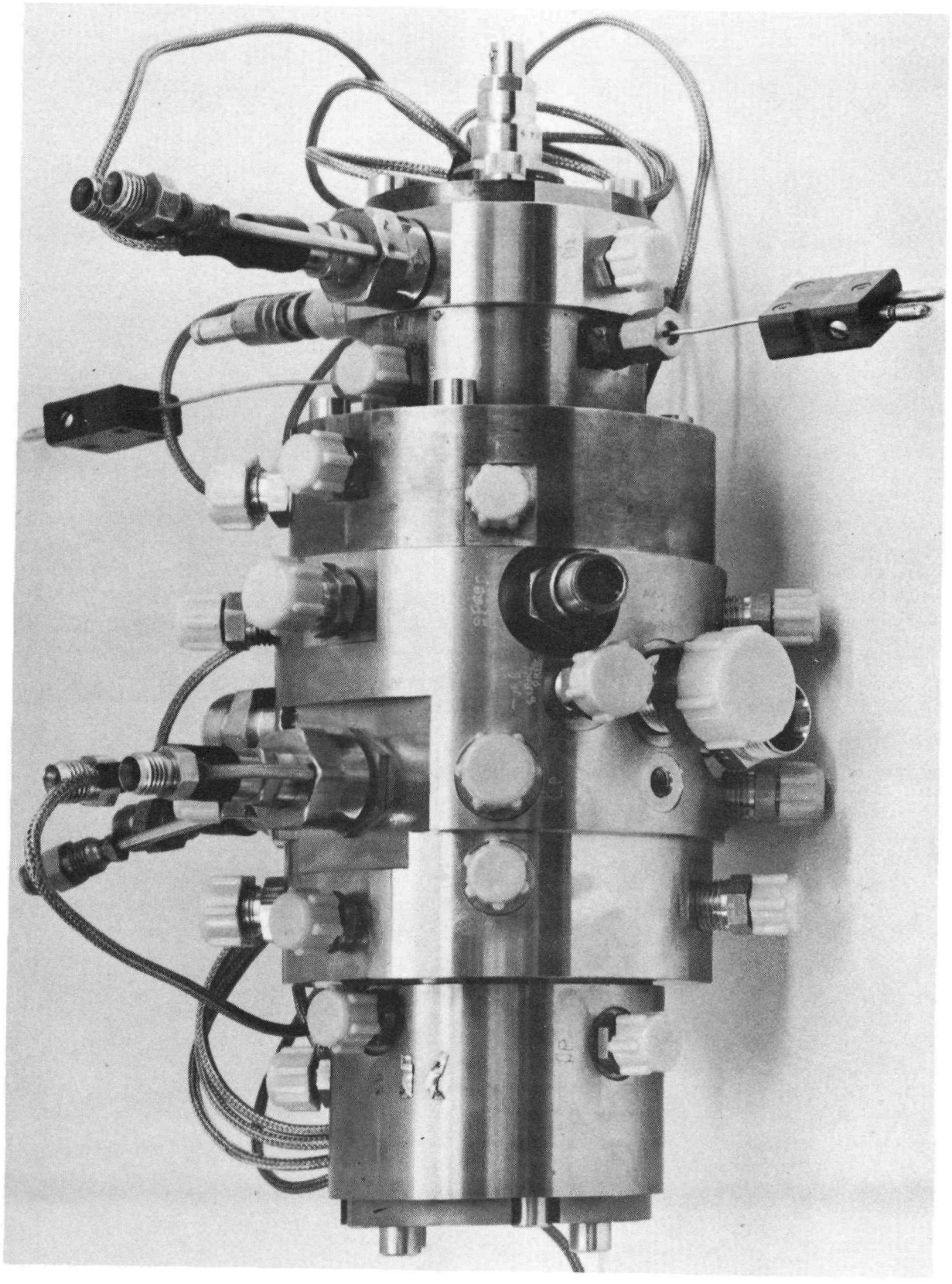

Figure 80. Assembled Dual Bearing Test Fixture

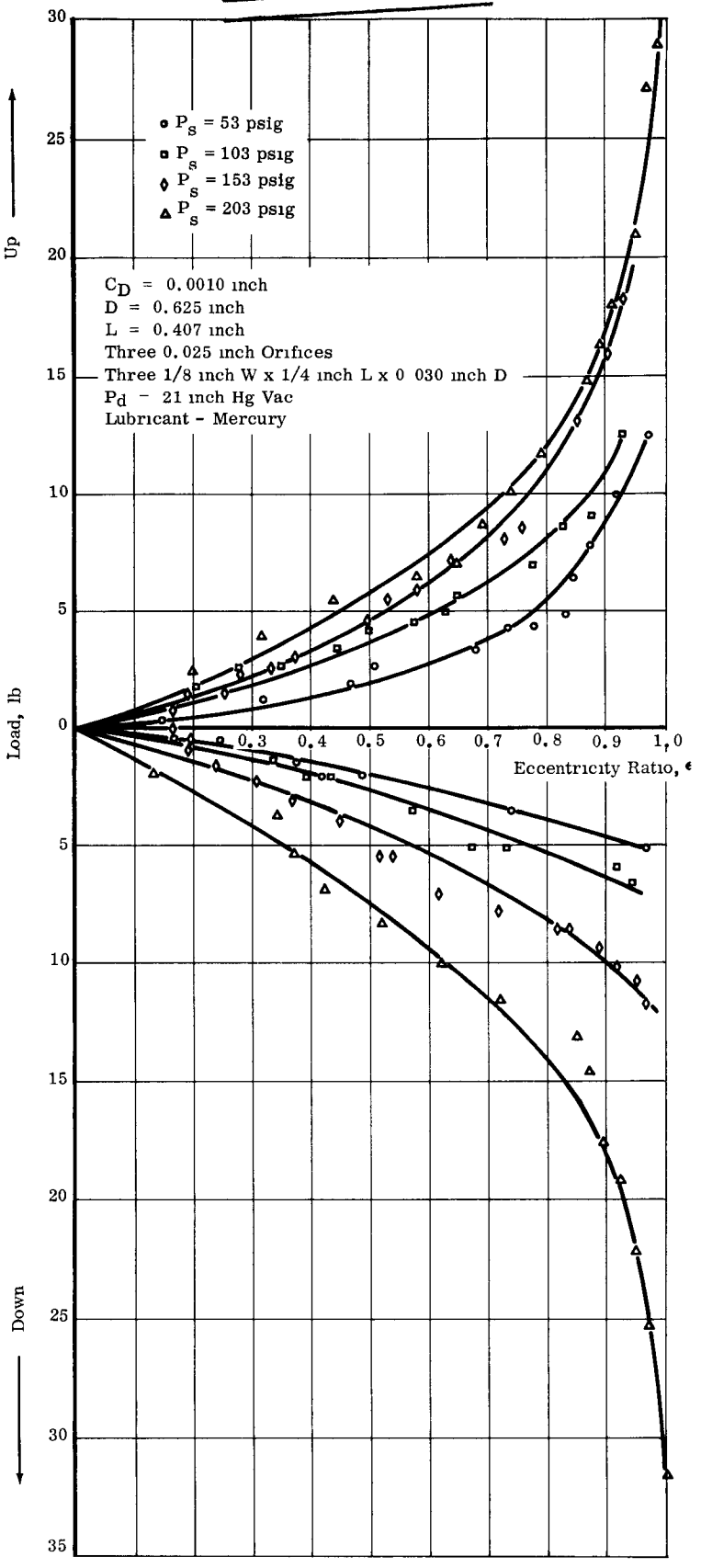

Figure 81 Static Load vs Eccentricity Ratio for a Three-Sector Partial Orifice Compensated Bearing DBTR 1 Test Series

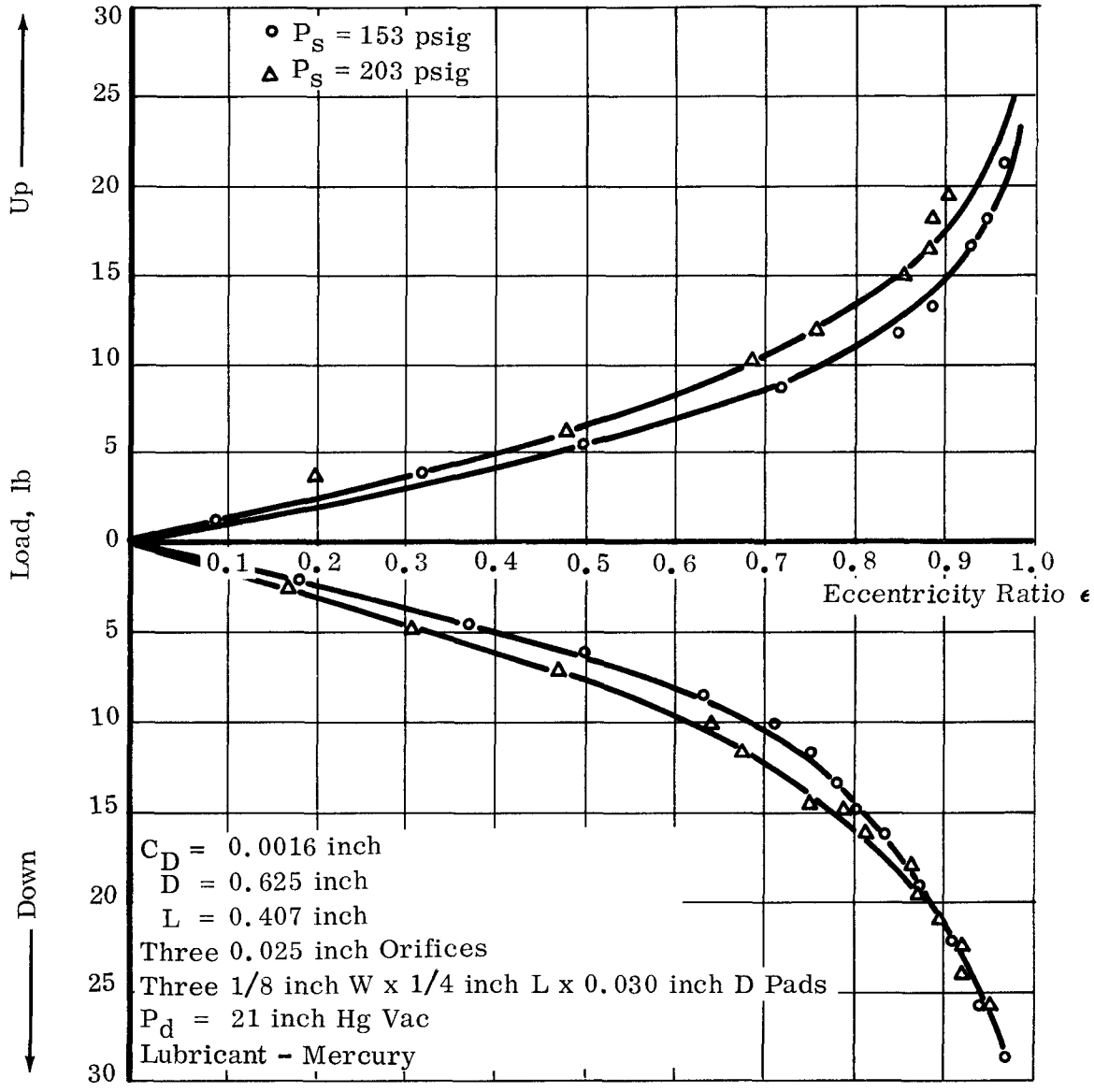

Figure 82. Load vs Eccentricity Ratio for a Three-Sector Partial Orifice Compensated Bearing at 15,000 rpm

DBTR 1 Test Series

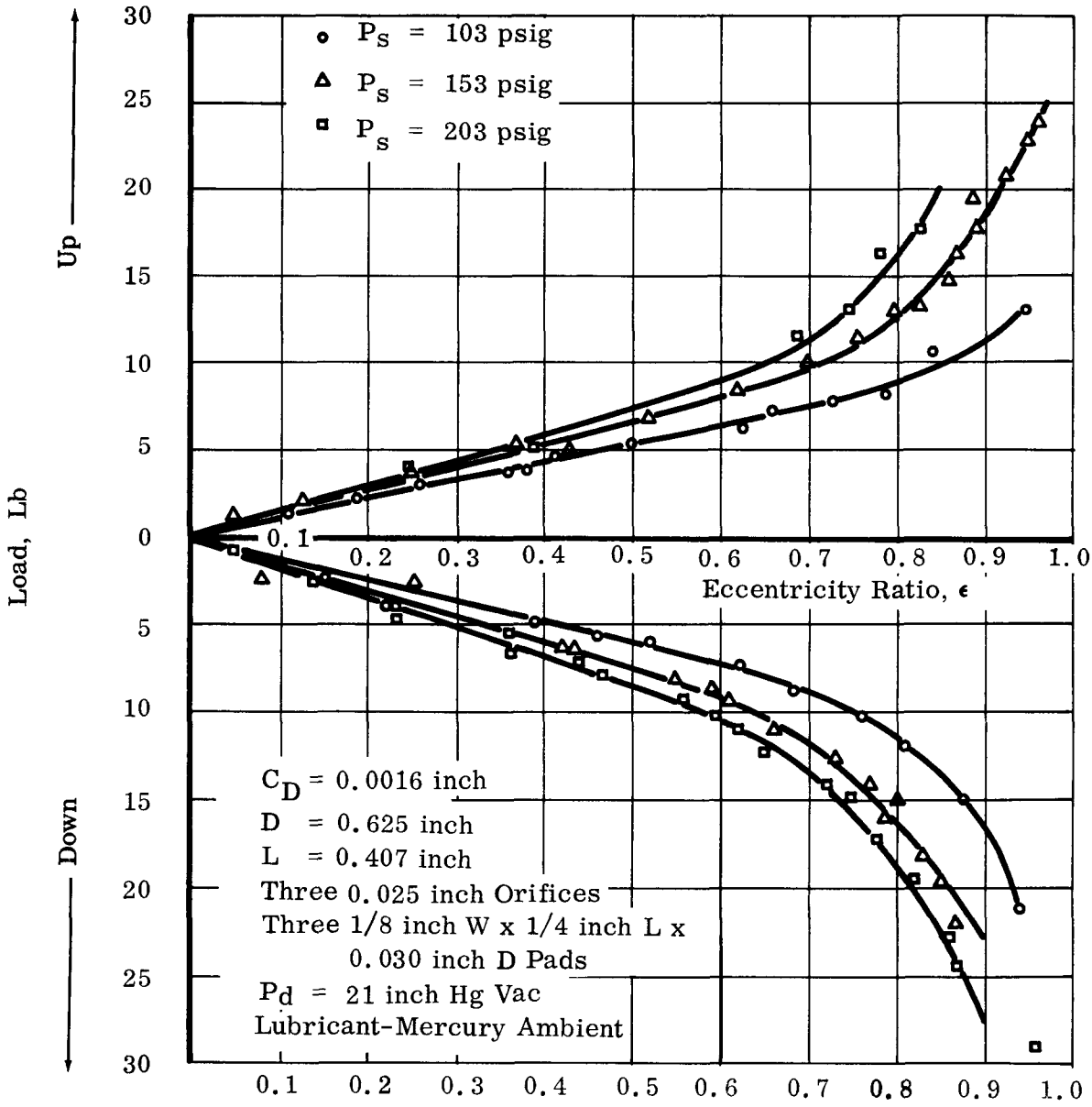

Figure 83. Load vs Eccentricity Ratio for a Three-Sector Partial Orifice Compensated Bearing at 20,000 rpm

DBTR 1 Test Series

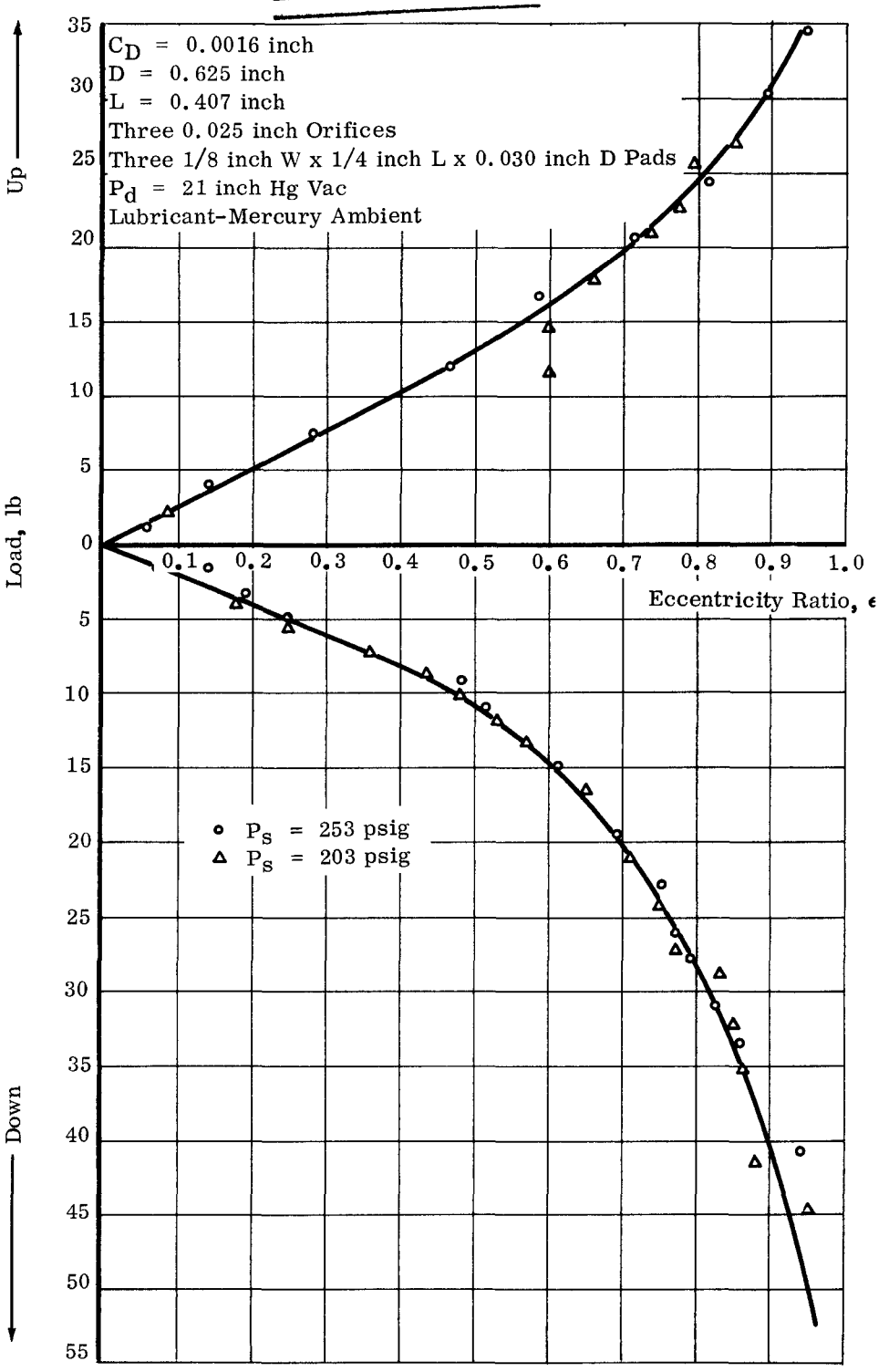

Figure 84. Load Carrying Capacity vs Eccentricity Ratio for a Three-Sector Partial Orifice Compensated Bearing at 30,000 rpm

DBTR 1 Test Series

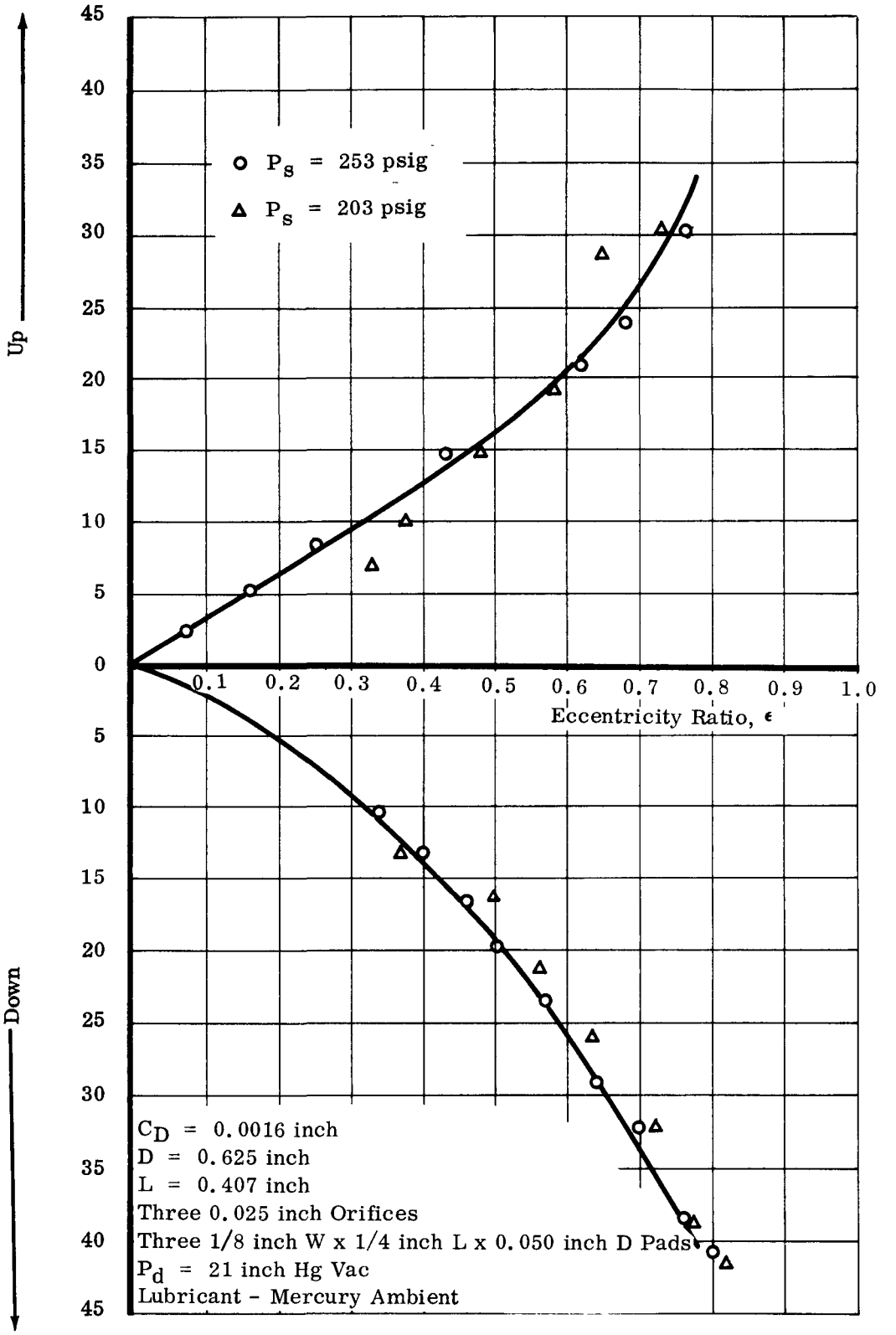

Figure 85. Load Carrying Capacity vs Eccentricity Ratio for a Three-Sector Partial Orifice Compensated Bearing at 40,000 rpm

DBTR 1 Test Series

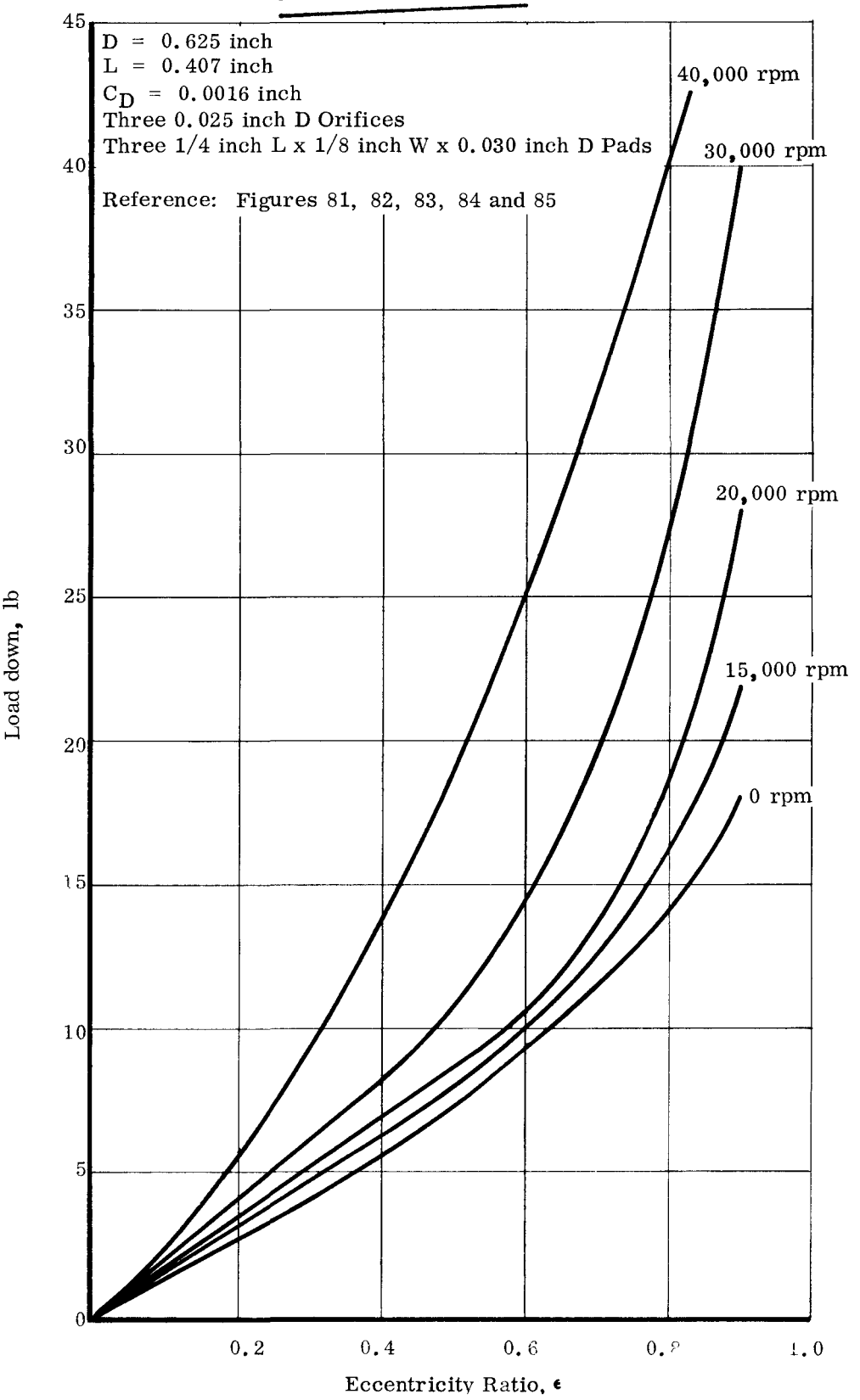

Figure 86. Load Deflection Characteristics of a Three-Sector, Partially Compensated Bearing at 203 psig Supply Pressure

DBTR 1 Test Series

At low values of eccentricity ratio the hybrid nature of the bearing results in a departure from hydrodynamic predictions, since this is the region where hydrostatic forces predominate. At larger eccentricity ratios, similar to higher speed, behavior is hydrodynamic and performance approaches laminar predictions. Figure 86 shows the increase in load capacity with speed for a constant supply pressure of 203 psig (loading down). Since the hydrostatic component is essentially constant, the increased load capacity with speed and eccentricity ratio is due to the hydrodynamic component. The increased pressure drop through the orifice resulted in a lower total load capacity, in comparison to the uncompensated case, at the lower eccentricity ratios. This characteristic represents one of the two disadvantages which result from orifice compensation. Flow-pressure, discussed later, is the second disadvantage.

b. Attitude Angle

The shaft locus is shown in Figures 87 through 91 for speeds from zero to 40,000 rpm. The loci reflect the increased hydrostatic influence as a result of the partial compensation. The larger the pressure, the smaller the attitude angle for a given speed and eccentricity ratio. Comparison with the completely uncompensated case (i.e., Figures 89 and 90 with Figure 68 (BETR 3) and Figure 41 (BETR 1) at 20,000 and 30,000 rpm, and Figure 87 with Figure 67 (BETR 3) and Figure 41 (BETR 1) at zero speed) clearly shows the influence of the partial compensation in minimizing the attitude angle at a given eccentricity ratio.

c. Stability

Threshold of half-frequency whirl was raised some 40 per cent over the uncompensated configuration. Furthermore, increasing supply pressure above 200 psig permitted complete suppression of whirl (at zero shaft weight) up to 40,000 rpm. The favorable attitude-eccentricity locus and partial compensation providing a sizable restoring force are responsible for the improved stability characteristics.

d. Flow-Pressure Characteristics

Increased pressure drop by reducing the orifice size and making the orifice restriction of the same order as the bearing clearance space restriction was the second penalty for improved stability. Figure 92 shows the flow characteristics of the partially compensated bearing as a function of speed. Statically the flow-pressure relationships were checked for three different shaft positions: shaft all the way on top of the bearing, shaft centered, and shaft slightly below center (equivalent to shaft weight position). Within the flow range of interest, 2 to 10 lb/min, the partial compensation assured essentially equal total flow regardless of shaft position. Superimposed in Figure 92 are the flow data from BETR 1. Statically the pressure drop due to compensation is severe. As expected, the pressure drop at low flows dynamically approaches zero and increases with higher flows.

Assuming that the 0.078-inch diameter orifice (BETR 1) has zero pressure drop through the orifice, the variation seen in Figure 92 represents a direct measure of

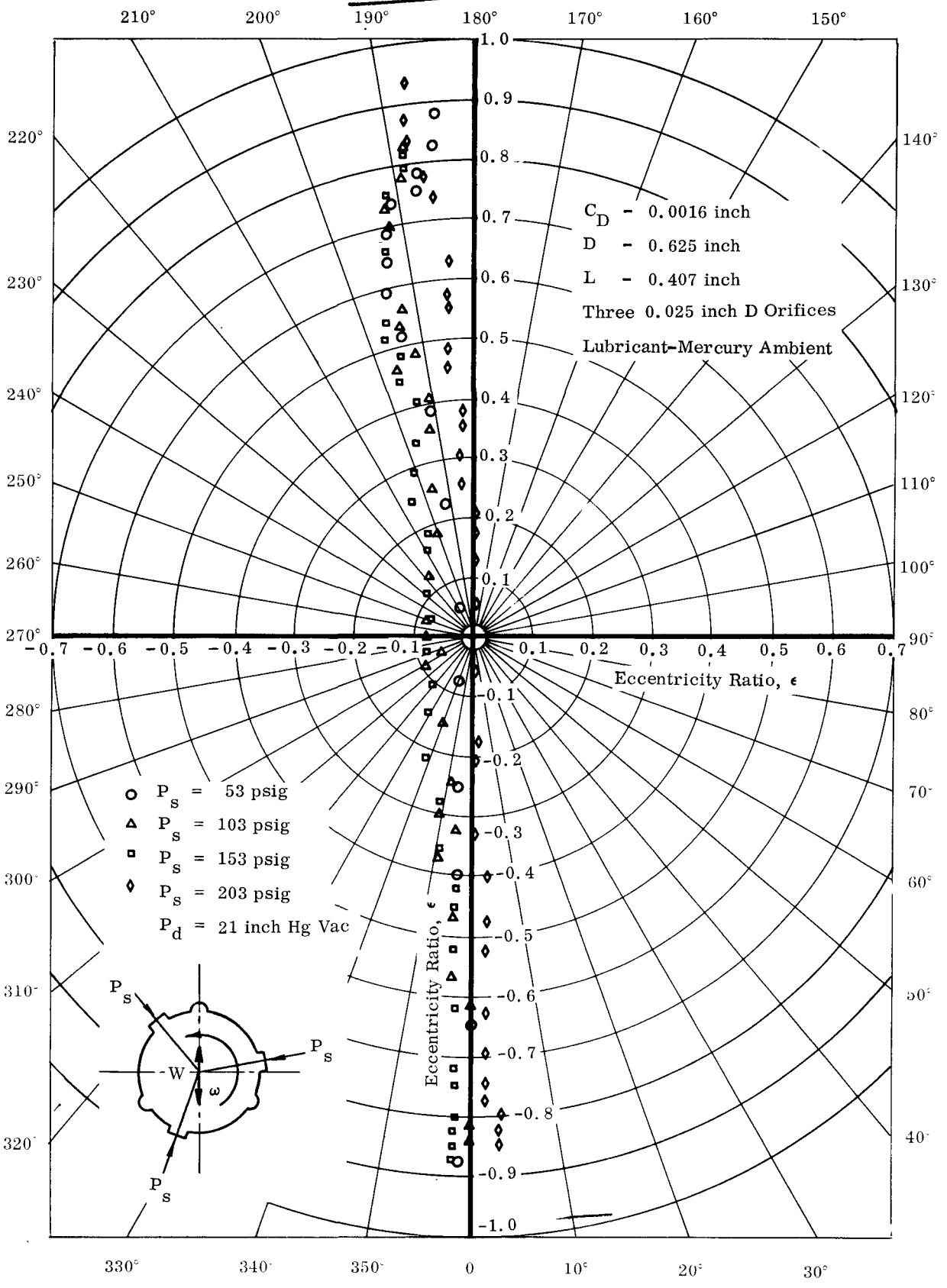

Figure 87. Static Attitude-Eccentricity Locus for a Partial Orifice-Compensated Three-Sector Bearing

DBTR 1 Test Series

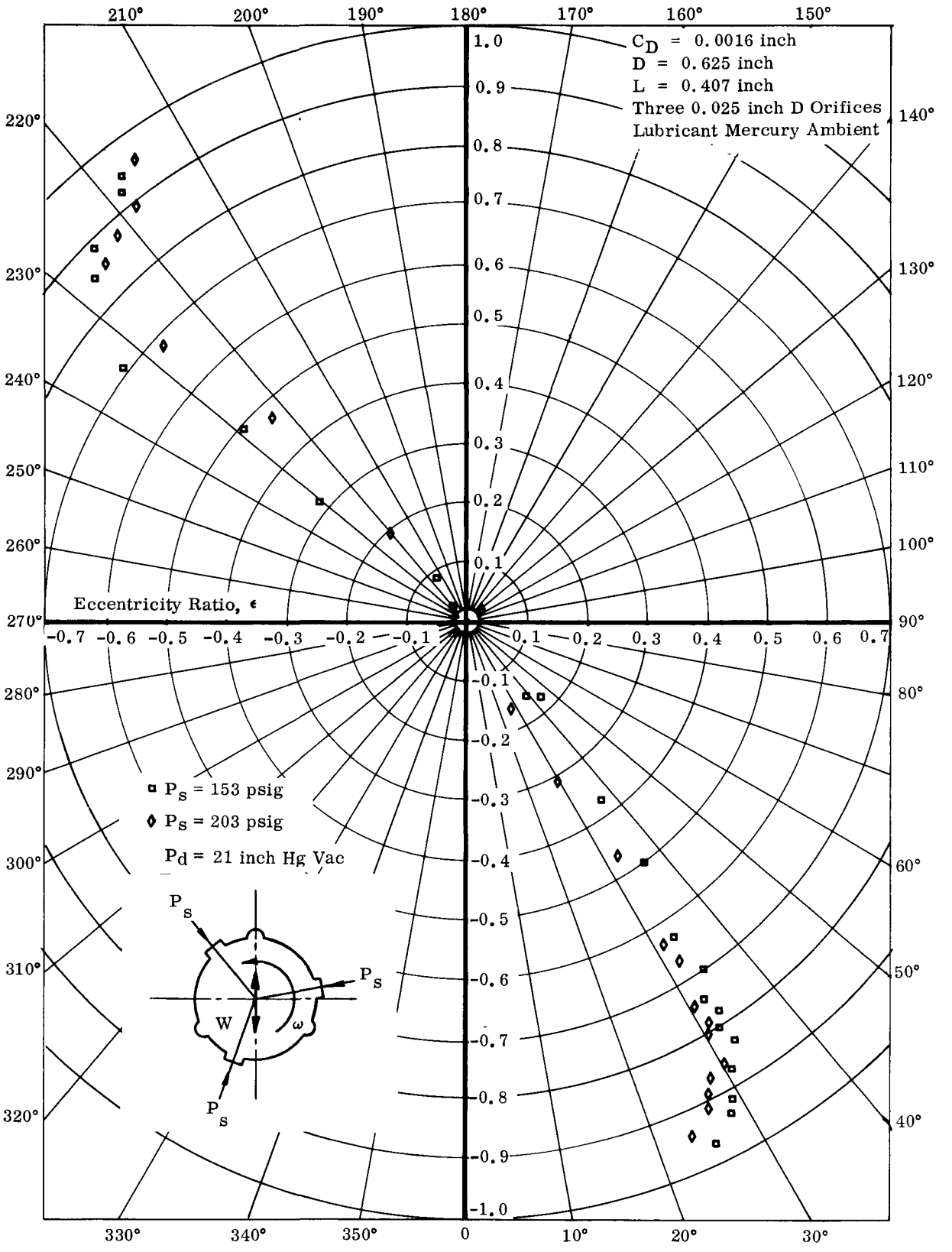

Figure 88. Attitude-Eccentricity Locus for a Partial Orifice-Compensated Three-Sector Bearing at 15,000 rpm

DBTR 1 Test Series

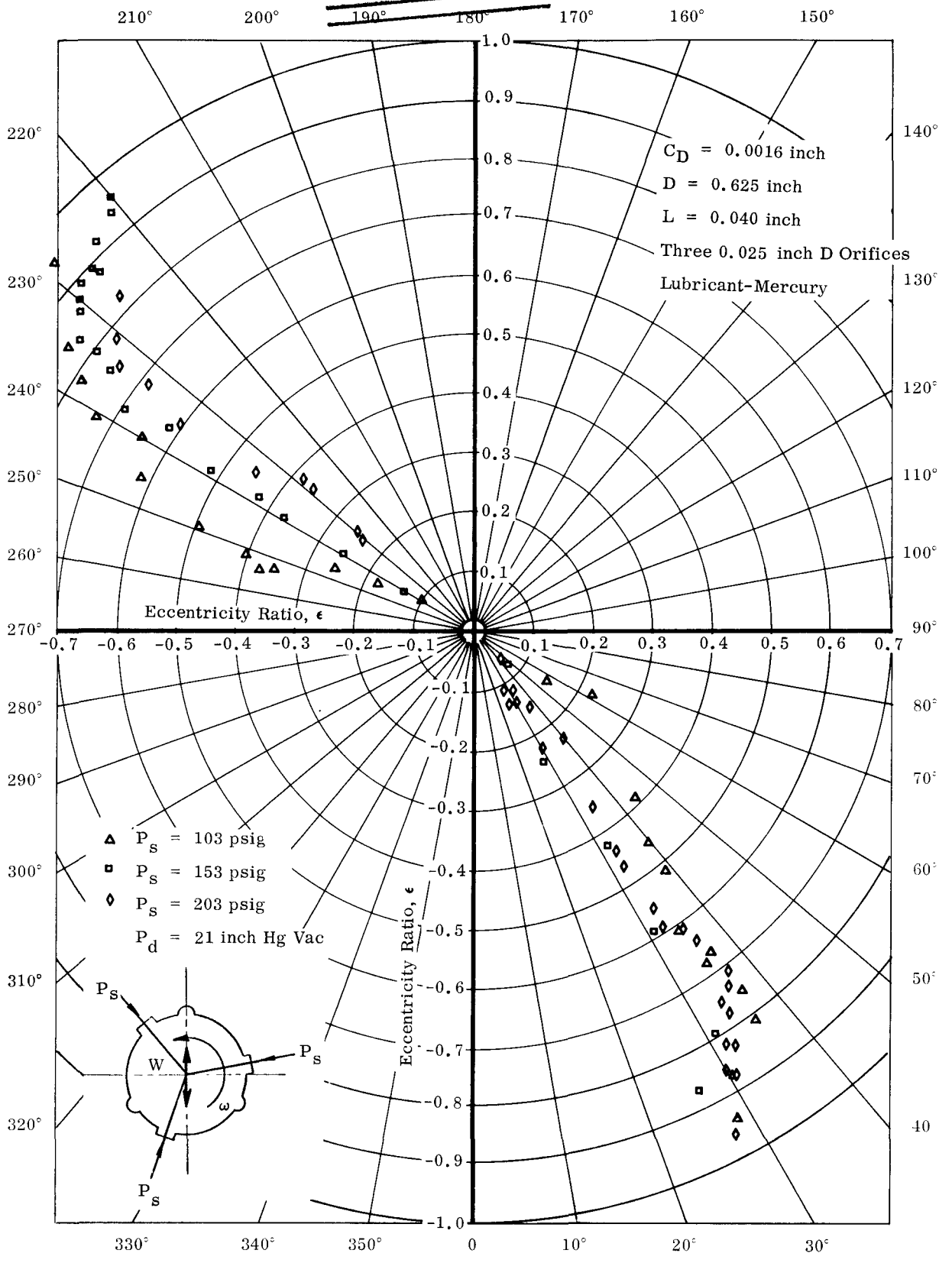

Figure 89. Attitude-Eccentricity Locus for a Partial Orifice-Compensated Three-Sector Bearing at 20,000 rpm

DBTR 1 Test Series

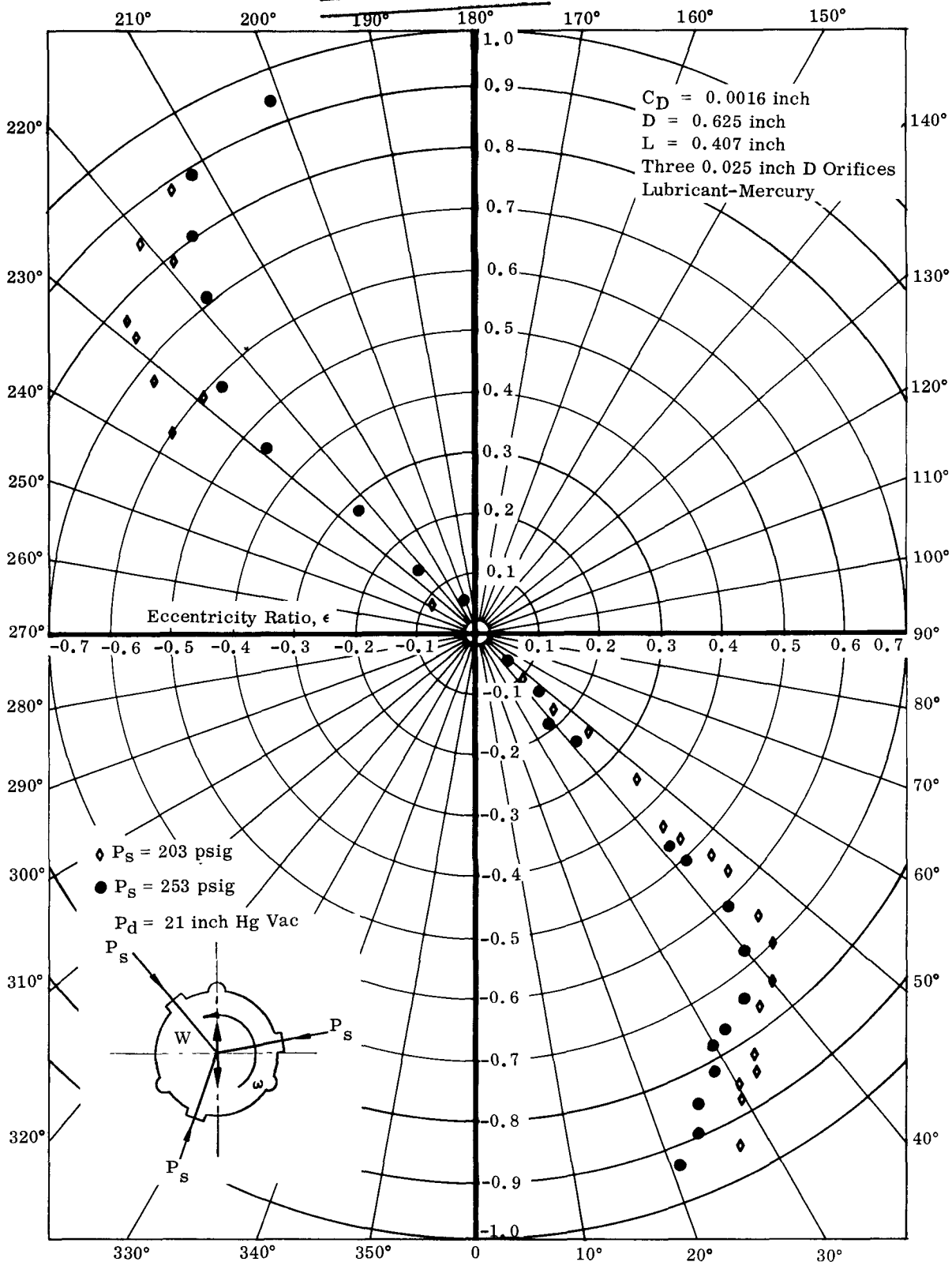

Figure 90. Attitude-Eccentricity Locus for a Partial Orifice-Compensated Three-Sector Bearing at 30,000 rpm

DBTR 1 Test Series

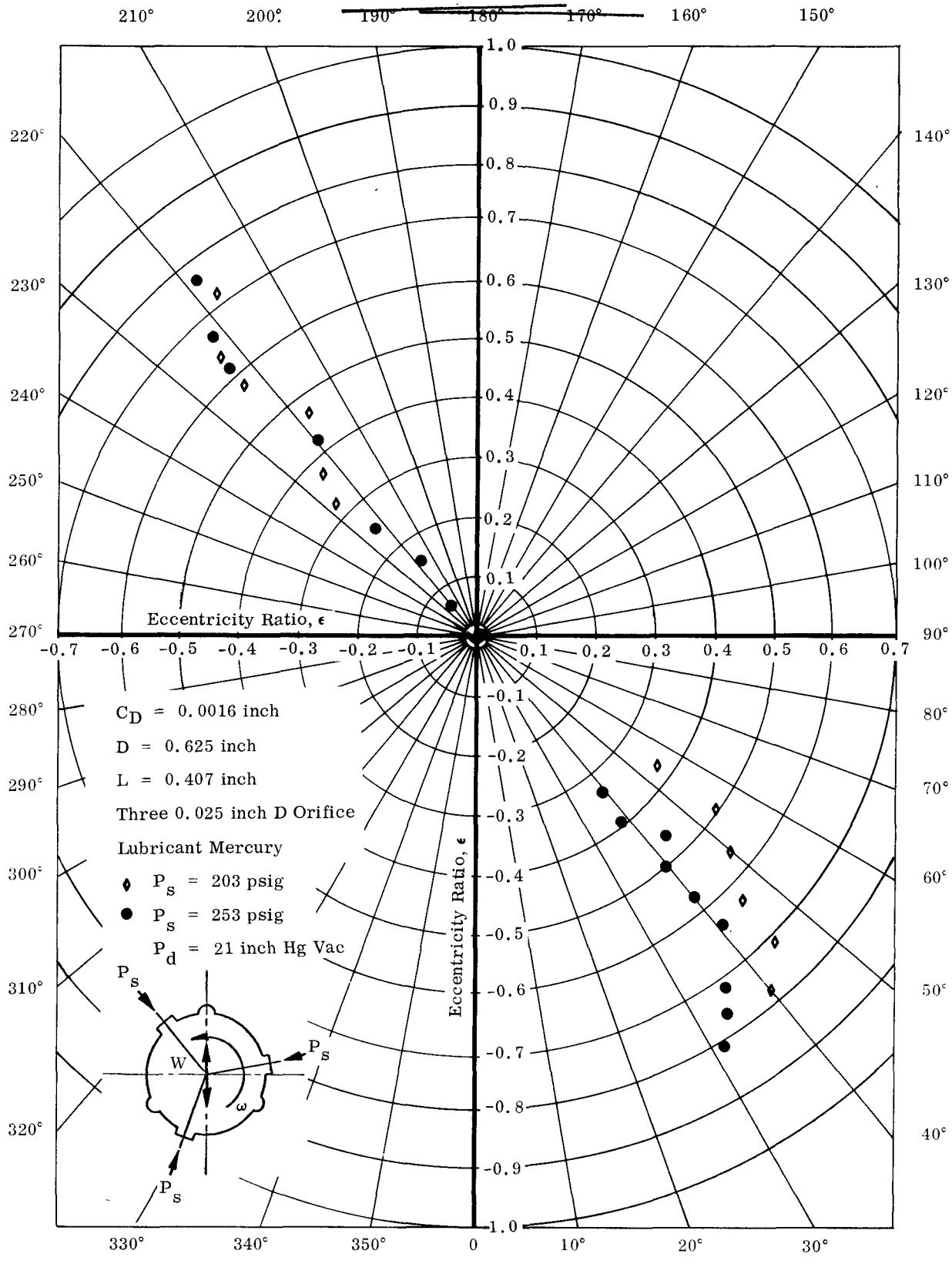

Figure 91. Attitude-Eccentricity Locus for a Partial Orifice-Compensated Three-Sector Bearing at 40,000 rpm

DBTR 1 Test Series

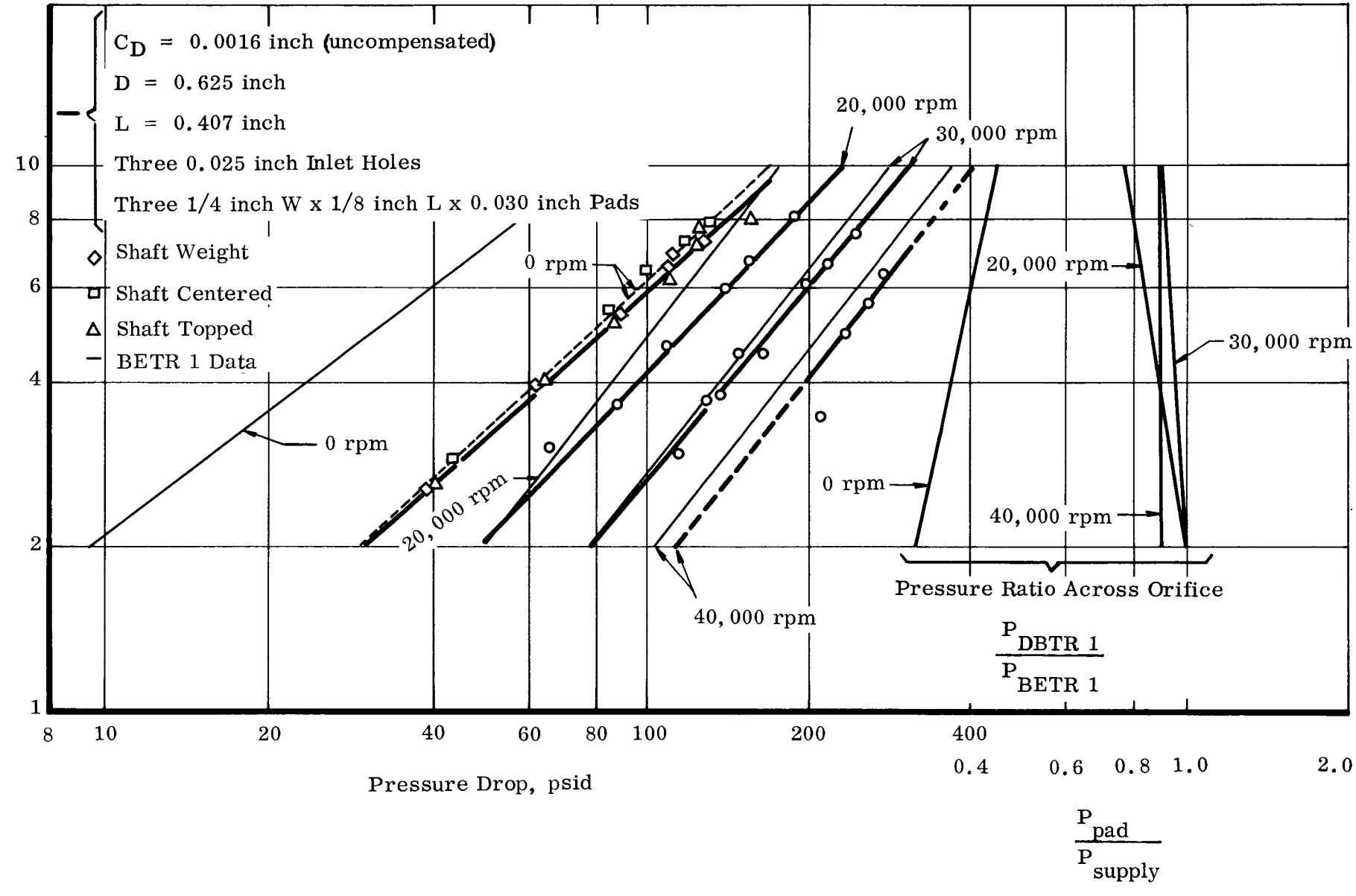

Figure 92. Flow Characteristics of a Partial Orifice-Compensated Three-Sector Bearing

DBTR 1 Test Series

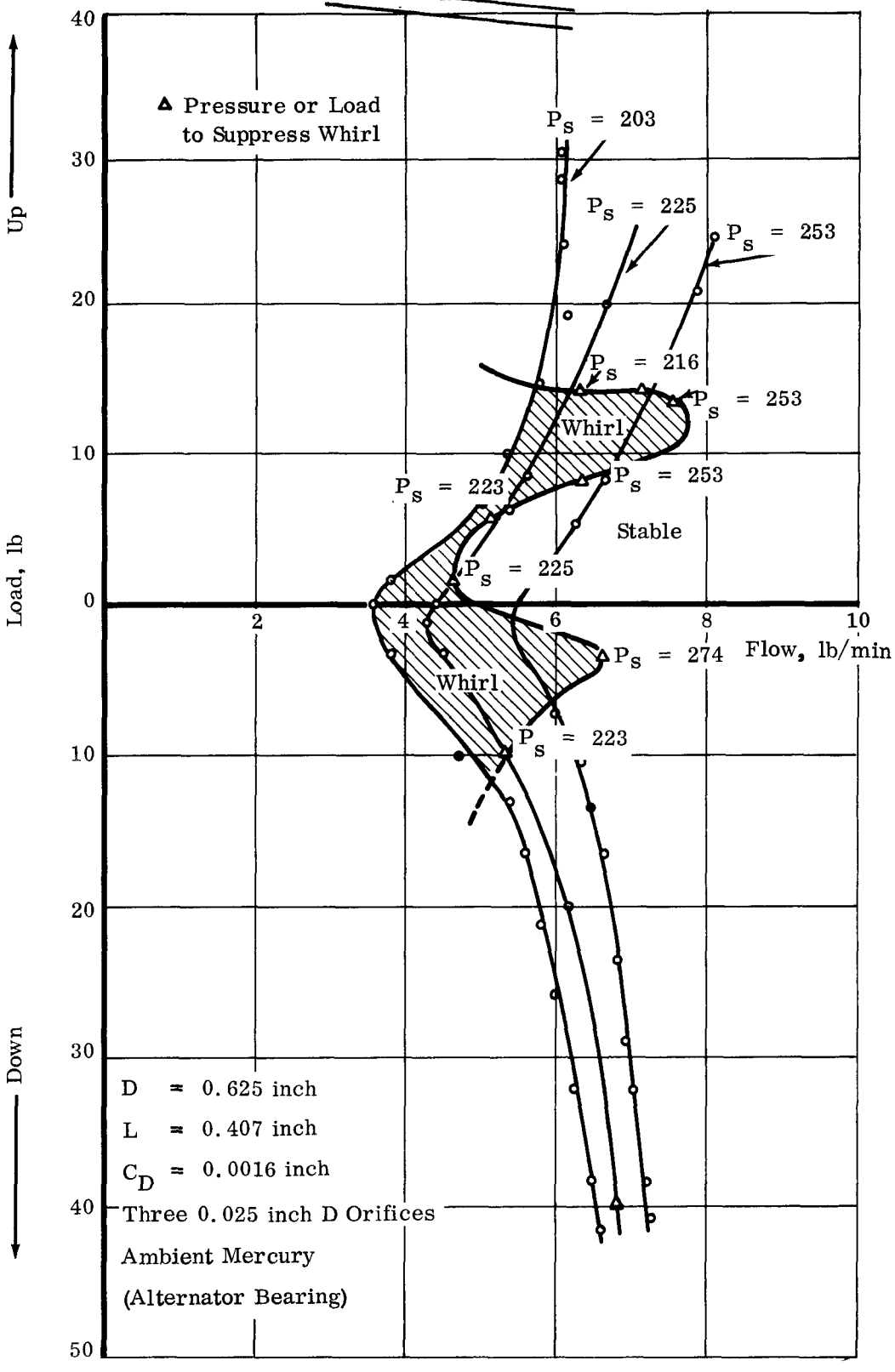

Figure 93. Load vs Flow for a Partial Orifice-Compensated Three-Sector Bearing at 40,000 rpm
DBTR 1 Test Series

pressure drop through a partially-compensated 0.025-inch diameter orifice because the bearing clearance restriction is identical in BETR 1 and DBTR 1. On this basis, the ratio of pressure in pad to supply pressure can be established; it is shown in Figure 92. The ratio is small dynamically, between 0.78 and 1.0; but it is statically quite large, from 0.32 to 0.45 (representing a large pressure drop).

The influence of load and stability on flow for fixed pressures at 40,000 rpm is shown in Figure 93. Superimposed are the pressures or load required to maintain stable operation at 40,000 rpm. Two distinct pockets of half-frequency whirl are evident. At a fixed pressure it is possible to be stable, but loads in either direction (up or down) will result in half-frequency whirl. Furthermore, at low loads it is possible to reduce pressure well below the threshold point without encountering whirl. Variation in total flow with load is still sizable, indicating that orifice compensation is not achieving constant flow with shaft displacement. Statically, however, variation from $-1.0 < \epsilon < 1.0$ is less than 1 lb/min.

2. DBTR 1A Test Series

The 0.0016-inch partially orifice-compensated bearing was modified to a 0.002-inch clearance, and the previous parametric test was repeated. As anticipated, the hydrostatic influence decreased further with the larger clearance. The net result was a weaker bearing at small eccentricity ratios where the hydrostatic component predominates.

a. Load Capacity

Figure 94 summarizes the load-deflection characteristics from zero to 40,000 rpm. Comparison with Figure 86 shows that at small eccentricity ratios the larger clearance bearing is considerably weaker. As $\epsilon \longrightarrow 1.0$, however, the predominating hydrodynamic forces result in the load capacity of the 0.002-inch clearance bearing approaching that of the 0.0016-inch bearing.

b. Attitude Angle

The clearance had little influence on the absolute attitude-eccentricity locus. Figure 95 shows the composite at 30,000 rpm. Varying the supply pressure from 153 to 203 psi has almost no influence on the locus. Comparison with Figure 90 at 153 and 203 psi is shown in Figure 96 and the good agreement permits the assumption that the locus of the partially orifice-compensated three-sector bearing over the range of clearances and speed tests (Reynolds numbers) is not too sensitive to clearance.

c. Stability

As anticipated, reduction in the hydrostatic component reduced the whirl threshold to 22,500 rpm. This still represents a sizable improvement in stability characteristics over the uncompensated 0.002-inch clearance bearing (which was 15,000 rpm). To

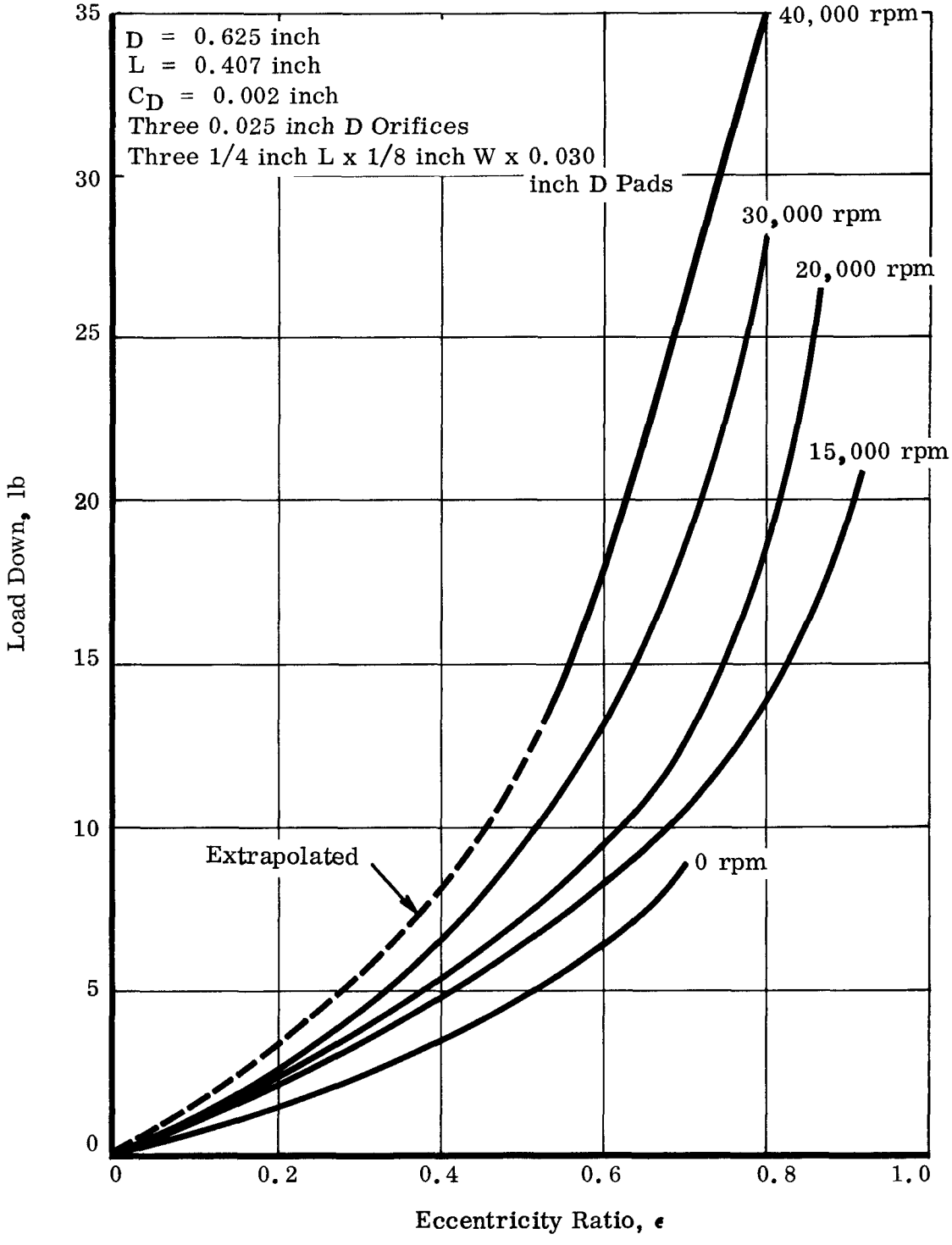

Figure 94. Load-Deflection Characteristics of a Three-Sector, Partially Compensated Bearing

DBTR 1A Test Series

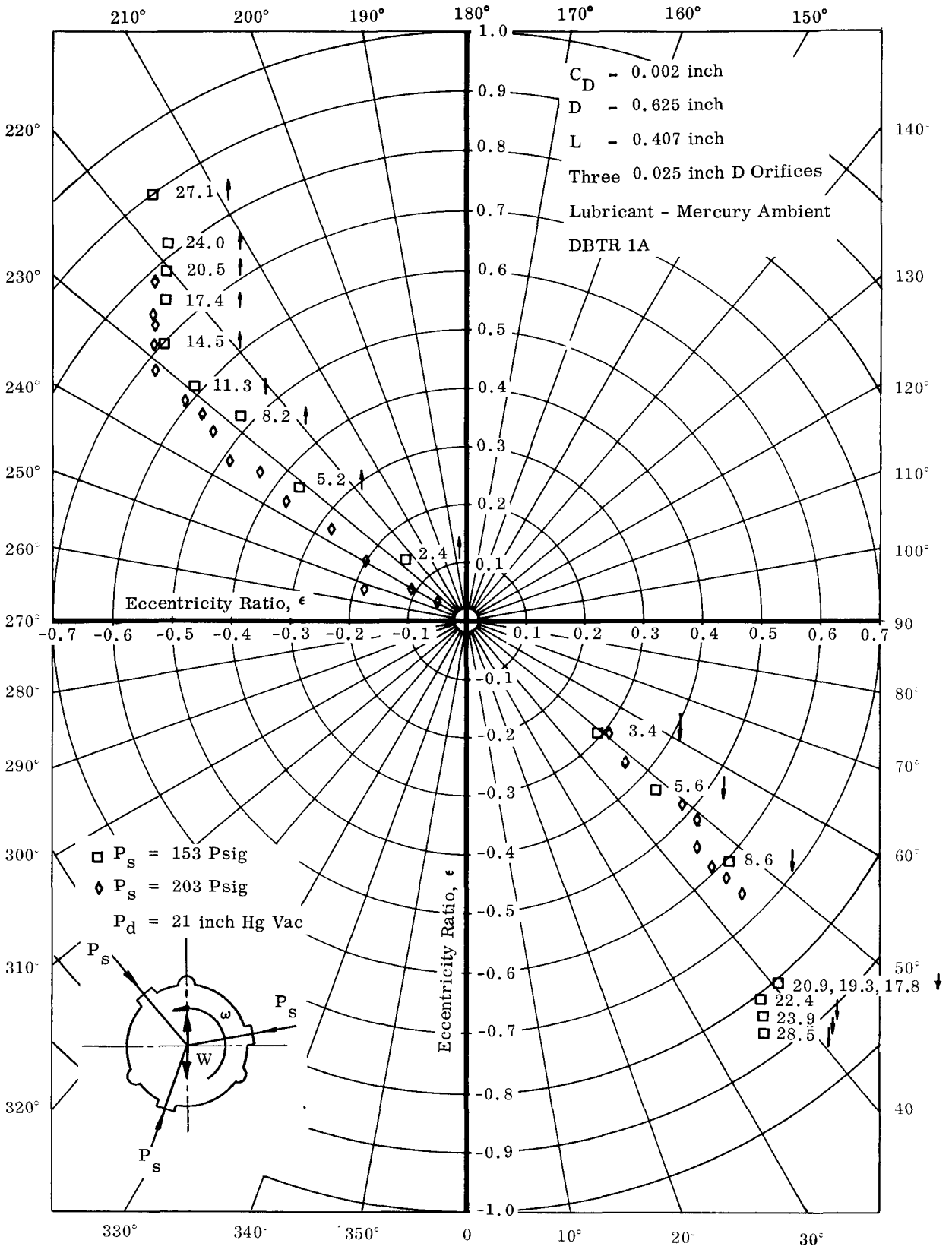

Figure 95. Attitude-Eccentricity Locus for a Three-Sector Partial Orifice-Compensated Bearing at 30,000 rpm

DBTR 1A Test Series

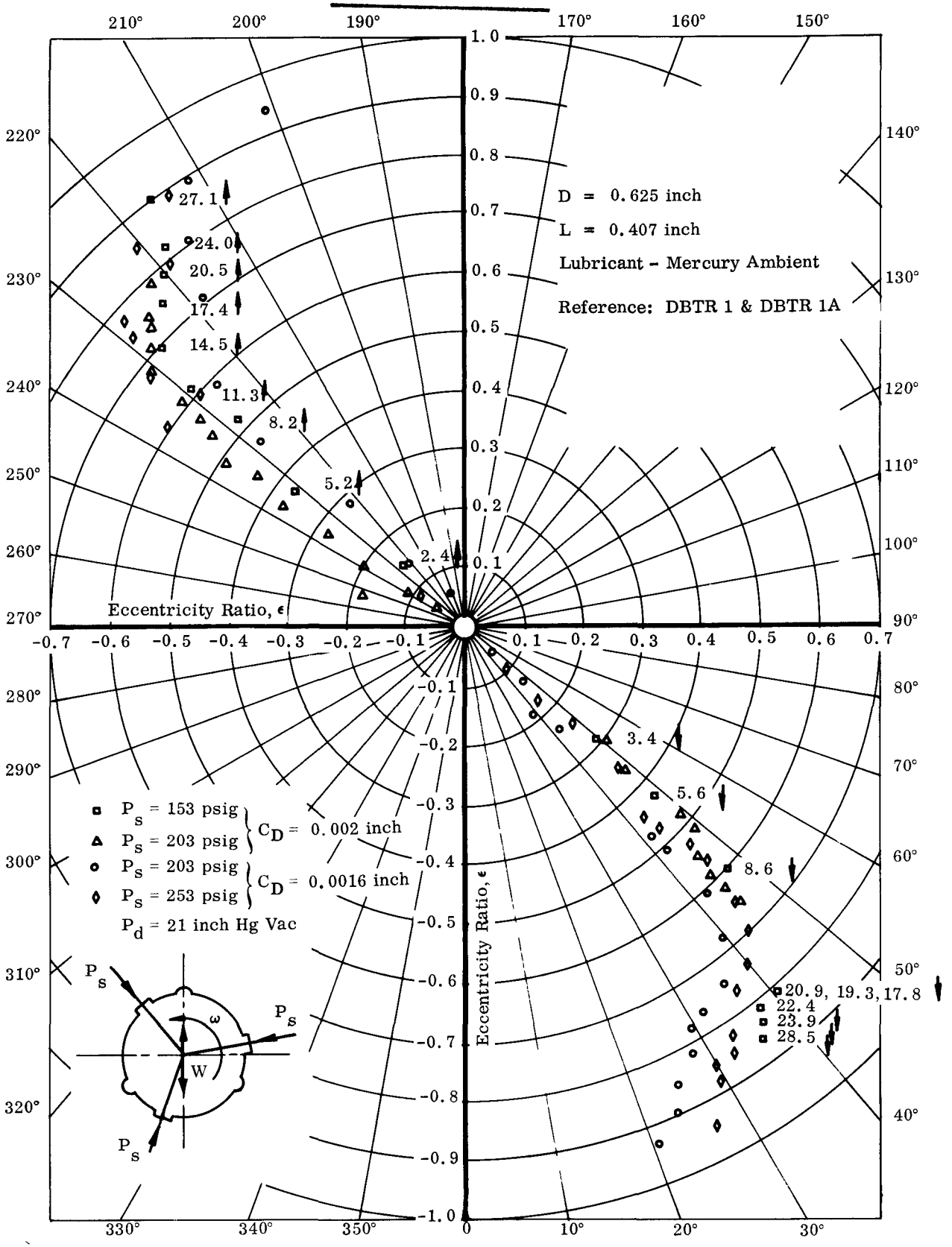

Figure 96. Comparison of Attitude Eccentricity Locus for Partial Orifice-Compensated Three-Sector Bearing at 30,000 rpm

(C_D = 0.0016 and C_D = 0.002)

assure that pure half-frequency whirl and not some other fractional or multiple frequency whirl was being encountered, the whirl frequency was measured at each speed. Figure 97 shows that the whirl frequency, i.e., ratio of whirl speed to rotating speed, varied from 0.492 to 0.513.

d. Flow Characteristics

Figure 98 shows the flow characteristic of the 0.002-inch partially compensated bearing, compares it to the uncompensated three-sector, and establishes the estimated pressure drop through the 0.025-inch orifice. The penalty for partial orifice compensation is clear in Figure 98. Since the orifice restriction remained unchanged between DBTR 1 and DBTR 1A, the static pressure drop (or P_{pad}/P_{supply} ratio) vs flow remained essentially unchanged by slightly varying the downstream restriction (clearance). Comparison of Figures 92 and 98 verify this. However, at 20,000; 30,000; and 40,000 rpm, the influence of larger Reynolds number in the clearance space influences the pressure drop. Increasing speed results in increased pressure drop at low flows (2 lb/min) while at larger flows ($\approx$ 10 lb/min) the pressure drop is equivalent to a P_{pad}/P_{supply} ratio of approximately 0.8.

e. Power Loss

Figure 99 shows the experimental power loss compared to that predicted by Smith and Fuller (Ref 6). Agreement is again good (180 watts at 40,000 rpm was assumed for the spiral-groove thrust bearing). Comparison with the power loss data generated for the 0.001-inch clearance three-sector bearing in BETR 3 (see Figure 78) shows that power loss decreases with increasing clearance as predicted by laminar flow and the turbulent correction by Smith and Fuller. The orifice compensation should have no influence on power loss. Figure 100 presents power loss as a function of speed for the 0.002- and 0.001-inch clearances.

3. Conclusions on Test Series

Completion of the DBTR 1A test concluded the scheduled test series on partially orifice-compensated three-sector bearings. Several important factors became evident as a result of these tests:

1) Partial orifice-compensation improved stability characteristics (half-frequency whirl).

2) The improved stability performance was obtained at the expense of reduced load capacity and increased pressure requirements for a fixed flow rate. However, load capacity was still far in excess of design loads and pressures were adequate for meeting flow requirements.

3) No plugging or reduction in orifice area was noted during 55 hours of testing under a variety of conditions.

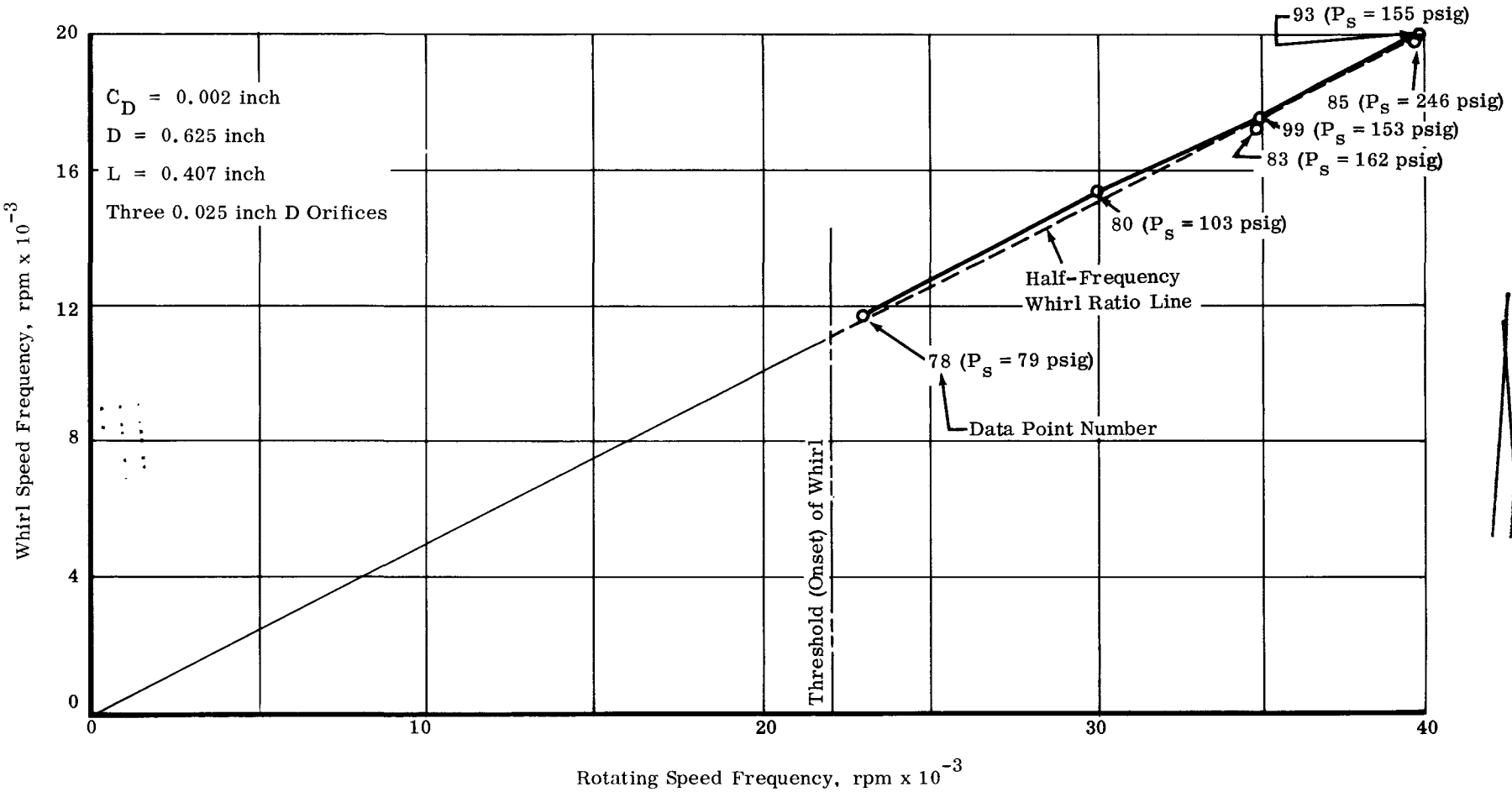

Figure 97. Whirl Frequency as a Function of Rotating Speed for a Partial Orifice-Compensated Three-Sector Bearing DBTR 1A Test Series

CONFIDENTIAL

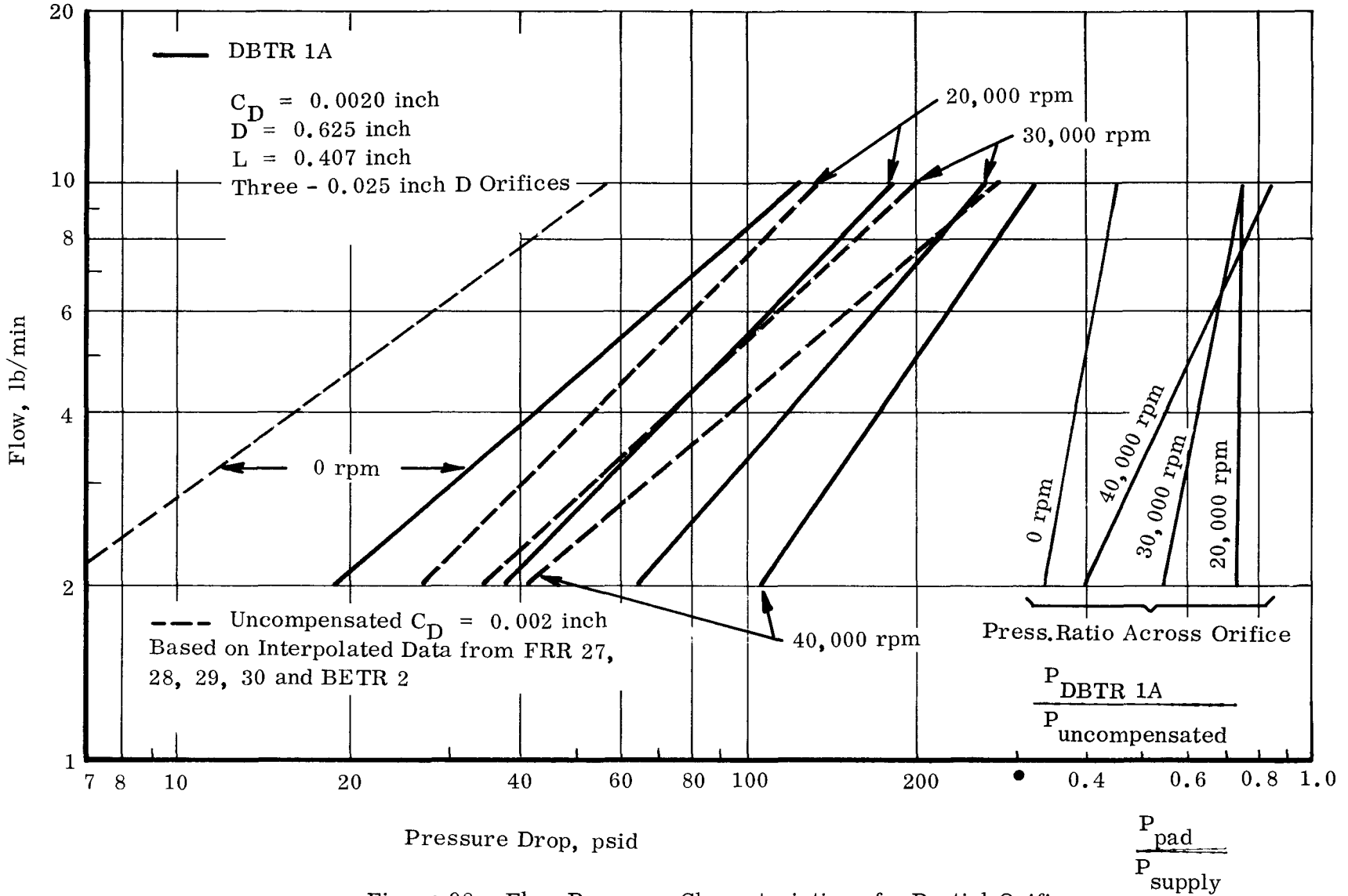

Figure 98. Flow Pressure Characteristics of a Partial Orifice-Compensated Three-Sector Bearing

DBTR 1A Test Series

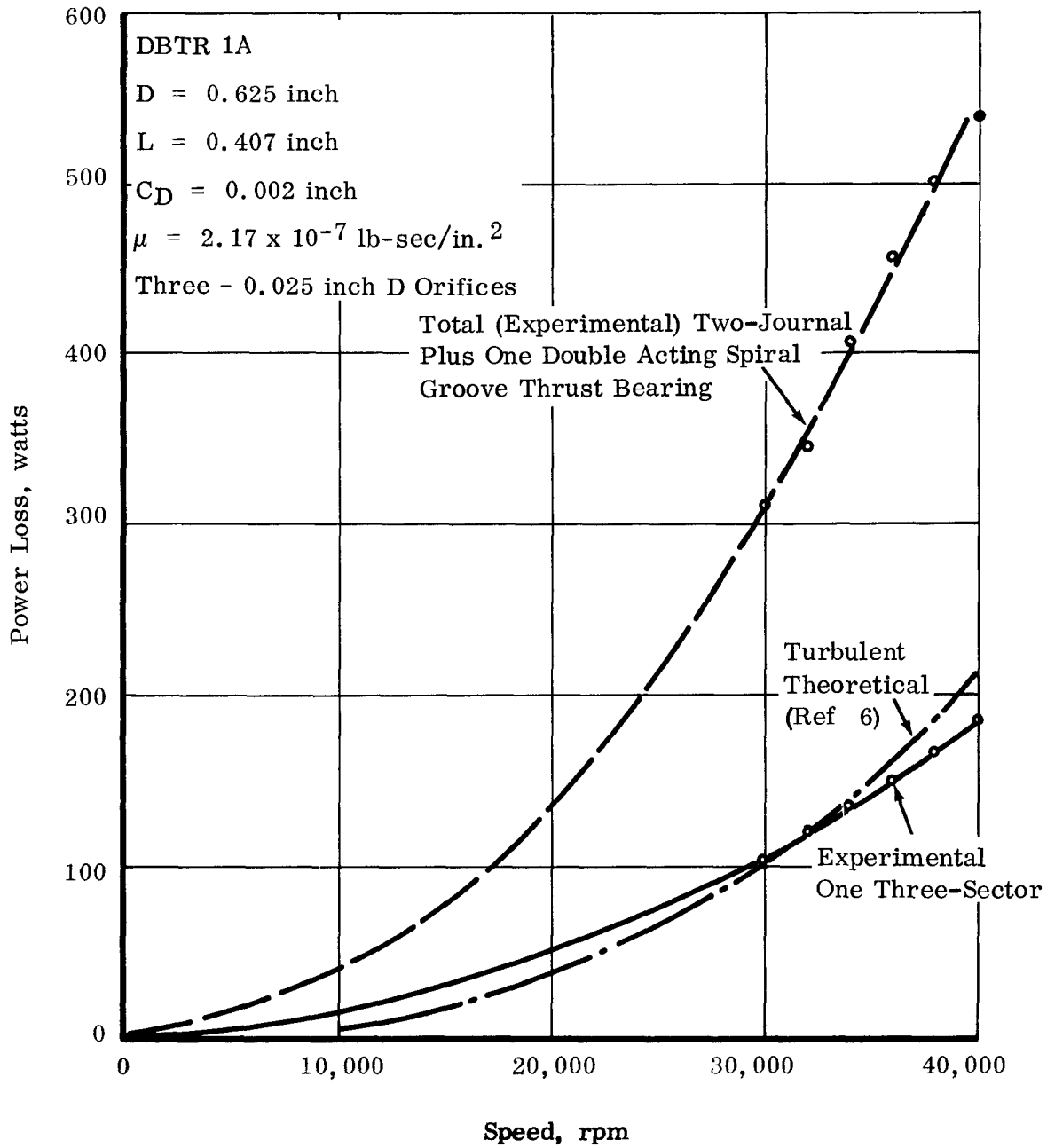

Figure 99. Power Loss vs Speed for a Three-Sector Partially Compensated Bearing

DBTR 1A Test Series

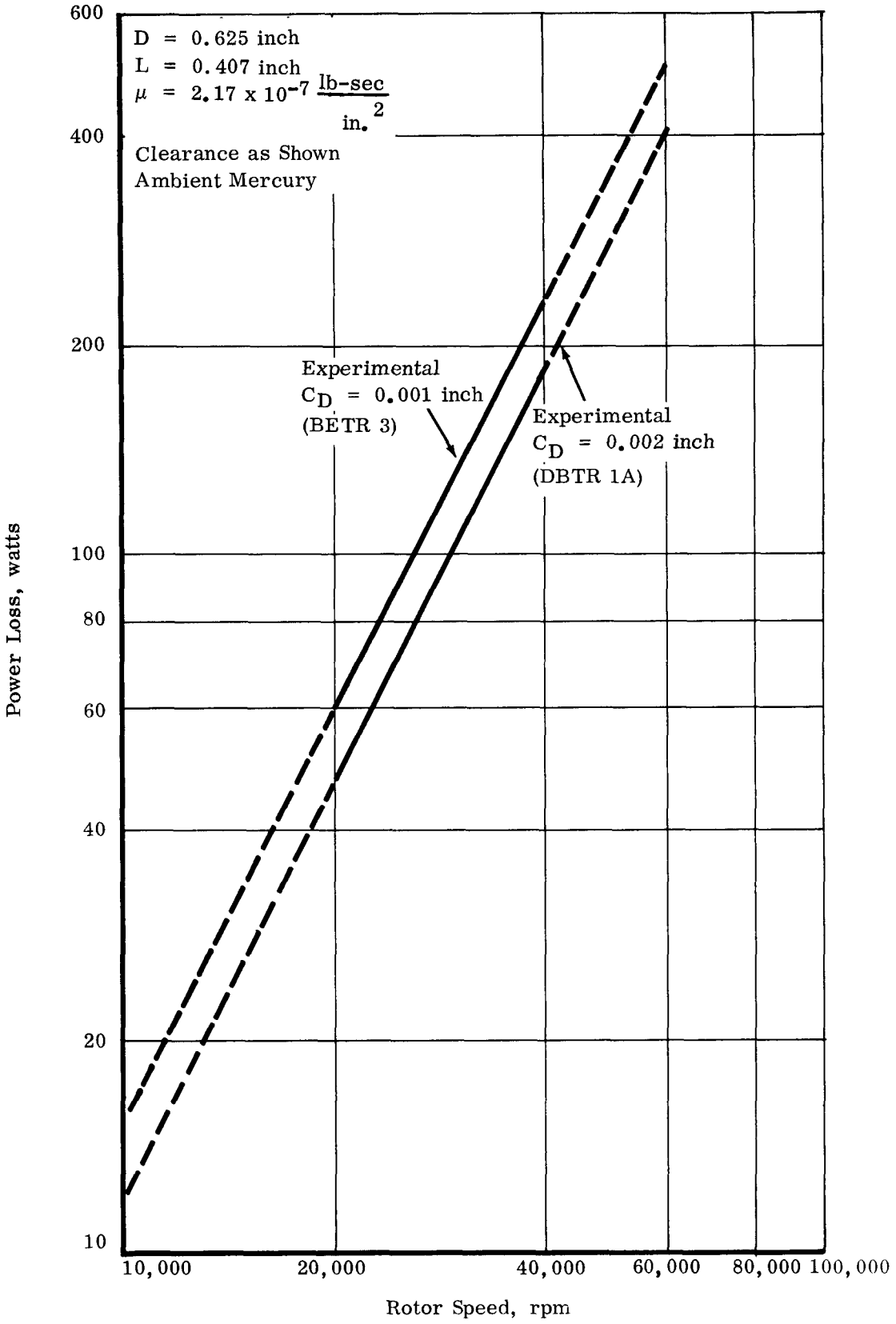

Figure 100. Experimental Power Loss vs Speed for a Three-Sector Bearing

4) Flow reliability was improved by taking a pressure drop across the orifice by increasing its restriction. This prevented all the flow from being dumped into the bearing's unloaded side.

5) The need for stability at all conditions up to speeds of 40,000 rpm was not achieved by partial orifice compensation. It remains to be determined if full compensation, which requires an orifice diameter of 0.020 inch, will assure freedom from half-frequency whirl for all possible conditions imposed on the bearing.

E. PROGRAM IV - FULLY ORIFICE-COMPENSATED THREE-SECTOR BEARING - DBTR 5 AND 6 TEST SERIES

The development of a high pressure, shaft mounted, centrifugal pump, coupled with the requirement for stable operation and the experience gained from the BETR 3, DBTR 1, and DBTR 1A test series, led to the development of a fully orifice-compensated three-sector bearing. The initial analysis of the orifice diameter required that orifice restriction $\geq$ bearing clearance restriction and established an orifice diameter of 0.020 inch. Consequently, a series of tests was conducted utilizing the dual bearing test rig on a three-sector bearing with a diameter (D) of 0.625 inch, a length (L) of 0.407 inch, and a diametral clearance (C_D) of 0.0015 and 0.002 inch. One 0.020-inch diameter orifice per sector and one 1/4-inch x 1/8-inch x 0.030-inch supply pad per sector were also used.

The objective of this test series was to establish the effect of clearance, speed, undirectional load, supply pressure and flow, and unbalance (rotating load) on the performance of a fully compensated three-sector bearing. The test designation and variables were as follows:

1) C_D = 0.0015 inch

DBTR 5	balanced rotor
DBTR 5A	15 lb/bearing unbalance at 40,000 rpm
DBTR 5C	30 lb/bearing unbalance at 40,000 rpm

2) C_D = 0.002 inch

DBTR 6	balanced rotor
DBTR 6A	15 lb/bearing unbalance at 40,000 rpm
DBTR 6C	30 lb/bearing unbalance at 40,000 rpm

The bearings were installed in the normal orientation with an axial drain groove on top. Figure 101 indicates the relationship of supply pads to the axial drain grooves.

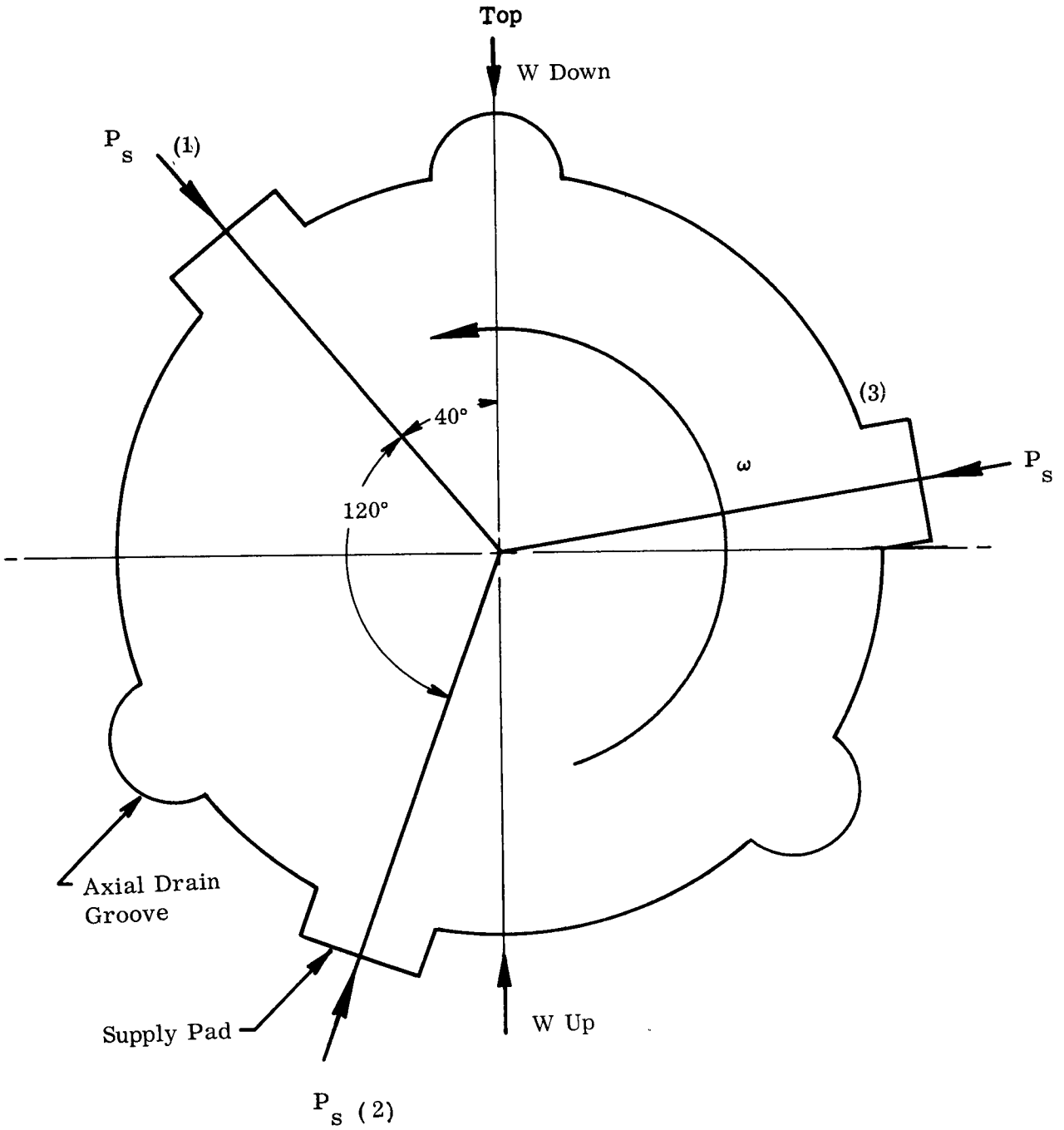

Figure 101. Three-Sector Bearing Schematic

The above test series was conducted using ambient temperature mercury (≈ 70°F) at the inlet. Load-eccentricity ratio, attitude-eccentricity ratio, flow-pressure, load-flow, and power loss measurements were made at speeds of zero; 10,000; 20,000; 30,000; 36,000; and 40,000 rpm for the balanced shaft and at 36,000 rpm for the unbalanced shaft. The influence of unidirectional and rotating load as well as supply pressure on the stability characteristics were established. Critical speed, radial stiffness, and damping characteristics were obtained for the unbalanced shaft tests. Shaft displacement data were obtained with two sets of probes - one set located approximately one inch from the "A" end bearing and the other set located outboard of the "B" end bearing over the shaft extension.

The total time accumulated during the dynamic portion of the tests was 64 hours during the DBTR 5 and 95 hours during the DBTR 6 test series. This included 43 start-stop tests for DBTR 5 and 50 start-stop tests for DBTR 6.

The results of this test series are summarized below in terms of load capacity, attitude-eccentricity locus, flow-pressure characteristics, load-flow characteristics, power loss, radial stiffness and damping characteristic, bearing-rotor system critical speed, and stability characteristics. Wherever applicable, comparisons of the different clearances and the rotating load performance are made.

1. Load Capacity

The static load deflection characteristics were obtained as a function of different supply pressures (held constant) and are plotted normally in Figure 102. Loading down into one of the sectors (rather than an axial slot) results in equal capacity regardless of clearance. This to be expected since the orifice restriction controls the pressure in the pad regardless of the bearing clearance restriction. Load capacity should, consequently, be relatively independent of bearing clearance in a fully orifice-compensated bearing. There are no Reynolds number effects at zero speed to prevent this characteristic. Minor variation with clearance occurs when loading up; i.e., capacity is greater for the smaller clearance, but this appears to be caused by the presence of the axial drain groove and the load and resultant shaft motion being directed into the groove.

Compensation, and the increase in hydrostatic force due to the built-in restoring force from orifice compensation, has made the bearing essentially equally strong regardless of load direction. The slope of the upward and downward load-deflection curves is almost equal. As a result the fluid film stiffness (dW/de) is essentially equal.

Full orifice compensation has therefore improved the three-sector bearing in two ways at zero speed:

1) It has made the static load capacity fairly insensitive to clearance (between 0.0015 and 0.002 inch).

2) Load capacity and stiffness are more uniform in both the up and down direction.

D = 0.625 inch

L = 0.407 inch

C_D = 0.020 inch

Mercury Lubricant

T_S = 70°F

Orifice Dia = 0.020 inch

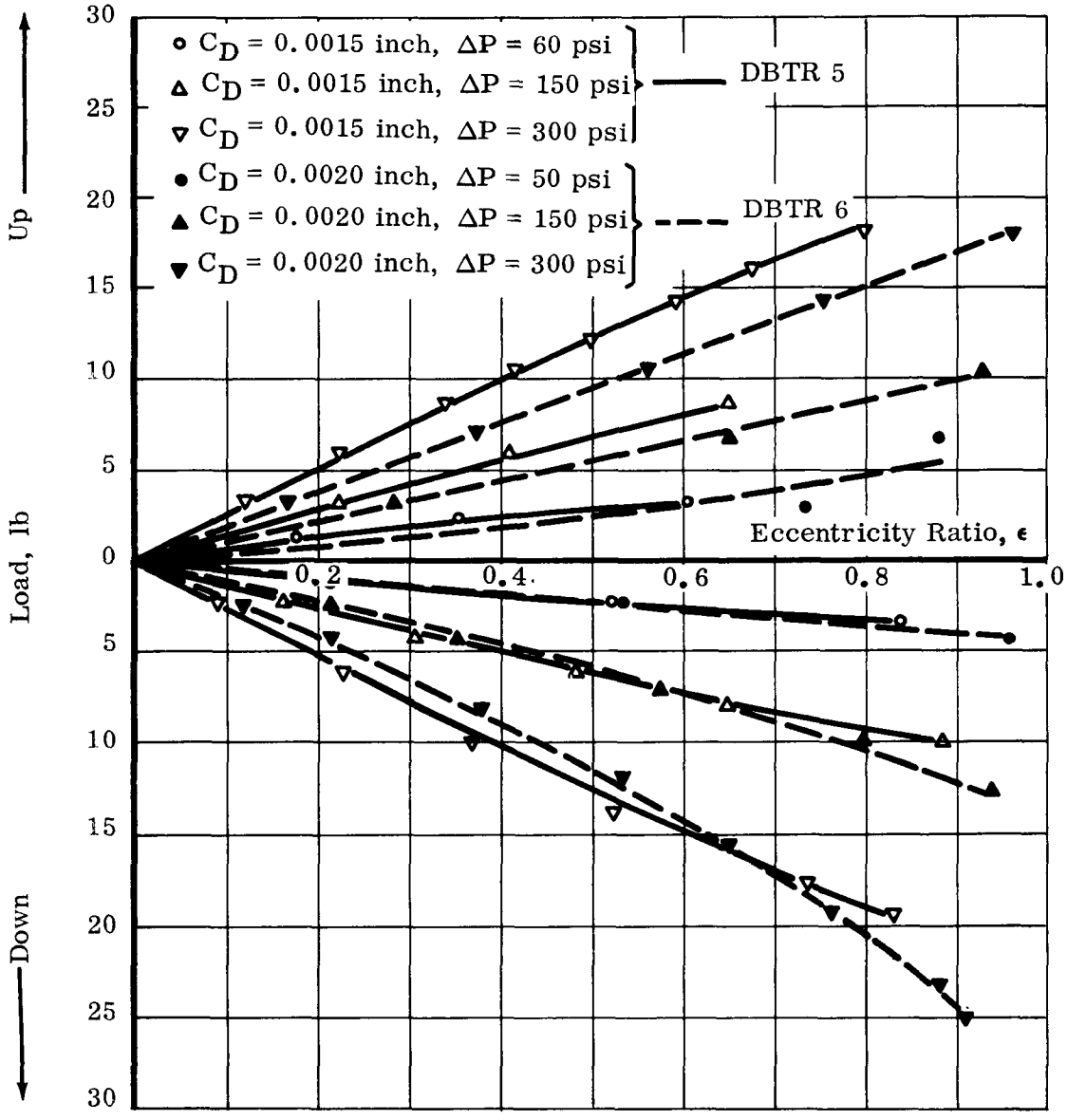

Figure 102. Static Load Carrying Capacity vs Eccentricity Ratio for a Three-Sector Orifice-Compensated Journal Bearing

DBTR 5 and 6 Test Series

Comparison with DBTR 1 and DBTR 1A test series at zero speed shows good correlation and demonstrates that full compensation, resulting in a further orifice pressure drop, is not accompanied by a further decrease in static load capacity.

The dynamic load-deflection characteristics for speeds of 10,000; 20,000; 30,000; 36,000;and 40,000 rpm are shown in Figures 103 through 107, plotted in dimensionless form as the reciprocal of the Sommerfeld number (S_n) versus eccentricity ratio, where

$$S_n = \frac{\mu N'}{W'} \left(\frac{D}{C_D} \right)^2$$

and $$W' = \frac{W}{L \times D}, \qquad N' = \frac{N}{60} \qquad \ldots 11$$

The data show the load capacity dependency on supply pressure for low speeds (10,000 and 20,000 rpm) and the gradual insensitivity to pressure at higher speeds. This verified the trend of having considerable hydrostatic capacity at low speeds and low eccentricity ratios, while the bearing becomes predominantly hydrodynamic at high speeds and large eccentricity ratios. These figures demonstrate the hybrid nature of the orifice compensated three-sector bearing. A purely hydrodynamic bearing with laminar flow in the clearance space would have the data points fall on a single line according to the predicted curves of Figure 4. This is obviously not the case because the bearing is hybrid and a certain degree of turbulence occurs in the clearance space.

In an effort to include the hybrid qualities of the bearing and achieve a dimensionless load-deflection curve, it is necessary to include the pressure drop of the lubricant across the bearing, i.e., $\Delta P = P_{supply} - P_{drain}$. A modified bearing number (Λ^*) is used where:

$$\Lambda^* = \frac{6 \mu \omega}{\Delta P} \left(\frac{D}{C_D} \right)^2 \qquad \ldots 12$$

Where: $$\omega = \frac{2 \pi N}{60} \text{ rad/sec}$$

(Bearing number commonly used in compressible flow lubrication is defined as

$$\Lambda = \frac{6 \mu \omega}{P_a} \left(\frac{D}{C_D} \right)^2 \qquad \ldots 13$$

Where:

P_a = ambient pressure.)

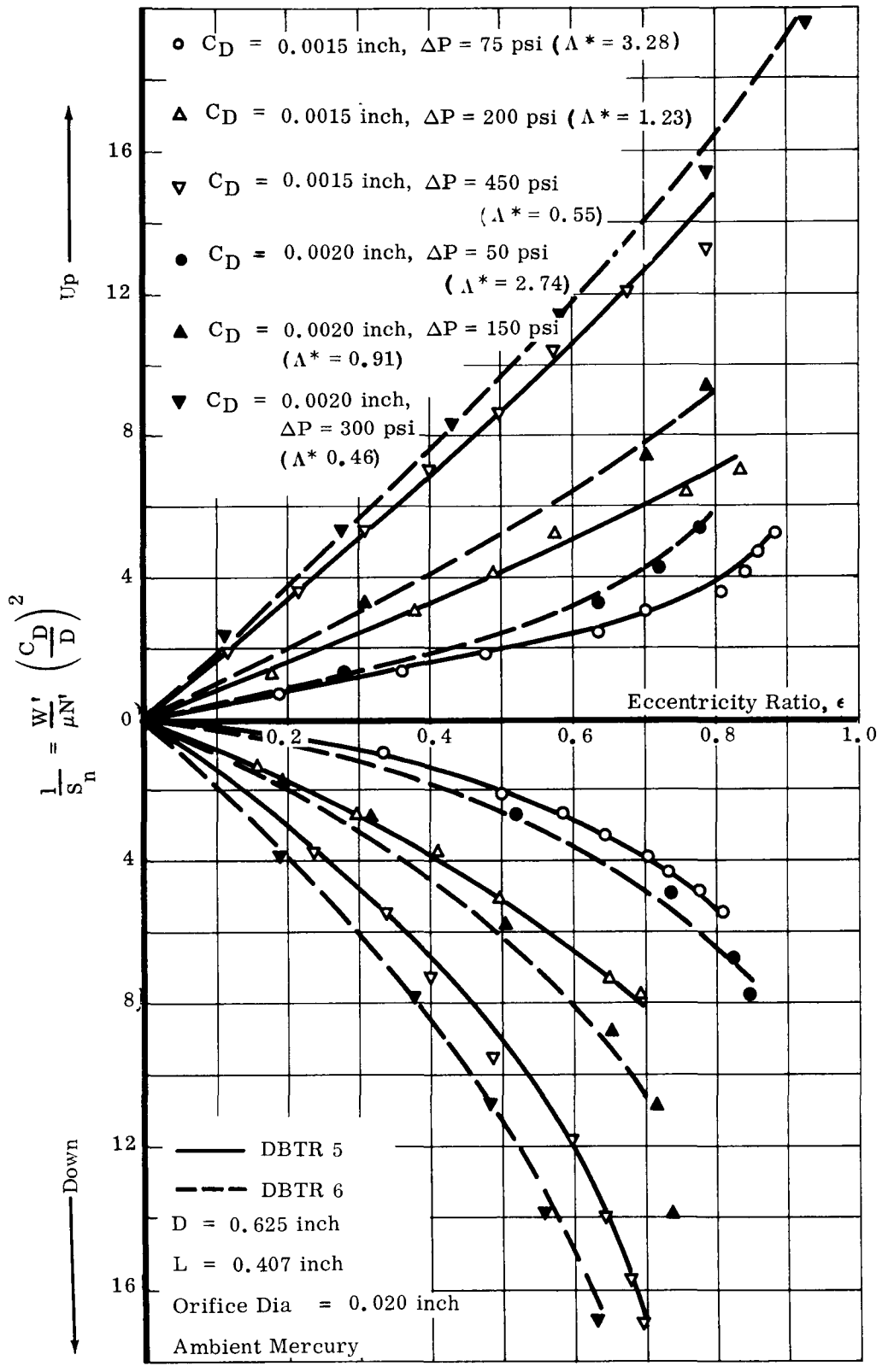

Figure 103. Dimensionless Load Carrying Capacity vs Eccentricity Ratio for a Three-Sector Compensated Journal Bearing at 10,000 rpm

DBTR 5 and 6 Test Series

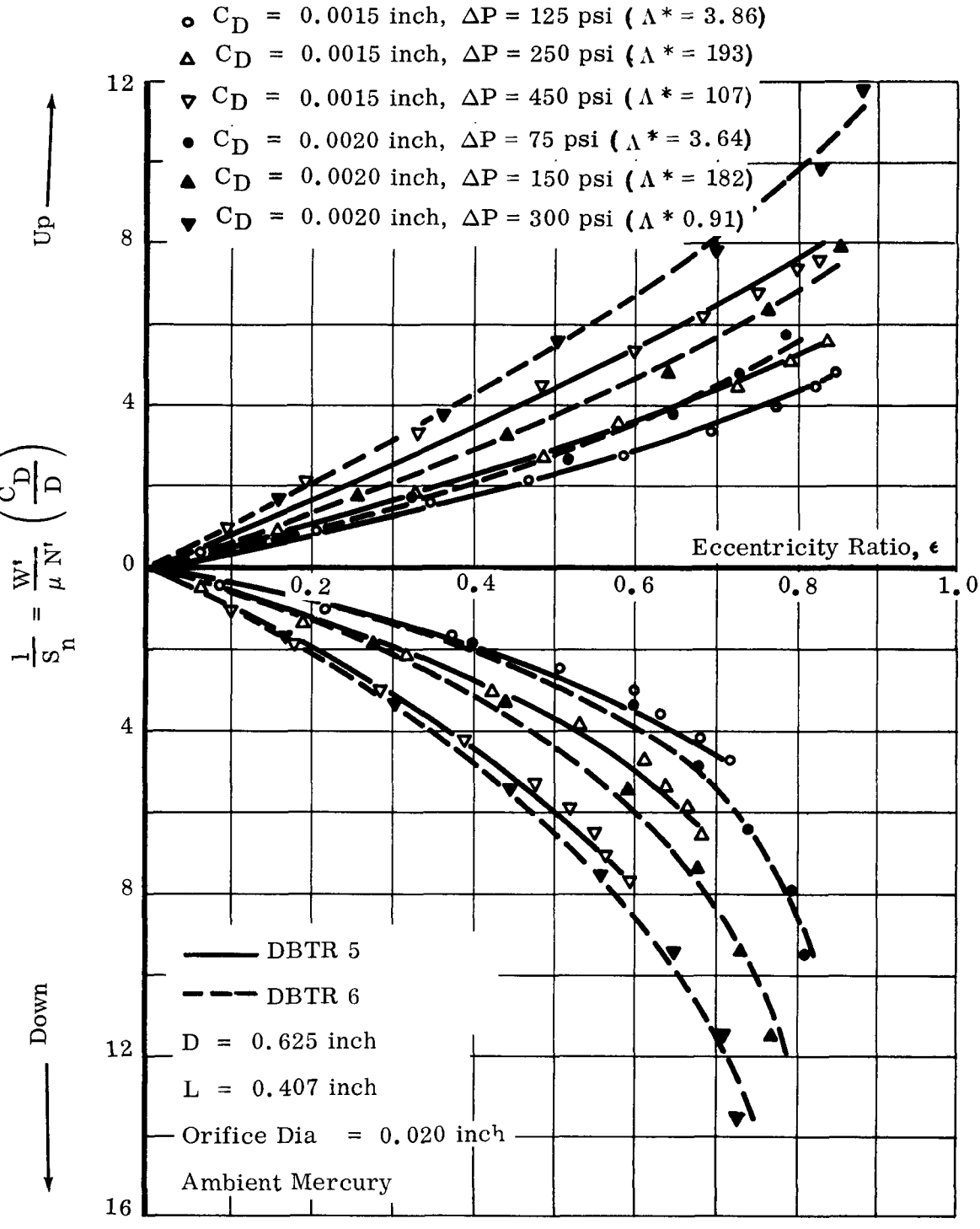

Figure 104. Dimensionless Load Carrying Capacity vs Eccentricity Ratio for a Three-Sector Compensated Journal Bearing at 20,000 rpm

DBTR 5 and 6 Test Series

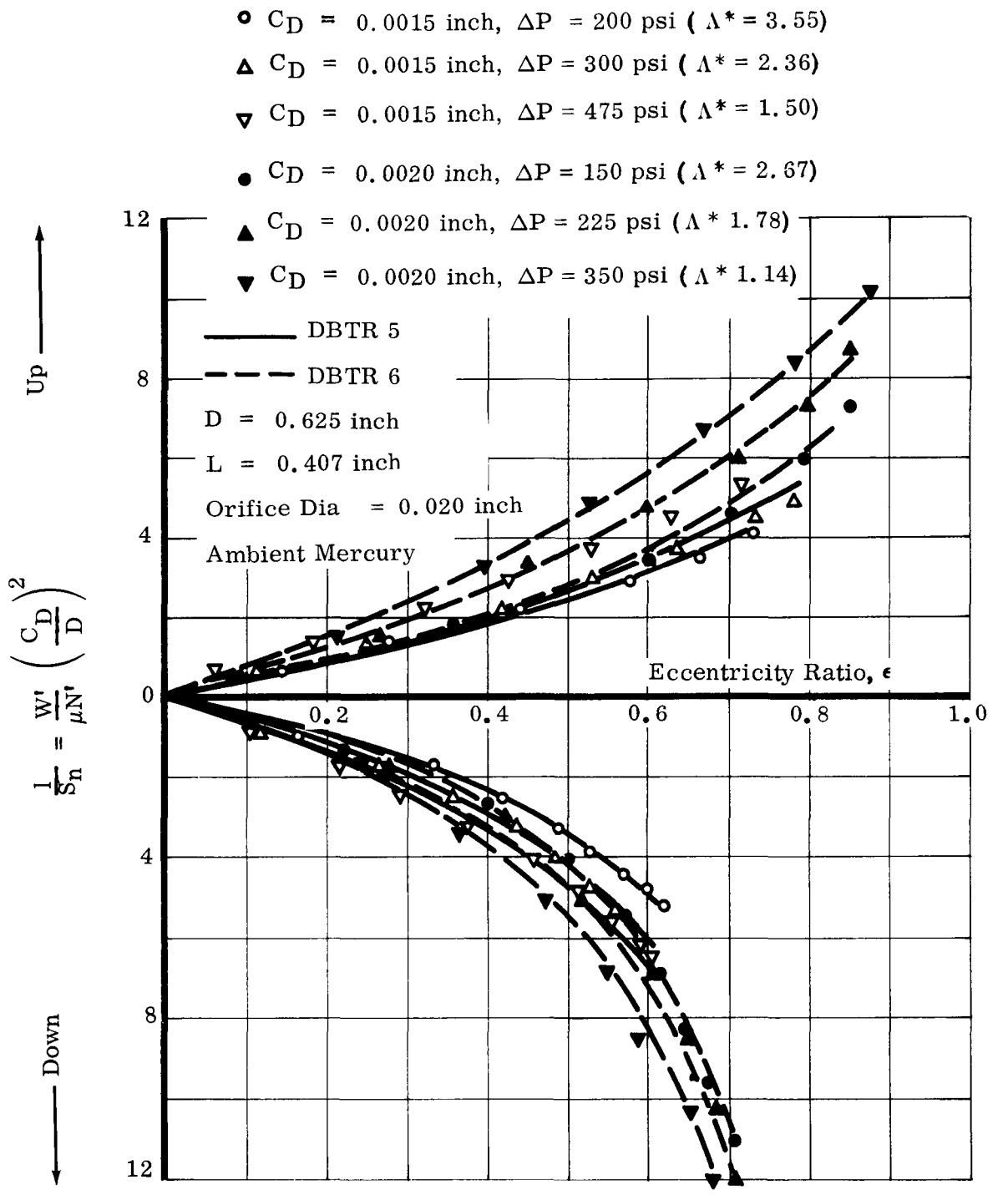

Figure 105. Dimensionless Load Carrying Capacity vs Eccentricity Ratio for a Three-Sector Compensated Journal Bearing at 30,000 rpm

DBTR 5 and 6 Test Series

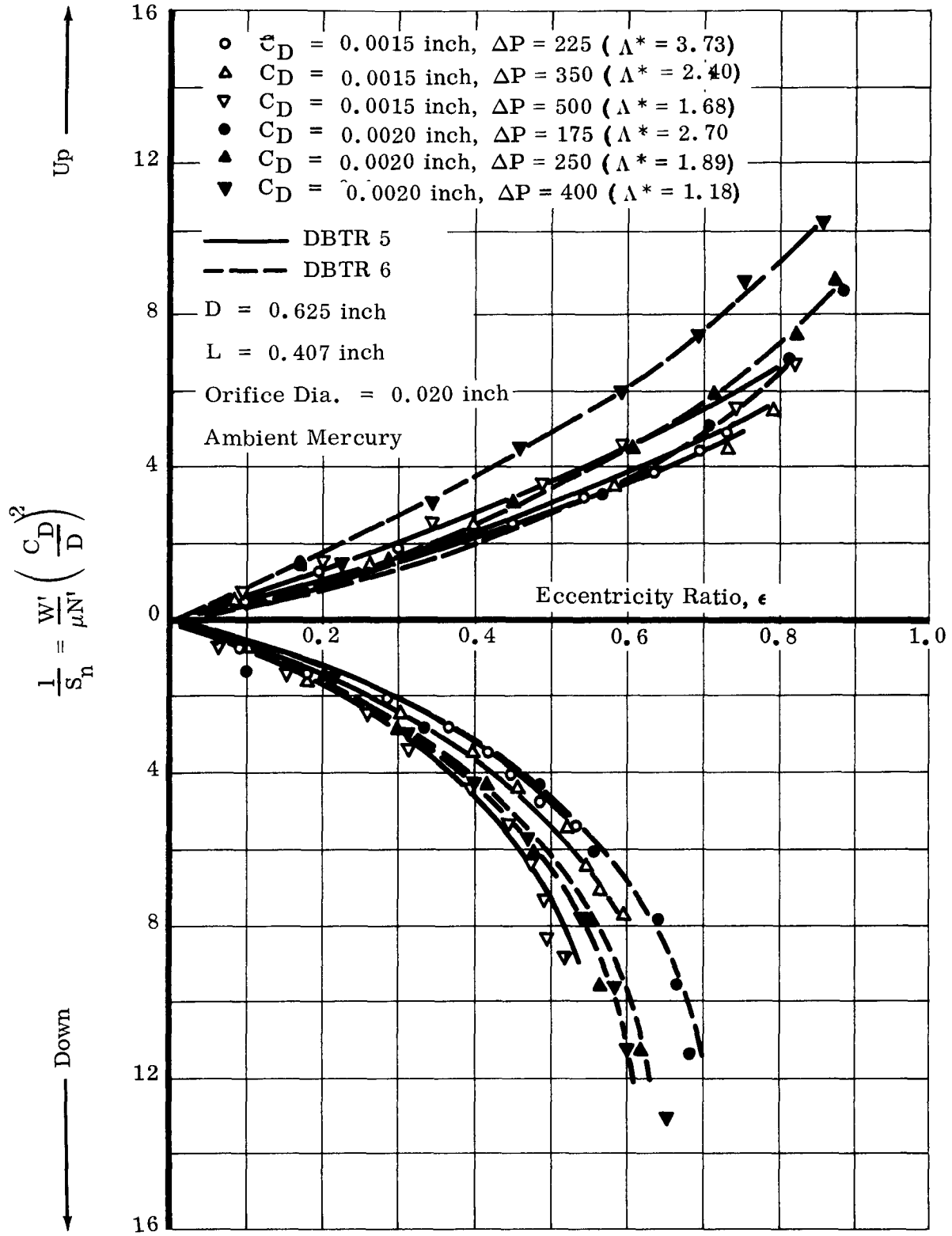

Figure 106. Dimensionless Load Carrying Capacity vs Eccentricity Ratio for a Three-Sector Compensated Journal Bearing at 36,000 rpm

DBTR 5 and 6 Test Series

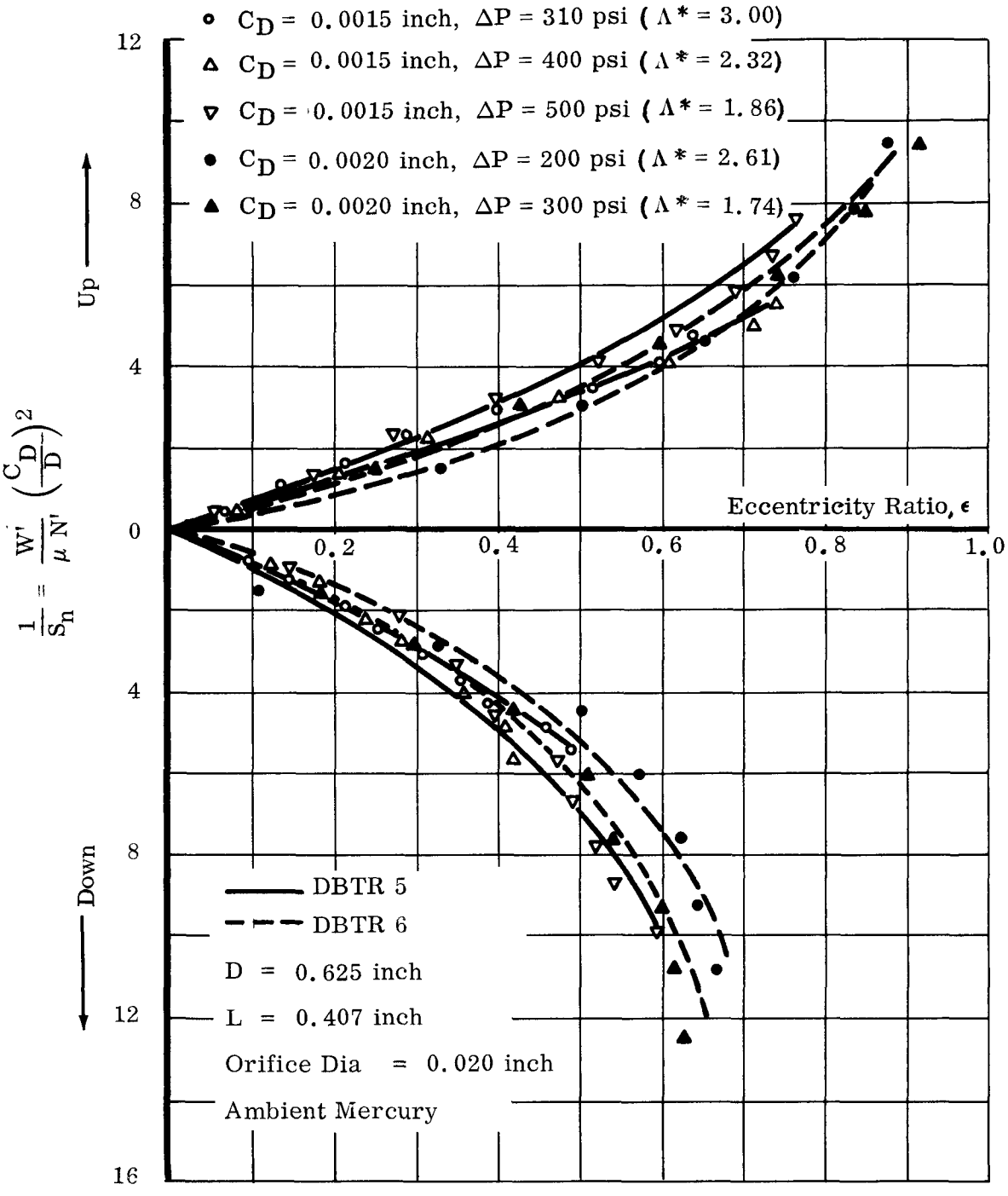

Figure 107. Dimensionless Load Carrying Capacity vs Eccentricity Ratio for a Three-Sector Compensated Journal Bearing at 40,000 rpm

DBTR 5 and 6 Test Series

Figures 103 through 107 were cross-plotted to give Figures 108 and 109 which are curves of $1/S_n$ vs Λ^* at constant eccentricity ratios for loads applied upward and downward, respectively. Calculated values for Λ^* at each speed, clearance and pressure are shown in Figures 103 through 109. Figure 108 shows that excellent results are obtained using this procedure for the load applied upward. A definite family of dimensionless curves are obtained for each eccentricity ratio from $0 < \epsilon < 0.8$ over the speeds from 10,000 to 40,000 rpm, for a pressure drop from 75 psi to 500 psi, and for a clearance range from 0.0015 to 0.002 inch. Cross plotting the data for loading downward results in greater scatter, yet the trend is identical and can be defined for values of eccentricity ratio from $0 < \epsilon < 0.5$. The greater the eccentricity ratio the larger the data scatter becomes. Two factors appear to influence the scatter when the procedure is used for downward applied loads.

1) Loading downward results in a predominantly hydrodynamic pressure force in the bearing at eccentricity ratios of $\epsilon > 0.5$. The rapidly increasing slope of Figures 103 through 107 for this load direction verify this trend. Loading upward the slope of the load-deflection curve is almost constant to $\epsilon = 0.5$ and then does not increase rapidly as $\epsilon \rightarrow 0.8$ or 0.9. This indicates that loading upward the bearing behaves as a hydrostatic bearing to larger eccentricity ratios than when loading downward.

   Recognizing the location of the axial drain grooves and the undisturbed arc of the bearing in relation to the minimum film thickness explains the variation of hydrostatic-hydrodynamic characteristics in the bearing with the direction of the applied load.

2) A Reynolds number influence is indicated since the deviations from the family of curves are greatest at large eccentricity ratios where the magnitude of the data for the small bearing clearance and for the lower speeds is lower than for the larger bearing clearance and the higher speeds.

To accommodate the performance for these turbulent effects, improved design curves might be possible by including a Reynolds number in the modified bearing number Λ^* as follows:

$$\frac{\Lambda^*}{(\mathrm{Re})^a}$$

Where: $$\mathrm{Re} = \frac{\rho U C_R}{\mu}$$

and $0 < a < 0.5$ based on the experimental data.

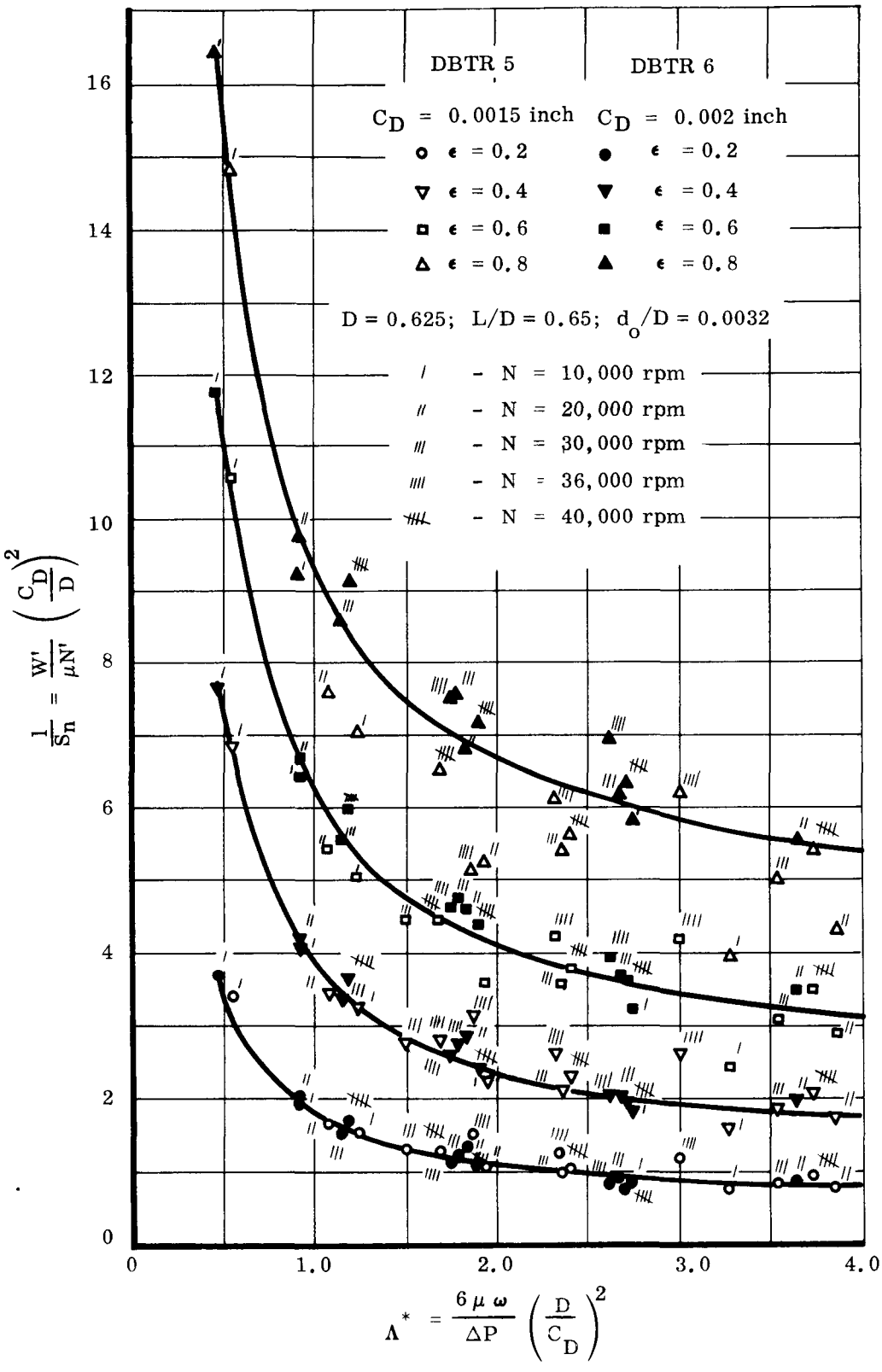

Figure 108. Dimensionless Load Capacity Upward vs Modified Bearing Number For a Three-Sector Orifice-Compensated Journal Bearing

DBTR 5 and 6 Test Series

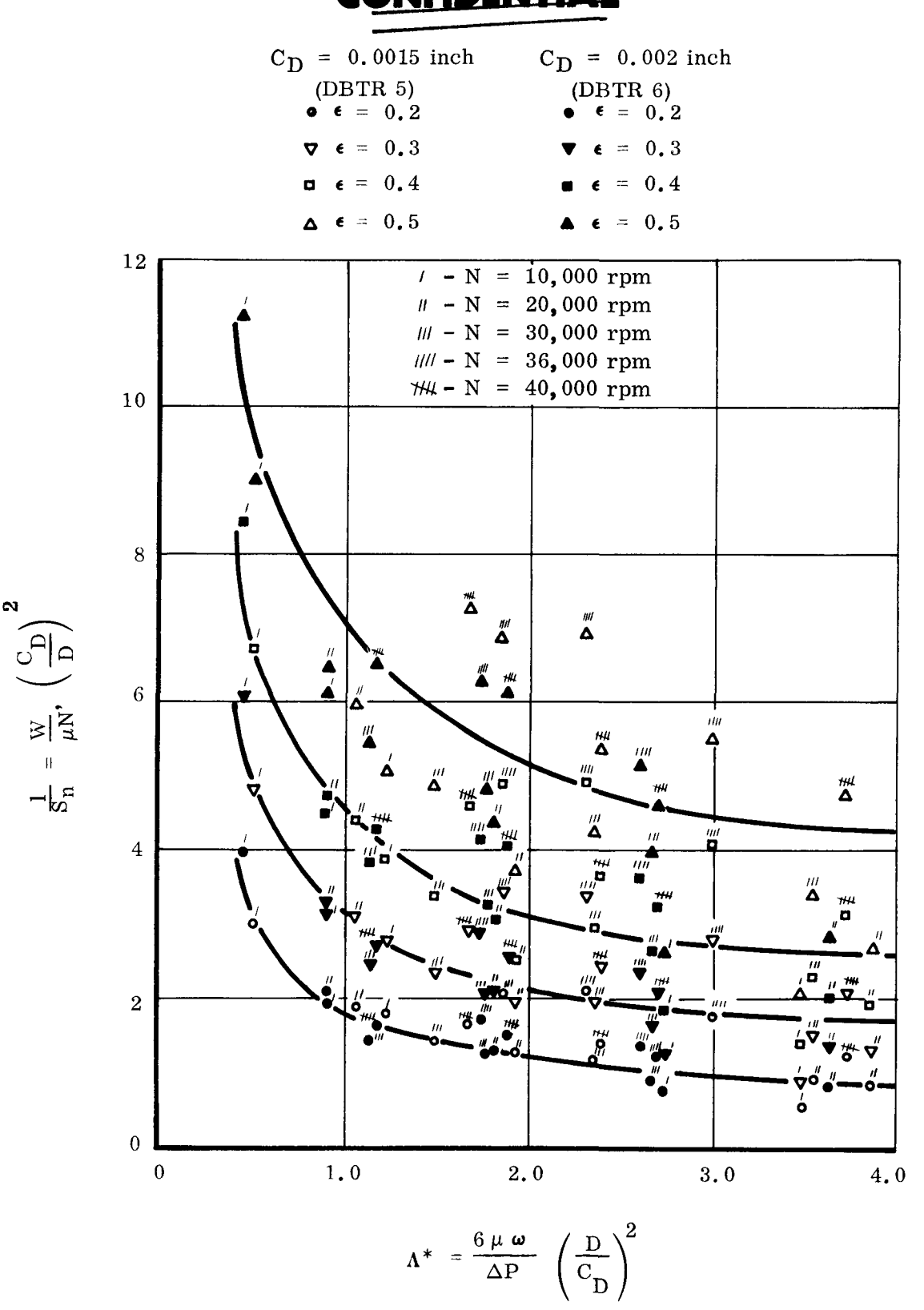

Figure 109. Dimensionless Load Capacity Downward vs Modified Bearing Number For a Three-Sector Orifice Compensated Journal Bearing

DBTR 5 and 6 Test Series

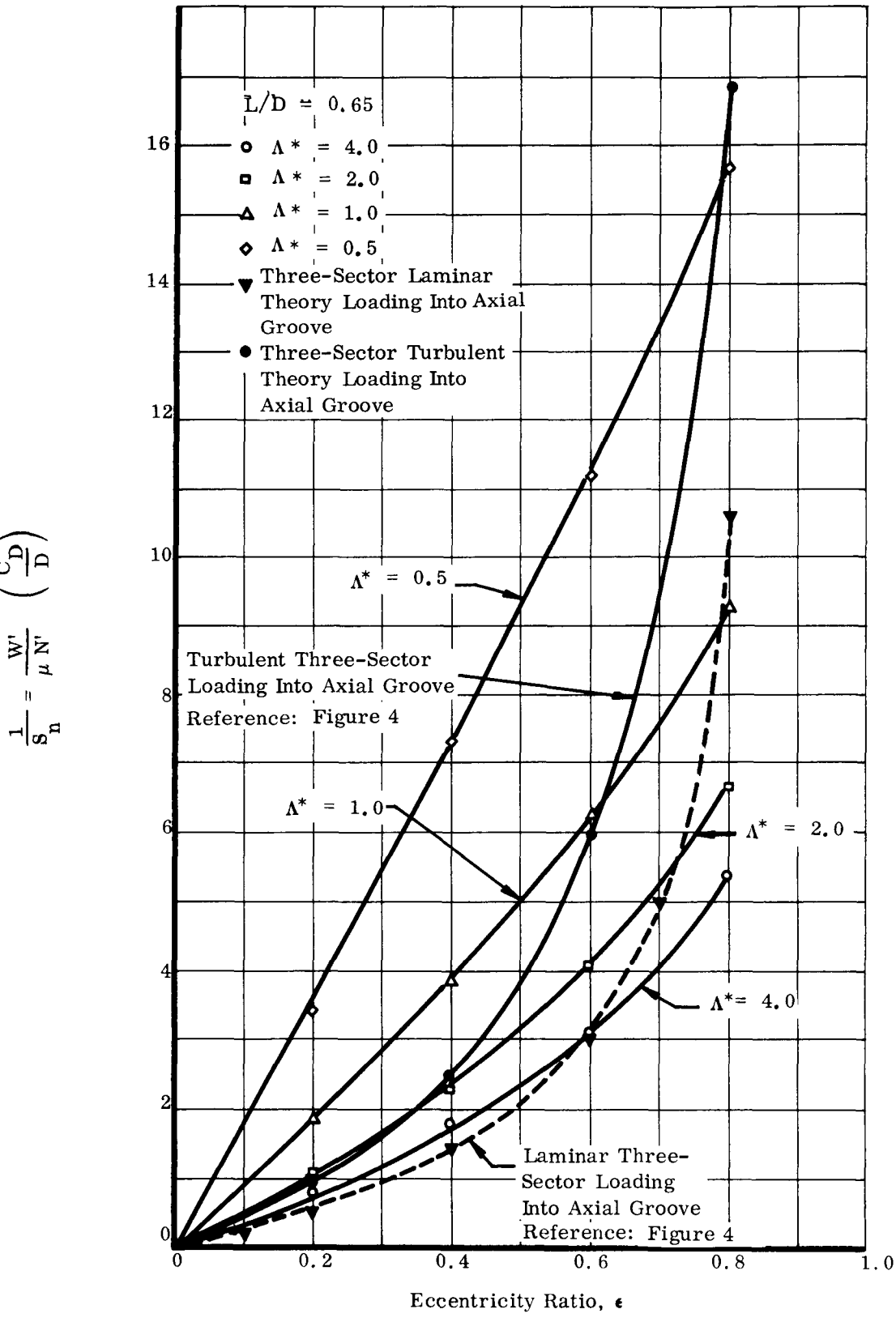

Figure 110. Dimensionless Load Capacity Upward vs Eccentricity Ratio For a Three-Sector Orifice-Compensated Journal Bearing

DBTR 5 and 6 Test Series

This approach was followed for the fully orifice-compensated three-pad bearing (see Volume V). Figures 108 and 109 represent valuable design curves for predicting the load capacity performance of this type of bearing. Although a Reynolds number is not included to account for turbulence, the data were obtained at Reynolds numbers up to 8000 based on the mean clearance. Consequently, the load capacity of hybrid three-sector bearings operating from $0 < Re < 10,000$ can be predicted.

Figures 108 and 109 define the lubrication regions where performance is primarily hydrostatic (strongly influenced by lubricant pressure drop), primarily hybrid (less influenced by lubricant pressure drop), and primarily hydrodynamic (not influenced by lubricant pressure drop).

Purely Hydrostatic: $0 < \Lambda^* < 1$

Hybrid: $1 < \Lambda^* < 4$

Purely Hydrodynamic: $4 < \Lambda^* < \infty$

A relationship between the journal velocity and the lubricant pressure drop which characterizes the three lubrication regions of interest is possible. The modified bearing number Λ^* approach indicates that a bearing may behave as a hydrostatic bearing not only because the velocity is small but also because the pressure drop is large or as a hydrodynamic bearing not only because the velocity is large but also because the pressure drop is small.

Figure 108 was cross plotted to obtain Figure 110 which is the standard curve (a generalized plot) of reciprocal Sommerfeld number versus eccentricity ratio. This could of course have been obtained from the load deflection data. However, it is cross plotted for constant values of Λ^*. Superimposed on Figure 110 is the predicted performance of the hydrodynamic three-sector bearing, loading into an axial slot based on the analysis outlined in Appendix G. The curve for $\Lambda^* = 4.0$, which according to the above criteria results in almost purely hydrodynamic lubrication, agrees fairly well with that predicted for laminar flow. At eccentricity ratios below 0.6,the actual performance is greater than the predicted, signifying the influence of turbulence in the clearance space. As $\epsilon \longrightarrow 0.6$,the influence of turbulence diminishes as demonstrated in previous tests. The trend of reestablishing laminar flow at small eccentricity ratios is verified. The lower than predicted performance as $\epsilon \longrightarrow 1.0$ is probably due to a combination of experimental error and sensitivity of assumed end leakage factors. Of particular interest, however, is the minor influence of Reynolds number (turbulence) on increasing load capacity.

For $\Lambda^* = 2.0$ and 1.0 the hybrid nature of the bearing influences the performance and results in departure from the predicted laminar performance. This is particularly true for $0 < \epsilon < 0.5$ where the hydrostatic forces predominate. For $0.5 < \epsilon < 1.0$ the hydrodynamic forces control. Combining with small film thickness results in performance which approaches the predicted laminar performance. The slope for

$\Lambda^* = 0.5$ is almost linear, verifying the almost pure hydrostatic characteristic of the bearings.

The design curves shown in Figures 108, 109, and 110 are based on a single L/D ratio of 0.65. However, using the work of DuBois and Ocvirk (Ref 9), it is possible to extend this technique to cover the range from $0 < L/D < 1.0$ by using the following relationship:

$$\left[\frac{1}{S_n}\right]_{L/D} = \frac{\left[\frac{1}{S_n}\right]_{L/D = 0.65} \times \left[\frac{L}{D}\right]^2}{(0.65)^2} \qquad \ldots 14$$

The above relationship was verified for the short journal bearings, but not for grooved bearings. Consequently, it must be applied with caution to other L/D ratio three-sector bearings operating at high (> 1000) Reynolds numbers.

The pad and orifice dimensions are two other critical dimensions that have a marked influence on performance. The design curves presented in Figures 108 and 109 are for a 1/4-inch axial and 1/8-inch circumferential pad. The depth has little influence as long as it is deep enough (> 0.005 inch) so that it does not act as a Rayleigh step. The orifice size is 0.020 inch, so that the orifice restriction is equal to or greater than the bearing clearance restriction. Consequently, when using Figures 108 and 109 for the performance prediction of larger (or smaller) three-sector bearings operating at Reynolds numbers where $1,000 < Re < 10,000$, the following procedure is recommended until a more fundamental approach is developed:

1) Maintain pad area in proportion to the bearing projected area.

2) Maintain the orifice restriction equal to or greater than the bearing clearance restriction.

The bearing clearance modulus for other size bearings is also maintained at the desired ratio established as optimum from a stability, flow-pressure, load capacity, power loss, critical speed and damping point of view for the 0.625-inch diameter bearing.

2. Fluid Film Stiffness for Balanced Rotor

Using the procedure outlined in Volume I, the generalized plots 1/S vs ϵ are used to establish fluid film stiffness at zero load.

$$K = \left[\text{slope}\right]_{1/S} \times \left[\frac{D}{C_D}\right]^3 \frac{\mu N L}{30} \qquad \ldots 15$$

or (DBTR 5) $K = \left[\text{slope} \right]_{1/S} \times 0.195 \times N$ for $C_D = 0.0015$ inch

and (DBTR 6) $K = \left[\text{slope} \right]_{1/S} \times 0.083 \times N$ for $C_D = 0.002$ inch

For zero eccentricity ratio (loading down) fluid film stiffness as a function of rotor speed at a constant flow of 5 lb/min for both 0.0015- and 0.002-inch bearings is shown in Figure 111. A later section will cross plot these values with the rotor-bearing critical speed.

3. Attitude Angle

The static attitude-eccentricity locus is shown in Figure 112 for the 0.0015-inch clearance. The influence of orifice compensation and the resultant hydrostatic characteristic of the bearing is evident by the almost vertical motion of the shaft center under the influence of vertically applied up and down loads. The almost vertical locus attests to the improved uniformity of the bearing. The improvement in the uniform forces acting in the bearing over the partially compensated and uncompensated bearing can be seen by comparing Figure 112 with Figures 87 (DBTR 1) and 41 (BETR 1).

The dynamic locus for the 0.0015-inch bearing from 10,000 to 40,000 rpm is shown in Figures 113 through 117. For the lower speeds, 10,000 and 20,000 rpm, the locus assumes the characteristic "S" shape of the hydrodynamic bearing.

However, the supply pressure has a marked influence on the locus as seen in Figures 113 and 114. For the low pressures, the large locus (big angles for small eccentricity ratios) characteristic of hydrodynamic bearings can be seen. At pressures above 200 psi the locus becomes narrow and assumes a characteristic hydrostatic appearance (small angles for all eccentricity ratios). The hydrostatic influence is gradually overcome by the hydrodynamic forces as speed is increased above 20,000 rpm. At 30,000; 36,000; and 40,000 rpm the bearing locus is predominantly hydrodynamic and only slightly affected by supply pressure. Attitude angle for upward loads is again greater than for downward loads. A composite of the loci is shown in Figure 118 for relatively constant pressures.

The similar performance was achieved with the larger clearance, 0.002-inch bearing as seen in Figures 119 through 125. The attitude-eccentricity locus, as shown in Figures 112 through 125, can be compared for various values of Λ^*. At large values of Λ^* the characteristic hydrodynamic "S" locus is obtained while the trend is toward a straight line, characteristic of hydrostatic performance, for small values of Λ^*. This substantiates the use of the modified bearing number Λ^* as an important dimensionless parameter when considering hybrid journal bearings.

4. Flow Characteristics

Flow-pressure calibration for the zero gravity case ($\epsilon = 0$) are shown in Figures 126 and 127 for the 0.0015- and 0.002-inch clearance bearings, respectively. The

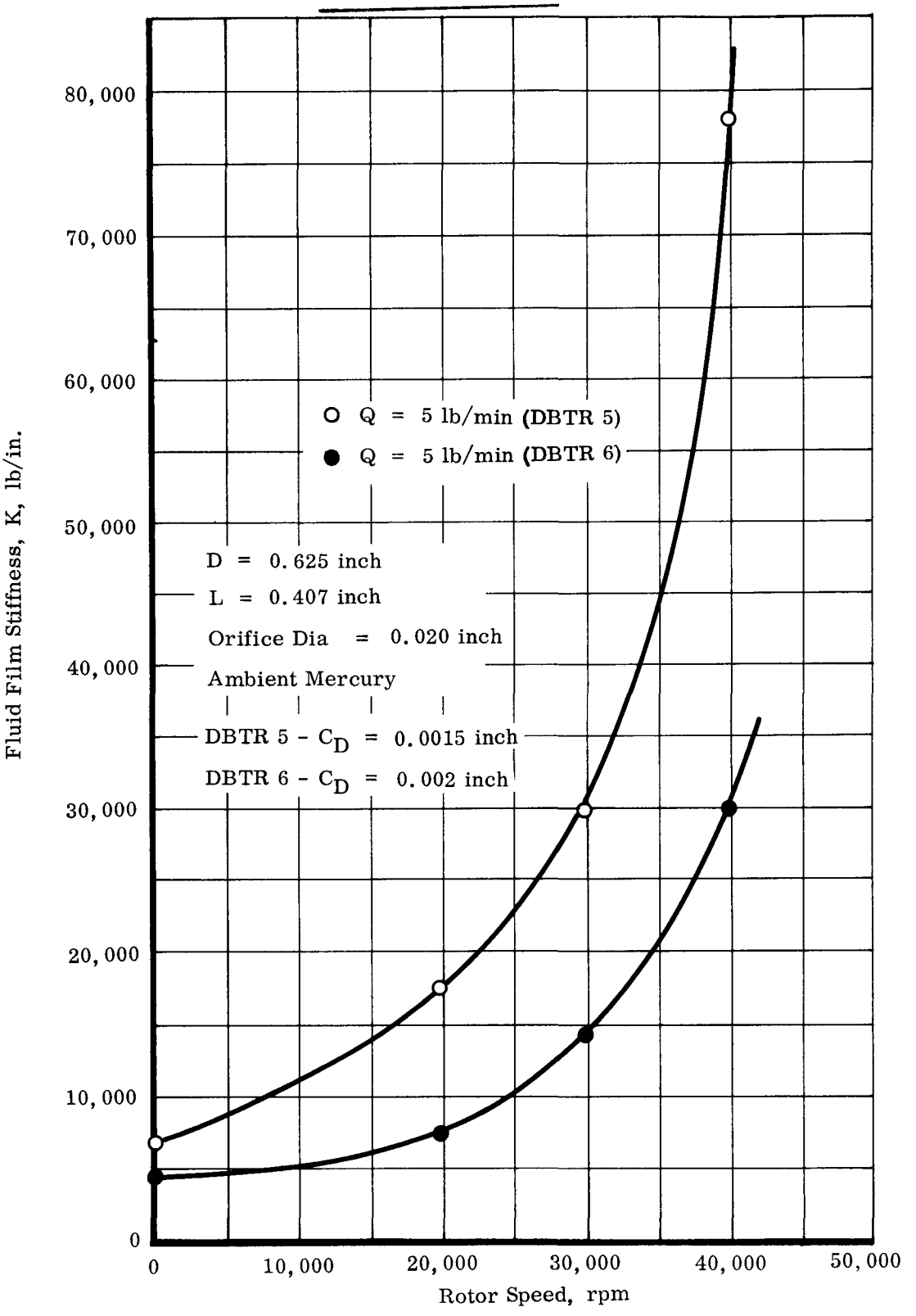

Figure 111. Fluid Film Stiffness vs Rotor Speed for a Three-Sector Orifice-Compensated Bearing at Zero Eccentricity Ratio

DBTR 5 and 6 Test Series

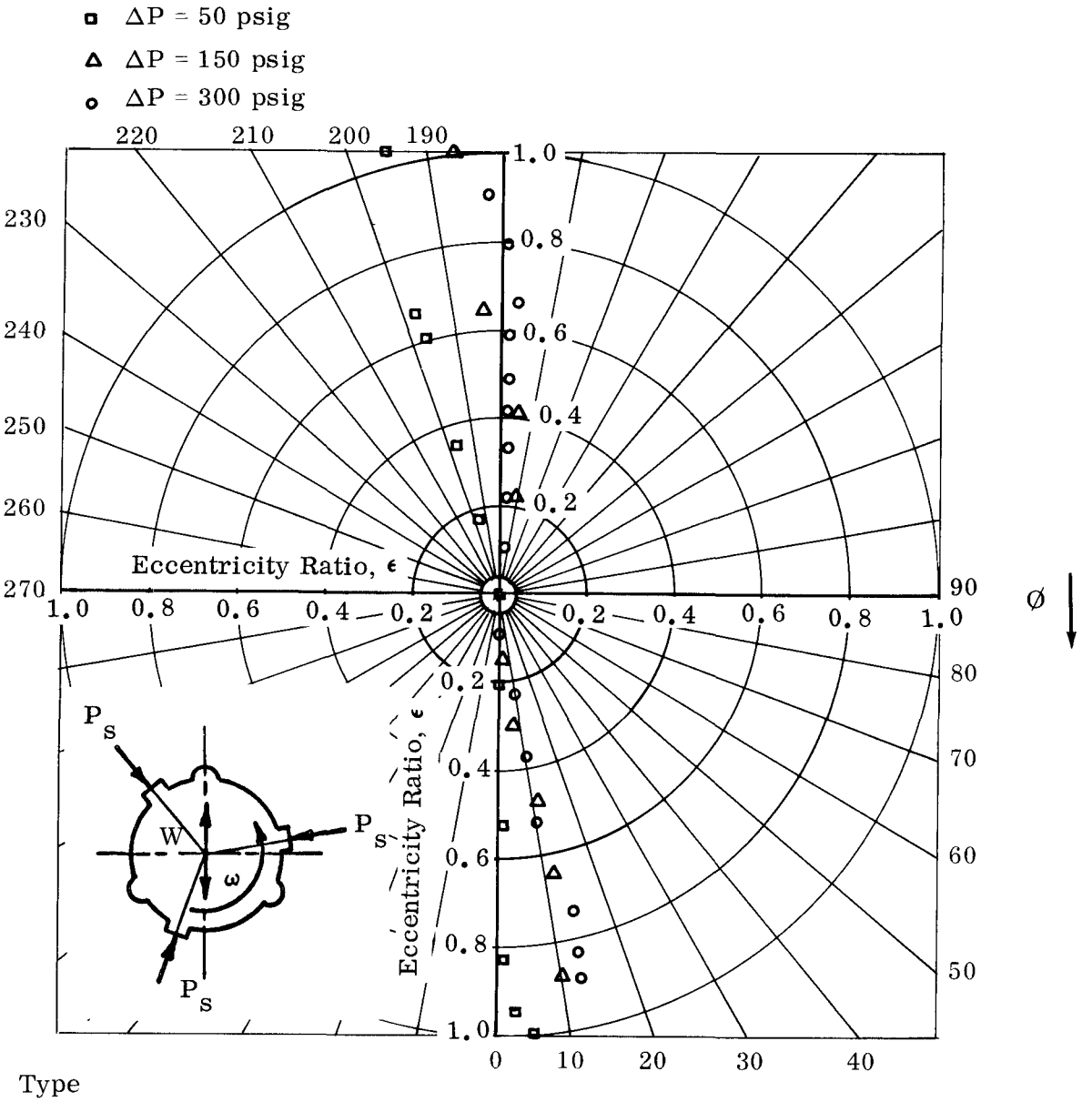

Type

C_D = 0.0015 inch

D = 0.625 inch

L = 0.407 inch

Orifice Dia = 0.020

Mercury Inlet Temperature = 70°

Figure 112. Static Attitude-Eccentricity Locus for a Three-Sector Compensated Bearing

DBTR 5 Test Series

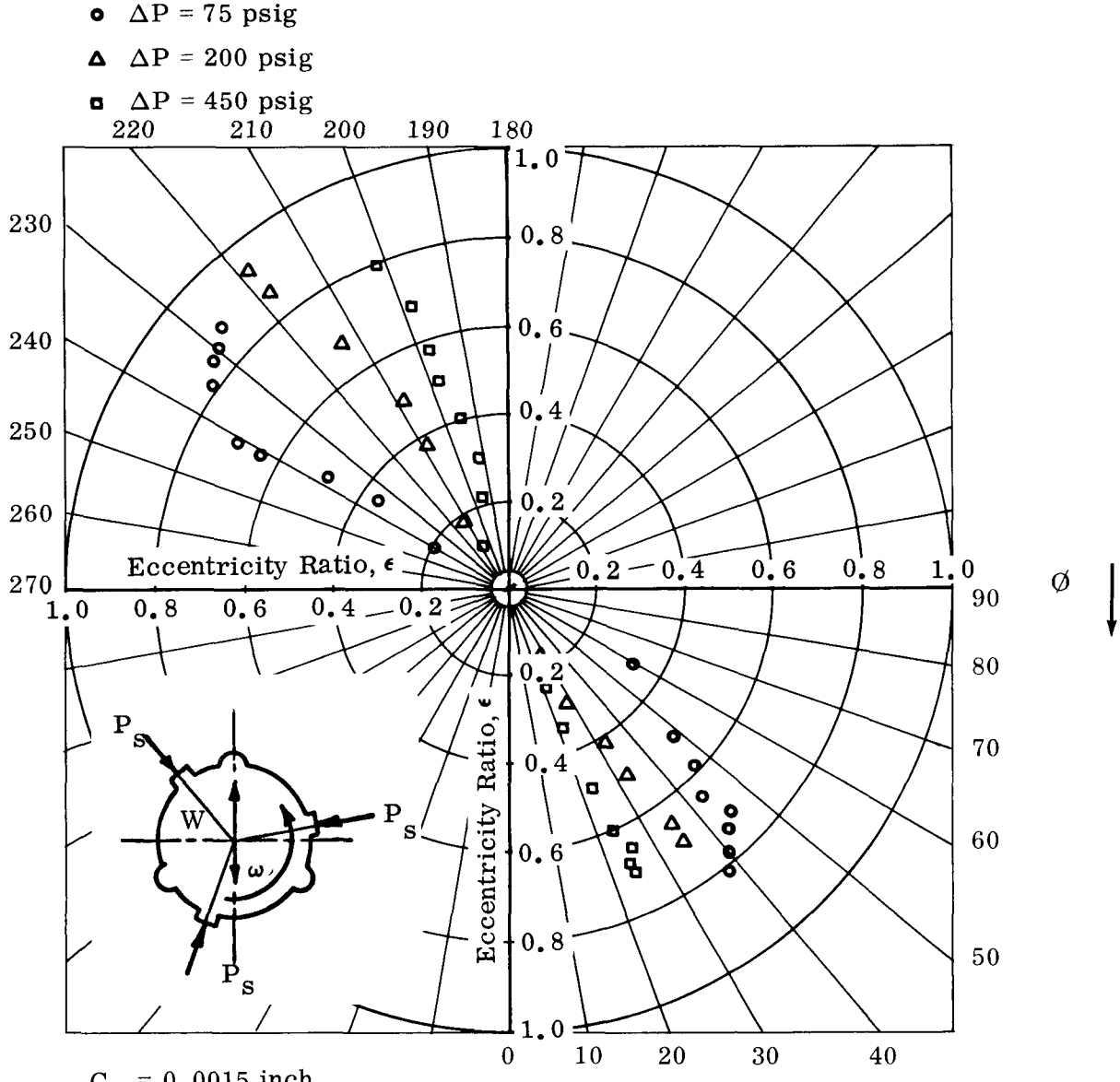

C_D = 0.0015 inch
D = 0.625 inch
L = 0.407 inch

Orifice Dia = 0.020 inch

Mercury Inlet Temperature = 70°

Figure 113. Attitude-Eccentricity Locus for a Three-Sector Compensated Bearing at 10,000 rpm

DBTR 5 Test Series

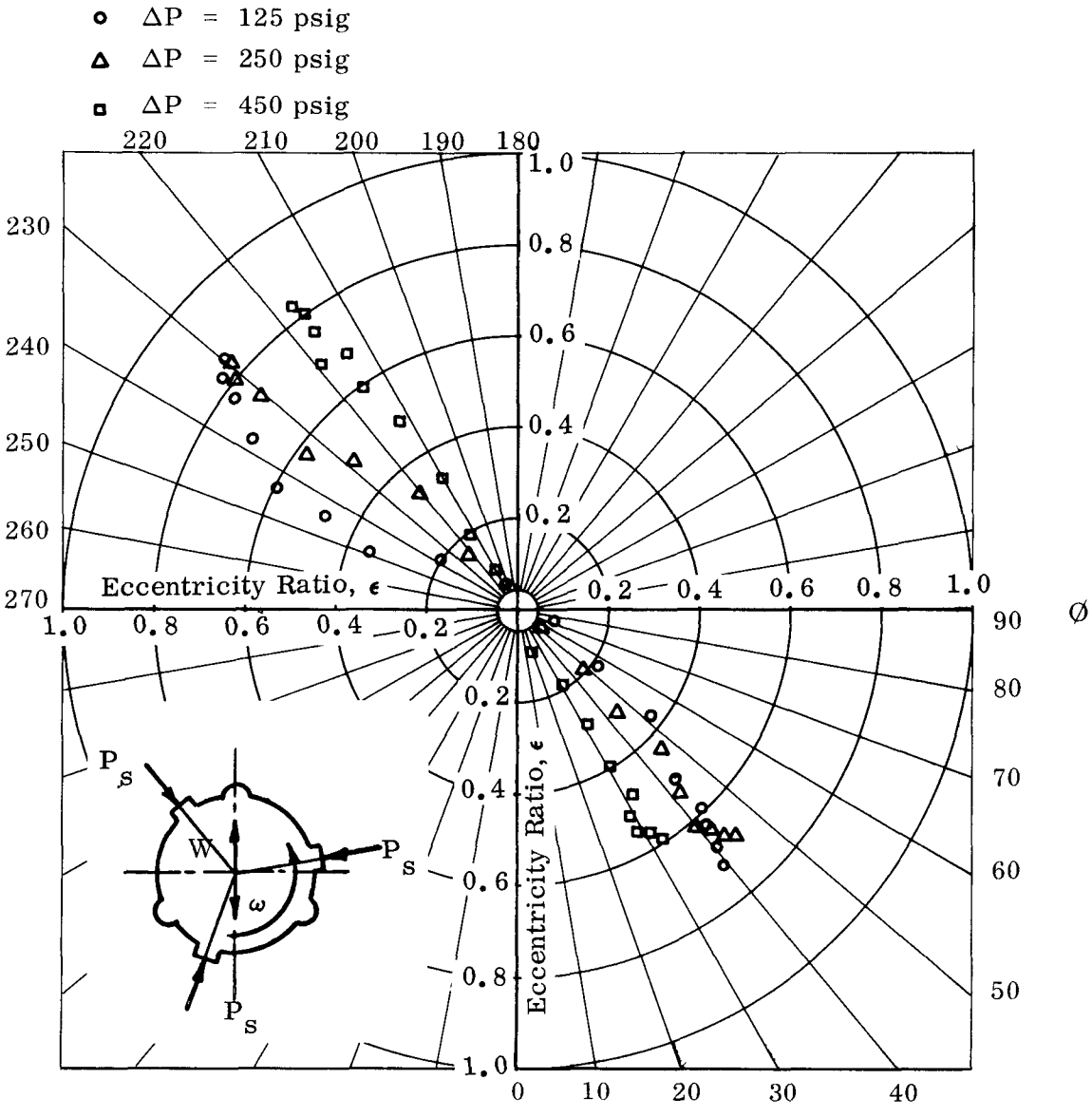

C_D = 0.0015 inch

D = 0.625 inch

L = 0.407 inch

Orifice Dia = 0.020 inch

Mercury Inlet Temperature = 70°F

Figure 114. Attitude-Eccentricity Locus for a Three-Sector Compensated Bearing at 20,000 rpm

DBTR 5 Test Series

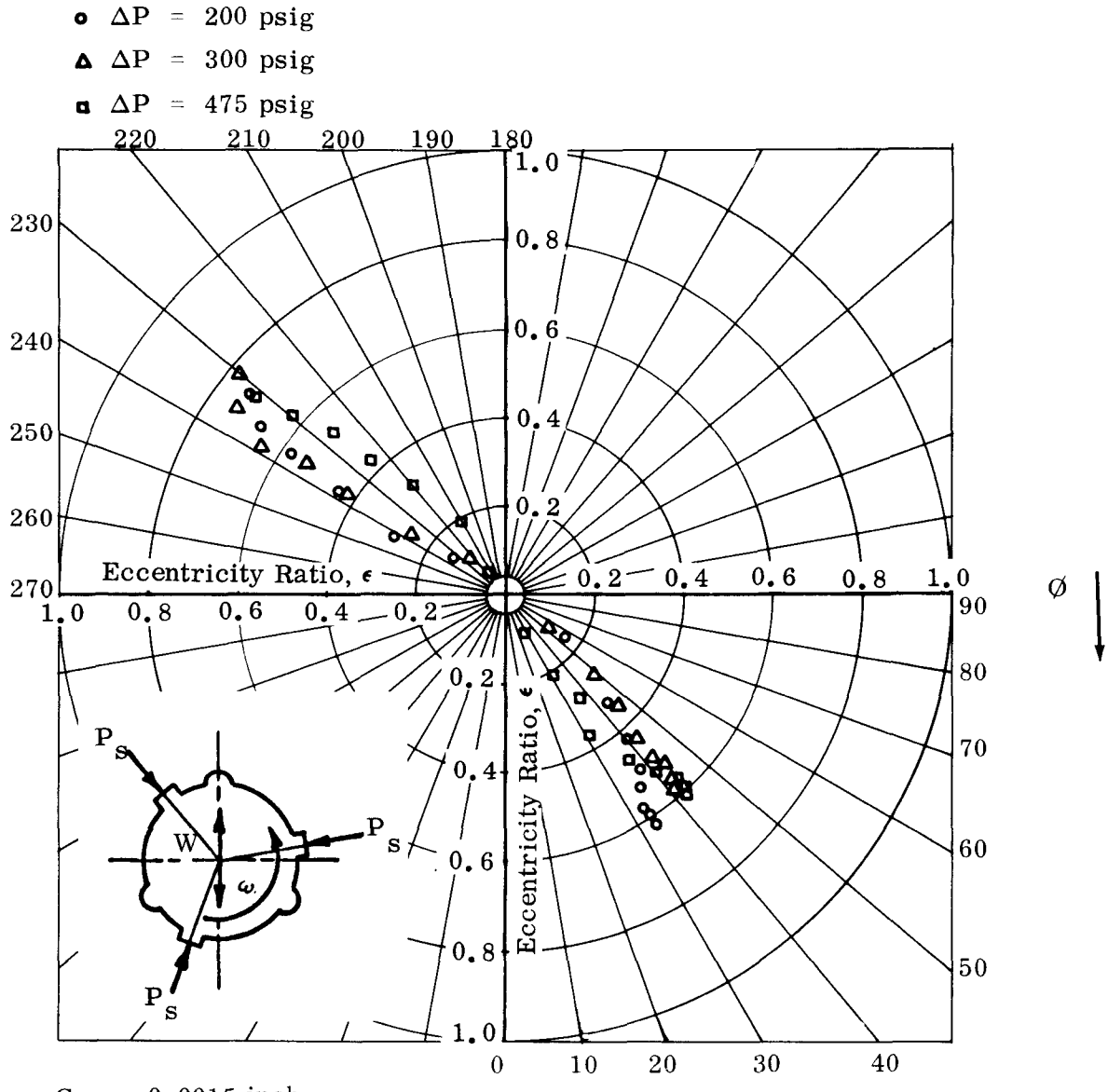

C_D = 0.0015 inch

D = 0.625 inch

L = 0.407 inch

Orifice Dia = 0.020 inch

Mercury Inlet Temperature = 70°F

Figure 115. Attitude-Eccentricity Locus for a Three-Sector Compensated Bearing at 30,000 rpm

DBTR 5 Test Series

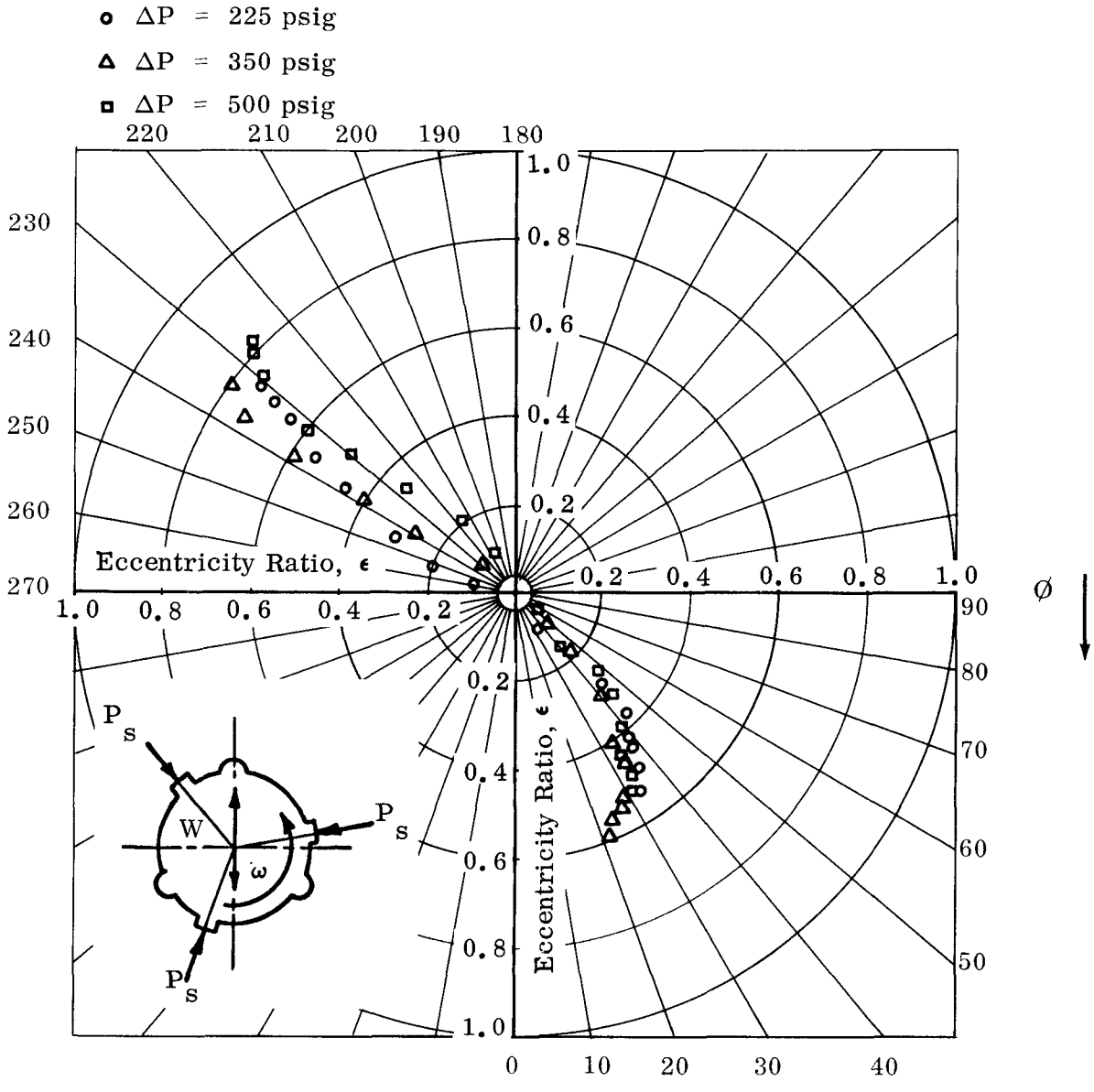

C_D = 0.0015 inch

D = 0.625 inch

L = 0.407 inch

Orifice Dia = 0.020 inch

Mercury Inlet Temperature = 70°F

Figure 116. Attitude-Eccentricity Locus for a Three-Sector Compensated Bearing at 36,000 rpm

DBTR 5 Test Series

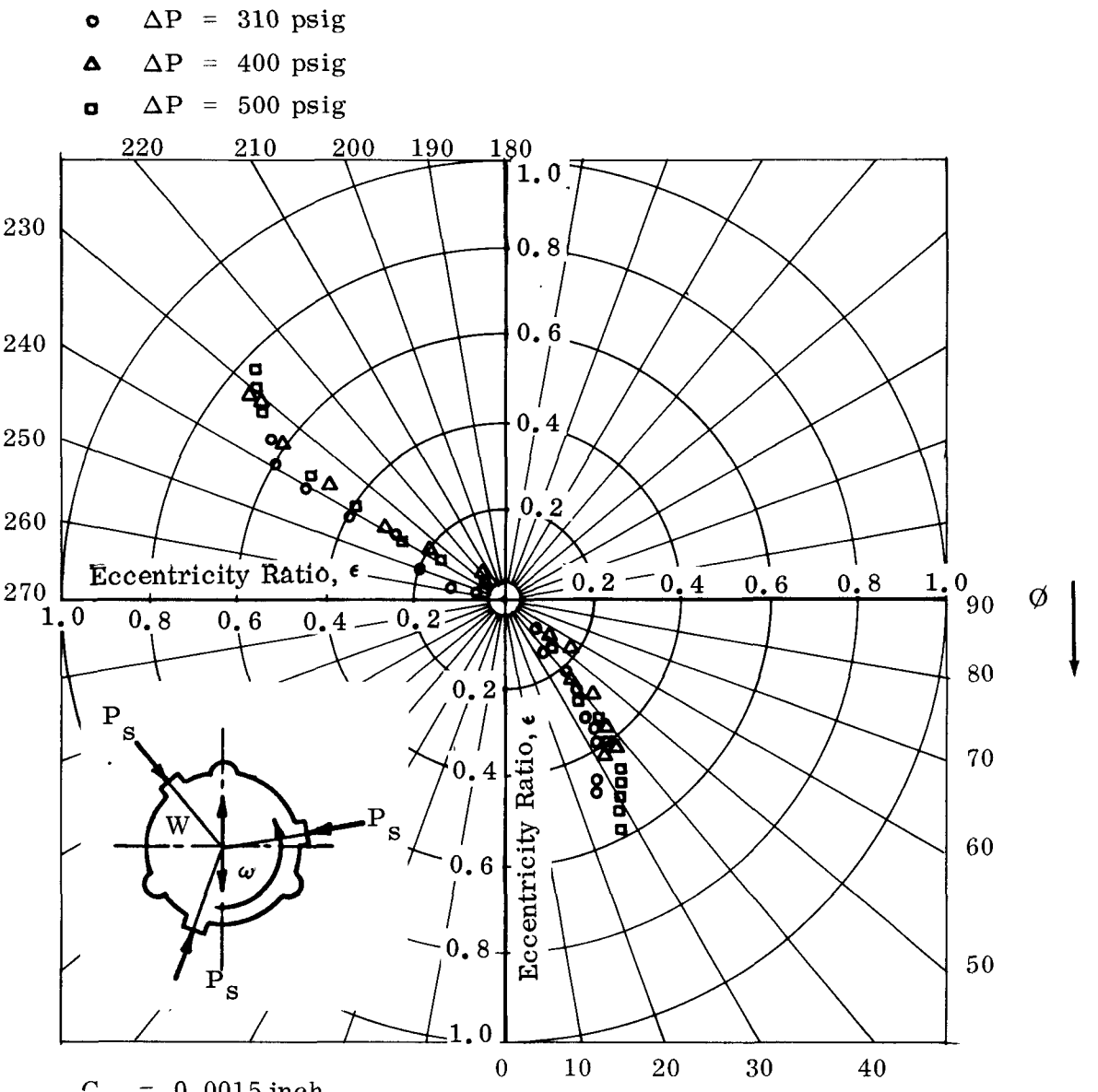

C_D = 0.0015 inch

D = 0.625 inch

L = 0.407 inch

Orifice Dia = 0.020 inch

Mercury Inlet Temperature = 70°F

Figure 117. Attitude-Eccentricity Locus for a Three-Sector Compensated Bearing at 40,000 rpm

DBTR 5 Test Series

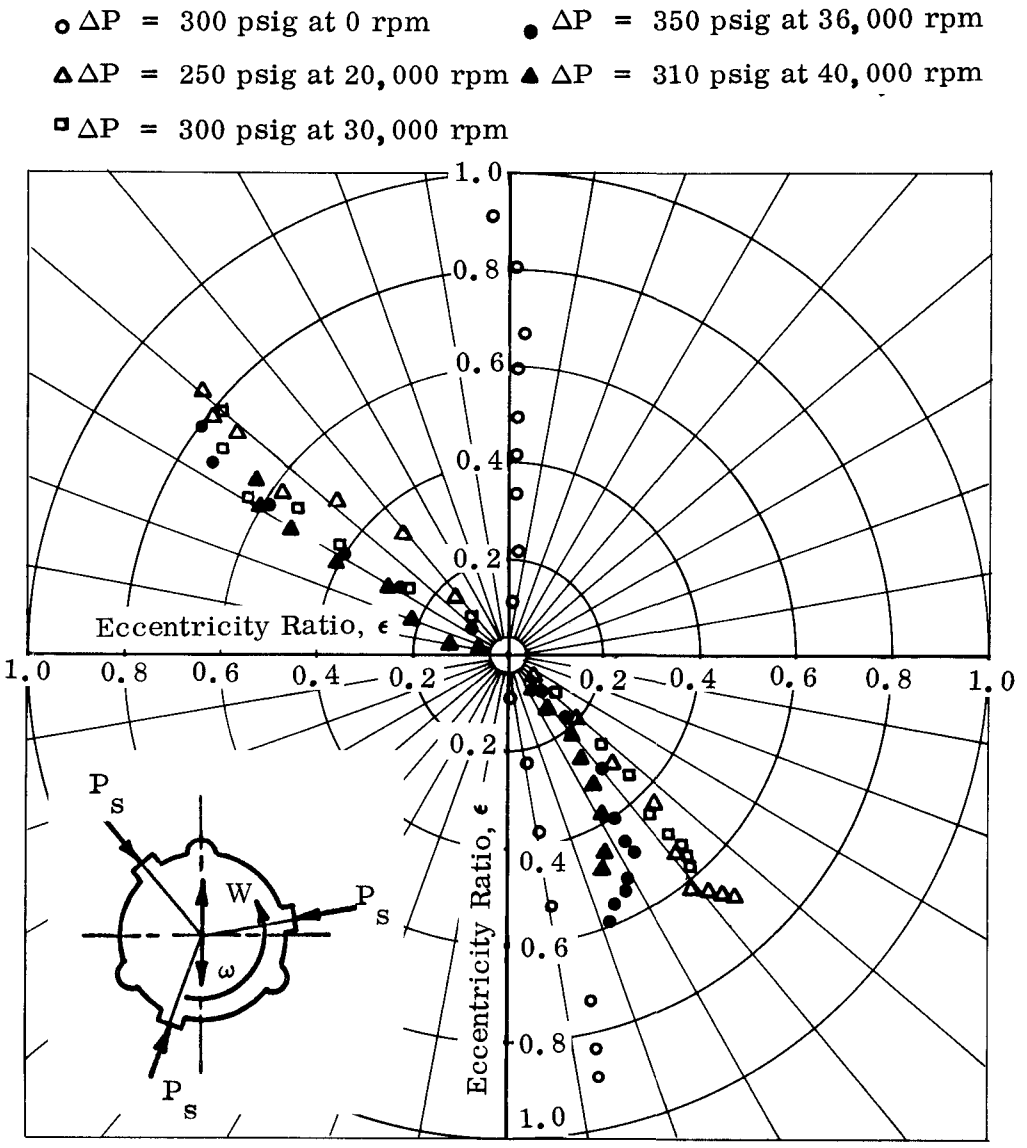

D = 0.625 inch

L = 0.407 inch

Mercury Inlet Temperature = 70°F

Figure 118. Attitude-Eccentricity Locus for a Three-Sector Compensated Bearing at C_D = 0.0015 Inch

DBTR 5 Test Series Summary

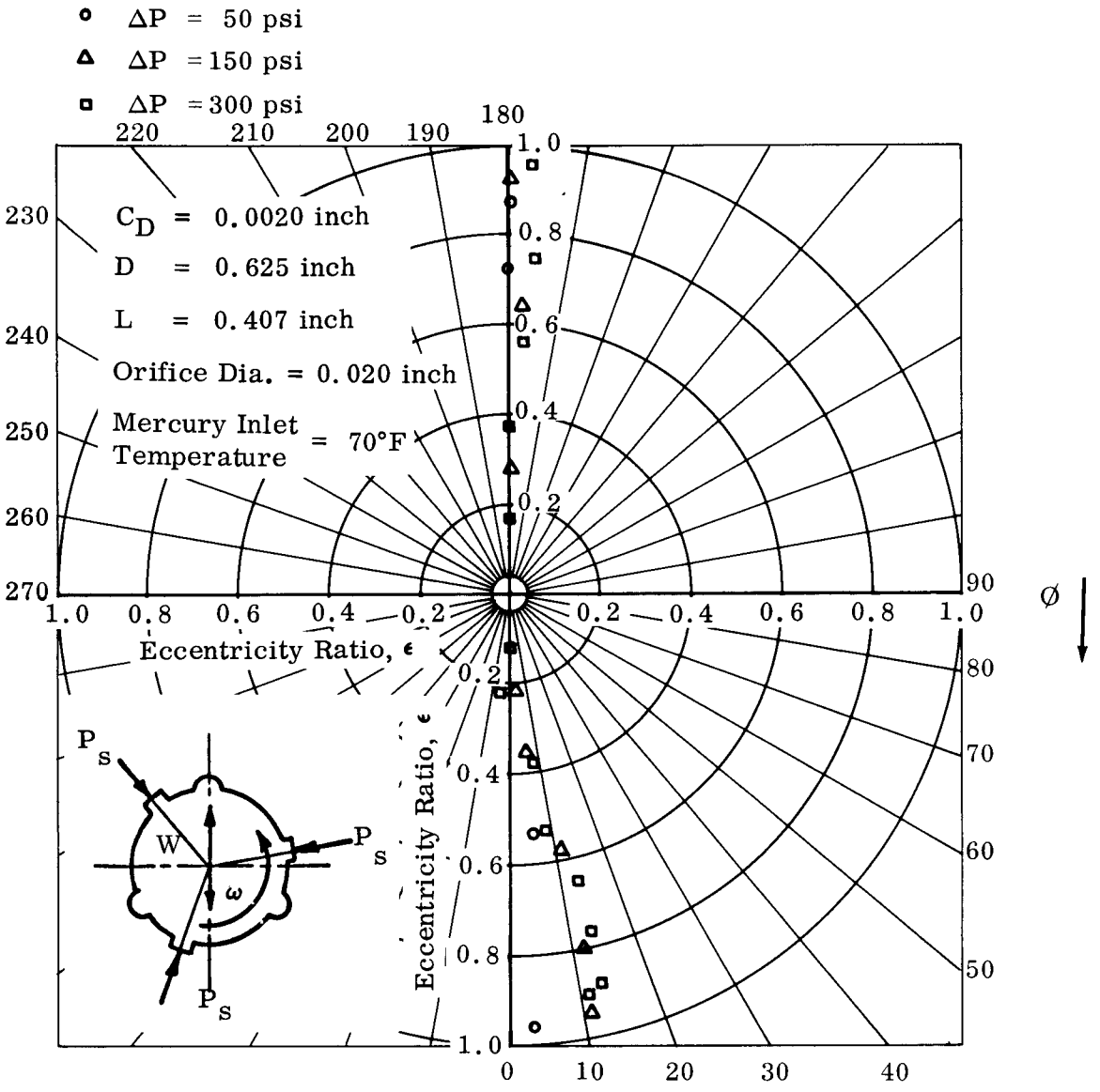

Figure 119. Static Attitude-Eccentricity Locus for a Three-Sector Compensated Bearing

DBTR 6 Test Series

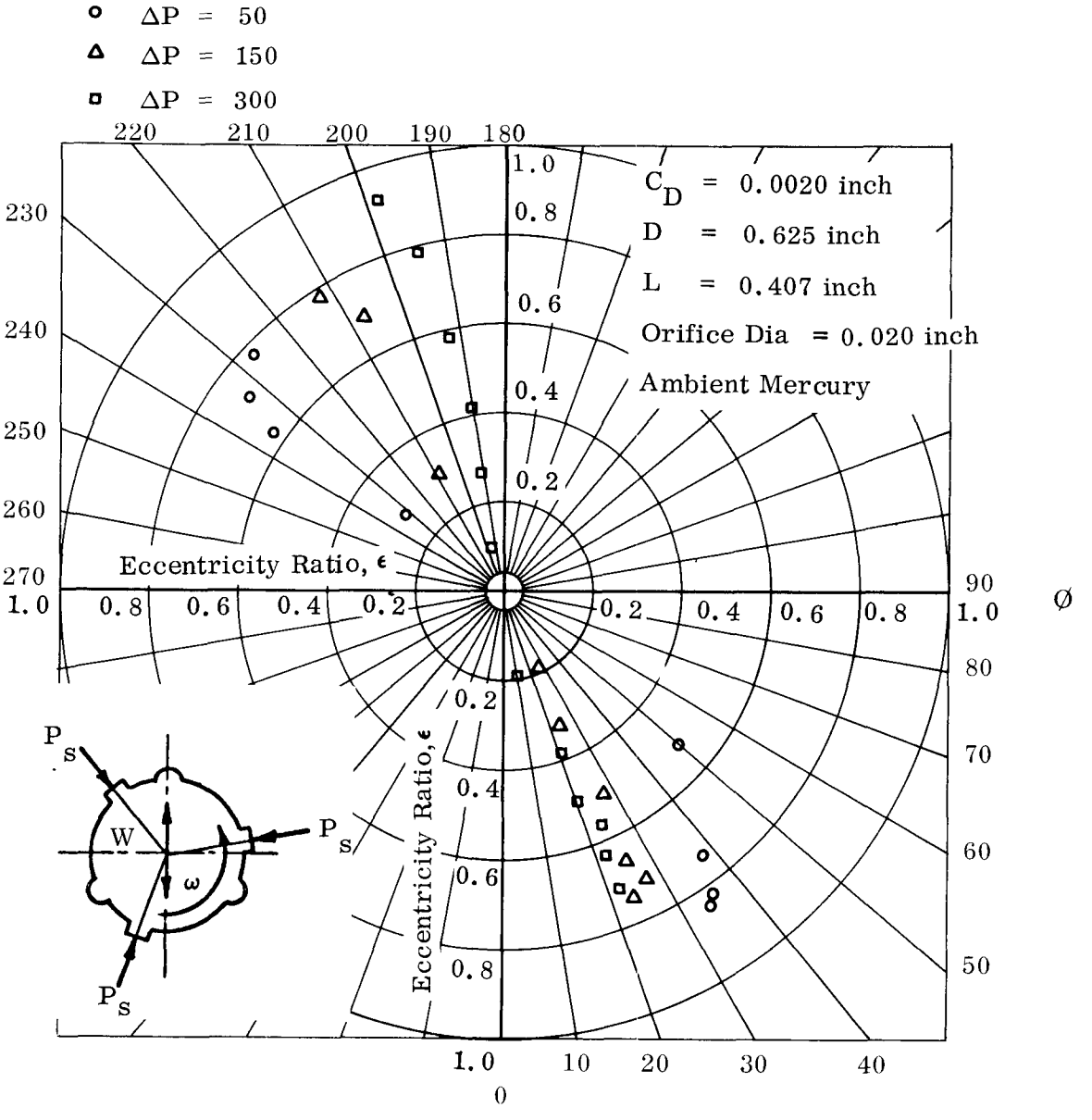

Figure 120. Attitude-Eccentricity Locus for a Three-Sector Compensated Bearing at 10,000 rpm

DBTR 6 Test Series

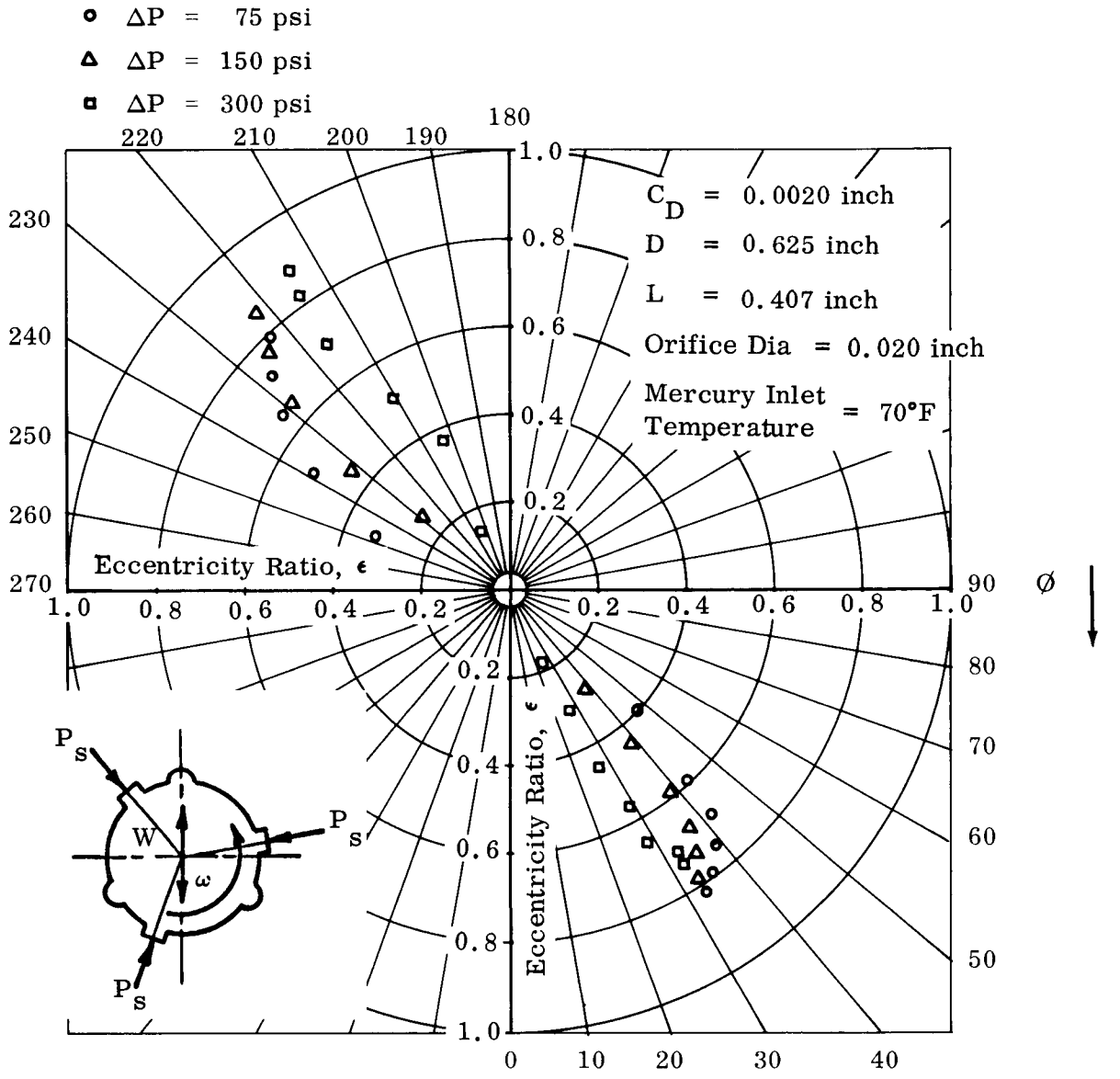

Figure 121. Attitude-Eccentricity Locus for a Three-Sector Compensated Bearing at 20,000 rpm

DBTR 6 Test Series

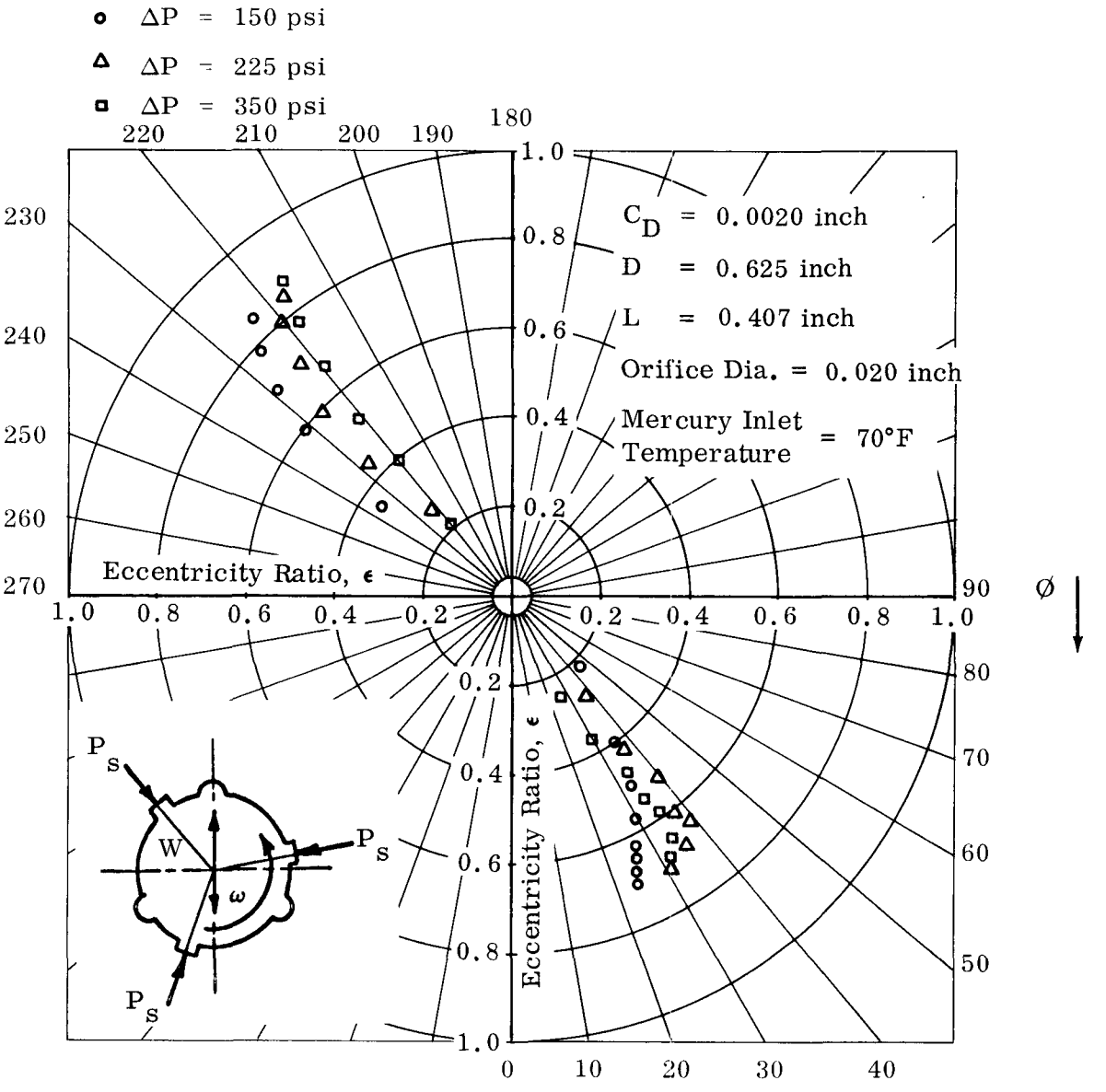

Figure 122. Attitude-Eccentricity Locus for a Three-Sector Compensated Bearing at 30,000 rpm

DBTR 6 Test Series

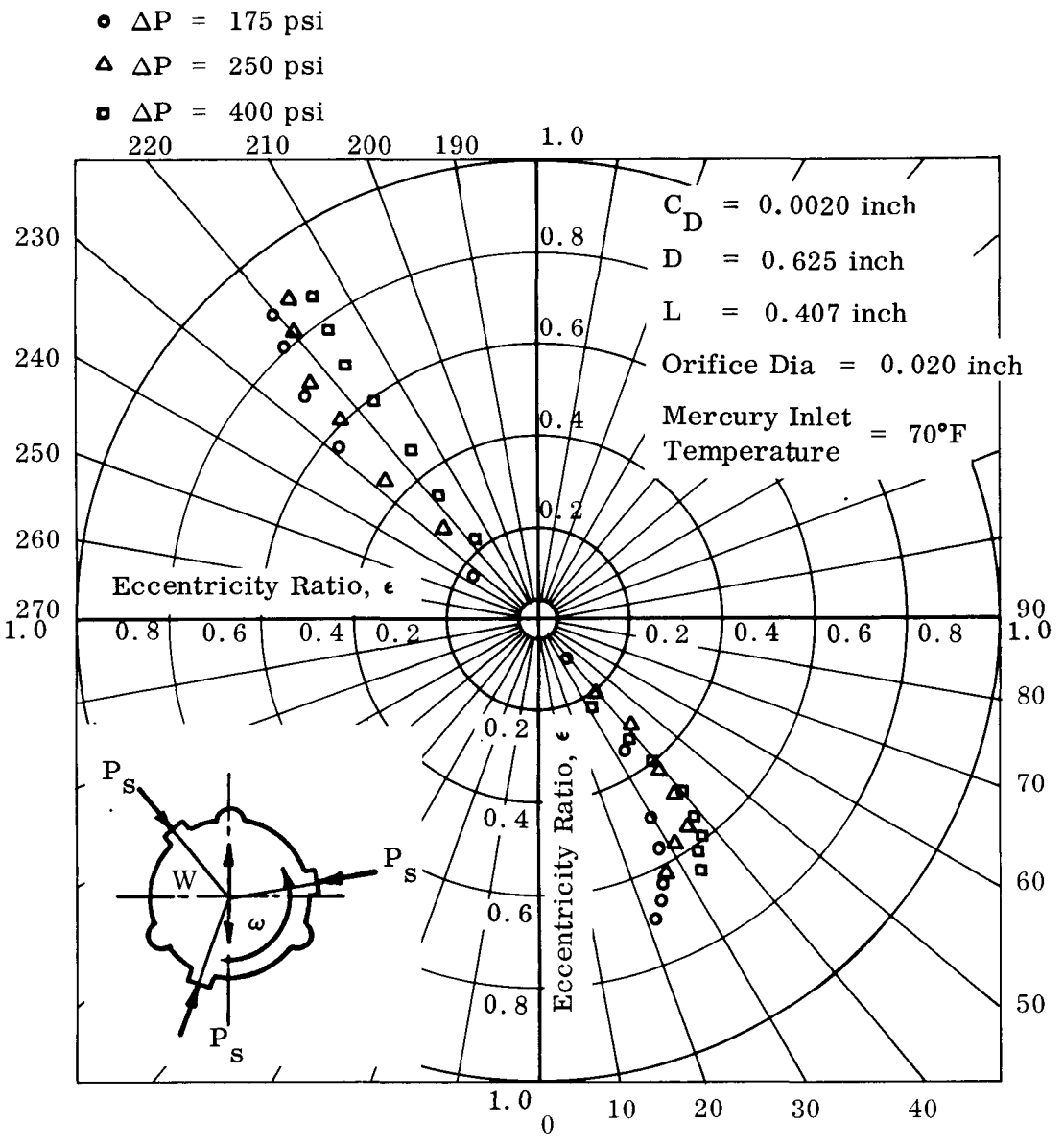

Figure 123. Attitude-Eccentricity Locus for a Three-Sector Compensated Bearing at 36,000 rpm

DBTR 6 Test Series

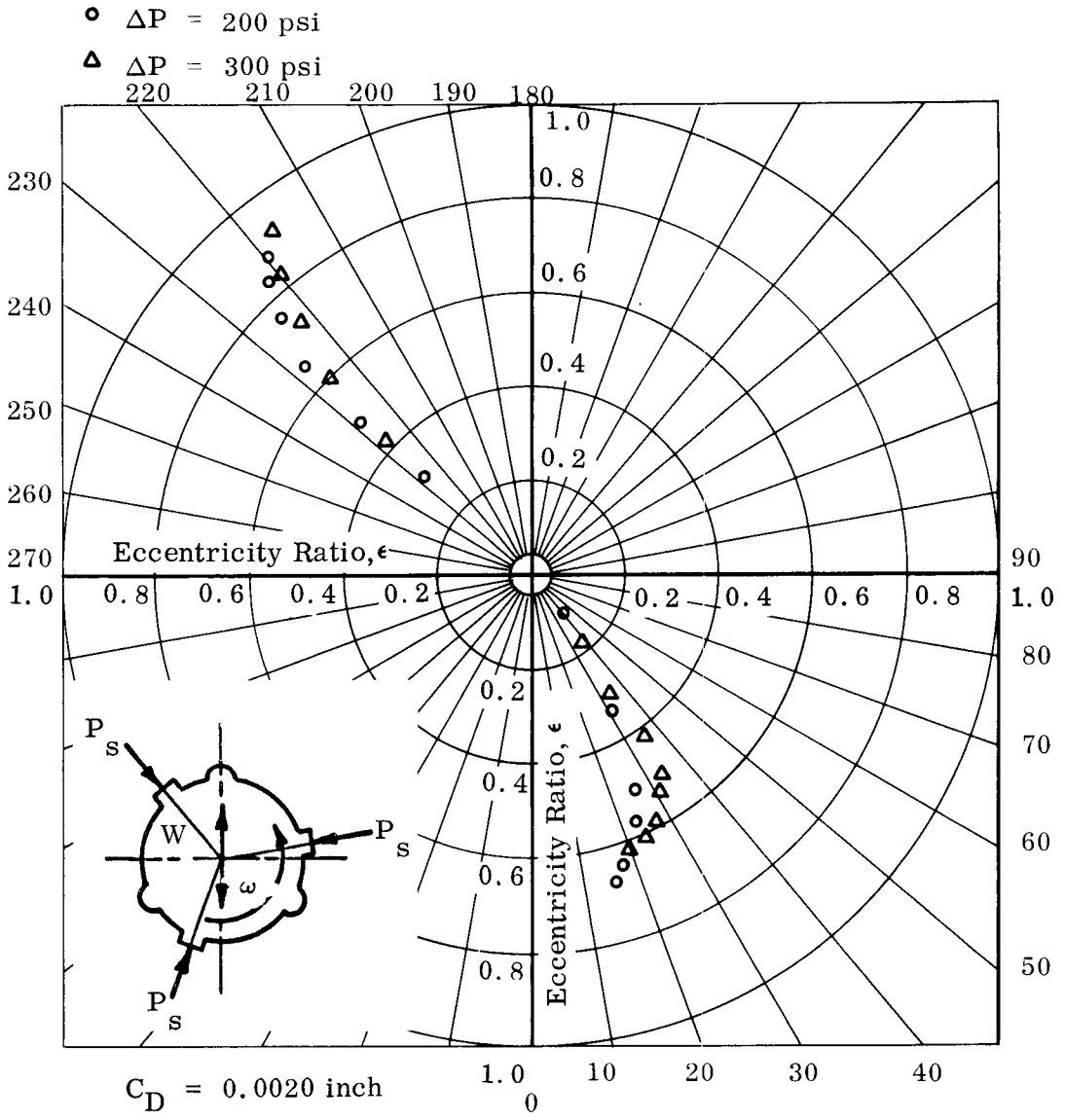

C_D = 0.0020 inch

D = 0.625 inch

L = 0.407 inch

Orifice Dia = 0.020 inch

Mercury Inlet Temperature = 70°F

Figure 124. Attitude-Eccentricity Locus for a Three-Sector Compensated Bearing at 40,000 rpm

DBTR 6 Test Series

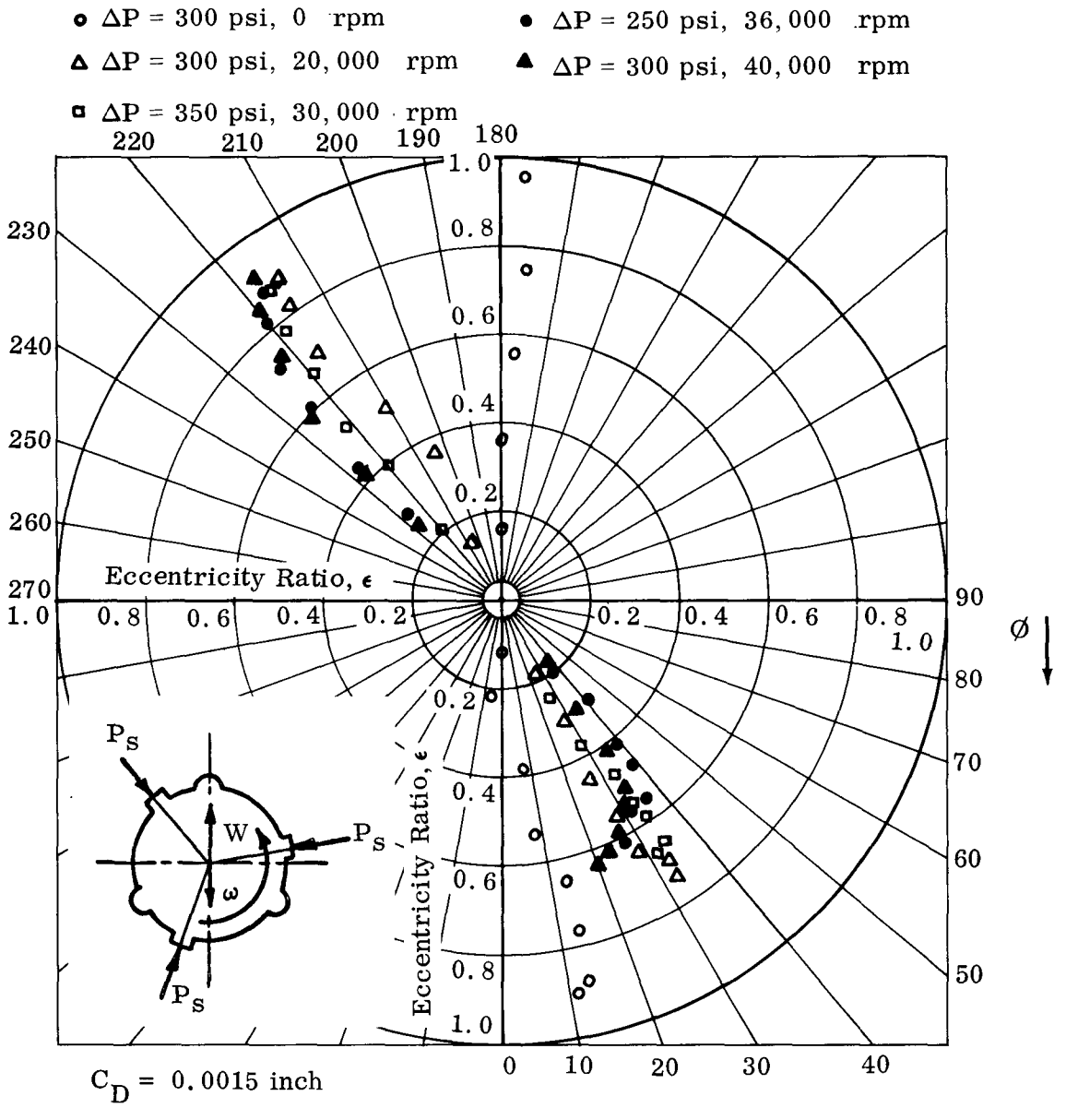

C_D = 0.0015 inch

D = 0.625 inch

L = 0.407 inch

Orifice Dia = 0.020 inch

Mercury Inlet Temperature = 70°F

Figure 125. Attitude-Eccentricity Locus for a Three-Sector Compensated Bearing

DBTR 6 Test Series

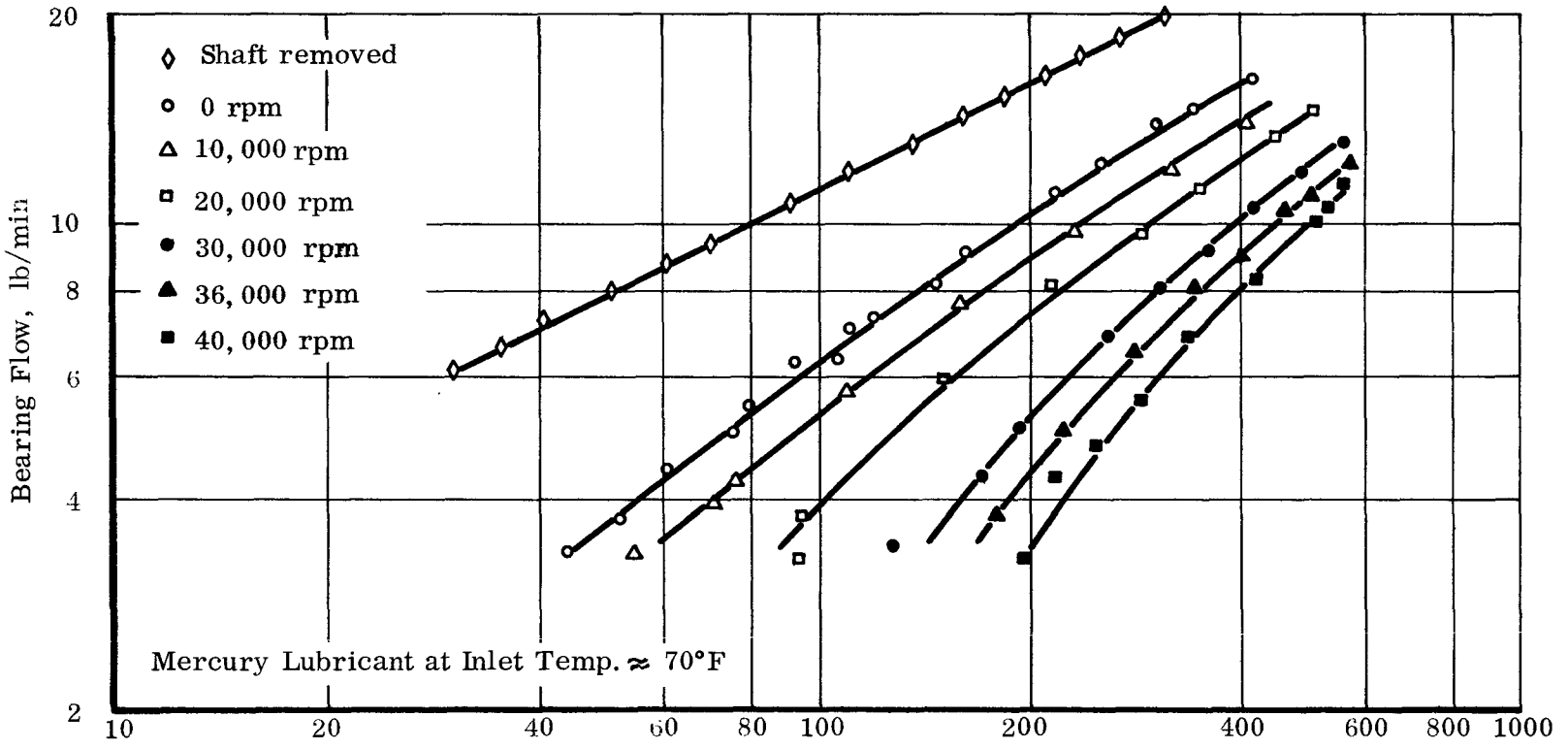

C_D = 0.0015 inch

D = 0.625 inch

L = 0.407 inch

Orifice Dia = 0.020 inch

Figure 126. Experimental Flow Calibration for a Three-Sector Compensated Bearing DBTR 5 Test Series

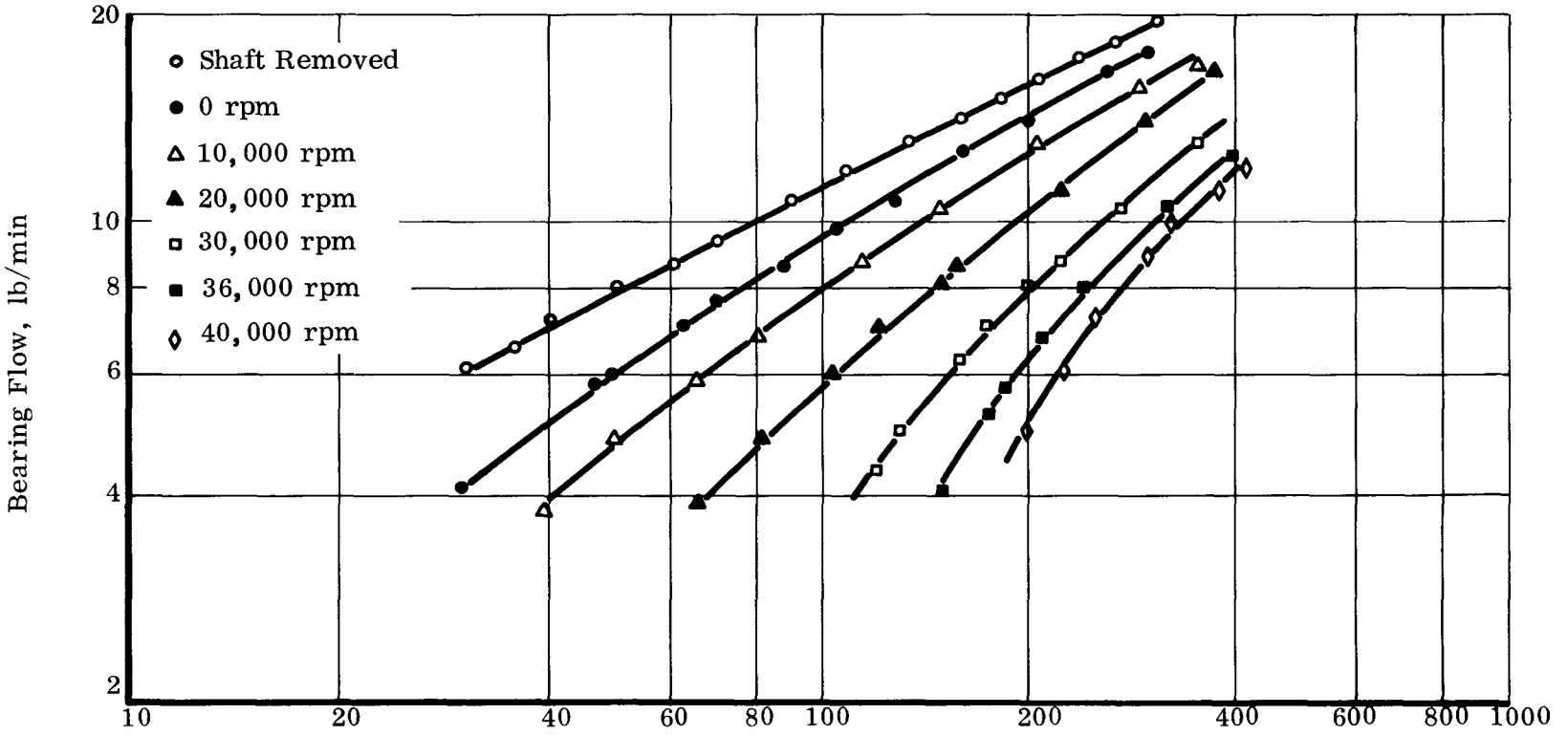

C_D = 0.002 inch

D = 0.0625 inch

L = 0.407 inch

Orifice Dia = 0.020 inch

Ambient Mercury = 70°F

Figure 127. Experimental Flow Calibration for a Three-Sector Orifice Compensated Bearing

DBTR 6 Test Series

CONFIDENTIAL

flow characteristics with the shaft removed are also included in these figures. Since the orifice restriction is equal for both bearing clearances and the downstream restriction is zero, the shaft-removed calibration is equal. With the shaft removed the flow-pressure characteristic represents an orifice calibration and the maximum flow obtainable.

Small variations in flow-pressure characteristics existed between the two journal bearings. However, a check of the calibration with the shaft removed indicated that they were due to minor differences in orifice size.

Figures 126 and 127 are useful for estimating operating clearances in actual units operating with these bearing types. Poor results were obtained by plotting a dimensionless flow factor (q_η) versus the bearing number (Λ^*) when

$$q_\eta = \frac{2Q}{\rho \pi DL C_D N} \qquad \ldots 16$$

Introducing a Reynolds number with the Λ^*, i.e., $\Lambda^* \mathrm{Re}$, resulted in excellent correlation as seen in Figure 128. The average value of the flow rate for the alternator and turbine end bearings was used. Figure 128, although a valuable design curve for flow estimation (for working back to calculate diametral clearance, for instance), is valid only for a particular bearing type and for zero load or $\epsilon = 0$. Nevertheless, its utility covers a large Reynolds number range (0 to 10,000) for flows from 2 to 15 lb/min, pressures from 0 to 500 psi, speeds from 0 to 40,000 rpm, and clearances from 0.0015 to 0.002 inch.

Figures 129 through 134 show the influence of load (shaft position) on alternator end bearing flow for both clearance bearings and at constant supply pressures. At the low Reynolds numbers (static, 10,000 and 20,000 rpm) the flow is very sensitive to load or shaft position. Maximum flow is achieved with the shaft in the center position at zero load. Flow-load characteristics are independent of load direction with flow under downward load influence being the mirror image of flow under upward load influence. This holds true for the higher speeds as well. Flow is quite insensitive to shaft position at speeds above 20,000 rpm (unless half-frequency whirl instability is encountered). At 40,000 rpm the flow variation is approximately 1 lb/min under the influence of loads in excess of 40 lb both up and down.

The 0.002-inch clearance encountered some half-frequency whirl (see later section) above 30,000 rpm at zero load and low supply pressures. A marked reduction in flow occurred on encountering whirl. Figure 132 shows that for a supply pressure of 150 psig whirl is encountered near a 5 lb load, resulting in a subsequent flow reduction. At 225 psi or above no instability was encountered at this speed at any load condition.

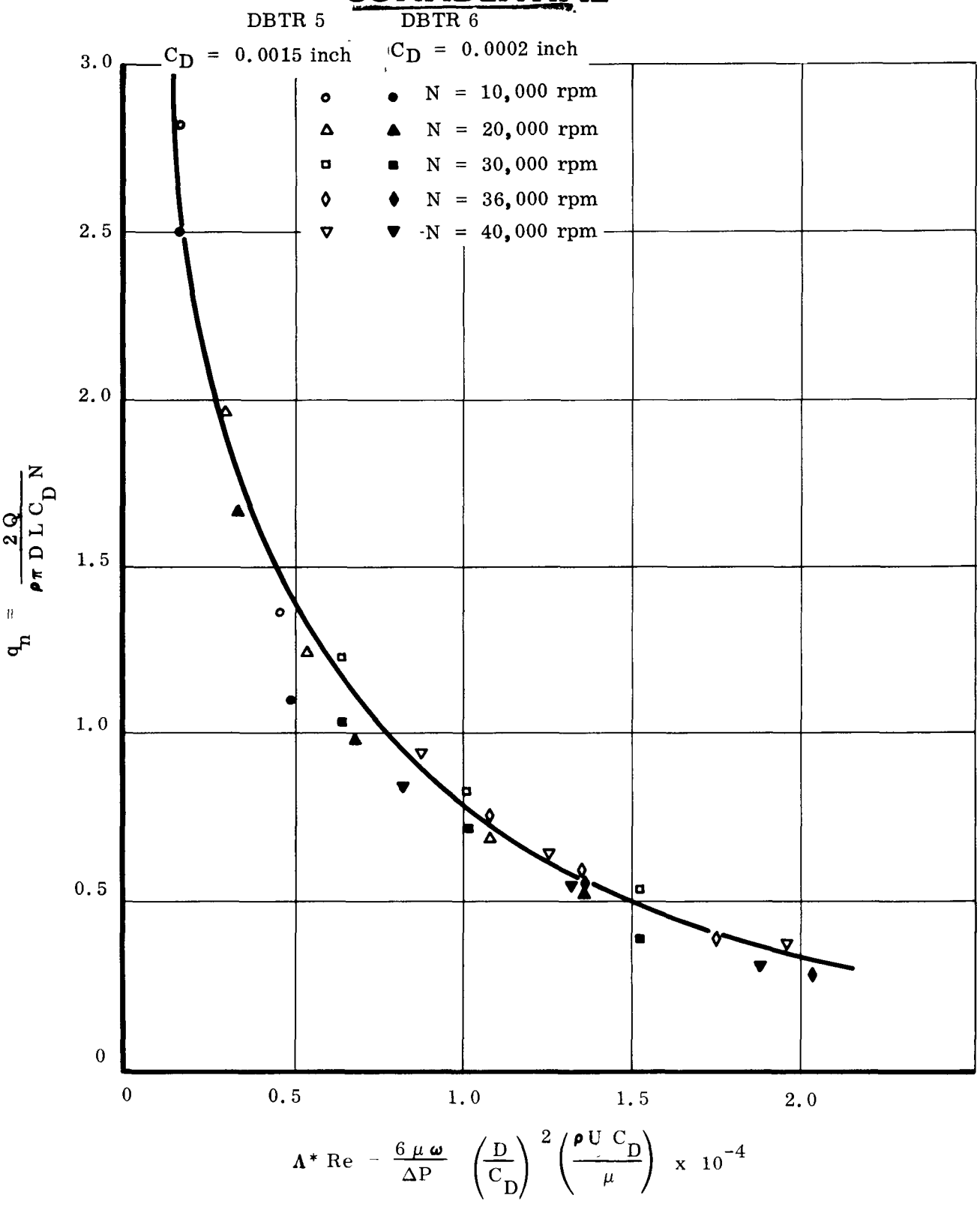

Figure 128. Dimensionless Flow Number vs the Modified Bearing Number and Reynolds Number Product for a Three-Sector Orifice-Compensated Journal Bearing for Zero Eccentricity

DBTR 5 and 6 Test Series

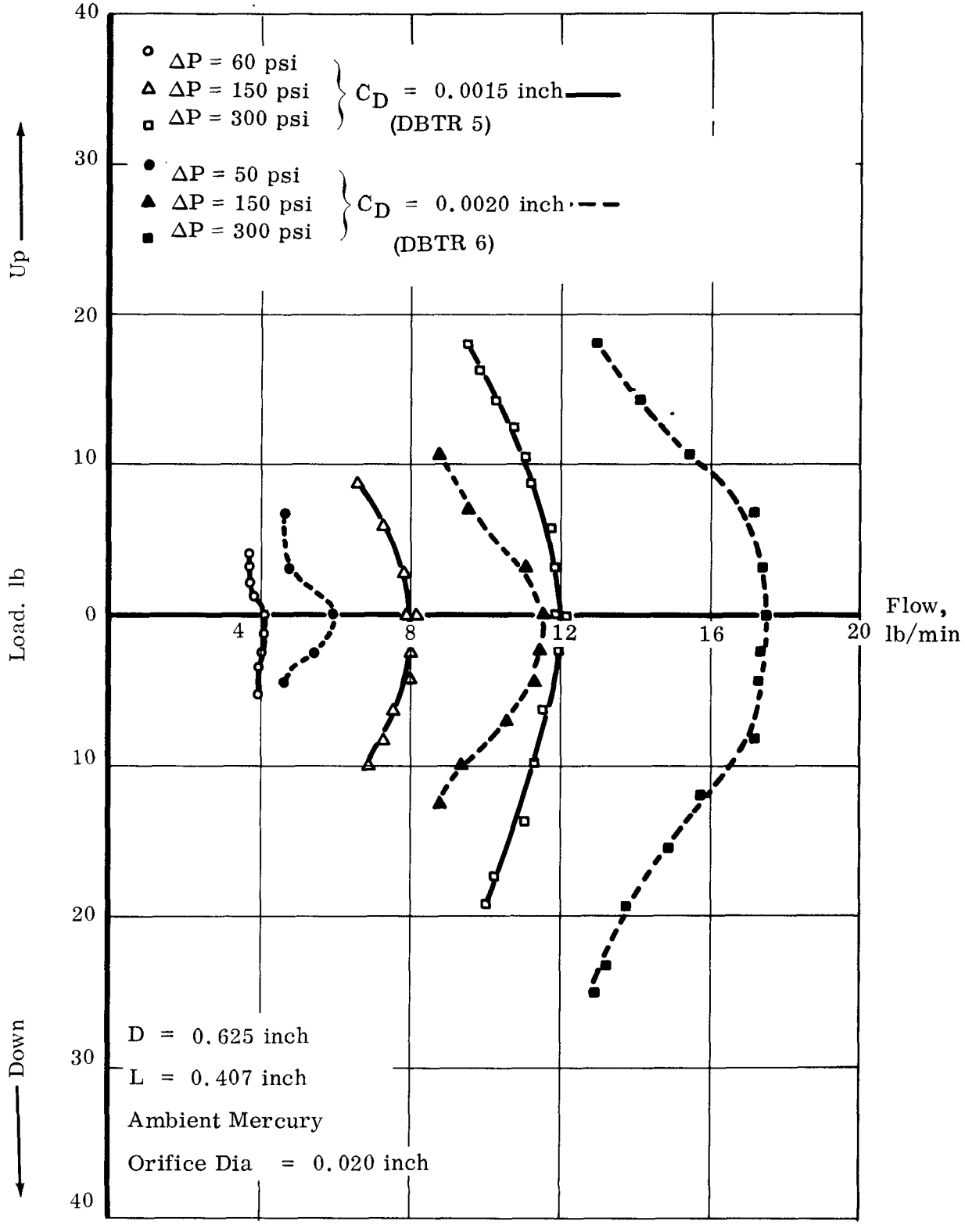

Figure 129. Static Load vs Flow for a Three-Sector Orifice-Compensated Bearing

DBTR 5 and 6 Test Series

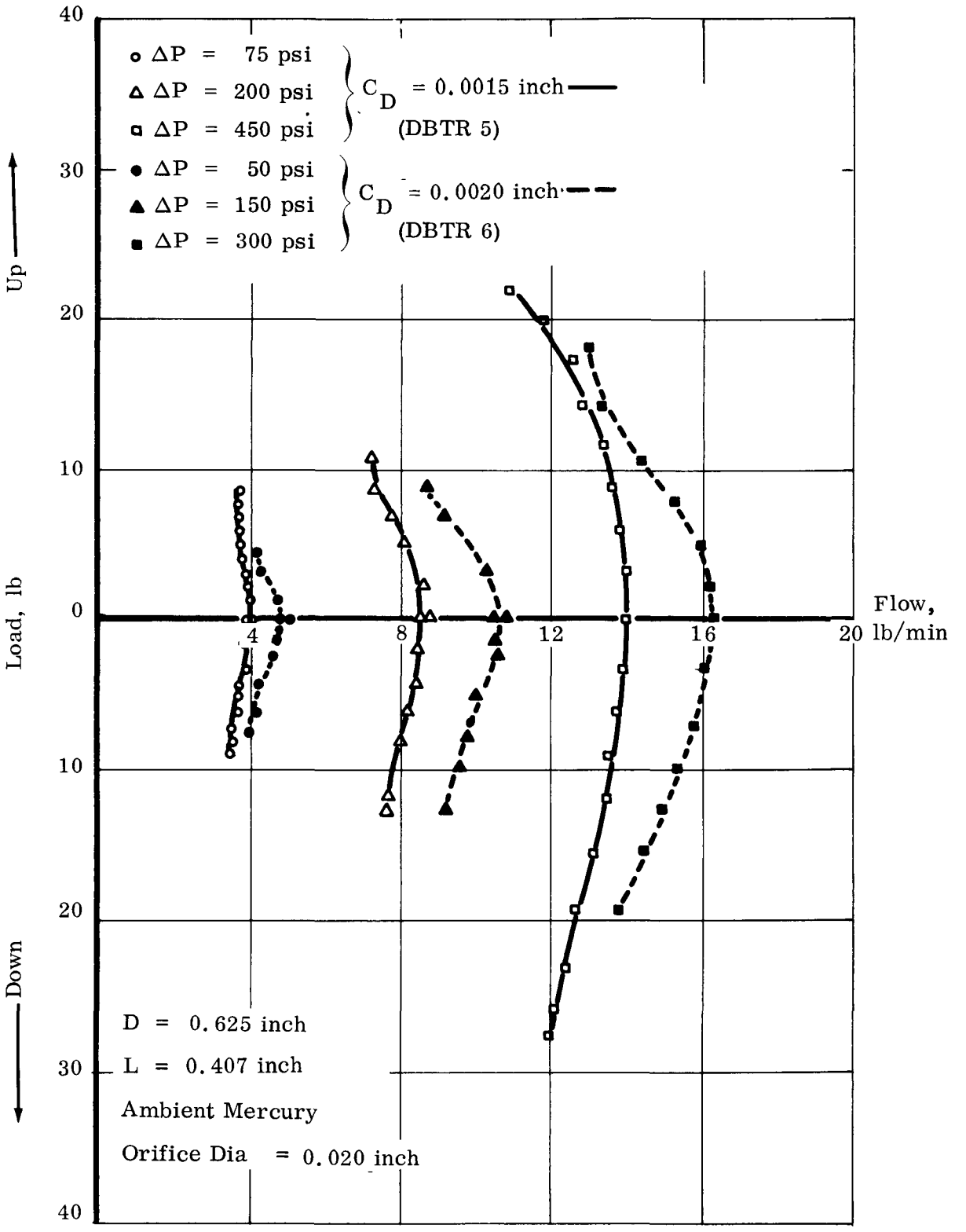

Figure 130. Load vs Flow for a Three-Sector Orifice-Compensated Bearing at 10,000 rpm

DBTR 5 and 6 Test Series

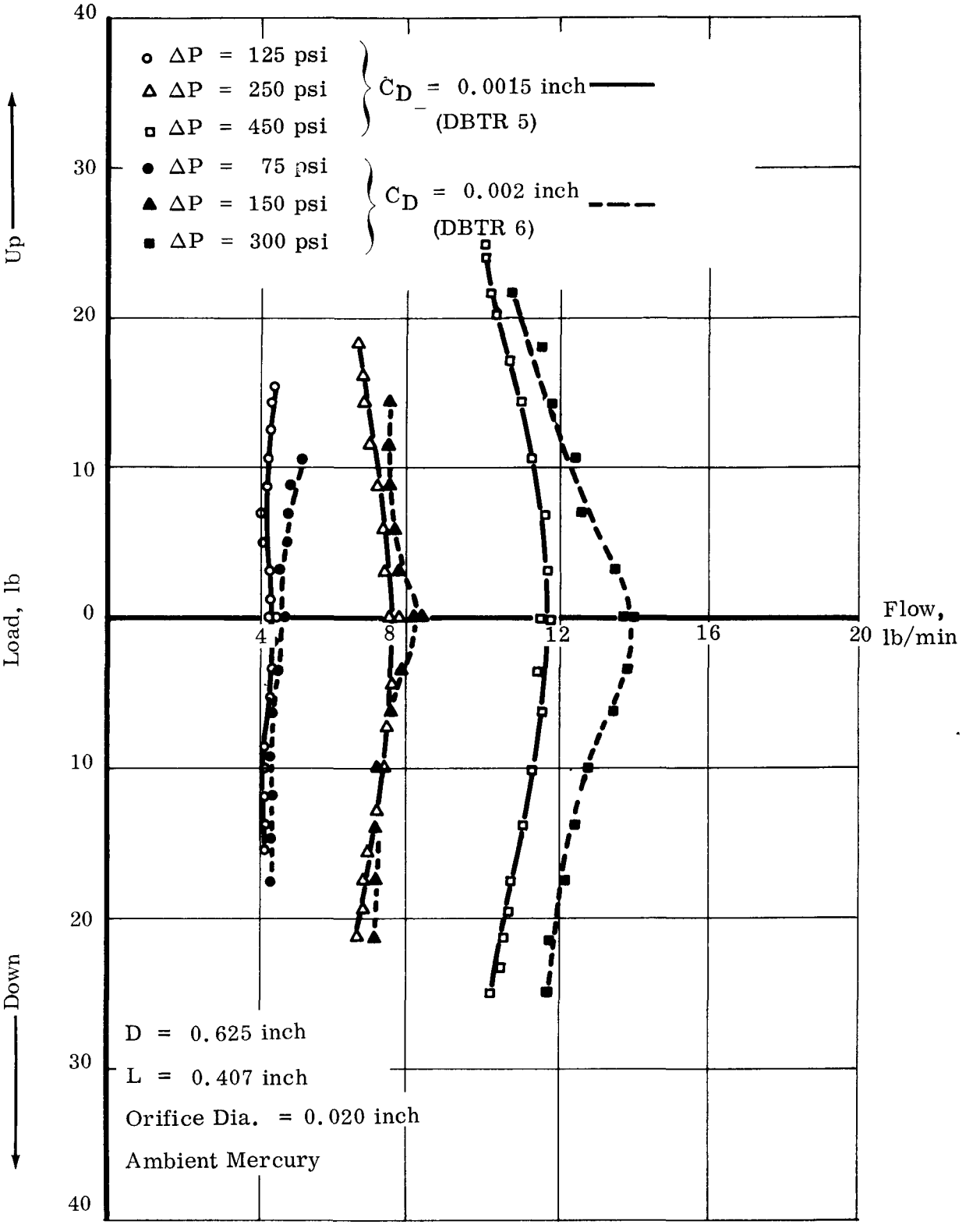

Figure 131. Load vs Flow for a Three-Sector Orifice-Compensated Bearing at 20,000 rpm

DBTR 5 and 6 Test Series

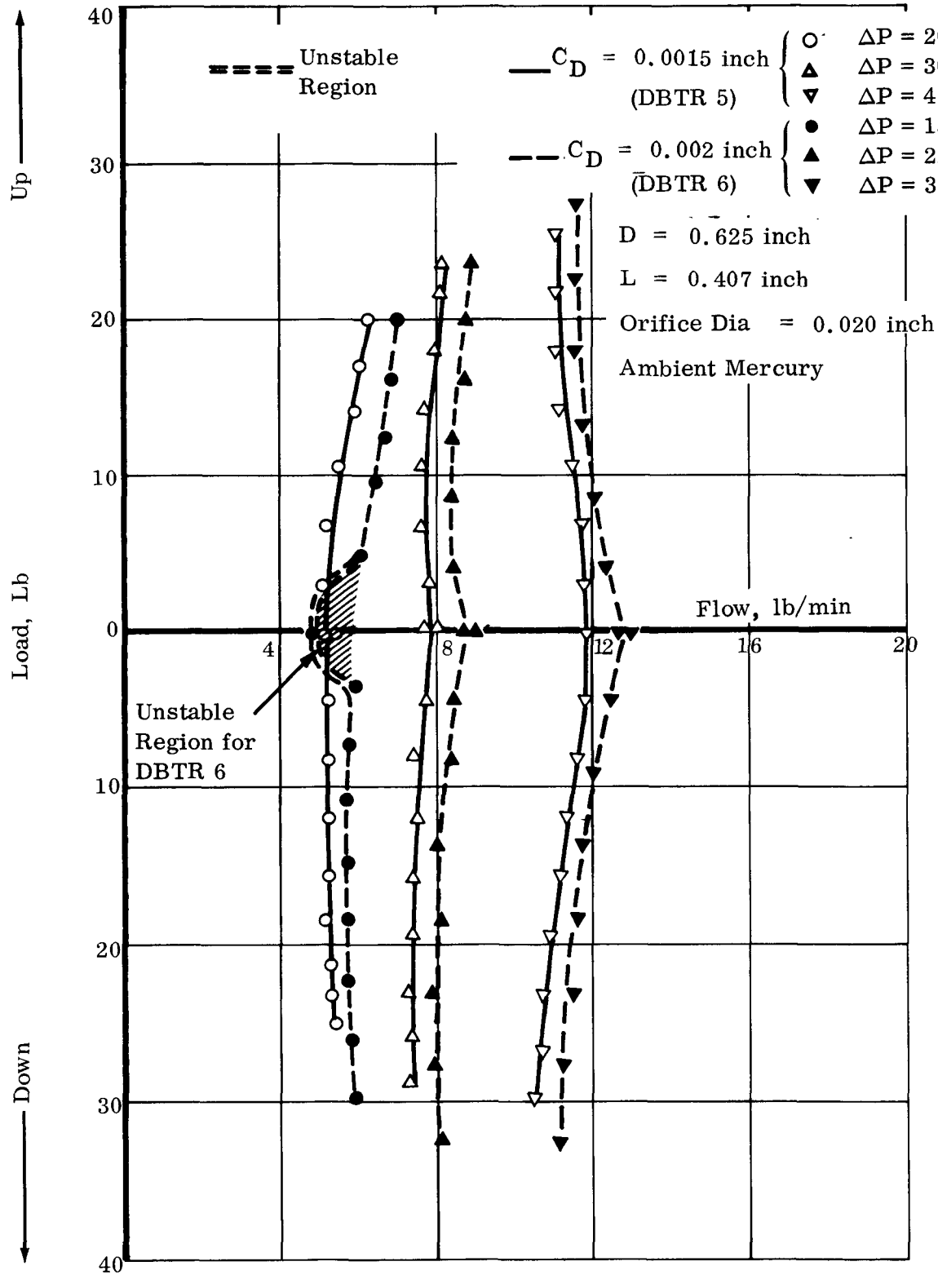

Figure 132. Load vs Flow for a Three-Sector Compensated Bearing at 30,000 rpm

DBTR 5 and 6 Test Series

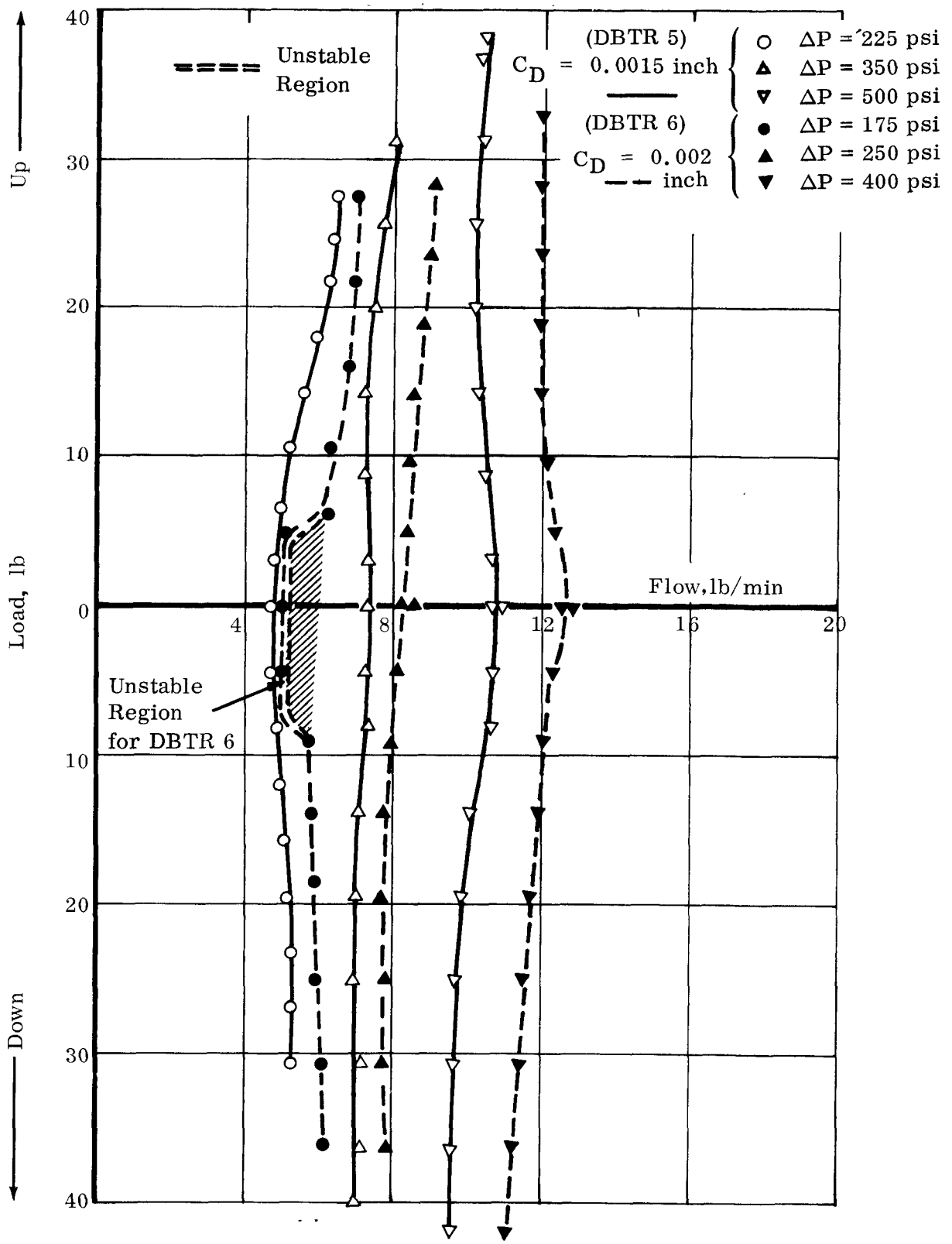

Figure 133. Load vs Flow for a Three-Sector Compensated Bearing at 36,000 rpm

DBTR 5 and 6 Test Series

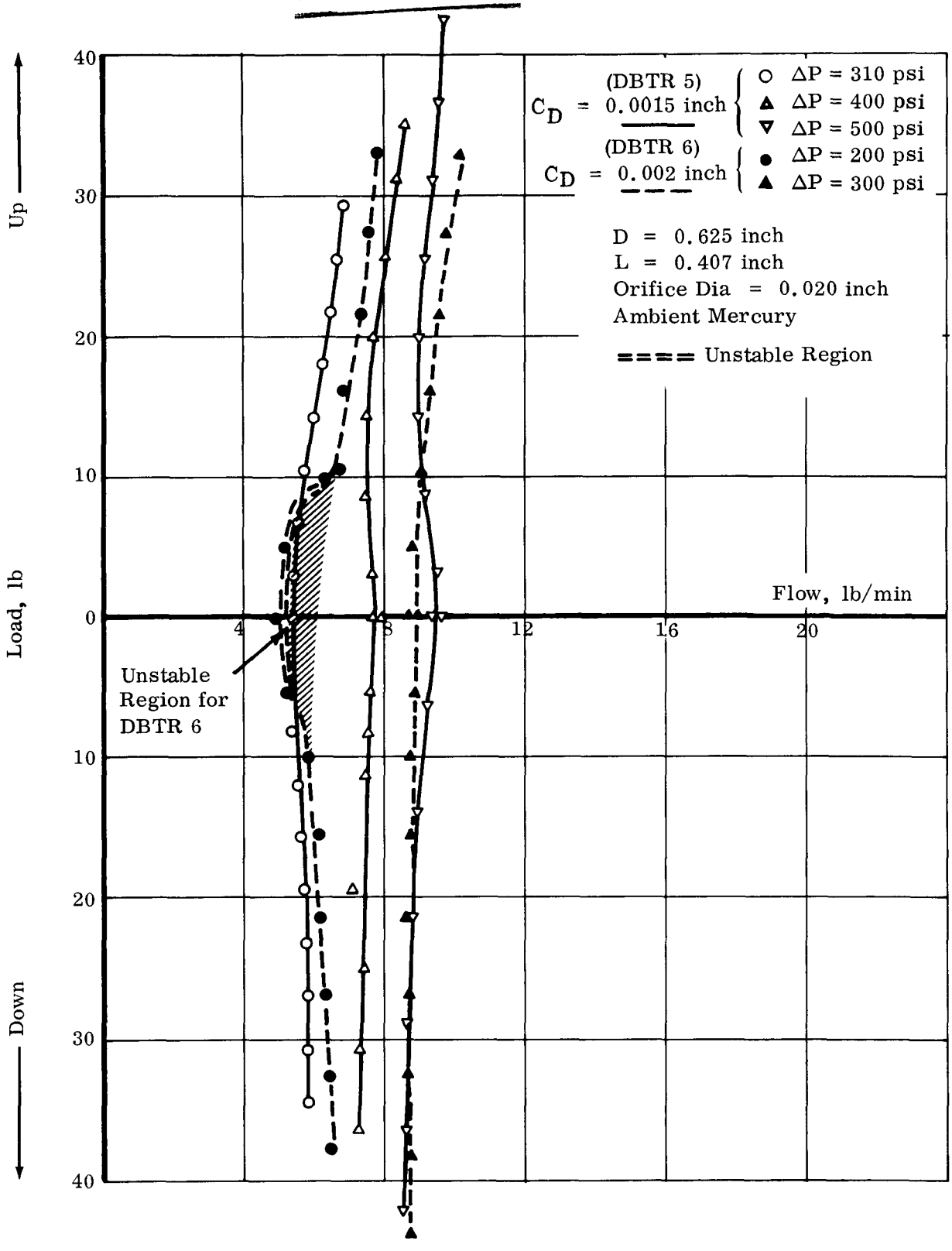

Figure 134. Load vs Flow for a Three-Sector Compensated Bearing at 40,000 rpm DBTR 5 and 6 Test Series

At 36,000 rpm the instability region increased somewhat as illustrated by Figure 133. Half-frequency whirl occurred at 175 psig and a load of approximately 7.5 lb (up or down). At higher pressures the rotor again remained stable. At 40,000 rpm the whirl region grew again to include 200 psi and loads of approximately 10 lb. At 300 psi the rotor retained its stability. Since at high speeds flow is quite independent of load, a dimensionless flow factor curve at different eccentricity ratios was not generated.

5. Power Loss

The frictional power loss was established by the normal speed decay method and is summarized in Figure 135. The shaft speed was measured as a function of speed decay by shutting off the turbine supply at 45,000 rpm and allowing the unit to spin down to 20,000 rpm. No data above 40,000 rpm were utilized to eliminate the possibility of surge in the turbine supply. An attempt was made to establish the influence of unidirectional and rotating loads, flow and pressure, and clearance on the power loss. The following ranges were imposed:

W (unidirectional)	0, 5, and 10 lb (up and down)
W (rotating)	0, 15 and 30 lb (at 40,000 rpm)
Q	7.0 and 10.0 lb/min
C_D	0.0015 and 0.002 inch

Only the bearing clearance had a measurable influence on power loss as shown in Figure 135. The unidirectional loads were kept small to protect the bearings and, consequently, did not cause a large shaft deflection and subsequent increase in power loss. At fixed speeds, increase in unidirectional load (decreasing film thickness) has been accompanied by an increase in power loss as predicted by theory. Rotating loads also had no measurable influence on power consumption. This is to be expected since the magnitude of the load is proportional to speed squared and, therefore, drops off rapidly with speed. Subtracting the power loss of the double acting thrust bearing permits determination of the journal bearing losses. Again the trend of power loss with clearance is as predicted by Smith and Fuller and laminar analysis, but the estimated loss is some 10 to 20 per cent higher than predicted by Smith and Fuller's turbulent equations. Comparison with uncompensated and partially compensated bearings reveals that these fully compensated bearings appear to have slightly greater power losses.

6. Stability Characteristics

The 0.0015-inch clearance orifice-compensated three-sector bearing was free from half-frequency whirl at all speeds to 45,000 rpm under all conditions of flow-pressure and load tested. Flows as low as 3.5 lb/min and the corresponding supply

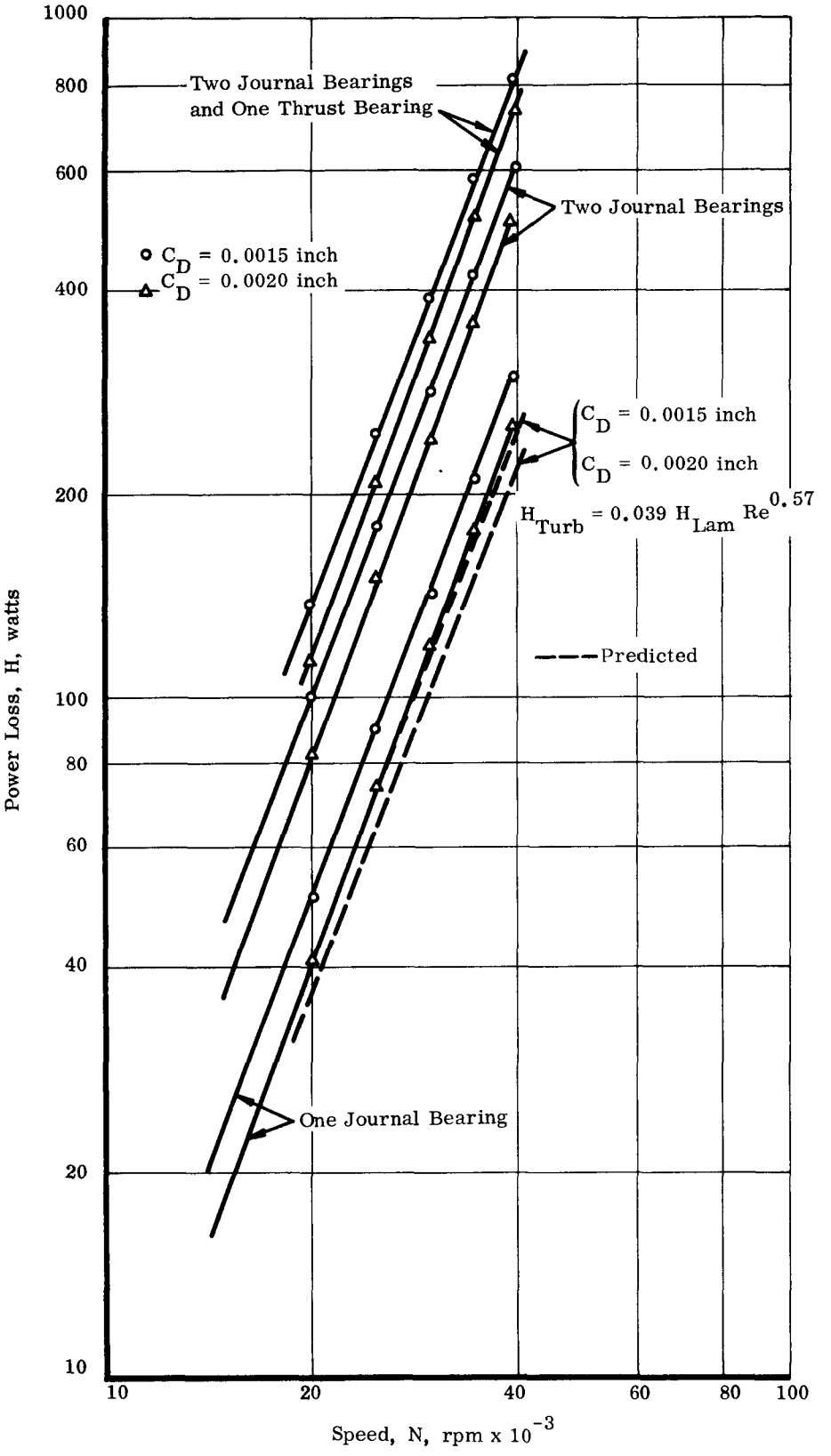

Figure 135. Frictional Power Loss vs Speed for a Three-Sector Orifice-Compensated Journal Bearing at Zero Eccentricity

DBTR 5 and 6 Test Series

pressure did not result in any whirl tendency. The 0.002-inch clearance bearing became unstable near 20,000 rpm, with pressures down to 75 psi and zero load.

The ratio of the whirl frequency to the shaft frequency was generally around 0.4, i.e., fractional frequency or multiple frequency whirl, under the influence of unidirectional loads. The large clearance bearing was more unstable when loading upward than downward. Figure 136 illustrates the combined effect of unidirectional load upward (into an axial groove) and supply pressure on the threshold of whirl. At constant pressure,increased load generally results in a higher whirl threshold. Increasing supply pressure at constant load similarly results in higher whirl threshold. Based on Figure 136, it is relatively easy to suppress the onset of half-frequency whirl above 44,000 rpm by the application of a supply pressure of 250 to 300 psi regardless of the size of the unidirectional load (from 0 to 10 lb/bearing). Since 250 to 300 psi is well within the system capacity and does not result in excessive bearing flows, this bearing with a clearance of 0.002 inch can be operated fully stable up to speeds of 44,000 rpm.

The lower whirl threshold achieved when loading up rather than down verifies the larger, less favorable attitude angle measured when loading upward. (See discussion of attitude-eccentricity loci.)

7. Influence of Rotating Load

The influence of rotating loads on the performance of the orifice-compensated three-sector bearing at both clearances was evaluated. Two specific objectives were accomplished by this series of tests:

1) The performance variations were established.

2) The data generated on the amplitude of the shaft motion under the influence of a known unbalance at a known location were used to establish radial film stiffness and damping characteristics.

a. Load Capacity

The addition of rotating unbalance had little influence on the load deflection characteristics other than to cause the shaft locus to have an increasing amplitude with speed. For small unidirectional loads,the shaft orbit in the bearing was the characteristic circle. As the unidirectional load was increased at a fixed speed, the circle became eliptical with the major axis staying relatively constant while the minor axis decreased with increasing eccentricity ratio. The unidirectional load-capacity measured at a fixed film thickness decreased but not at the same proportion as the increased rotating load.

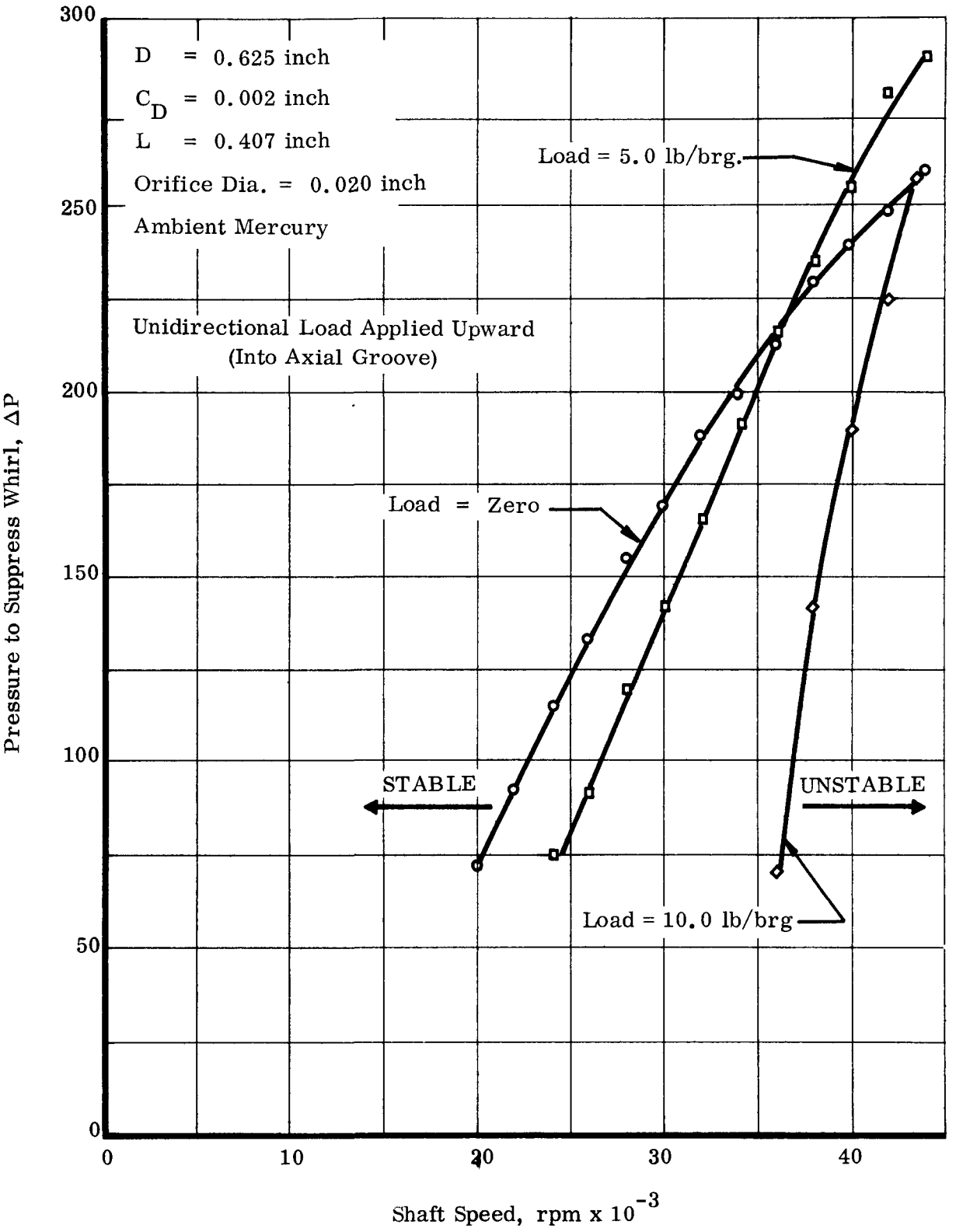

Figure 136. Pressure to Suppress Whirl vs Speed for a Three-Sector Orifice Compensated Bearing

DBTR 6 Test Series

b. Attitude-Eccentricity Locus

Attitude-eccentricity ratio remained unchanged although the attitude angle was again represented by an orbit instead of a point locus so that there was a minimum and maximum, i.e., time dependent, attitude angle at each load and speed.

c. Flow Characteristics

The effect on flow by the unbalanced loads was minor and negligible. A slight reduction in flow can be expected with rotating loads which correlates with the effect of unidirectional load on flow mentioned earlier.

d. Stability

Rotating load had a measurable influence on the threshold of whirl, the frequency of the whirl ratio, and the additional pressure required to suppress whirl completely. It had absolutely no effect on the 0.0015-inch clearance bearing since the bearing was stable at all conditions up to 45,000 rpm. The addition of rotating loads (in the quantities applied here) did not decrease the stability of this bearing. Its beneficial influence on the 0.002-inch clearance bearing is evident in Figure 137. As the rotating load was increased, the whirl threshold for a fixed pressure increased. Similarly, to achieve stability at a given speed required lower supply pressures with increased rotating load. This phenomenon is characteristic of fluid film bearings. Increasing the rotor unbalance to achieve stable operation is a standard practice in the field.

Unbalancing the rotor is, therefore, a relatively simple method for achieving stable operation at reasonable supply pressures in the absence of adequate unidirectional loads. The addition of downward unidirectional loads further improved the stability characteristics so that they required smaller supply pressures. However, no definite trend was observed with the application of upward unidirectional loads. The unidirectional load would either increase or decrease the whirl threshold depending on the relative magnitude of the load vectors.

The hysteresis, observed to be sizable with uncompensated three-sector and plain journal bearings, was found to be quite small in this case. As a result, regardless of whether the speed, load, or pressure was increased, the same whirl threshold was obtained.

The ratio of the whirl frequency to the shaft frequency under the influence of both rotating and unidirectional loads was generally 0.5 or true half-frequency whirl. Without rotating loads the ratio was around 0.4. Typical oscilloscope photographs are shown in Figure 138. Figure 138a represents fractional frequency whirl obtained at 42,000 rpm during DBTR 6C at zero unidirectional load. Figures 138b and 138c represent half-frequency whirl obtained at 22,000 and 36,000 rpm during DBTR 6C with unidirectional loads of 5 lb and 10 lb/bearing upward, respectively. Figure 138b clearly shows that the locus is a combination of rotating load (small

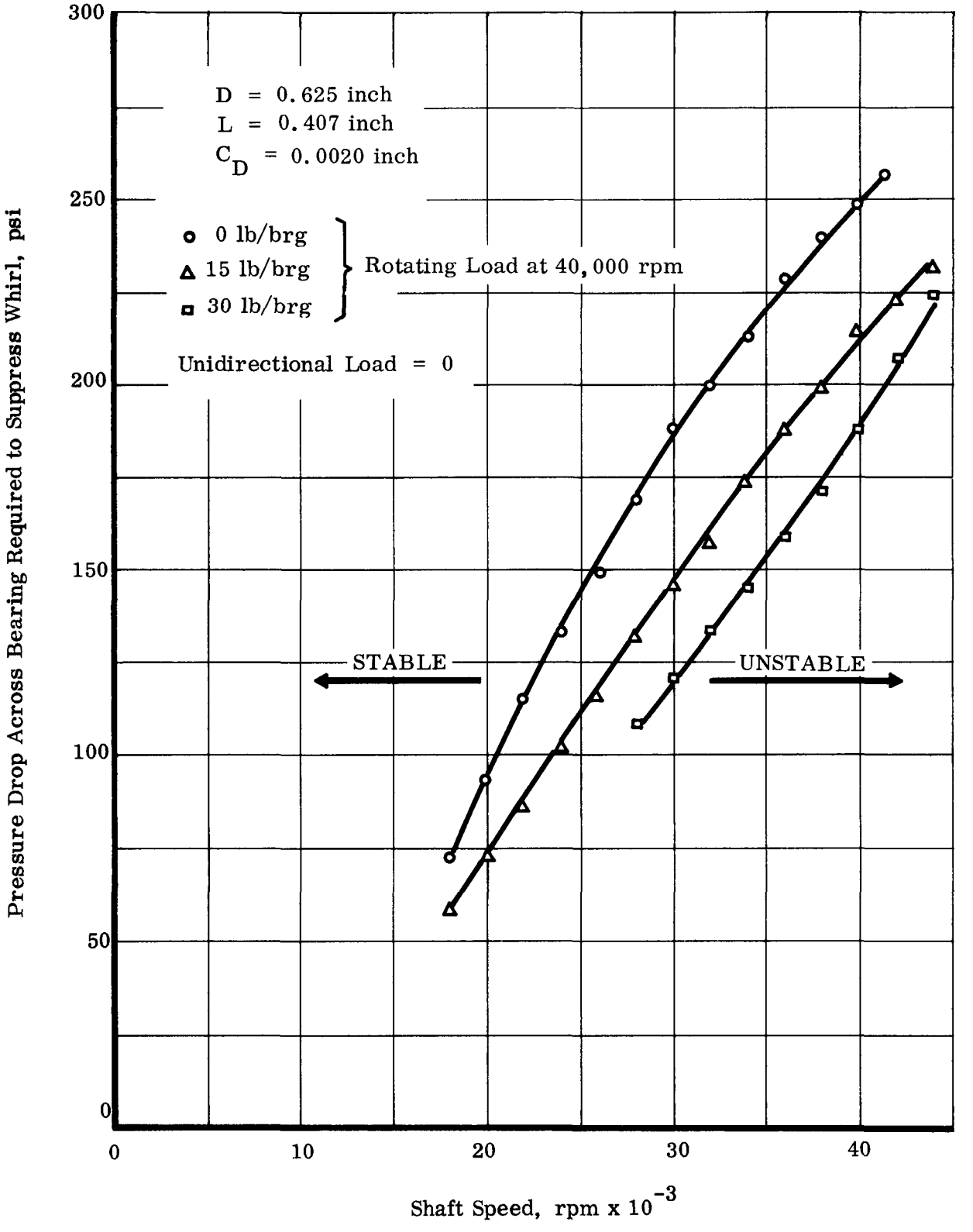

Figure 137. Pressure to Suppress Whirl vs Shaft Speed for an Orifice-Compensated Three-Sector Bearing

DBTR 6 Test Series

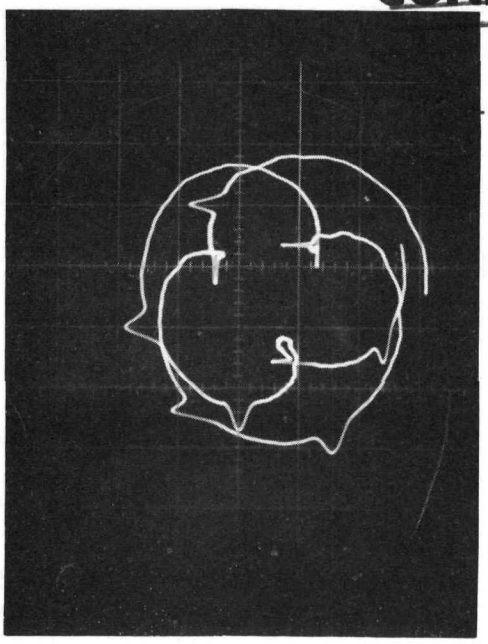

(a) DBTR - 6C at 42, 000 rpm
10-1-63
DP #3

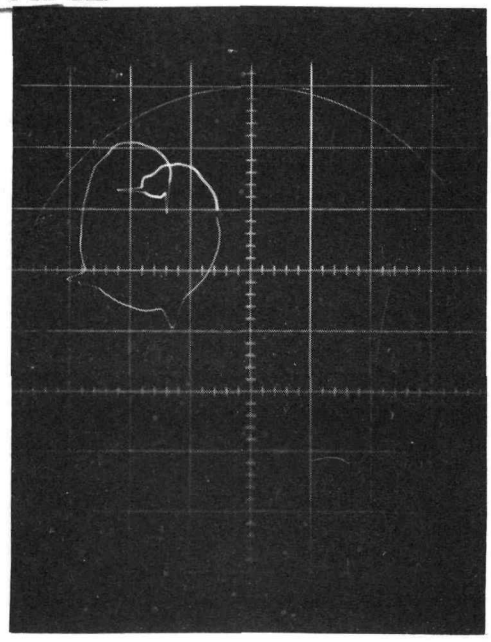

(b) DBTR - 6C at 22, 000 rpm
Load = 5 lb
10-2-63
DP #3

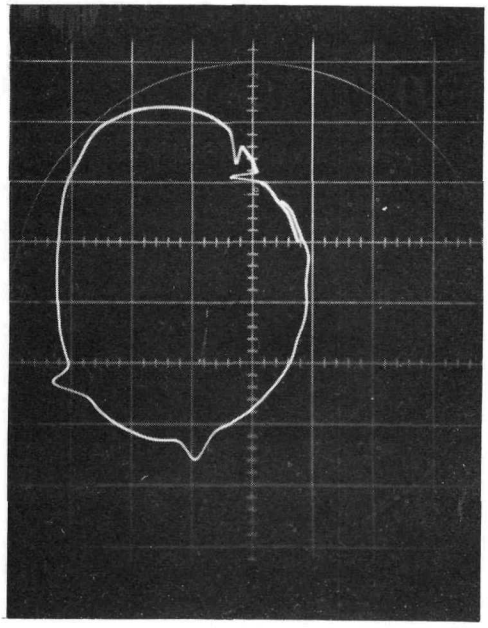

(c) DBTR - 6C at 36, 000 rpm
Load = 10 lb
10-2-63
DP #42

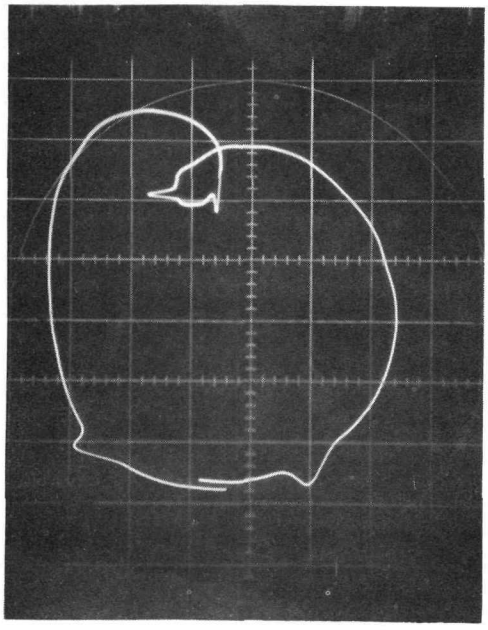

(d) DBTR - 6A at 36, 000 rpm
Load = 11. 55 lb
10-8-63
DP #78

Figure 138. Oscillograph Photographs Showing Fractional Frequency Whirl in Orifice Compensated Three-Sector Bearings

DBTR 6 Test Series

circle) and half-frequency whirling motion (large circle). In Figure 138c the half-frequency whirling motion has overcome the rotating load (unbalance) and represents the major influence on the shaft orbit. Figure 138d represents half-frequency whirl obtained during DBTR 6A at 36,000 rpm with an additional 11.5 lb/bearing uni-directional load. In these instances the fractional frequency whirl is characterized by a non-repeating orbit, although if it were a whole fraction of the rotating speed (1/2, 1/3, 1/4, 1/5, etc.), even these orbits would be repetitively stable. The half-frequency orbit is generally a closed, repeating type locus although the circle does not close as it departs from pure half-frequency (either > 0.5 or < 0.5) by a small amount. This is seen especially in Figures 138c and 138d. The whirl ratio can be established by using a wave analyzer, of course, but most easily by counting the number of shaft revolutions (vertical or horizontal blips) per shaft orbit.

8. Radial Stiffness and Damping

The radial film stiffness (K_R) and damping coefficient (C) were determined from data generated during the unbalanced tests. The method used is based on a theoretical model which assumes a lumped mass, stiff shaft rotor with a known direction and magnitude of unbalance. The stiffness and damping are found from a force summation on the shaft. Appendix I presents the theoretical discussion and procedure followed to establish radial film stiffness and damping coefficient. Experimentally it is only the shaft orbit and the phase angle (angle between the unbalanced load vector and the shaft displacement vector) which need to be measured. The shaft orbit and phase angle are obtained from photographs of the oscillograph trace which is a measure of the horizontal and vertical probe outputs. The notch on the shaft combined with capacitance probe output establishes the phase angle.

The final magnitude of the unbalance and direction relative to the shaft notch is given below:

Test	Unbalance in.-oz	Magnitude lb/brg at 40,000 rpm	Angle Relative to Notch* degrees
DBTR 5C	0.0053	15	0
DBTR 5A	0.0106	30	0
DBTR 6C	0.00594	17	-30
DBTR 6A	0.0106	30	0

*Positive angles are in the direction of shaft rotation.

Test data were obtained as a function of speed at increments of 2,000 rpm for either constant supply pressure (DBTR 5A) or constant flows (DBTR 5C, 6C, and 6A).

Figures 139and 140 show stiffness and damping coefficient as functions of speed for the unbalanced 0.0015-inch bearing and Figures 141 and 142 for the unbalanced 0.002-inch bearing. The results show that the radial film stiffness increases for speeds below 30,000 rpm as either pressure or flow is increased. Above this speed, pressure and flow have little effect on stiffness, indicating the predominantly hydrodynamic characteristics of the bearing.

Calculating the zero speed stiffness from the static load-deflection curves indicates a decreasing trend in radial film stiffness to approximately 15,000 rpm for the 0.0015-inch bearing. Since this bearing is predominantly hydrostatic to 30,000 rpm, the increasing hydrodynamic component (due to unbalance and speed) may be out of phase with the hydrostatic component, causing the initial drop in radial film stiffness. Figure 140 clearly demonstrates the hydrostatic nature of the 0.0015-inch bearing and the influence of pressure on increasing radial bearing stiffness.

The damping coefficient is relatively constant with speed. For the 15 lb/bearing unbalance Figure 139 indicates a range from 16 to 20 lb-sec/in. The 30 lb/bearing unbalance in Figure 140 indicates a range from 12 to 16 lb-sec/in.

For the 0.002-inch bearing Figures 141 and 142 show the decreasing hydrostatic influence, even at the lower speeds. Radial stiffness for constant flows of 5 and 7 lb/min. appear relatively insensitive to amplitude of unbalance. Comparison of Figure 141 with the 0.0015-inch bearing data of Figure 139, shows a similar insensitivity of radial film stiffness to clearance at speeds above 30,000 rpm.

Damping coefficient shows a large increase with speed for the 15 lb/bearing unbalance test, from a low of approximately 6 lb-sec/in. to a high of 22 lb-sec/in. The increase is only small, from 5 lb-sec/in. to approximately 9 lb-sec/in., for the 30 lb/bearing unbalance case. This indicates that increasing unbalance results in smaller damping coefficients.

Radial film stiffness for the balanced rotor DBTR 5 and DBTR 6 can be calculated from the slope of the radial force versus eccentricity ratio curve ($W \cos \phi$ vs ϵ), or from the nondimensional plot of $1/S \cos \phi$ vs ϵ, as indicated in Volume I. Static damping coefficients can also be experimentally obtained by shock loading the rotor and measuring the decay rate of the shaft displacement.

9. Critical Speed

The predicted first and second mode critical speeds of the DBTR rotor-bearing system as a function of bearing stiffness is shown in Figure 143. First and second mode critical predictions are based on the modified Prohl method programmed on an IBM 7070 digital computer. Reference 23 describes the calculation method. Figure 143 also shows the stiff shaft critical which assumes that the shaft stiffness is very much greater than the bearing stiffness so that:

$$N_{CR} = \frac{1}{2\pi} \sqrt{\frac{K}{M}}$$

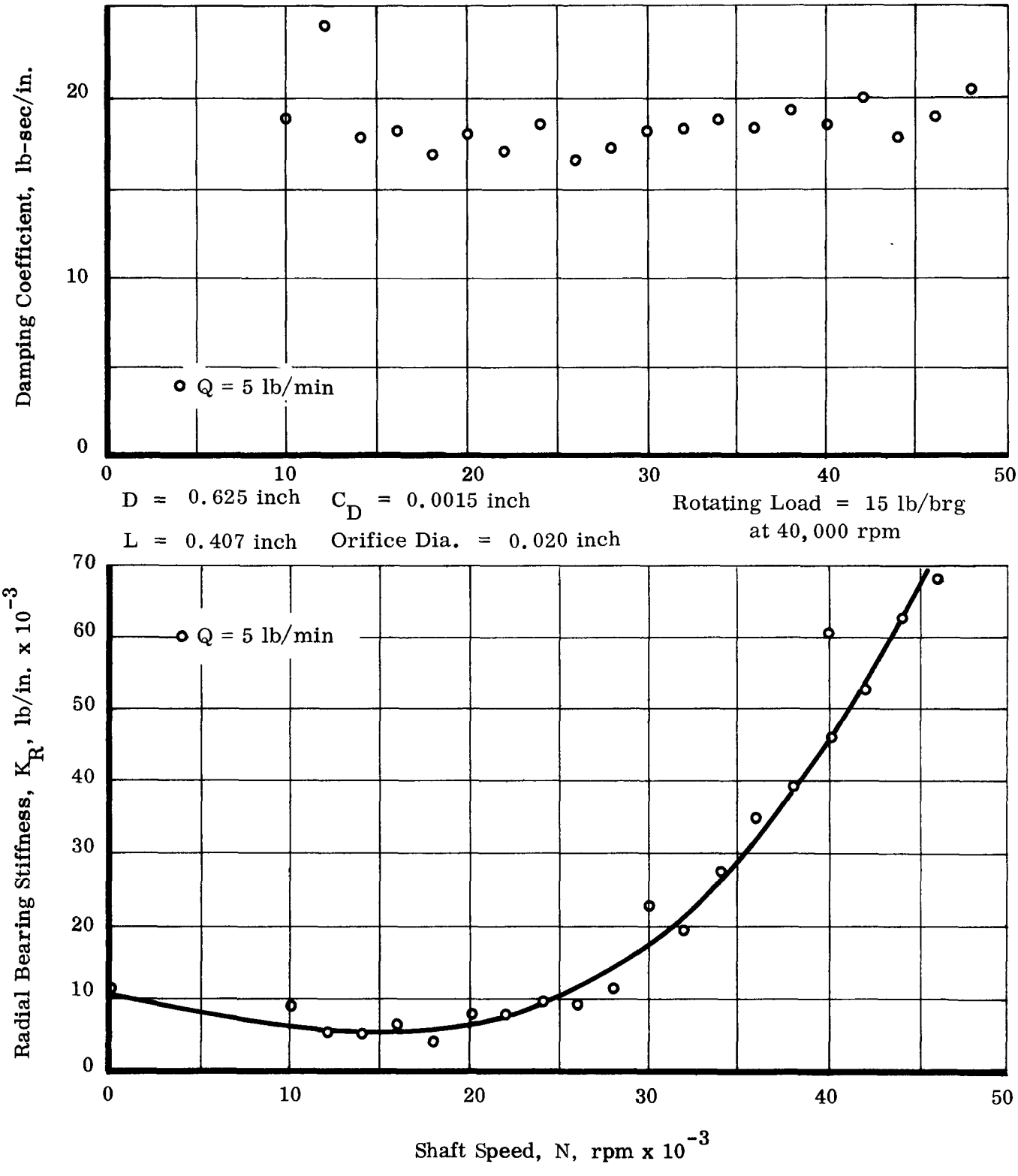

Figure 139. Damping Coefficient and Radial Film Stiffness vs Shaft Speed for a Three-Sector Orifice Compensated Journal Bearing

DBTR 5C Test Series

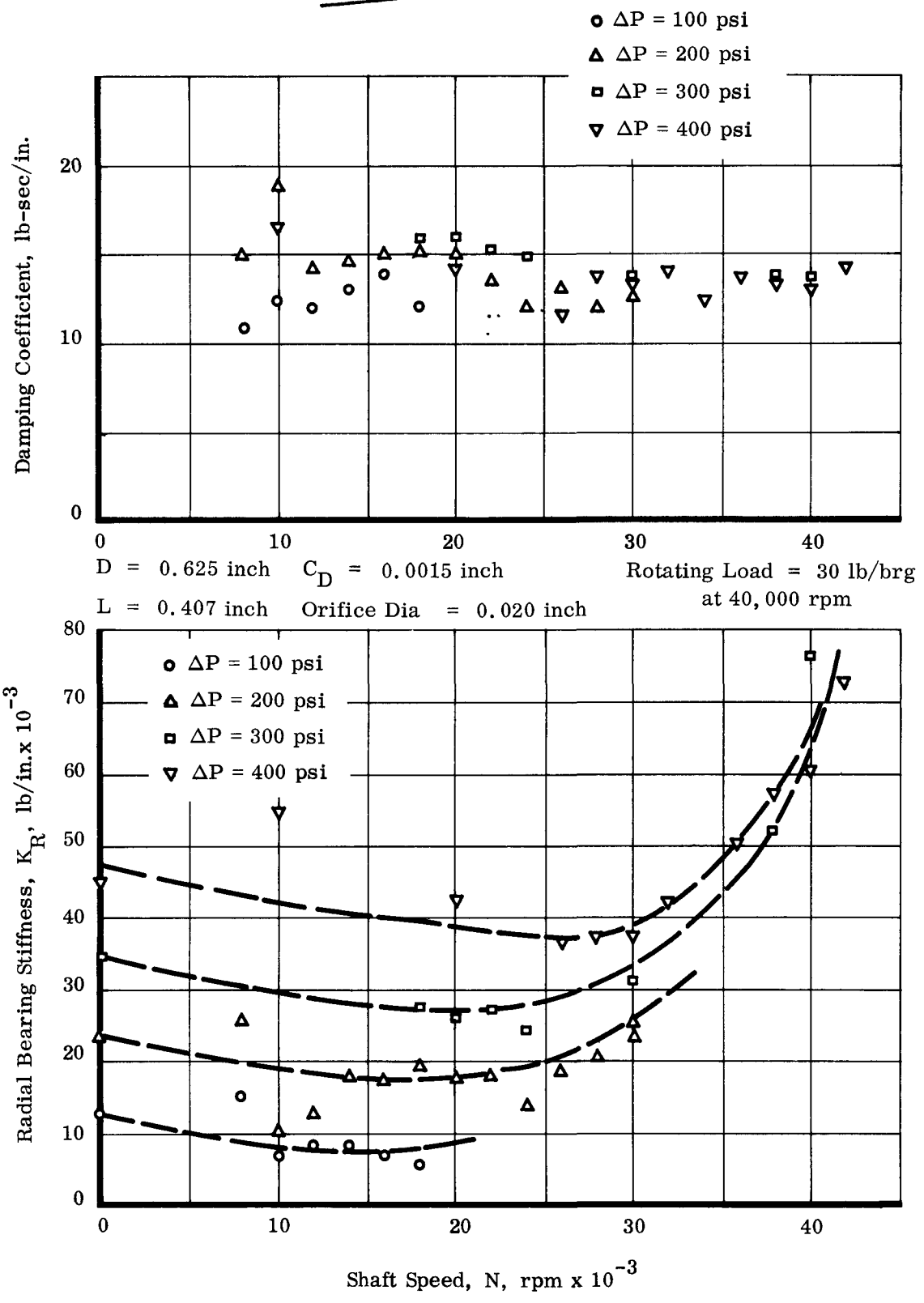

Figure 140. Damping Coefficient and Radial Stiffness vs Shaft Speed for a Three-Sector Orifice-Compensated Journal Bearing

DBTR 5A Test Series

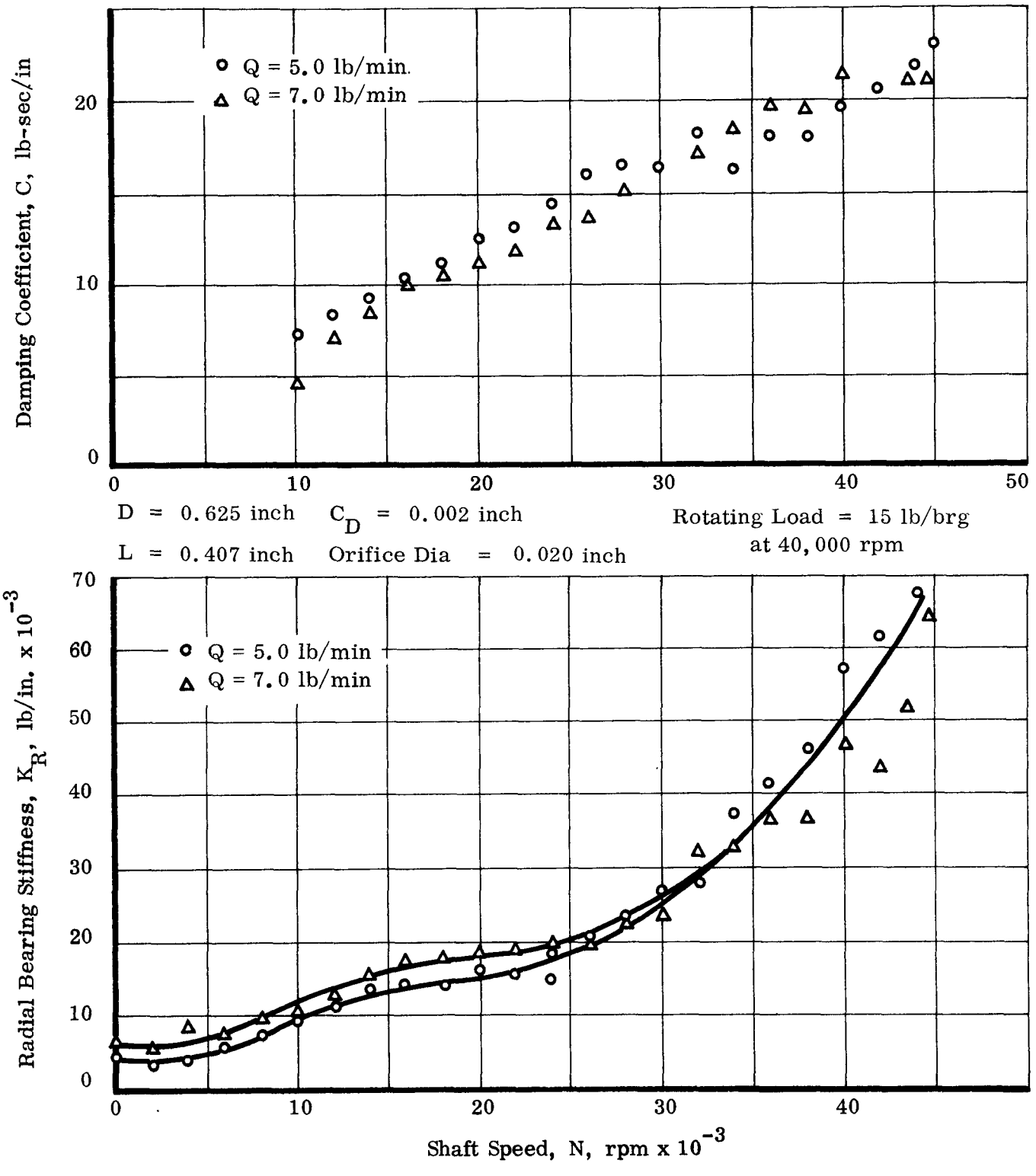

Figure 141. Damping Coefficient and Radial Film Stiffness vs Shaft Speed for a Three-Sector Orifice-Compensated Journal Bearing

DBTR 6C Test Series

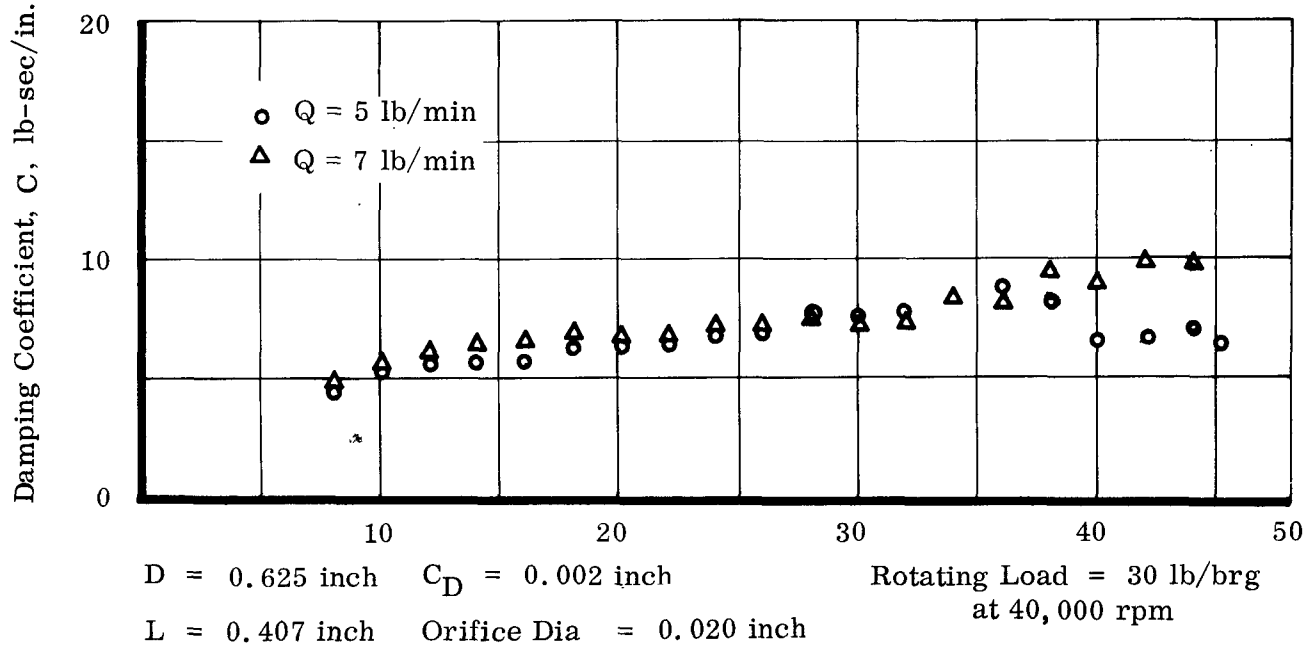

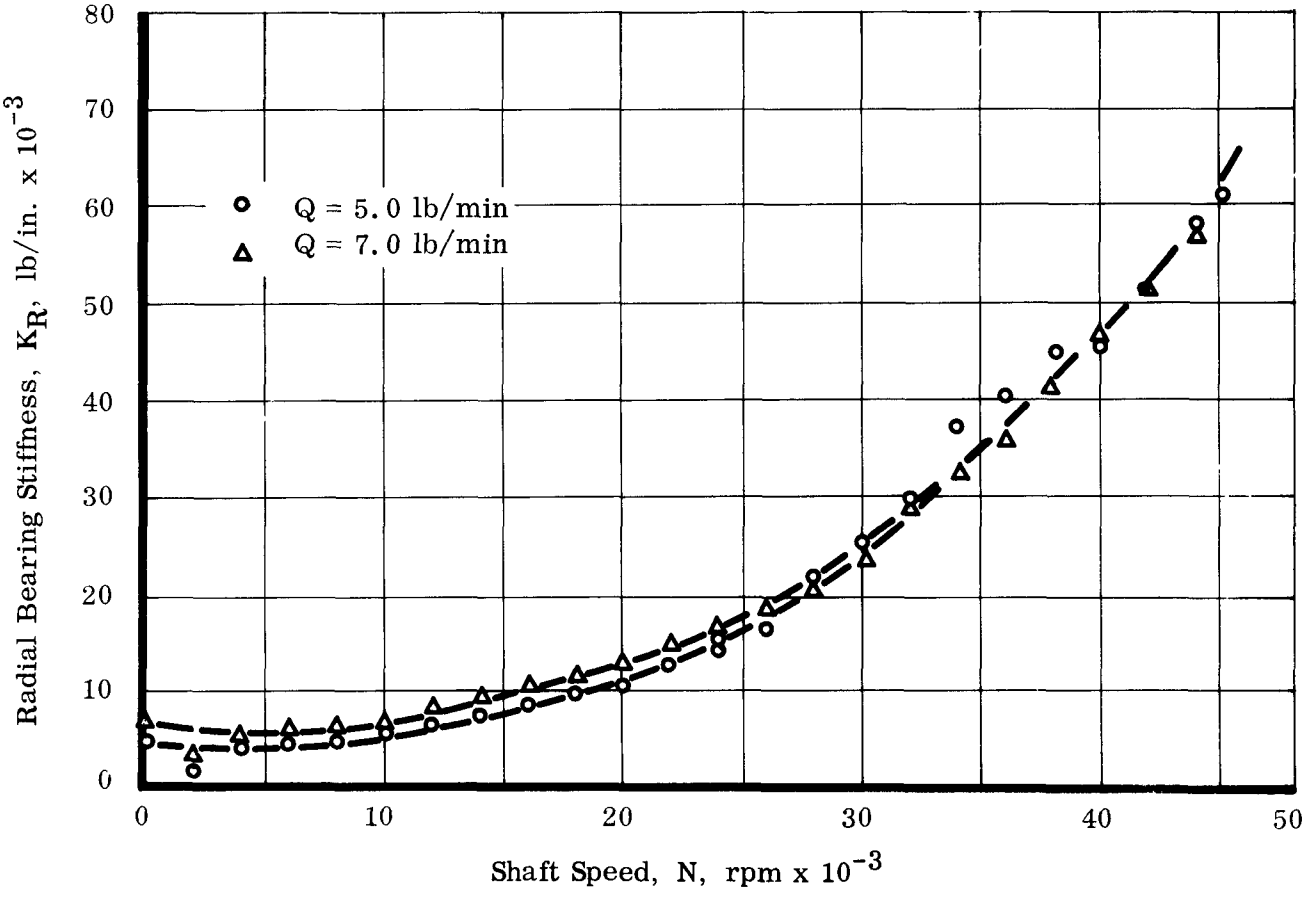

Figure 142. Damping Coefficient and Radial Film Stiffness vs Shaft Speed for a Three-Sector Orifice-Compensated Journal Bearing

DBTR 6A Test Series

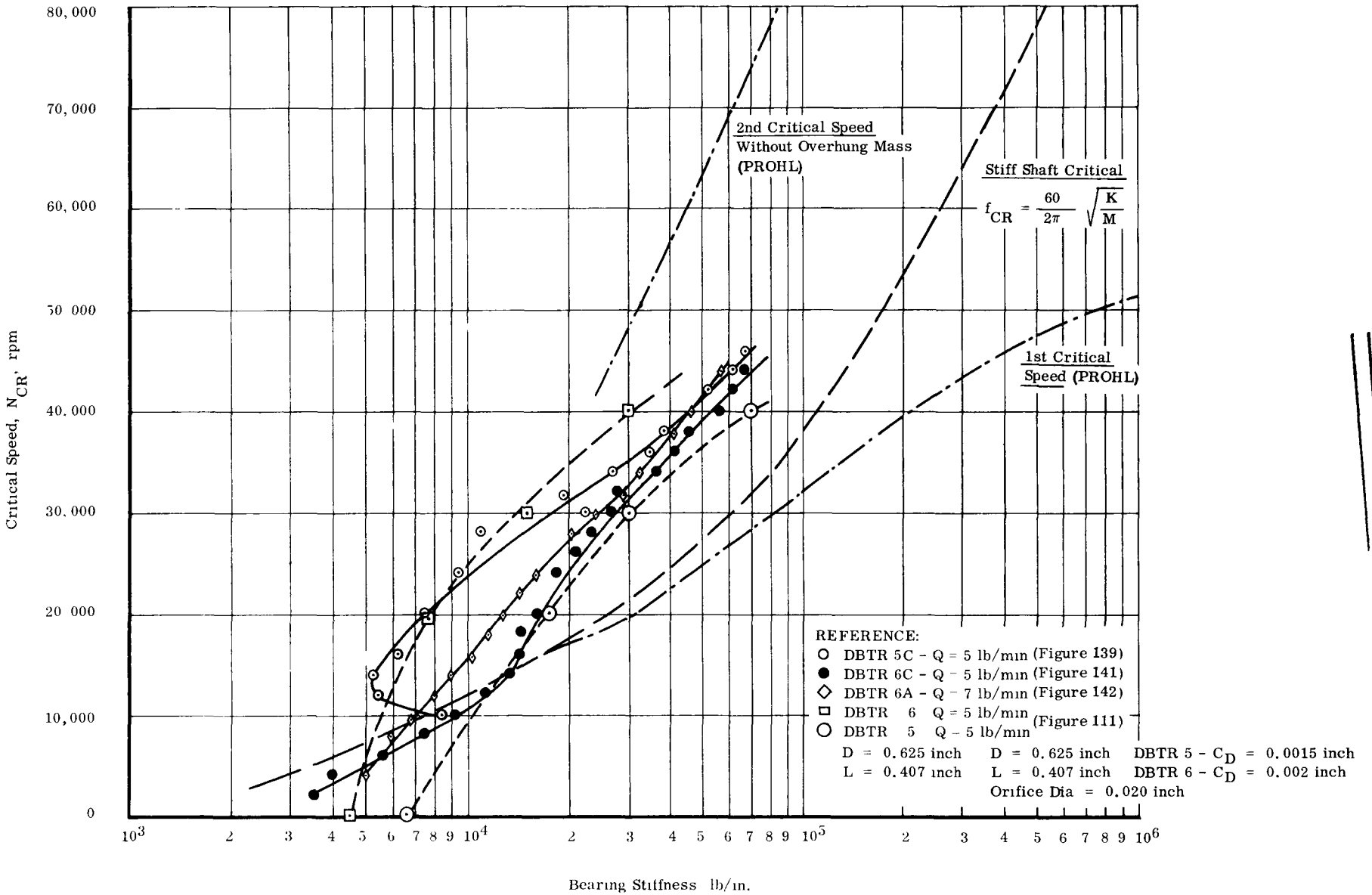

Figure 143. Critical Speed Characteristic of Dual Bearing Test Rig
(DBTR as Function of Bearing Stiffness
Orifice Compensated Three Sector)

Where:

K = bearing fluid film stiffness

M = mass supported by the bearing in question

Figure 143 shows that for values of bearing stiffness below 5×10^4 lb/in. the Prohl and stiff shaft equations predict essentially the same critical speed.

The bearing stiffnesses established during the DBTR 5 and 6 unbalance test series are superimposed in Figure 143. Based on these stiffness values (bearing stiffness under influence of rotating loads), the first mode critical speeds (predominantly influenced by bearing stiffness) are as follows:

DBTR 5C (Q = 5 lb/min)	N_{CR} = 10,500 rpm
DBTR 6C (Q = 5 lb/min)	N_{CR} = 14,000 rpm
DBTR 6A (Q = 7 lb/min)	N_{CR} = 9,000 rpm

Experimental verification of the presence of critical speeds was not possible on the basis of increasing amplitude. At these low speeds the high damping prevented a measurable amplitude change, and, even though amplitude increased with speed, it could not be differentiated from the increase caused by increasing unbalance. Consequently, experimental verification depended on the phase angle variation with speed. Figure 144 shows the measured phase angle (angle between the unbalanced load vector and the shaft displacement vector) for the corresponding test series. Since encountering the first mode critical is accompanied by a 90 degree phase angle change (180 degrees to pass all the way through), Figure 144 can be used to estimate first mode criticals. Assuming the phase angle to be zero at zero speed (DBTR 5A and 6A were unbalanced in this manner, while DBTR 6C was corrected for its 30 degree initial phase angle), the critical speeds can be expected to be:

DBTR 5C (Q = 5 lb/min)	N_{CR} = 10,800 rpm
DBTR 6C (Q = 5 lb/min)	N_{CR} = 13,600 rpm
DBTR 6A (Q = 7 lb/min)	N_{CR} = 10,000 rpm

Excellent agreement exists between the value based on cross-over between measured film stiffness and measured phase angle.

Figure 143 shows that operation at design speed is between first and second critical speeds. Furthermore, the influence of increasing rotating load from DBTR 6C to DBTR 6A is accompanied by a decreased radial stiffness and a subsequent lower critical speed. At higher speeds, the bearing stiffness seems to merge, indicating the small influence of clearance and rotating load on the bearing stiffness.

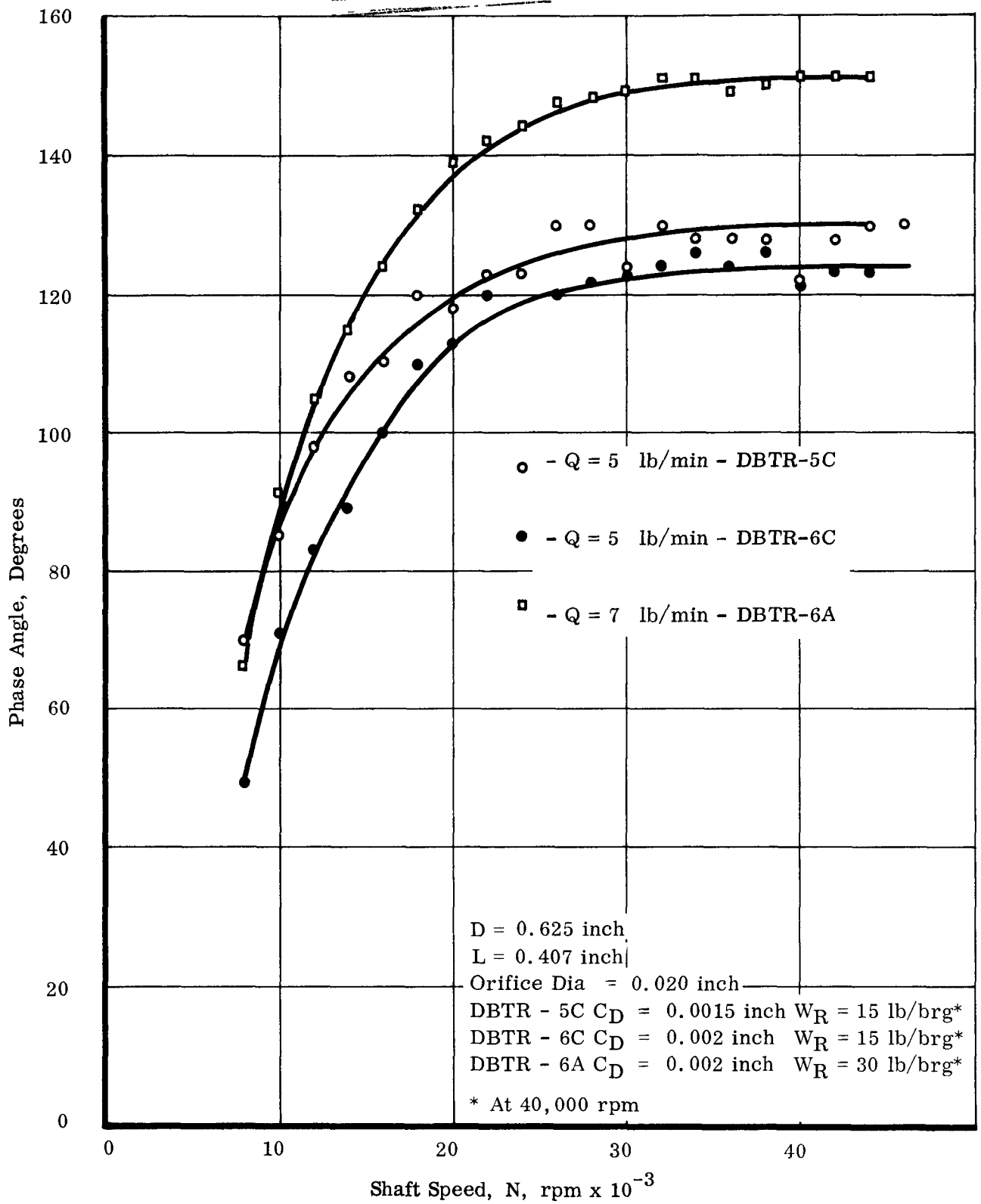

Figure 144. Phase Angle vs Shaft Speed for a Three-Sector Orifice Compensated Bearing

DBTR 5 and 6 Test Series

The value of fluid film stiffness shown in Figure 111 for DBTR 5 and DBTR 6 (balanced rotor) are also plotted in Figure 143. Based on a 5/lb/min flow the first mode bearing-rotor critical occurs at 14,000 rpm for DBTR 5 (C_D = 0.0015 inch) and 7,500 rpm for DBTR 6 (C_D = 0.002 inch). Since phase angles were not monitored during the balanced rotor test and amplitudes were very small, verification of these criticals was not obtained.

10. Conclusion for DBTR 5 and 6 Test Series

Specific conclusions based on the results of the DBTR 5 and 6 test series are summarized below:

1) Orifice compensation improved the stability characteristics of the three sector bearing.

2) The 0.0015 inch diametral clearance bearing was free of fractional frequency whirl for all operating modes of loads, pressures,flows,and speeds up to 45,000 rpm.

3) The 0.002 inch diametral clearance bearing had areas of instability starting at 20,000 rpm for low supply pressures of 75 psi and zero applied load. The whirl ratio was 0.4.

4) The threshold of fractional frequency whirl could be suppressed to above 44,000 rpm with the application of 250 to 300 psi supply pressures at zero applied load.

5) Addition of rotating load improved stability characteristics of the 0.002 inch clearance bearing, increased the whirl ratio to 0.5 but had no stability effect on the inherently stable 0.0015 inch clearance bearing.

6) With orifice compensation improved stability was achieved at the expense of load capacity and increased pressure requirements for a fixed flow rate.

7) Load capacity into the axial groove (loading up) was considerably less than the load capacity into a pad (loading down).

8) A non-dimensional load capacity design curve explained the behavior of the bearing over a range of diametral clearance, (0.0015 to 0.002 inch), eccentricity ratio (0 to 0.8), speed (0 to 40,000 rpm), and supply pressures, (0 to 500 psi).

9) A similar non-dimensional plot explained the flow characteristics of the bearing.

10) Three predominant performance regions were established:

    a) At zero and low speed and low loads the bearing is predominantly hydrostatic.

    b) At medium speeds and loads the bearing is predominantly hybrid.

    c) At high speeds and large loads the bearing is predominantly hydrodynamic.

11) In the hydrostatic region, bearing load capacity was influenced by supply pressure, while flow was influenced by applied load. Also, bearing performance could be predicted by hydrostatic theory without Reynolds number corrections.

12) In the hydrodynamic region, the bearing load capacity was relatively independent of pressure, and flow was insensitive to load. For small eccentricity ratios, a Reynolds number correction was indicated; but at eccentricity ratios > 0.5, laminar behavior was approached, and a Reynolds number modification was not required.

13) Power loss was 10 to 20% higher than predicted. At 40,000 rpm power loss of the 0.0015- and 0.002-inch clearance bearings were 300 and 250 watts respectively.

14) Bearing-rotor critical speed was approximately 10,000 to 15,000 rpm depending on the clearance, applied load, and flow rate. Operation at 36,000 rpm and 40,000 rpm was between the first and second critical speed modes. Good agreement exists between predicted critical speed (based on measured bearing film stiffness) and measured phase angle.

15) The bearing is highly damped and for the 0.0015-inch clearance damping coefficient is relatively independent of speed. For the 0.002-inch clearance bearing, damping coefficients are lower and dependent on speed.

16) No evidence of cavitation-erosion was detected during the test series which consisted of 159 hours of dynamic operation and some 93 stop-starts.

III. THREE-SECTOR BEARING - MAJOR CONCLUSIONS

The analytical and experimental bearing development program revealed the ability of the three-sector bearing to meet the specified requirements of stable operation at any possible operating mode with orifice compensation but at a considerable compromise in load capacity. However, on the basis of experimental tests, the load capacity was still greater than required by CRU specifications.

Other advantages offered by the three-sector bearing were verified during component testing:

1) Improved flow reliability was achieved by orifice compensation, and pressures required for the specified flows were well within the system capacity at the desired clearance of 0.0015 inch.

2) No evidence of cavitation-erosion damage was detected during any of the three-sector bearings (compensated or uncompensated) tests.

3) Stable operation was achieved at reasonable clearances with orifice compensation and could be assured at clearances up to 0.002 inch with 250 to 300 psi supply pressures.

4) Critical speed could be controlled within reasonable limits in the orifice-compensated three-sector by flow selection. Operation between first and second mode critical was assured with the bearing clearances suitable for CRU application.

5) Crudding of small orifices was not encountered. The component tests did reveal a compromise in load capacity to achieve stability, i.e., by orifice compensation.

The influence of the reduction in load capacity and long term operating characteristics of the compensated three-sector bearing remained to be verified at the conclusion of the period covered by this report.

The operational history of the uncompensated three-sector bearing, primarily in CRU III, was very poor. The longest test on an uncompensated three-sector bearing CRU III was 300 hours. Some units failed bearings after short runs. The primary cause for these early failures was diagnosed as a combination of large amplitude half-frequency whirl, bearing misalignment, operation at or close to the second critical speed (overhang NaK pump rotor resulted in a second critical speed close to 40,000 rpm for the uncompensated three sector bearing), large unbalance loads, and conical mode operation.

The performance characteristics of the orifice-compensated three-sector bearing in a CRU remained unknown at the conclusion of the period covered by this report.